

CHEMISTRY AND STABILITY OF THIOL BASED POLYETHYLENE GLYCOL
SURFACE COATINGS ON COLLOIDAL GOLD AND THEIR RELATIONSHIP TO
PROTEIN ADSORPTION AND CLEARANCE IN VIVO

By

PAUL CARPINONE

A DISSERTATION PRESENTED TO THE GRADUATE SCHOOL
OF THE UNIVERSITY OF FLORIDA IN PARTIAL FULFILLMENT
OF THE REQUIREMENTS FOR THE DEGREE OF
DOCTOR OF PHILOSOPHY

UNIVERSITY OF FLORIDA

2012

© 2012 Paul Carpinone

To all who nurtured my intellectual curiosity, academic interests, and sense of scholarship throughout my lifetime, making this milestone possible

ACKNOWLEDGMENTS

First and foremost, I would like to acknowledge the support from my advisor, Kevin Powers, who gave me the freedom to pursue this topic with a high level of autonomy. I would also like to acknowledge the support of my other committee members: Brij Moudgil, Hassan El-Shall, Rajiv Singh, Spyros Svoronos, and Steve Roberts. Special thanks go to Steve Roberts, Dave Barber, and John Munson of the Center for Environmental and Human Toxicology who made the animal experiments possible and provided many helpful discussions on toxicology. I would also like to thank Nancy Denslow and Georgia Hinkley from the CEHT for their helpful discussions and collaboration. I would like to acknowledge Nick Komninakis for his assistance in performing experiments when an extra set of hands were needed and Kerry Siebein for her collaborative work with microscopy. Finally, I acknowledge the faculty, staff, and coworkers at the Particle Engineering Research Center and the Center for Environmental and Human Toxicology for their assistance over the years.

TABLE OF CONTENTS

	<u>page</u>
ACKNOWLEDGMENTS	4
LIST OF TABLES	8
LIST OF FIGURES	10
LIST OF ABBREVIATIONS	19
ABSTRACT	21
CHAPTER	
1 INTRODUCTION	23
Nanotechnology	23
Nanomaterials for Biological Applications	24
Surface Modification for Biological Applications	25
Nanotoxicology	27
Research Goals	29
2 SYNTHESIS AND CHARACTERIZATION OF GOLD NANOMATERIALS	34
Chapter Introduction	34
Overview of Gold Chemistry	35
Particle Synthesis	36
Characterization Methods	37
Sedimentation	37
Equations governing sedimentation	39
Sedimentation for characterizing adsorbed species	42
<i>In vivo</i> particle size analysis by sedimentation	45
Dynamic Light Scattering	47
Microscopy	49
Raw Particle Properties	51
Chapter Summary	52
3 PROPERTIES AND STABILITY OF PEG COATINGS	78
Adsorption and Desorption on Gold Surfaces	78
Measurements of Adsorption	80
Colorimetric methods	84
Sedimentation methods	87
Electrophoresis	90
Ultraviolet absorption methods	95
Thermogravimetric analysis	98

Other measurements	102
Surface Conformation	103
Preparation and Properties of PEG Coated Particles	104
Reagent Purity	108
PEG Coating Stability	116
Coating Stability Kinetics	118
Factors Affecting Coating Stability	119
Dissolved gases	122
Thermal stability	125
Effects of reagent impurities	127
Salt and solute effects	129
pH	133
Chapter Summary	135
4 IN VITRO PARTICLE - PROTEIN INTERACTIONS	195
Chapter Introduction	195
Selection of Model Proteins	196
Interactions of Proteins with Gold Particles	196
Measurements of Protein Adsorption	197
Colorimetric assay methods	197
Electrophoretic techniques	198
Other measurements	199
Protein Adsorption and Binding Behavior	200
Properties of Coated Particles	205
Differential Binding of Serum Proteins	206
Interactions of Proteins with PEG Coated Gold Particles	208
Time Dependent Interactions of Proteins with PEG Coated Gold Particles	208
Protein Binding	209
Reagent Purity	213
Suspension Stability	215
Chapter Summary	217
5 IN VIVO BEHAVIOR OF NANOMATERIALS	242
Chapter Introduction	242
Polyethylene Glycol Surface Coatings for Improved Circulation Time	242
Clearance of particles from the bloodstream	244
<i>In vivo</i> Clearance and Biodistribution of PEG Coated Gold Particles	246
Chapter Summary	252
6 SUMMARY AND CONCLUSIONS	263
APPENDIX	
A ESTIMATION OF PARTICLE SPECIFIC SURFACE AREA BY IMAGE ANALYSIS	277

B	ADDITIONAL PHYSICOCHEMICAL CHARACTERIZATION DATA	282
C	EFFECTS OF CONTAINER TYPE ON DEGRADATION RATE MEASUREMENTS	288
	LIST OF REFERENCES	295
	BIOGRAPHICAL SKETCH.....	320

LIST OF TABLES

<u>Table</u>	<u>page</u>
1-1	List of coatings used to improve biocompatibility, particle stability, and circulation time <i>in vivo</i> 31
1-2	List of nanomaterials typically cited for current or projected widespread use. 33
2-1	Summary of preparation methods for differential sedimentation analysis of gold particles in whole mouse blood..... 70
3-1	Differences in estimated specific surface area values for gold particles..... 140
3-2	Literature reported adsorption densities of PEG on gold surfaces..... 141
3-3	Summary of selected methods used for quantitative determination of coating density. 145
3-4	Summary of selected methods used for qualitative analysis of coating density. 149
3-5	Effects of interferences in colorimetric and fluorimetric assays when used to determine adsorption density by the depletion method. 151
3-6	Typical UV absorption range for selected organic functionalities 160
3-7	Apparent coating densities for various gold particles as measured by TGA. 162
3-8	Summary of common misconceptions regarding adsorption measurements of PEG coatings of gold particles..... 168
3-9	Sulfur content of thiolated PEG reagents as determined by ICP. 180
3-10	Sulfur and thiol content of dialysis permeate and retentate (Reagent 2). 180
3-11	Summary of selected compounds possessing properties which are likely to influence the rate and mechanism of PEG coating degradation. 186
3-12	Degradation times for the least stable samples listed in Table 3-11 under buffered conditions. 186
3-13	Summary of samples prepared to screen for relationships between rate of coating degradation and common storage conditions. 188
3-14	Summary of samples prepared for analysis of the relationship between thiourea impurities in PEG reagents and particle degradation..... 191
3-15	Literature reported salt effect parameters for selected salts ²¹² 192

3-16	Degradation times for the least stable samples listed in Table 3-15.....	193
4-1	Literature reported isoelectric points for some common proteins.	222
5-1	Literature reported clearance characteristics of gold particles <i>in vivo</i>	255
5-2	Summary of particles tested <i>in vivo</i>	256
A-1	Comparison of mean specific surface area values produced by various models of particle shape (by TEM image analysis)	281
C-1	Summary of leaching experiment results at 65C	293
C-2	Summary of samples prepared for analysis of container sealing and oxygen availability in plastic containers.....	293

LIST OF FIGURES

<u>Figure</u>		<u>page</u>
1-1	Illustration of several coating possibilities utilizing functional polyethylene glycol coatings on gold particles.....	32
2-1	UV/Visible absorption spectra of several gold (III) complexes.....	54
2-2	Speciation diagram of gold chloride in water.....	54
2-3	Speciation of the Au ³⁺ /Cl ⁻ system as a function of pH and chloride ion concentration.....	55
2-4	Pourbaix diagram of the Au/Cl system where [Cl ⁻] = 1M.....	55
2-5	Illustration of differential and integral sedimentation.....	56
2-6	Illustration of a modern disc centrifuge geometry for differential sedimentation analysis.....	56
2-7	Response curve to nominally 40nm gold suspensions of different concentrations.....	57
2-8	Calculated relative light scattering cross section (407nm) of spherical gold particles at sizes below 1µm.....	57
2-9	Particle size distributions of various gold suspensions as measured by differential sedimentation.....	58
2-10	Sedimentation velocity distributions of various coated 40nm gold particles.....	58
2-11	Calculated net densities of coated gold particles.....	59
2-12	Calculated apparent particle size relative to core particle size for various coated gold particles.....	60
2-13	Variance of calculated coating thickness with assumed coating density.....	63
2-14	Electron micrographs of human blood cells.....	65
2-15	Sedimentation velocity distribution of whole blood.....	66
2-16	Equivalent particle size of whole blood components.....	66
2-17	Sedimentation velocity distribution of lysed whole blood.....	67
2-18	Equivalent particle size of lysed whole blood components.....	67

2-19	Obstruction of analysis range by blood relative to particle density..	68
2-20	Sedimentation velocity distribution of blood with PEG coated gold particles	69
2-21	TEM image analysis particle size distributions of gold particles prepared by the citrate method.....	70
2-22	Aggregates of uncoated gold particles in mouse gastric fluid.....	71
2-23	Distribution of gold particles in mouse gastric contents.....	71
2-24	Identification of gold particles by EDS mapping.....	72
2-25	Transmission electron micrographs of gold particles as prepared.....	73
2-26	Zeta potential titration of nom. 50nm gold particles as determined by DLS.....	74
2-27	Zeta potential of a 50ppm suspension of nom. 40nm gold particles titrated with sodium chloride.....	74
2-28	Photograph of spherical and monodisperse gold particles ranging in size from approximately 40nm (left) to 100nm (right).....	75
2-29	Visible absorption spectrum of gold particles at various sizes.....	75
2-30	UV/Visible absorption spectrum of gold particles with increasing concentration of salt (increasing from S1 to S3).....	76
2-31	Particle size distribution of nominally 20nm gold particles by DLS.....	76
2-32	DLS particle size distribution of nominally 20nm gold particles before and after coating with PEG.....	77
3-1	Frequency of literature reported PEG coating densities on gold particles.....	144
3-2	Typical effects of impurities listed in Table 3-5 for a high affinity adsorption isotherm.....	151
3-3	UV/Visible absorption spectrum of Ellman's Reagent with various concentrations of mercaptoethanol.....	152
3-4	Comparison of response curves for two 5kDa PEG-thiol reagents from two sources to a cysteine standard using Ellman's Reagent.....	152
3-5	Adsorption isotherm of thiol-PEG to the surface of nominally 20nm gold particles.....	153
3-6	Sedimentation velocity and calculated coating thickness for various concentrations of PEG.....	154

3-7	Effects of gradient contamination with excess PEG on analyzed particle size.....	155
3-8	Measured relative sedimentation velocity vs. core particle size for PEG coated gold particles.....	156
3-9	Diagram of a charged particle migrating under an applied electric field.	157
3-10	Mobility of nom. 20nm PEG coated particles with increasing PEG density..	157
3-11	Schematic showing the relationship between electrophoretic mobility and PEG coating density.....	158
3-12	Separation of PEG coated nom. 20 and 45nm gold particles by electrophoresis.	158
3-13	Near ultraviolet absorption spectra of PEG (hydroxyl terminated) and thiol functionalized methoxy PEGs in water.	159
3-14	Near ultraviolet absorption spectra of selected compounds in water.....	159
3-15	UV response curves for thiolated PEG at various wavelengths.....	160
3-16	Near UV absorption curves of thiolated PEG mixed with deionized water and particle supernatant.....	161
3-17	Near UV absorption curve of thiolated PEG after exposure to a gold sputter coated glass slide.	161
3-18	Coating mass relative to total particle and core particle mass as a function of coating surface density for various core sizes.	163
3-19	TGA curves of thiolated PEG (Reagent 2) up to 1000C under inert (N ₂) and reactive (Air) atmospheres.	164
3-20	TGA curves for sodium citrate dihydrate up to 1000C under inert (N ₂) and reactive (Air) atmospheres.	164
3-21	TGA curve of coated nom. 20nm PEG coated (Reagent 2) gold particles under an oxidative atmosphere.	165
3-22	TGA curve of uncoated nom. 20nm gold particles under an oxidative atmosphere.....	165
3-23	Particle size increase of nom. 20nm gold particles on coating with PEG as determined by DLS.....	166
3-24	Zeta potential neutralization of nom. 20nm gold particles on coating with PEG (as determined by DLS).....	166

3-25	TEM images of negatively stained nom. 40nm PEG coated and uncoated gold particles..	167
3-26	Illustration of the adsorbate surface structure with increasing coating density..	169
3-27	Sedimentation velocity distributions at different points during PEG coating (Reagent 1) with a large mixing volume.	170
3-28	Apparent hydrophobicity exhibited by gold particles in salt solutions and when coated with sub-optimal coating densities.....	170
3-29	Salt induced aggregation of particles with sub-optimal PEG coatings.....	171
3-30	Sedimentation velocity distributions of mixed nom. 20nm PEG coated and nom. 45nm uncoated particles after incubation at 37C for approximately 24h..	171
3-31	Sedimentation velocity distributions of mixed nom. 20nm PEG coated (Reagent 2) and nom. 45nm uncoated particles initially.....	172
3-32	Sedimentation velocity distributions of mixed nom. 20nm PEG coated (Reagent 2 as received) and nom. 45nm uncoated particles after 24h under various conditions.....	173
3-33	Sedimentation velocity distributions of mixed nom. 20nm PEG coated (Reagent 2 purified) and nom. 45nm uncoated particles after 24h at 37C..	174
3-34	Sedimentation velocity distributions of nom. 45nm particles added to supernatants from PEG coated (Reagent 2 as received) nom. 20nm particles after 24h at 37C.....	175
3-35	Rate of thiol activity loss in PEG-thiol solutions (0.1mM Reagent 2) based on storage condition.	176
3-36	Near UV absorption spectra of aqueous solutions of selected compounds used for thiolation..	176
3-37	Near UV absorption spectra of aqueous solutions of thiolated PEG (as received), dialysis permeate, and retentate of the thiolated PEG compound (3kDa MWCO).....	177
3-38	Images of a gold suspension before and after exposure to the PEG reagent (Reagent 2 as received), dialysis permeate, retentate, and thiourea.....	177
3-39	UV response curves of thiourea at concentrations below 0.2mM.....	178
3-40	Near UV absorption spectra of aqueous solutions of thiolated PEG (Reagent 2 as received), dialysis permeate, and retentate of the thiolated PEG compound (100-500Da MWCO).....	179

3-41	Relative mobility of PEG coated nom. 20nm gold particles with increasing concentration of thiolated PEG.	179
3-42	Deconvolution of the UV absorption spectrum of the dialysis permeate (from Figure 3-37).	181
3-43	Potential thiourea mediated oxidation processes.	181
3-44	Chromatograms of A) dialysis permeate (100-500Da) and B) pure thiourea. ...	182
3-45	Comparative measurements of purified and as received PEG reagent (Reagent 2) using several coating characterization techniques.	183
3-46	Sedimentation analysis demonstrating the effects of thiourea impurities on the PEG coating.	184
3-47	Adsorption isotherm of thiourea on nom. 20nm gold particles.	184
3-48	Time dependent mobility and coating density of PEG coated gold particles incubated at 37C in deionized water.	185
3-49	Change in mobility of buffered particles exposed to various compounds at 37C for 23 days..	187
3-50	Dissolved oxygen content in deionized water equilibrated with air at STP. ²¹¹ ..	188
3-51	Comparison of particle mobilities in equilibrated and degassed media after 5 days under various conditions.	189
3-52	Relative mobilities of PEG coated gold particles incubated for 5 days at 37C in deionized water which was degassed and subsequently saturated with various gases and gas mixtures.	189
3-53	Relative particle mobility as a function of temperature and time over the first three days of incubation for A) Equilibrated water and B) Degassed water.	190
3-54	Time required to degrade approximately 90% of the PEG coating on nom. 20nm gold particles as a function of temperature in equilibrated and degassed water.	190
3-55	Time dependent relative mobilities of particles coated with purified and as-received thiolated PEG (Reagent 2).	191
3-56	Relative mobilities of PEG coated (Reagent 2) particles in various 100mM salt solutions after approximately one month of incubation at 37C.	192
3-57	Concentration dependent mobility of coated gold particles (Reagent 2) as a function of salt (NaCl) concentration after incubation for 4 days at 37C.	193

3-58	Time dependent degradation of PEG coated gold particles (Reagent 2) at various pHs.....	194
4-1	UV/Visible absorption spectrum of the Bradford Assay with various concentrations of BSA.	222
4-2	Typical response curves for the Bradford Assay using BSA.....	223
4-3	Schematic showing the effect of protein adsorption on the electrophoretic mobility.	223
4-4	Transmission electron micrographs of negatively stained serum protein coated nom. 40nm gold particles.....	224
4-5	Dynamic light scattering particle size distributions of nom. 40nm gold particles showing an increase in size of approximately 40nm on coating with human plasma proteins.	224
4-6	Adsorption isotherm of BSA onto as-prepared nom. 20nm gold particles with regions of colloidal stability and instability indicated.....	225
4-7	Aggregation of protein coated particles upon dilution with deionized water.....	225
4-8	Adsorption density of BSA as a function of suspension pH on as prepared nom. 20nm gold particles.	226
4-9	Adhesion of BSA coated gold particles to hydrophobic polypropylene containers.....	226
4-10	Adsorption density of Lysozyme as a function of suspension pH on as prepared nom. 20nm gold particles.	227
4-11	Zeta potential titration of BSA coated nom. 20nm gold particles.	227
4-12	Zeta potential titration of lysozyme coated nom. 20nm gold particles.....	228
4-13	Zeta potential titration of serum protein coated 40nm gold particles.....	228
4-14	Comparison of serum protein binding characteristics for gold particles and titania.....	229
4-15	Size dependent binding of serum proteins to uncoated gold particles.....	229
4-16	Adsorption of BSA relative to PEG coating density on nom. 20nm gold particles.....	230
4-17	Adsorption of BSA relative to PEG coating density on nom. 20nm gold particles using a lower quality reagent.....	230

4-18	Time dependent integrated mobility of PEG coated gold particles (Reagent 1) in BSA and Human Serum. Particles incubated in: A) BSA (concentration approximately equal to reference serum albumin levels) B) Human plasma. ...	231
4-19	Estimated quantities of protein adsorbed (as BSA) to PEG gold particles based on data shown in Figure 4-18.	232
4-20	Time dependent BSA adsorption on PEG coated (Reagent 1) gold particles quantified by the Bradford total protein assay.	233
4-21	Mobility spectra of PEG coated gold particles (Reagent 1) incubated with BSA for various periods of time.	233
4-22	Time dependent integrated mobility of PEG coated gold particles (Reagent 2) in human plasma.	234
4-23	Protein adsorption in cleaned and as prepared PEG coated (Reagent 1) gold particles after incubation at 37C for three days under different conditions.	234
4-24	Competitive desorption of BSA from fully protein coated particles at physiological pH by thiolated PEG (Reagent 2).	235
4-25	Illustration of the proposed relationship between impurity adsorption and protein binding on gold particles.	236
4-26	Time dependent integrated mobility of PEG coated gold particles (Reagent 2) before and after purification in BSA and Human Serum.	237
4-27	Single point adsorption measurement of BSA onto PEG coated (Reagent 2) nom. 20nm gold particles using the Bradford Assay after 5 day incubation at 37C.	238
4-28	Sedimentation velocity distributions of PEG coated gold particles (Reagent 1) incubated at 37C in whole mouse blood for various times.	239
4-29	Optical micrographs of aggregated gold particles (uncoated) in whole blood after lysing cells in deionized water.	239
4-30	Optical micrograph of aggregated gold particles (uncoated) in whole blood. ...	240
4-31	Sedimentation velocity distributions of blood before and after addition of uncoated gold particles.	240
4-32	Optical micrographs of uncoated gold particles added to human plasma under different mixing conditions.	241
5-1	Clearance pathways for particles in the bloodstream.	254
5-2	Percent of dose recovered in the blood and body tissues.	257

5-3	Gold concentration and primary particle peak intensity in blood as a function of time.....	259
5-4	Ratio of gold concentration in blood by ICP-MS to primary particle peak intensity.	259
5-5	Histology section of liver tissue from mice after dosing with uncoated gold particles.	260
5-6	Transmission electron micrographs of clusters of gold particles in liver tissue after administration of uncoated particles.	260
5-7	Histology sections of liver tissues from mice dosed with PEG coated (Reagent 1) gold particles.	261
5-8	Transmission electron micrographs of liver tissues after administration of uncoated particles.	261
5-9	EDS analysis of dark features observed in tissue sections to confirm composition.	262
A-1	Image analysis schemes for approximating the specific surface area of certain anisotropic particles.	279
A-2	Image analysis scheme based on finite element analysis using truncated conical elements.	280
B-1	Relative near ultraviolet absorption spectra of thiourea at various concentrations.	283
B-2	Ratio of absorbance peak intensities at 236nm and 196nm as a function of thiourea concentration.	283
B-3	Raman spectra of various PEG and functionalized PEG reagents.	284
B-4	Raman spectrum of thiourea.	285
B-5	TGA curve of C ₁₆ TAB in air up to 1000C.	286
B-6	TGA curves of thiourea under nitrogen and air up to 1000C.	286
B-7	Titration curve of thiourea.	287
C-1	Near ultraviolet absorption curves of water after leaching in various plastic containers for approximately 24h at 65C.	292
C-2	Relative mobilities of PEG coated (Reagent 2) gold particles under various conditions.	292

C-3 Relative mobilities of PEG coated (Reagent 2) gold particles under various conditions to illustrate the influence of dissolved oxygen availability on coating degradation..... 294

LIST OF ABBREVIATIONS

BSA	Bovine Serum Albumin
BSE	Backscattered Electron
CTAB	Cetyltrimethylammonium Bromide
DLS	Dynamic Light Scattering
EDS	Energy Dispersive Spectroscopy
FTIR	Fourier Transform Infrared Spectroscopy
FWHM	Full width at half maximum
HPLC	High Performance Liquid Chromatography
HSA	Human Serum Albumin
ICP	Inductively Coupled Plasma
IEP	Isoelectric Point
MWCO	Molecular Weight Cutoff
PBS	Phosphate Buffered Saline
PEG	Polyethylene Glycol
pI	Isoelectric Point
PVP	Polyvinyl Pyrrolidone
RES	Reticuloendothelial System
SDS	Sodium Dodecyl Sulfate
SE	Secondary Electron
SEM	Scanning Electron Microscopy
TAE	Tris-Acetate-EDTA Buffer
TCEP	tris(carboxyethyl) phosphine
TEM	Transmission Electron Microscopy
TGA	Thermogravimetric Analysis

TOC

Total Organic Carbon

XPS

X-Ray Photoelectron Spectroscopy

Abstract of Dissertation Presented to the Graduate School
of the University of Florida in Partial Fulfillment of the
Requirements for the Degree of Doctor of Philosophy

CHEMISTRY AND STABILITY OF THIOL BASED POLYETHYLENE GLYCOL
SURFACE COATINGS ON COLLOIDAL GOLD AND THEIR RELATIONSHIP TO
PROTEIN ADSORPTION AND CLEARANCE IN VIVO

By

Paul Carpinone

December 2012

Chair: Kevin Powers

Major: Materials Science and Engineering

Nanomaterials have presented a wide range of novel biomedical applications, with particular emphasis placed on advances in imaging and treatment delivery. Of the many particulate nanomaterials researched for biomedical applications, gold is one of the most widely used. Colloidal gold has been of great interest due to its chemical inertness and its ability to perform multiple functions, such as drug delivery, localized heating of tissues (hyperthermia), and imaging (as a contrast agent). It is also readily functionalized through the use of thiols, which spontaneously form sulfur to gold bonds with the surface. Polyethylene glycol (PEG) is the most widely used coating material for these particles as it provides both steric stability to the suspension and protein resistance. These properties extend the circulation time of the particles in blood, and consequently the efficacy of the treatment. Despite widespread use of PEG coated gold particles, the coating chemistry and stability of these particles are largely unknown. The goal of this work was to identify the mechanisms leading to degradation and stability of thiol based polyethylene glycol coatings on gold particles and to relate this behavior to protein adsorption and clearance *in vivo*. The results indicate that the protective PEG

coating is susceptible to sources of oxidation (including dissolved oxygen) and competing adsorbates, among other factors. The quality of commercially available thiolated PEG reagents was also found to play a key role in the quality and protein resistance of the final PEG coating. Analysis of the stability of these coatings indicated that they rapidly degrade under physiological conditions, leading to the onset of protein adsorption when exposed to plasma or blood. Paralleling the protein adsorption behavior and onset of coating degradation observed *in vitro*, blood clearance of parenterally administered PEG coated particles in mice began after approximately 2h of circulation time. Taken together, the data presented in this work indicates that the stability of the PEG coating and the many factors affecting it represent a fundamental limitation to the use of these particles.

CHAPTER 1 INTRODUCTION

Nanotechnology

Though definitions and terminology vary¹, one of the earliest and most often used definition of a 'nanomaterial' or 'nanotechnology' is a material with at least one dimension less than 100nm^{2, 3}. Due to the vast number of possible exceptions and special cases, it is difficult to ascribe a concise definition to nanotechnology. As a result, modern definitions have grown to be far more complex and/or broad^{4, 5}. Factors such as porosity, surface roughness, and atomic scale defects challenge the "features under 100nm" definition. Many would not consider a boulder to be a nanomaterial; however if magnified appropriately, the surface would almost certainly contain features less than 100nm. Another example may be a protein such as albumin. Albumin is considered to have a size of 30 x 30 x 80Å in crystalline form⁶ and approximately 14nm^{7, 8} in solution. If albumin was compared to a laboratory synthesized gold particle of a similar (or even smaller) size, many would argue that the protein is not a nanomaterial while the gold particle is. Ultimately, the definition of a nanomaterial is subjective. Perhaps one of the caveats in the definition of 'nanomaterial' proposed by the American Chemical Council in 2007⁴ best illustrates the intent and subjectivity of most definitions:

Exclusions: 1. Materials that do not have properties that are novel/unique/new compared to the non-nanoscale form of a material of the same composition.

Nanomaterials are not a new phenomenon. Smoke, for example, is among the many natural sources of nanoscale particles. In contrast to the modern manufactured/engineered nanomaterials, the physical and chemical properties of most naturally generated nanomaterials are highly heterogeneous. The ability to produce

unique nanoscale structures and particles with a high degree of uniformity has generated revolutionary technology in a vast array of industrial and research applications.

Nanomaterials for Biological Applications

In addition to the various industrial and electronics applications, nanomaterials have presented a wide range of novel biomedical applications, with particular emphasis placed on advances in imaging and treatment delivery.^{9, 10} These emerging technologies unite the burgeoning global market in nanotechnology and the continuous demand for more advanced therapeutic and diagnostic tools. The US market for nanotechnology based medical products is increasing at an annual rate of 17% and is projected to reach \$75.1 billion in 2014, with the majority of the demand directed toward pharmaceutical applications¹¹. This is a small fraction of the total market for nanomaterials, which is estimated to reach the trillion dollar mark by 2015¹².

Much attention has been given to inorganic nanomaterials for biomedical applications. The size dependent ability of nanomaterials to permeate certain compartments of the body combined with unique physical properties and the ability remain in circulation for considerable amounts of time¹³⁻¹⁵ form the basis for most applications. Three of the most widely used and studied inorganic nanomaterials for injectable therapeutic and imaging purposes are gold (imaging, drug delivery, hyperthermia), iron oxide (imaging, drug delivery, hyperthermia), and silica (imaging, drug delivery). Drug conjugated gold particles have already demonstrated their use as an effective delivery method for solid tumors¹⁶ and are currently in Phase II clinical trials¹⁷. Gold particles, such as nanorods and nanoshells, have been found effective for advanced non-invasive imaging¹⁸ and localized heating of tumors upon exposure to

appropriate electromagnetic radiation¹⁸⁻²⁰. Iron Oxide has seen considerable use as an MRI contrast agent²¹ for years, and is studied as an agent for localized heat generation via an alternating magnetic field²². Silica, particularly dye doped silica, has many advantages as a contrast material for bioimaging²³, and like most other nanomaterials, it can be easily functionalized to carry therapeutic or diagnostic payloads. In addition to encapsulation of various materials, silica particles can be synthesized with a regular pore structure which results in extremely high specific surface area (known as mesoporous colloidal silica), greatly increasing its drug payload²⁴⁻²⁶.

Suspensions of these inorganic materials in their native form have one common limitation: they tend to be unstable under physiological conditions. The lack of dispersion stability and rapid recognition by the reticuloendothelial system (RES) can severely decrease efficacy and circulation time. To combat this, the particles are coated with a polymer, most often polyethylene glycol (PEG), which will both stabilize the particles and provide protection from nonspecific protein adsorption. The stability of this coating is critical to the effectiveness of the particle while in circulation; however the coating behavior during exposure is not well known.

Surface Modification for Biological Applications

The majority of particulate nanomaterials are unstable under physiological conditions, necessitating some type of dispersant for use. Hydrophilic polymers are the standard choice for this application due to the steric stability imparted by the grafted polymer chains. Ideally these surface modifications also decrease or eliminate binding of biological molecules which elicit a response from the immune system, allowing the particle to pass throughout the body undetected. Although the exact structural elements

which resist protein binding are poorly understood²⁷, the characteristics desired for such a coating include²⁸:

- Capable of imparting colloidal stability on the nanomaterials; steric stabilization is preferred.
- Resist desorption from the surface; hydrophilic polymers 'grafted' to the surface by one or more reactive functionalities are preferred.
- Prevent or minimize nonspecific binding of proteins and other opsonins.
- Lack charged²⁹ or hydrogen bonding moieties (such as hydroxyls and amines) which can aid in protein adsorption and trigger the complement system³⁰.

Since its first use in 1977 to improve circulation times of proteins³¹, polyethylene glycol (PEG) and PEG derivatives continue to be the most effective and widely used polymer for improving nanomaterial stability in the bloodstream^{32, 33}. Though other materials such as polysaccharides, protein based biopolymers, and other hydrophilic polymers have been investigated and are used, most fail to fulfill one or more of the aforementioned characteristics as effectively as PEG. Some of the coatings used for enhancing particle stability and biocompatibility *in vivo* are outlined in Table 1-1. Like other polymers, PEG can be functionalized for a variety of purposes. This is typically carried out by addition of terminal functionalities to the polymer chain. The simplest case involves one terminal group which is reactive to the particle surface and the other containing a non-reactive group (typically methoxylated). Additional functionality can be imparted to the particle via the use of bi- or multi- functional polymers, which allow one or more functional components to be added to the end of the PEG chain. Some of these schemes are illustrated in Figure 1-1 for gold particles. Many of these schemes would not be possible without the presence of the PEG coating. Addition of antibodies, proteins, or other biologically active molecules to the surface can result in

conformational changes on adsorption^{34, 35}, which may alter their activity. These molecules alone also may not be capable of stabilizing the particle suspension, and can induce aggregation of the suspension. Attachment of molecules to the terminal end of an adsorbed PEG chain eliminates many of these problems, as suspension stability is achieved through the PEG coating alone and restriction of the biomolecule attachment to a single point may decrease the likelihood of conformational changes. Attachment of a fluorophore is another option made possible by bifunctional PEG coatings, as fluorescence quenching will occur in the proximity of the metal surface. PEG chains of sufficient length can provide the distance required to decrease quenching³⁶. Functional PEG compounds are available in a seemingly endless number of possibilities, and provide the researcher with a flexible tool with which to construct customized functional particles and surfaces.

Nanotoxicology

The past several decades have seen a rapid rise in synthesis and utilization of nanomaterials for a vast array of applications. Though nanomaterials were not new at the time³⁸, initial reports from the 1990s showed greater than expected toxic responses to nanomaterials as compared to larger particles of the same composition in inhalational studies^{39, 40}. Subsequent reports in 2003 showed additional cases where the size of nanomaterials influenced their *in vivo* behavior⁴¹. In 2004, the Royal Society and Royal Academy of Engineering published a seminal report on nanomaterials and their potential health risks⁴². In the years that followed, increasing attention has been placed on studying the unique effects and potential toxicity of nanomaterials on biological systems.

The continued rapid proliferation of nanomaterials in medicine and other fields has left many questioning whether the technology is moving too far ahead of the toxicological risk assessments⁴³. The long term impacts of these materials in the body are not well known, and conflicting literature reports on the toxicity of many popular nanomaterials add to the uncertainty⁴⁴. Major differences between formulations based on the same material and even batch to batch variations^{45, 46} have demonstrated the need for effective characterization to better understand the biological interactions of nanomaterials⁴⁷. Characterization of these materials, though, can be complex and difficult to perform⁴⁷. This gap in the current understanding of nanomaterial biological interactions has led to increasing interest from both the scientific and regulatory communities^{12, 42, 48-51}. Concerns about potential dangers of manufactured nanotechnology led the city of Berkeley, California to become the first municipality in the US to formally regulate nanomaterials⁴⁹, though these regulations only include a requirement to report activity involving nanomaterials and associated safety information. Recent reports from the Organisation for Economic Co-operation and Development (OECD) highlight the regulatory interests and activities in a number of member countries⁵⁰.

Concerns about the toxicity of nanomaterials are largely centered on one particular class of nanomaterial: nanoscale particulates. Particulate nanomaterials have the highest risk of release/exposure and are potentially more mobile than their larger counterparts. These particles are used in countless consumer products, such as sunscreen, cosmetics, antimicrobial silver preparations, and many others. Inhalation, ingestion, and dermal contact with these materials are the most likely routes of

incidental exposure. Medicinal nanomaterials which may also be injected are emerging, and several are already in widespread use^{52, 53}. Certain nanomaterial compositions are of particular concern to scientists and regulators due to their current or potential widespread use, and many agencies have compiled lists of nanomaterials of concern^{48, 54}. Most of these lists encompass the materials listed in Table 1-2. Some materials of particular concern include carbon nanotubes due to their asbestos-like fiber morphology, zinc and titanium oxides due to their widespread use in sunscreen, quantum dots due to their heavy metal content, and silver due to its antimicrobial behavior.

Research Goals

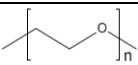
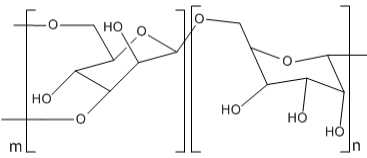
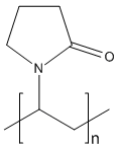
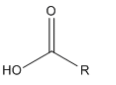
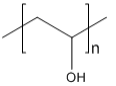
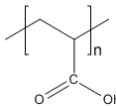
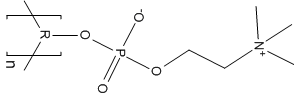
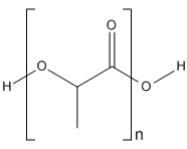
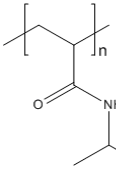
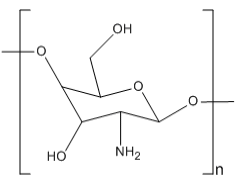
The previous introductory sections highlighted the important role played by the coatings applied to therapeutic nanomaterials. The stability and efficacy of the particles *in vivo* are ultimately controlled by the properties of the applied coating. Toxicological concerns about the unique activity and biodistribution of nanomaterials present an additional driving force to understand the behavior of therapeutic particles *in vivo*. Since gold particles are among the most widely used vehicles for the plethora of new therapeutic and diagnostic biomedical applications, are considered by some to be a 'standard' nanomaterial for toxicological testing⁵⁵⁻⁵⁹, and are poorly characterized in many aspects, additional information about the properties and behavior of these particles is important. Uncertainty exists regarding several important facets of gold based nanotechnology, including accurate particle characterization, properties and stability of thiol based PEG coatings, and time dependent *in vivo* behavior. To address some of these issues, the following main research objectives were formulated:

- Development of characterization methods to facilitate efficient analysis of the dispersion stability *in vivo* and coating properties *in vitro* of PEG coated gold particles.
- Identify mechanisms of degradation and stability in thiol based polyethylene glycol coatings on gold particles under various *in vitro* conditions.
- Identify, if possible, relationships between the coating stability, protein adsorption behavior, colloidal stability, and clearance *in vivo*.

This work was divided into chapters representing increasing system complexity.

Chapter 2 will cover the development of characterization methods for analyzing various physicochemical properties of the selected nanomaterials. Chapter 3 will discuss the formation and stability of the chemisorbed PEG coatings on gold particles. Chapter 4 will introduce protein interactions with the coated and uncoated particles. Finally, chapter 5 will examine the *in vivo* behavior of various coated and uncoated particles.

Table 1-1. List of coatings used to improve biocompatibility, particle stability, and circulation time *in vivo*. Adapted from Gupta and Gupta³⁷.

Coating	Structure	Advantages*
Polyethylene Glycol (PEG/PEO)		Immobilization of PEG on the surface improves the biocompatibility, blood circulation time and internalization efficiency of the nanoparticles
Dextran		Enhances the blood circulation time, stabilizes the colloidal solution
Polyvinylpyrrolidone (PVP)		Enhances the blood circulation time and stabilizes the colloidal solution
Fatty Acids		Colloidal stability, terminal functional carboxyl groups
Polyvinyl Alcohol (PVA)		Prevents coagulation of particles, giving rise to monodisperse particles
Polyacrylic Acid (PAA)		Increase the stability and biocompatibility of the particles and also helps in bioadhesion
Polypeptides	Variable; Amino acids	Good for cell biology, e.g. targeting to cell
Phosphorylcholine (PC)		Poorly complement and coagulation activating, colloidal solution stabilizer
Poly (d, l lactide)		Biocompatible, low cytotoxicity
Poly(N-isopropylacrylamide) (Poly NIPAAM)		Thermosensitive drug delivery and cell separation
Chitosan		Widely used as non-viral gene delivery system, biocompatible, hydrophilic, used in agriculture, food, medicine, biotechnology, textiles, polymers, and water treatment
Gelatin	Variable; Amino acids	Used as a gelling agent, emulsifier hydrophilic, biocompatible, natural polymer

*Advantages listed are the comments of the authors Gupta and Gupta³⁷ and are specifically related to the behavior of coated iron oxide particles.

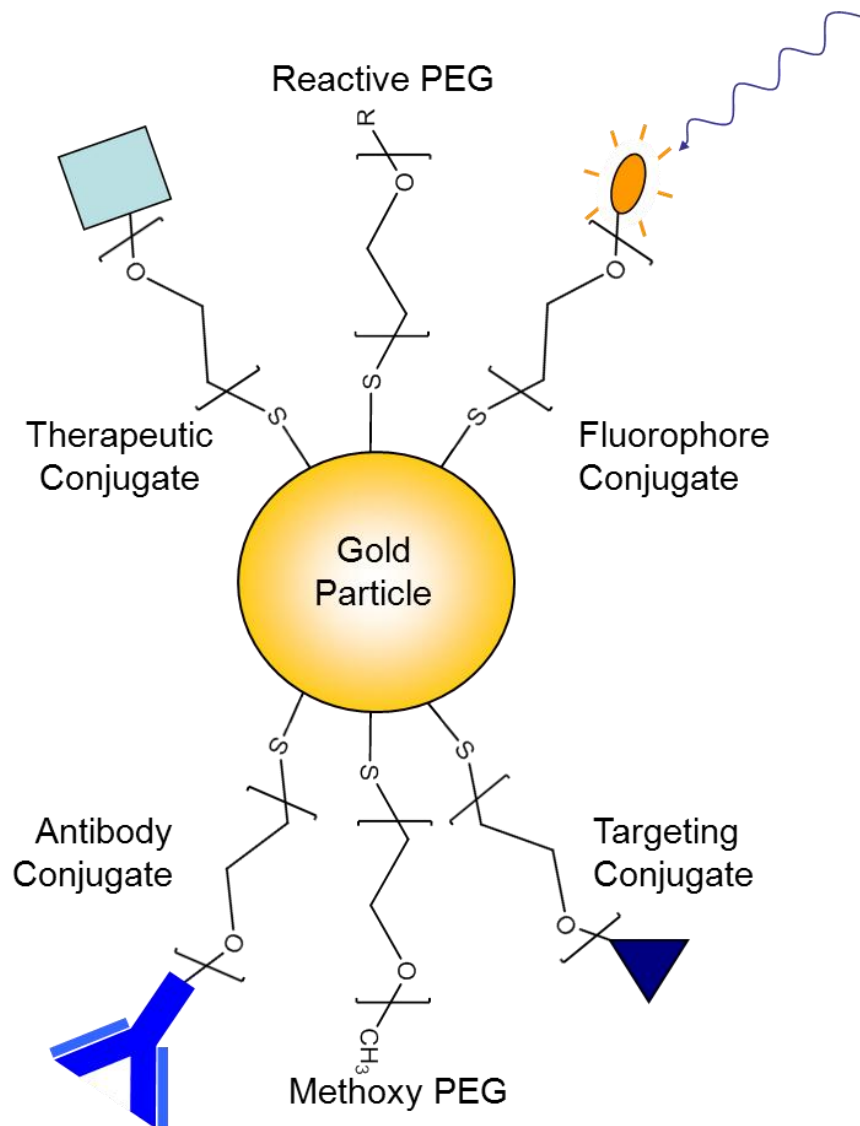


Figure 1-1. Illustration of several coating possibilities utilizing functional polyethylene glycol coatings on gold particles.

Table 1-2. List of nanomaterials typically cited for current or projected widespread use.

Material	Uses
Aluminum Oxide	Abrasives/polishing, coatings, catalysts
Cerium Oxide	Diesel additive, polishing, coatings
Carbon Nanotubes	Structural materials (composites), conductive films and coatings, brushes in electric motors, electronics
Carbon Black	Rubber products, coatings, pigments
Clays	Structural materials (composites), packaging, fire retardants
Dendrimers	Therapeutic and diagnostics agents, sensors
Fullerenes	Coatings, cosmetics. Many emerging uses in electronics and optics, industrial and pharmaceutical chemistry, and advanced materials.
Iron	Catalysts, magnetic materials (ferrofluids, magnetic storage media, etc.), batteries and electrodes
Polystyrene	Coatings, inks
Quantum dots (multiple materials)	Lighting, displays, electronics/computing/semiconductors, sensors, imaging, photovoltaics
Silica	Composites, coatings, abrasives/polishing, food, fillers, catalysts, paper, absorbent materials
Silver	Antimicrobial preparations of various types, coatings, catalysts
Titania	Sunscreen, paints and coatings, photocatalytic agent (for cleaning, purification, environmental remediation, etc.), batteries and solar cells, cosmetics
Zinc Oxide	Sunscreen, coatings, semiconductors, antimicrobial coatings

CHAPTER 2 SYNTHESIS AND CHARACTERIZATION OF GOLD NANOMATERIALS

Chapter Introduction

Colloidal gold is the most researched nanomaterial for intravenously administered therapeutic applications, and one of the most studied colloidal systems of all time⁶⁰. Colloidal gold has been used since ancient times for imparting a red or purple color to glass and ceramic materials, although the reason for this color was not initially known. It was not until the mid 1800s that Michael Faraday correctly identified colloidal gold as being composed of “diffused” and “exceedingly fine” gold particles, which were the cause of suspension’s red color³⁸. Some of his gold suspensions remain stable to this day at the Royal Institution of Great Britain Museum. Colloidal gold has been of great interest due to its chemical inertness and its ability to perform multiple functions such as drug delivery, localized heating of tissues (hyperthermia), and imaging (as a contrast medium). A colloidal gold based series of chemotherapy drugs has already been established with at least six products in stages varying from development to phase II clinical trials as of October 2012.¹⁷ In one of these applications, functionalization of gold particles with PEG and tumor necrosis factor alpha (TNF- α) allowed targeted parenteral administration far in excess of its LC50 as a free molecule⁶¹. Gold particles of various shapes, sizes, and compositions have been used for optical heating applications to exploit the vulnerability of tumor cells to heat^{19, 62}. Gold particles have demonstrated their effectiveness as contrast agents for PAT⁶³, CT⁶⁴, and NIR imaging²¹. Coupled with their ease of functionalization through a sulfur-metal bond, gold particles are a leading vehicle for nanomaterial based therapeutics.

Overview of Gold Chemistry

Gold exists primarily in two valences, +1 and +3. Gold (III) salts are the most common, and form planar tetracoordinate complexes with suitable ligands. Some ligands which form complexes with gold in aqueous solutions include halogens, cyanide, various organic and inorganic sulfur compounds, phosphines, amines, etc. Gold (III) halides are most often used in the laboratory as a source of soluble gold. In its pure form, the chloride exists as the dimer Au_2Cl_6 , which hydrolyses when dissolved in water. In the presence of acid and chloride, the chloroaurate ion is formed ($[\text{AuCl}_4]^-$). This compound can be dried to yield tetrachloroauric acid (HAuCl_4), one of the most common sources of soluble gold. The stability of the tetracoordinate halides increases down the group with iodide complexes yielding the highest stability. For this reason, the halide complexes will undergo ligand exchange reactions when in the presence of a higher halogen. These exchanges can be observed optically as a color change in the complex (Figure 2-1) as well as by the decreasing strength of the reduction potential. Halide ligands can be displaced by hydroxyls dependent on the pH of the solution, ultimately yielding the colorless $[\text{AuOH}_4]^-$ complex. The speciation diagram for the substitution of chloride by hydroxyls is shown in Figure 2-2 and Figure 2-3, and the Pourbaix diagram of gold chloride is shown in Figure 2-4. Many of these gold complexes are soluble in a variety of polar solvents such as alcohols, ketones, esters, and ethers. Solubilization of gold in certain nonpolar solvents such as aliphatic and aromatic hydrocarbons requires the use of a phase transfer catalyst (typically an oil soluble quaternary ammonium compound).

Dissolution of metallic gold can be achieved by a variety of methods, but typically involves the presence of an oxidizer and suitable ligand, which may be the same.

Depending on the stability of the complex formed and solution chemistry, the oxidizer may even include dissolved oxygen, as is the case with cyanide. Other ligands capable of forming particularly stable complexes with gold can utilize dissolved oxygen, but often at a slower rate. External oxidizers are used in this process to increase the rate of dissolution. Aqua regia is traditionally used for dissolution of gold, where the chloride ions provide the ligand and the nitrate ions provide the oxidizer.

Particle Synthesis

One of the major advantages of colloidal gold is its relative ease of synthesis. Colloidal gold is typically prepared via reduction of a gold salt with a suitable reducing agent. The most popular technique involves reduction of gold (III) chloride with sodium citrate, which was first described in 1951 by Turkevich⁶⁶ and subsequently expanded by Frens in 1973⁶⁷. This method results in a stable suspension of gold particles with a negative surface charge. Synthesis is performed under boiling conditions, and particle size is controlled by the concentration of sodium citrate (increasing citrate concentration causes an exponential decrease in the particle size). Particles between approximately 8nm and 80nm can be produced using this method. The syntheses of these particles proceeds by the formation of large network or aggregate like particles which subsequently break up to form the final suspension. This is the cause of the blue-black color initially observed during synthesis.

Due to ease of reduction, gold particles can and have been synthesized using a plethora of different methods, resulting in varying particle sizes, shapes, and qualities. Smaller particles can be produced using stronger reducing agents such as hydrides or via the incorporation of a surface active compound to moderate growth. The smallest particles (including sub-nm particles) typically require a compound which binds strongly

to the particle surface in order to achieve such a particle size. The presence of compounds used during synthesis that interact strongly with the surface are a major consideration when the particles are to be surface modified post-synthesis, as many of these compounds can not be easily desorbed. These adsorbates can alter the particle surface properties and interfere with or decrease the efficiency of other coatings, as well as unfavorably interact with biological systems (if the desired purpose involves biological testing).

Characterization Methods

Although nanomaterials are frequently characterized as received and prior to exposure, the behavior of nanomaterials during the course of an *in vivo* exposure has traditionally been difficult to analyze⁶⁸. The ability to track particle behavior during the course of an exposure can greatly enhance the understanding of the interactions between surface chemistry, colloidal stability, and clearance. These relationships can be employed to understand or engineer particles with controlled biodistribution and/or clearance rates. Several methods were employed in this work to characterize particle size, charge (zeta potential), and sedimentation properties. Careful attention to method selection is important, as certain particle size analyzers are capable of producing significant errors which may not always be obvious to the operator.

Sedimentation

Sedimentation is one of the earliest known particle sizing techniques. Originally, gravitational sedimentation of suspended particles was the primary method of analysis. Quantification of the sedimentation velocity was performed gravimetrically using apparatus such as the Andreasen Pipette^{69, 70} to sample the suspension at various time intervals. Although useful for larger particles, the sedimentation velocity of small and

light particles is exceedingly long, decreasing the utility of the technique. Modern instruments based on this technique (which are still available) utilize gravitational sedimentation with more efficient detection methods. These methods include visible light obscuration detectors, and more frequently, x-ray obscuration detectors⁷¹. Use of these non-intrusive detection techniques eliminates error due to mechanical sampling; however these instruments still rely on gravitational acceleration to induce sedimentation. Addition of a scanning detector can decrease analysis time, but use of a centrifuge to accelerate sedimentation is necessary for timely analysis of slowly sedimenting particles. Instruments specifically designed for particle sizing based on centrifugal sedimentation are now widely available in many different formats and are capable of analyzing nanoscale particles⁷²⁻⁷⁵.

There are two major methods of particle analysis by sedimentation: integral and differential. The methods differ in their initial conditions, and are illustrated in Figure 2-5. In integral sedimentation, particles are initially dispersed homogeneously throughout a medium and sediment out of the suspension. Differential sedimentation differs in that the particles are initially present in a thin layer over a fluid and sediment through the clean fluid in a band (or bands). Although integral sedimentation analysis has been described for over 100 years, differential sedimentation was not described for particle size analysis until the early 1930s⁷⁶ and not fully utilized until decades later^{77,78}. Since particles begin sedimentation at essentially the same position and separate based on velocity differences, velocity analysis is direct. As a result, differential sedimentation techniques typically have a higher resolution compared to integral sedimentation due to minimization of overlap. Data from differential sedimentation is also intuitively

interpretable, whereas data from integral sedimentation often requires software for data interpretation and deconvolution. Modern centrifuge based differential sedimentation particle sizing instruments include a light obscuration detector which analyzes band intensity as shown in Figure 2-6. More sophisticated analytical ultracentrifuges include full UV/Vis optics and Rayleigh interference optics⁷⁹. These detectors can be used for quantitative analysis of materials passing through the disc or rotor as demonstrated in Figure 2-7 with nominally 40nm gold particles.

All sedimentation analysis in this work was performed by differential sedimentation with a disc centrifuge (CPS Instruments model DC24000). This instrument uses a transparent vertical disc loaded with a sucrose based density gradient and a 405nm light source and detector to track the passage of particles. Particles are introduced into the center of the disc and sediment to the edge while the detector measures light obscuration as a function of time. This curve is then mathematically transformed into a particle size distribution.

Equations governing sedimentation

Sedimentation based techniques are all governed by the Stokes equation⁸⁰:

$$D^2 = \frac{18\nu\mu}{(\rho - \rho_f)a} \quad (2.1)$$

Where D is the particle diameter, ν is the sedimentation velocity of the particle, μ is the dynamic viscosity of the fluid through which the particles are sedimenting, ρ is the particle density, ρ_f is the fluid density through which the particles are sedimenting, and a is the applied acceleration. The Stokes equation is a simple solution to the terminal velocity of a particle moving through a fluid under ideal flow conditions. During sedimentation, three major forces act on the particle in balance: applied or gravitational

forces, drag, and buoyancy (typically combined with the gravitational/applied force). The Stokes equation is valid under laminar flow conditions with smooth, spherical, homogeneous particles which do not interact with other suspended particles. The influence of some of these factors on sedimentation analysis will be addressed later. The Stokes equation can be modified to include the operating parameters and geometry of a disc centrifuge using differential sedimentation as shown in equation 2.2.

$$t = \frac{18\mu \ln\left(\frac{r_d}{r_f}\right)}{D^2(\rho - \rho_f)\omega^2} \quad (2.2)$$

Where t is the sedimentation time (time to the detector), μ is the dynamic viscosity of the fluid through which the particles are sedimenting, r_d is the distance from the center of the disc to the detector, r_f is the distance from the center of the disc to the fluid surface, D is the particle diameter, ρ is the particle density, ρ_f is the fluid density through which the particles are sedimenting, and ω is the angular velocity of the centrifuge. Disc centrifuge instruments time the passage of particles through the gradient, and using Equation 2.2, can convert the time to apparent particle size. In addition, light scattering models (not shown) are employed to convert the obscuration of the light source to particle number and mass, as particles differentially scatter light based on size (Figure 2-8). These sedimentation and light scattering models are combined to generate particle size distributions, such as those shown in Figure 2-9.

One of the principal advantages of sedimentation based techniques is the relatively high resolution that can be achieved. Manufacturers of modern sedimentation instruments claim to be capable of resolving particle populations that differ by as little as 2% in size⁷⁴. Although the technique has many advantages, it also has several

important limitations. The first and possibly most important is that sedimenting particles are assumed to be smooth and spherical. Although this is also the case for most other particle size analyzers, sedimentation can be particularly sensitive to deviations in particle shape. Stokes sedimentation assumes that the fluid flow relative to the spherical particle is completely within the laminar flow regime. The presence of surface roughness or particle anisotropy can induce turbulent flow around the particle and/or cause non-uniform sedimentation (much like a leaf falling through the air) respectively. These factors will affect the sedimentation properties of the particles and therefore the computed particle size. Another issue which is particularly important in the analysis of smaller particles is diffusion during analysis. Particle diffusion due to Brownian motion (thermal drift) can cause the distribution of particles to broaden during analysis and resolution to decrease. Analysis of aggregate particles by sedimentation is also problematic. Aggregation of particles generates or exacerbates many of the aforementioned limitations of sedimentation analysis. An aggregate particle is composed of smaller particles, which may (but almost certainly will not) exist as a uniform superlattice. The typical random packing of primary particles in aggregates results in particles with variable density, which can confound sedimentation analysis. Additionally, these aggregates have rough surfaces and are typically polydisperse in both shape and size, each of which are confounding variables in sedimentation analysis. An example of this complexity is illustrated later in Figure 2-22. The strength of the aggregates may also play a role, as breakup of aggregates upon sample introduction or due to shear during analysis can result in an altered size distribution.

These factors must be considered when planning a study based on sedimentation as they can provide misleading information.

Sedimentation for characterizing adsorbed species

In addition to particle sizing, sedimentation can be utilized for analysis of certain surface coatings. Addition of a surface coating to a particle causes a change in size and/or density, which in turn will alter the sedimentation velocity of the particle under many circumstances. Comparison of the sedimentation velocity of a coated particle to the sedimentation velocity of the core particle can allow for (at a minimum) a qualitative comparison of coating thickness among samples. If the density of the coating is known, these sedimentation velocities can be used to calculate the shell thickness of the coating. A separate equation (2.3) was derived from the Stokes Equation to allow for this calculation:

$$\frac{v_s}{v_c} = \frac{D_m^2}{D_c^2} = \frac{D_c(\rho_c - \rho_s)}{(D_c + 2t)(\rho_c - \rho_f)} + \frac{(\rho_s - \rho_f)(D_c + 2t)^2}{D_c^2(\rho_c - \rho_f)} \quad (2.3)$$

Where v_s is the sedimentation velocity of the coated particle, v_c is the sedimentation velocity of the core particle, D_c is the core particle diameter, D_m is the coated particle equivalent diameter (density assumed to be equivalent to core particle density), t is the coating thickness, ρ_c is the core particle density, ρ_s is the coating density, and ρ_f is the fluid density through which the particles are sedimenting.

Adsorption of large organic species such as PEG or protein to the surface of a gold particle causes a marked decrease in density due to the low density of the coating relative to the core particle density (19.3g/cc for gold). The computed net density of particles with PEG and serum proteins is included in Figure 2-11. A density of 1.1g/cc was selected for the coating density of adsorbed PEG and protein. This number is

consistent with the densities of adsorbed protein layers on various surfaces as measured by quartz microbalance⁸¹, the densities of protein solutions in water⁸²⁻⁸⁴, and the density of PEG solutions in water⁸⁵⁻⁸⁷. The selected density is somewhat lower than the density of solid PEG at 1.14g/cc^{85, 88, 89} and the density of 1.33g/cc^{81, 90} generally used for hydrated protein. The region of highest slope largely occurs in the nanoscale range (<100nm), indicating that the largest differences in sedimentation velocities between coated and uncoated particles should be observed in this region. Given that the coating influences two factors which have opposite effects on the sedimentation velocity of a coated particle (particle size – velocity increases with increased size, and density – velocity decreases with decrease in density), there exists the possibility that at a certain core particle size, sedimentation velocity does not change with the application of a coating. This point would occur when the effects of the decrease in density and increase in particle size balance. It is important that this balance point does not occur within the range of sizes of interest and that the change in sedimentation velocity relative to size is monotonic over the core size range of interest. The relationship between apparent size and core particle size for gold particles is shown in Figure 2-12. For gold particles where the thickness of the organic coating is smaller than the particle size, the balance of these factors causes a decrease in the sedimentation velocity under almost all conditions. The point at which the coated and uncoated particle sedimentation velocities are equivalent occurs at a size less than 1nm, placing it well below the smallest particle used in this study as well as the minimum size limit of the disc centrifuge.

Knowledge or estimation of the shell density is a critical parameter in the computation of the shell thickness by sedimentation as demonstrated in Figure 2-13. The solution to equation 2.3 using data collected from nom. 40nm gold particles is shown in Figure 2-13A. The curve has a vertical asymptote at the point where the fluid density (ρ_f) and coating density (ρ_c) equal. It can be seen from the shape of this curve that for coating densities higher than the asymptotic value, two possible coating thicknesses can satisfy the measured sedimentation conditions while only one solution is possible below the asymptote. These two solutions again arise from the balance between the increase in size on coating and the decrease in density. The higher of the two solutions occurs where the coating is sufficiently large that the increased sedimentation velocity due to the increase in particle size equals the decrease in sedimentation velocity due to decreased density. These higher thicknesses are typically much larger than what would be feasible for the self assembled monolayer systems of interest. The smaller solutions that are feasible for the monolayer systems of interest are detailed in Figure 2-13B. Below the asymptotic value, only one possible solution exists, as the balance of factors will never favor a higher particle size over the decrease in density. Application of such a coating in a large enough size would eventually result in the particles becoming buoyant, preventing the particles from being analyzed in the first place. For core particles with an extremely high density (such as gold) coated with a low density material (such as PEG), the variance in computed thickness with small changes in coating density is relatively small. Over the density range of 1g/cc (de-ionized water) to 1.14g/cm³ (solid PEG)^{85, 88, 89}, the computed coating thickness varies less than 4% from the selected density of 1.1g/mL (Figure 2-13).

To summarize, the following characteristics are required for analysis of coating thickness by differential sedimentation:

- The coating must be significant in size relative to the particle in order to generate a measurable change in sedimentation velocity.
- The combination of coating thickness and density must be capable of generating a measurable change in the sedimentation velocity of the particles.
- Particles should be spherical and monodisperse.
- The coating must be adhered to the core particle such that changes to the coating will not occur during analysis. Care must be taken if the coating is disturbed by changes in the solution environment (ex. when the particles enter the gradient).

***In vivo* particle size analysis by sedimentation**

The complexity of the mixture present in whole blood represents a unique challenge for *in vivo* particle characterization. Most ensemble particle characterization techniques are confounded by samples which contain non-isotropic particles, complex mixtures, particles with varying optical properties, etc{{76 Powers, KW 2012; }}. Techniques such as image analysis require either extensive sample manipulation and/or are time consuming, making time dependent measurements difficult or impossible. As discussed previously, understanding the behavior of particles *in vivo* is critical to elucidating potential mechanisms of clearance but is largely not performed. To address some of these issues, differential sedimentation was investigated as a method for *in vivo* particle characterization.

Whole blood consists primarily of three cell types: erythrocytes, leukocytes, and platelets. Human erythrocytes are in the vicinity of $6-8\mu\text{m}^{91, 92}$, leukocytes are typically in the range of $10-20\mu\text{m}^{93}$, and platelets are $1.5-3.5\mu\text{m}$ in size⁹³. These cells possess many of the properties which complicate size measurement by sedimentation: non-

uniform densities, a widely varying and complex non-spherical shape, and/or a rough or textured surface as shown in Figure 2-14. In order to characterize suspended fine particles in whole blood by sedimentation, the sedimentation velocity of blood cells must significantly differ from those of the particles of interest. To assess the sedimentation velocity of blood cells, heparinized whole mouse blood was diluted 1:20 in 1x PBS for analysis. Buffered isotonic density gradients were used for analysis in the centrifuge rather than the typical de-ionized water based gradients to prevent lysing of blood cells during analysis. The sedimentation velocity distribution of whole mouse blood is shown in Figure 2-15, and the equivalent size as a spherical gold particle is shown in Figure 2-16. Large peaks corresponding with erythrocytes were observed as well as peaks for other blood components. These peaks generate significant background which can obscure wide regions of the analysis range (Figure 2-16). In an attempt to minimize this interference, the analysis was repeated using lysed blood to remove or reduce the concentration of blood cells. In this case, whole blood was diluted 1:20 in deionized water, and the gradient utilized in the centrifuge contained no salts and was not pH adjusted or buffered. Upon addition of blood to deionized water, the normally opaque blood became transparent, indicating that the cells were lysed. Sedimentation analysis of these samples showed that the large peaks observed in whole blood were largely removed. Only a single relatively low intensity peak was observed across the analysis range used. This peak likely corresponded to either cell fragments or platelet residues generated during lysis. Replication of these measurements with blood samples from a larger number of individuals provided sufficient data to outline the practical range of particle sizes not obstructed by blood components (Figure 2-19). Due to variations

between individuals, the actual amount of interference may differ within the indicated ranges and yield a wider (but unpredictable) analysis range. This can be illustrated by comparing the size range obstructed by residues in Figure 2-18 and the obstructed region highlighted in Figure 2-19B. PEG coated particles were then introduced into whole mouse blood and analyzed using both the isotonic and lysed methods described previously. The resulting sedimentation velocity distributions using the isotonic and lysed preparation methods compared to the same blood without particles are shown in Figure 2-20. In both cases, the PEG coated particles were clearly separated from the blood. No interferences were observed due to the preparation methods used, and the peak corresponding to the gold particles was in the same location both before and after analysis.

One of the primary purposes for *in vivo* particle size analysis is the determination of the state of agglomeration. To achieve this, both the primary particle size analysis range and the size where agglomerates occur must be clear from background. Selection of the preparation technique is dependent on the type of data desired as outlined in Table 2-1. For example: if characterization of the primary particle concentration, distribution shape, and intensity are desired, the isotonic preparation method would be most suitable. For characterization of aggregates, the lysed method is most applicable as it has the widest unobstructed range at higher particle sizes.

Dynamic Light Scattering

Dynamic light scattering is one of the most widely used sizing and zeta potential measurement techniques for fine particles. Dynamic light scattering relies on relating the diffusivity (Brownian motion) of suspended particles to particle size via measurement of fluctuations in light scattered by suspended particles. Particles in

suspension move in a stochastic fashion due to thermal (Brownian) motion, which is related to the size of the particle and physical properties of the fluid (ex. density, temperature, and viscosity) by the Stokes-Einstein equation:

$$D_h = \frac{k_B T}{3\pi\eta D} \quad (2.4)$$

Where D_h is the hydrodynamic radius, k_B is Boltzmann's constant, T is the temperature, η is the dynamic viscosity, and D is the diffusion coefficient. If the physical properties of the fluid are well known and the diffusivity measured, this leaves only one principal unknown – the particle size. In order to measure the particle size, the mean drift velocity of the particles in suspension must be measured. This measurement is accomplished by analyzing the intensity fluctuations of laser light scattered from the particles. Using the optical properties of the fluid and particle, a correlation algorithm is employed to compute the particle size distribution from the light scattering data. The particle size measured by this technique is not the 'hard sphere' measurement one would see via microscopy. The size reported by dynamic light scattering instruments is the hydrodynamic size of the particles, which is the calculated sphere of equivalent diffusivity to the particles being analyzed. This typically includes any adsorbed species, such as surfactants, around the particles⁹⁵. Commercial instruments are capable of measuring particle and molecule sizes from angstroms up to several microns⁹⁶. Analysis can be performed on small sample volumes in various fluids and is non-invasive. It is, however, not particularly well suited for broad or polydisperse particle size distributions. Like most other ensemble particle sizing techniques, the shape of the particle is assumed to be spherical. These factors can present a significant problem if the desired

application involves characterization of aggregation, where particles are rarely spherical, homogeneous, and uniform in size.

Dynamic light scattering is one of the few ensemble techniques capable of zeta potential measurements, and instruments are frequently equipped for such measurements in addition to sizing. Zeta potential analysis by dynamic light scattering involves analysis of light scattering while the particles are under the influence of an applied electric field rather than thermal (Brownian) motion alone. One of the most common methods of relating the measured particle mobility to zeta potential is by phase analysis (also known as laser Doppler electrophoresis). In this scheme, a laser beam is split into reference and sample beams with the sample beam passing through the suspension. The sample beam is scattered by the suspended particles, which, if charged, are in motion due to the applied electric field. Some of this scattered light is collected and recombined with the reference beam, and the Doppler shift in the sample beam is measured relative to the reference beam. This data is used to calculate the velocity of the particles, which is then related to the apparent charge using the known fluid properties and applied electric field strength.

Dynamic light scattering was used to measure the particle size and zeta potential of many particles used in this study. A representative size distribution is shown in Figure 2-31. Like sedimentation, dynamic light scattering is sensitive to the adsorption of molecules to the particle surface. Adsorption of PEG increases the particle size considerably and can easily be measured (Figure 2-32).

Microscopy

All of the previously described ensemble particle characterization techniques provide a variety of useful physical information but lack detailed information such as

particle composition and shape. Factors such as shape irregularity can confound or interfere with particle sizing measurements based on ensemble techniques such as light scattering or sedimentation. Microscopy (particularly electron microscopy) provides a clearer picture of the particle system and aides in identifying interferences in ensemble measurements (Figure 2-21). In addition to imaging, electron microscopy can yield structural and chemical information about the particles of interest via electron diffraction, energy dispersive spectroscopy (EDS), and electron energy loss spectroscopy (EELS). Analysis and conclusive identification of particles by these means is important to determining biodistribution and pathways of clearance *in vivo*. An example of this can be seen in Figure 2-22 and Figure 2-23, where aggregates of nom. 40nm gold particles were identified in gastric fluid after an initially well dispersed suspension was administered orally. The smaller particles composing the aggregates can clearly be seen, and were identified compositionally by EDS (Figure 2-24). Although electron microscopy provides many benefits for particle characterization, its use for analyzing the distribution of particles in suspension is considerably more limited. Most electron microscopy techniques require a dry sample under vacuum for analysis, though techniques exist for imaging of wet samples under certain circumstances⁹⁷. Drying processes for sample preparation can easily introduce artifacts, restricting the utility of the technique when the state of dispersion is a factor of interest.

Though the resolution of optical microscopy is not sufficient to directly image nanoscale materials, it is useful in identifying collections or aggregates of particles (Figure 2-23). Gold particles, for example, are optically dense and can easily be distinguished from most other biological materials, as will be shown later (Figure 4-29,

Figure 5-7). Optical microscopy has the added benefit of analyzing samples without drying or preparation, eliminating those sources of interference.

Raw Particle Properties

Production of gold particles via the sodium citrate reduction method is the most widely used synthesis technique for nanoscale gold particles. Although other methods may produce particles of higher monodispersity in size and shape, particles produced by citrate reduction were used throughout this study due to their widespread (nearly exclusive) use. The particles produced by this method are typically spherical or nearly spherical at smaller sizes and less spherical at larger sizes as shown in Figure 2-25B/C and Figure 2-21. As the particle size increases beyond 20-30nm, the particles show a certain level of anisotropy with average aspect ratios of approximately 1.3 at a nominal particle size of 40nm (measured by image analysis). Beyond this point, the polydispersity in shape and size continues to increase rapidly.

The particles generated by this method have a negative surface charge which remains negative over the range of pH values (approximately pH 2 - 12) where the particles are stable (Figure 2-26). Though immediate aggregation was not observed over this range, it is likely that aggregation will occur slowly at the highest and lowest pH samples. The concentration of salts in the suspension plays a key role in the particle zeta potential and stability. As shown in Figure 2-27, salts can cause the zeta potential to decrease exponentially due to charge screening until the suspension is destabilized. The precise origin of the charge on the particles is not well known, though it is either attributed to the presence of citrate ions or ionized gold groups on the surface.

Well dispersed suspensions of these particles exhibit an intense red to pink color when the particle size is in the 10s of nanometers due to a strong optical absorption in

the green region. This optical absorption spectrum varies based on particle size, with small particles (<2-3nm) appearing as a tan colored suspension with no single strong optical absorbance and large particles exhibiting a broader apparent absorption due to higher light scattering (Figure 2-28, Figure 2-29). The visible absorbance maximum is dependent on particle size and ranges from 500-570nm for nanoscale particles. These unique optical properties are perhaps one of the most valuable features of gold particles, as it allows for immediate qualitative assessment of the suspension size and stability. Aggregation of these particles leads to a color change from red to purple to blue/black as absorption shifts to higher wavelengths and polydispersity increases. This behavior can be easily identified both visually and by UV/Visible spectroscopy (Figure 2-30).

Chapter Summary

Synthesis of gold particles by reduction of gold chloride with sodium citrate produces particles of varying sphericity and monodispersity based on size (Figure 2-25B/C, Figure 2-21). At lower sizes, the particles are roughly spherical, while larger particles tend to be increasingly anisotropic (mean aspect ratio of 1.3 measured at approximately 40nm). Methods and theory for particle sizing and characterization of adsorbed species on gold particles by differential sedimentation were presented. Chemisorption of species (such as the thiolated PEG used to coat gold surfaces) alters both the particle size and net density, which in turn affect the sedimentation velocity. The adsorption of low density coatings such as PEG typically results in a marked decrease in the measured sedimentation velocity compared to the core particle (Figure 2-12). Calculations indicate that for the coatings (PEG and serum protein) and core particles (nanoscale gold) of interest, this decrease occurs at almost all sizes (with the

exception of exceedingly small particles). Two possible coating thickness solutions can satisfy the measured sedimentation data when the coating density is greater than the fluid density, the smaller of which is relevant to the particles of interest (Figure 2-13). Use of sedimentation for analysis of particles in biological fluids (such as blood) was investigated. Gold particles in blood could be separated from other constituents by sedimentation velocity (Figure 2-20); however interferences from various components in blood obscured certain particle size ranges (Figure 2-19). Certain interferences from blood components can be removed by lysing the blood sample prior to analysis. Selection of the method used for sample preparation is dependent somewhat on the range of analysis desired (Figure 2-19, Table 2-1). Particle size characterization was performed by several techniques, including sedimentation, dynamic light scattering, and microscopy (Figure 2-9, Figure 2-31, Figure 2-21). As-prepared gold particles exhibited a negative charge which varied in magnitude across the pH range of 2-12 where the particles were stable (Figure 2-26).

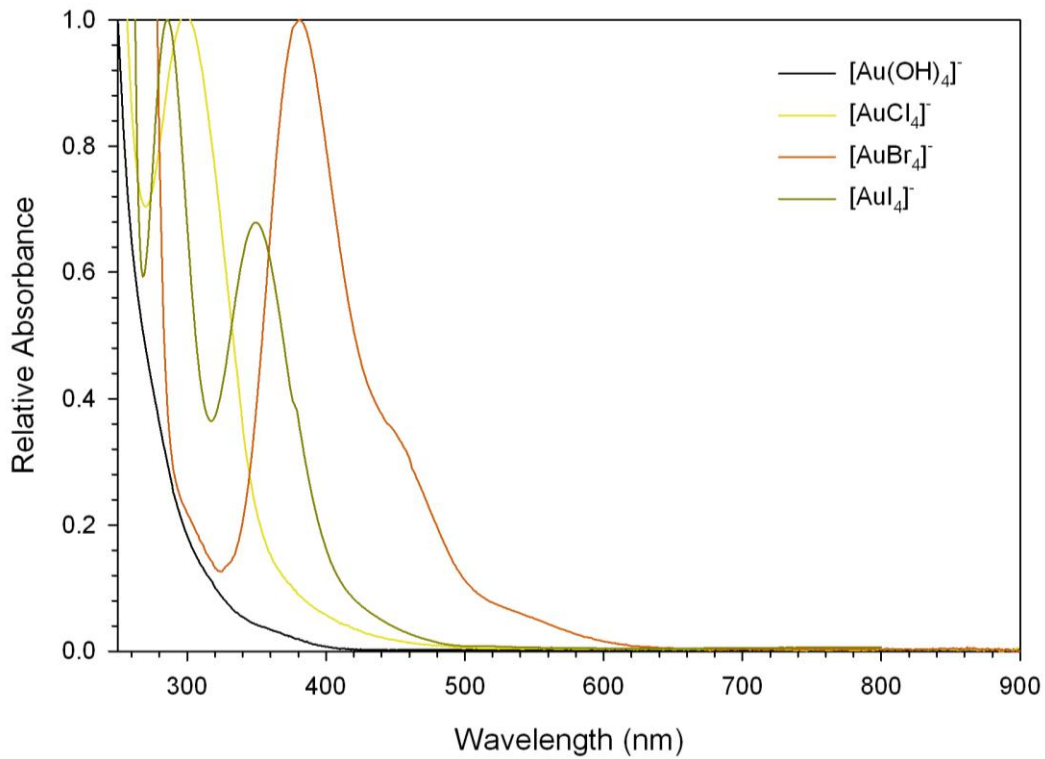


Figure 2-1. UV/Visible absorption spectra of several gold (III) complexes.

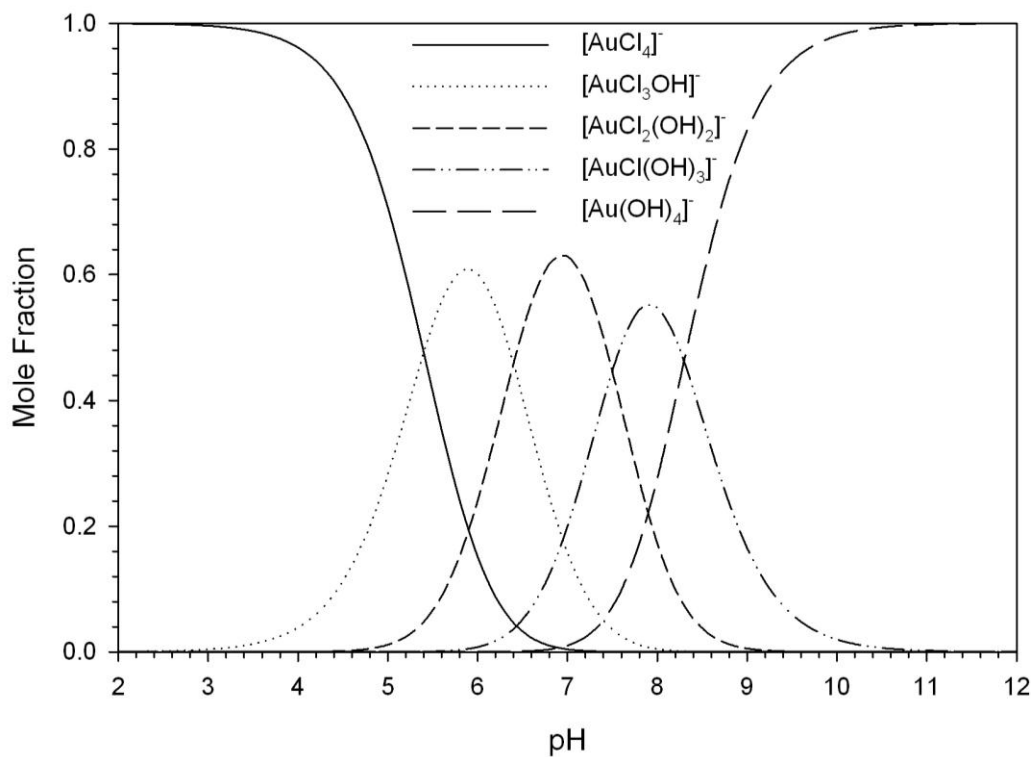


Figure 2-2. Speciation diagram of gold chloride in water.

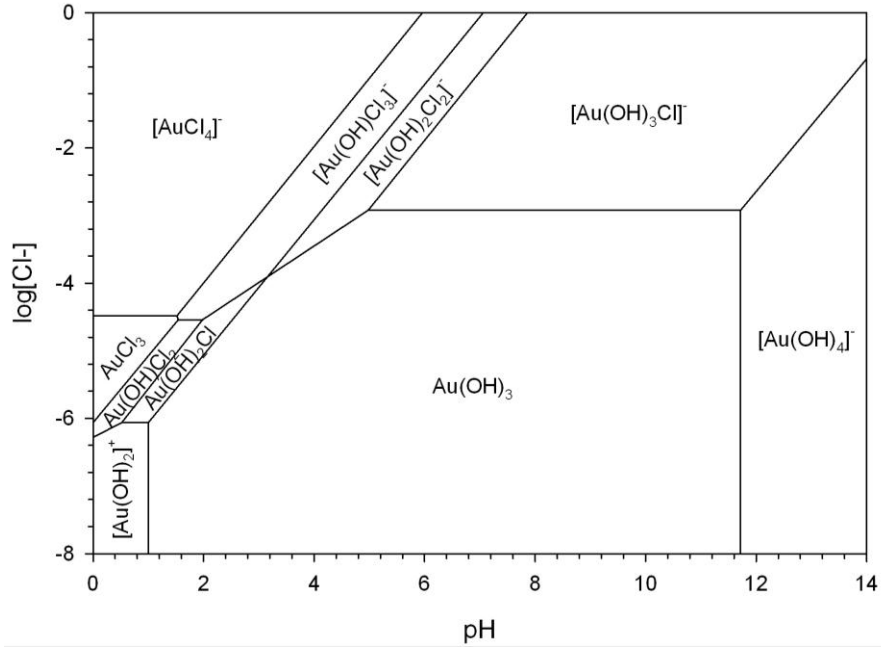


Figure 2-3. Speciation of the $\text{Au}^{3+}/\text{Cl}^-$ system as a function of pH and chloride ion concentration. Adapted from Baes and Mesmer⁶⁵.

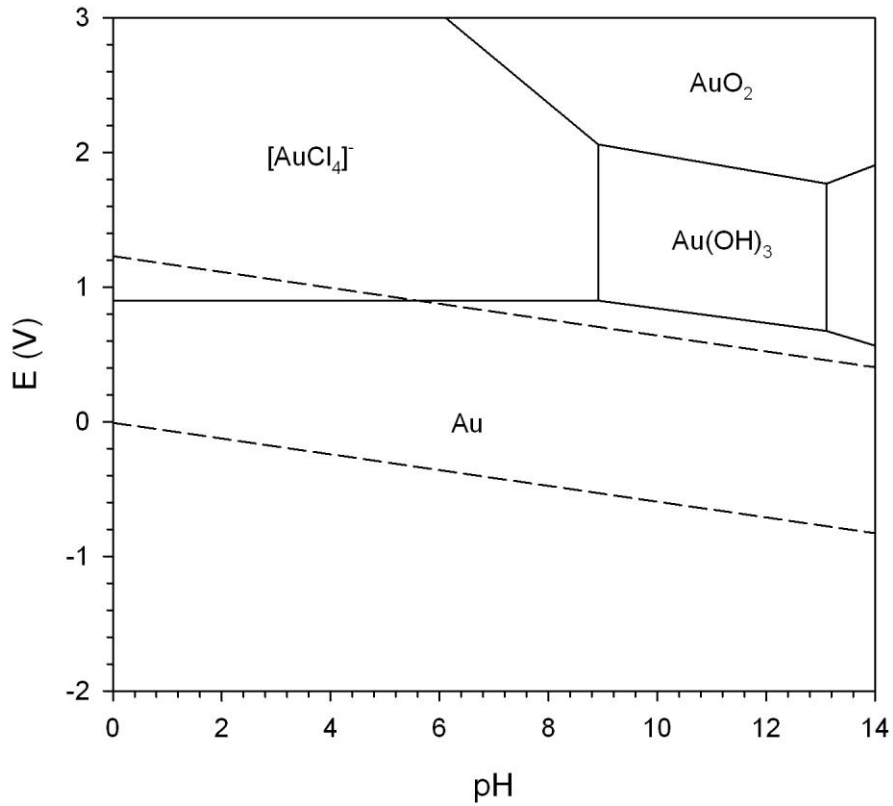


Figure 2-4. Pourbaix diagram of the Au/Cl system where $[\text{Cl}^-] = 1\text{M}$.

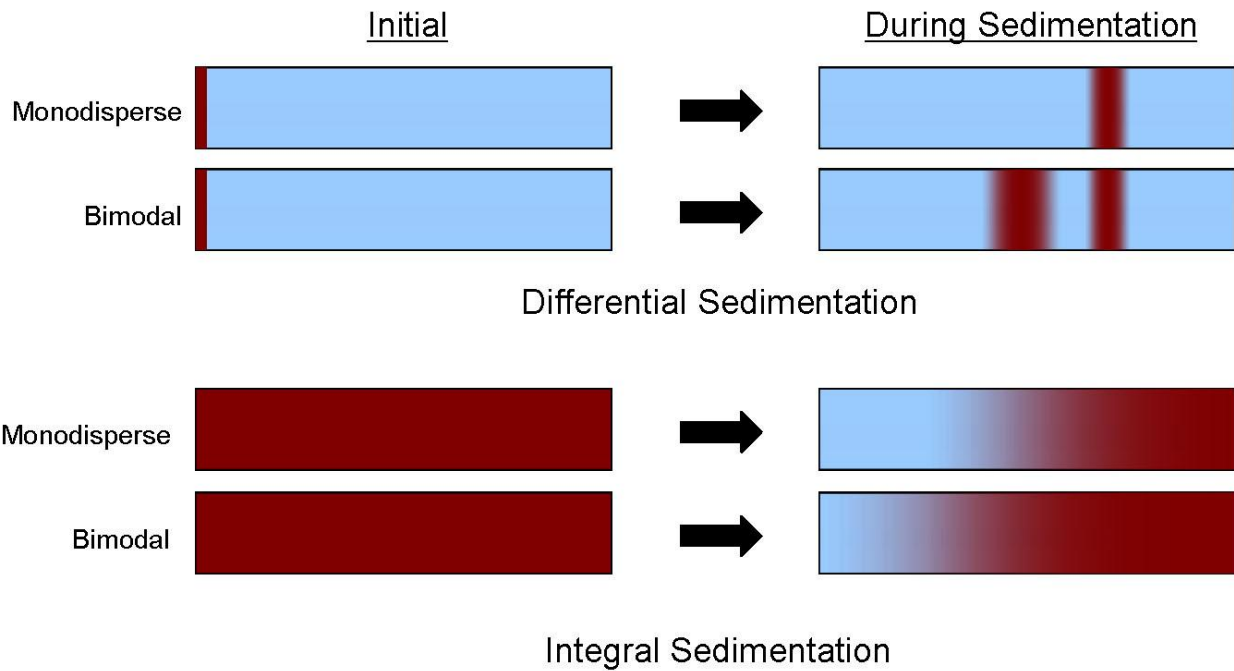


Figure 2-5. Illustration of differential and integral sedimentation. A suspension of particles (red) is sedimenting through a medium (blue).

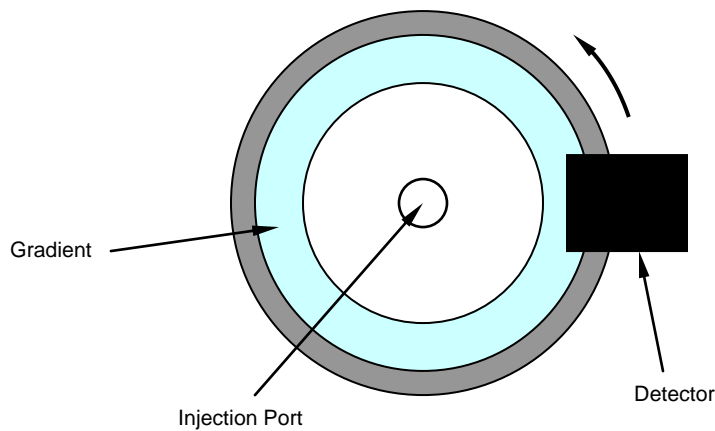


Figure 2-6. Illustration of a modern disc centrifuge geometry for differential sedimentation analysis. Samples are introduced into the center of a hollow transparent disc and move toward the edge of the disc through a pre-loaded density gradient fluid. A light obscuration detector placed near the edge of the disc monitors the passage of particles over time.

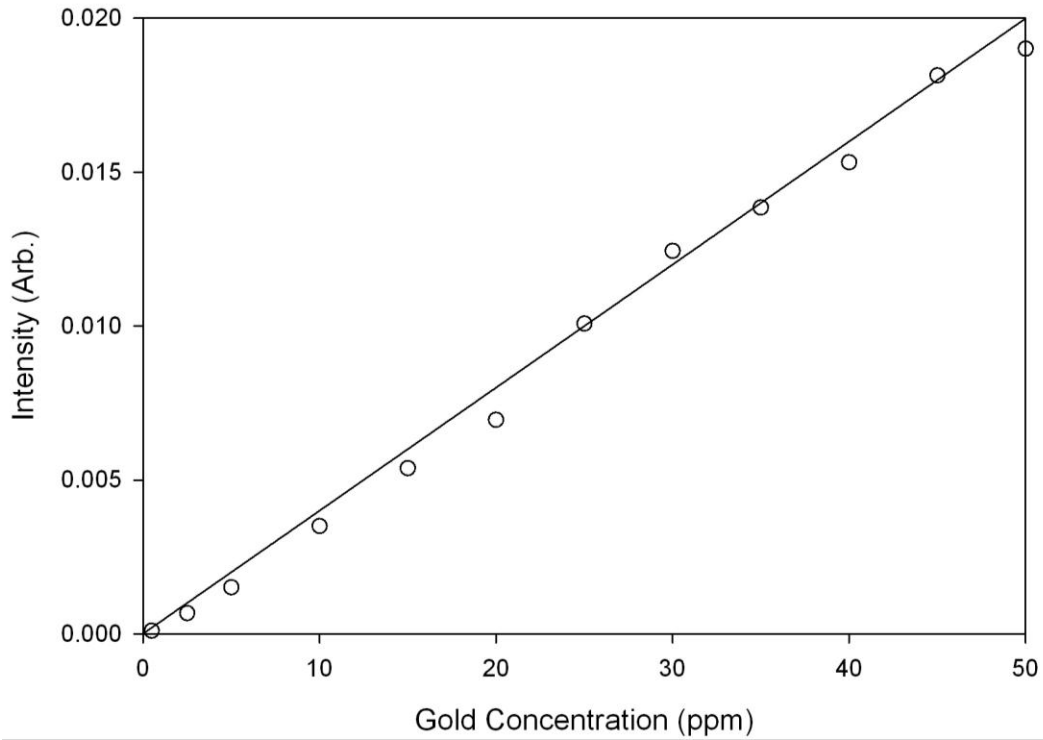


Figure 2-7. Response curve to nominally 40nm gold suspensions of different concentrations. The peak obscuration was proportionally related the concentration of gold in the suspension.

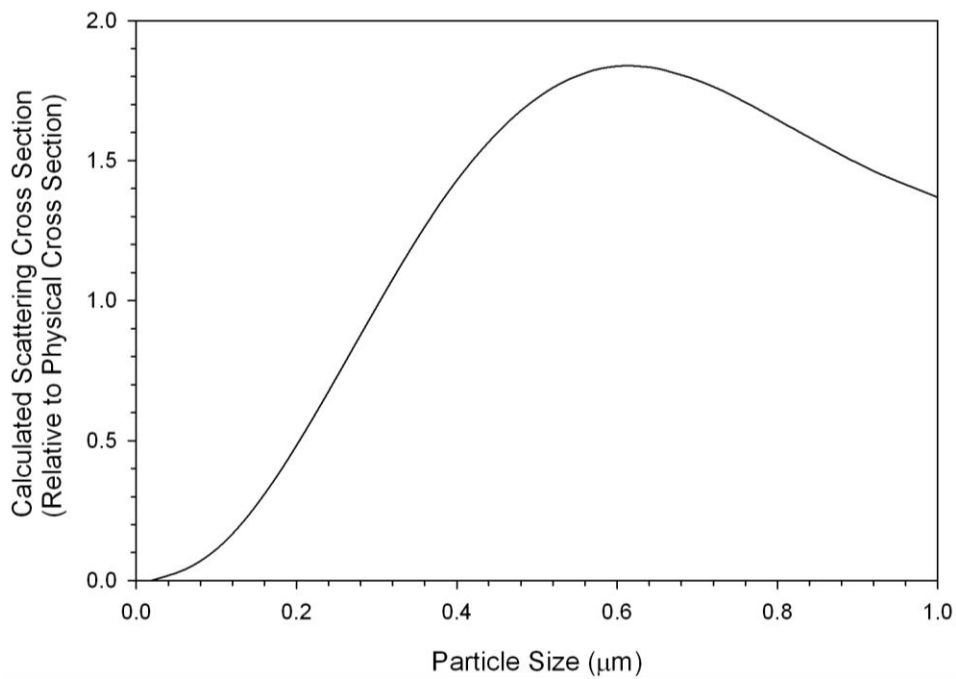


Figure 2-8. Calculated relative light scattering cross section (407nm) of spherical gold particles at sizes below 1μm.

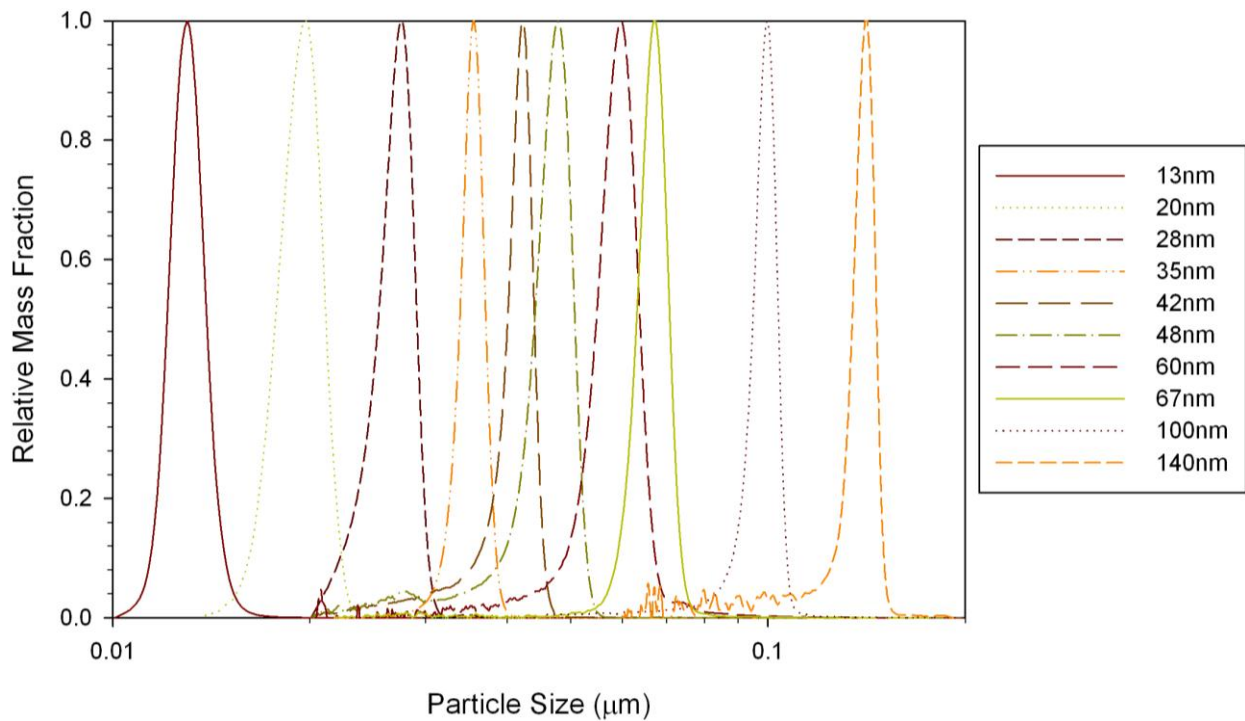


Figure 2-9. Particle size distributions of various gold suspensions as measured by differential sedimentation.

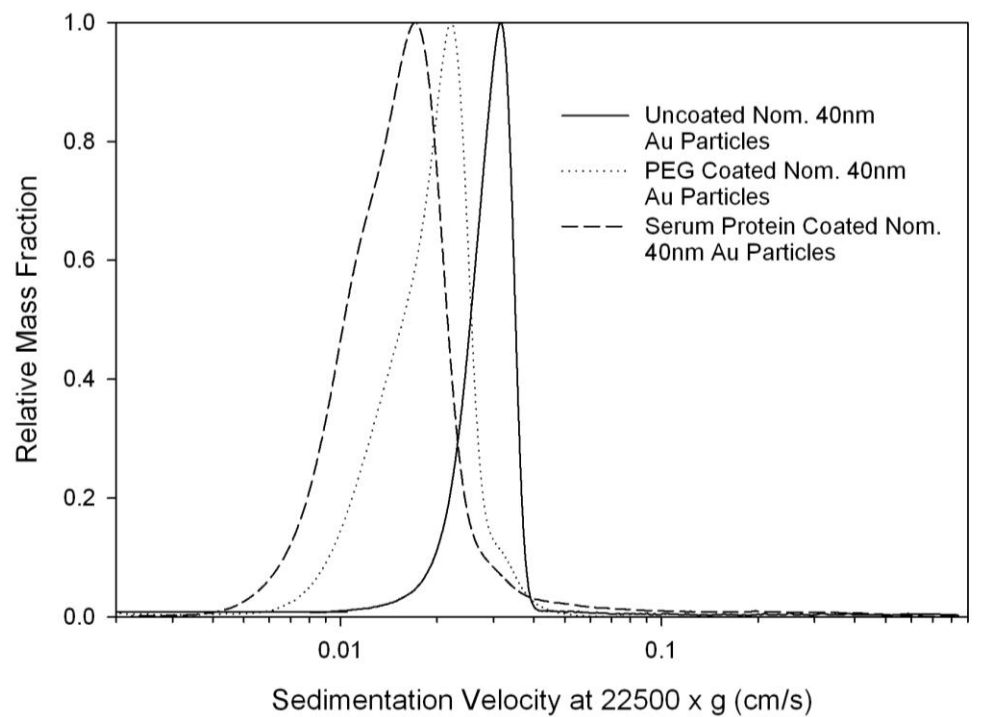


Figure 2-10. Sedimentation velocity distributions of various coated 40nm gold particles.

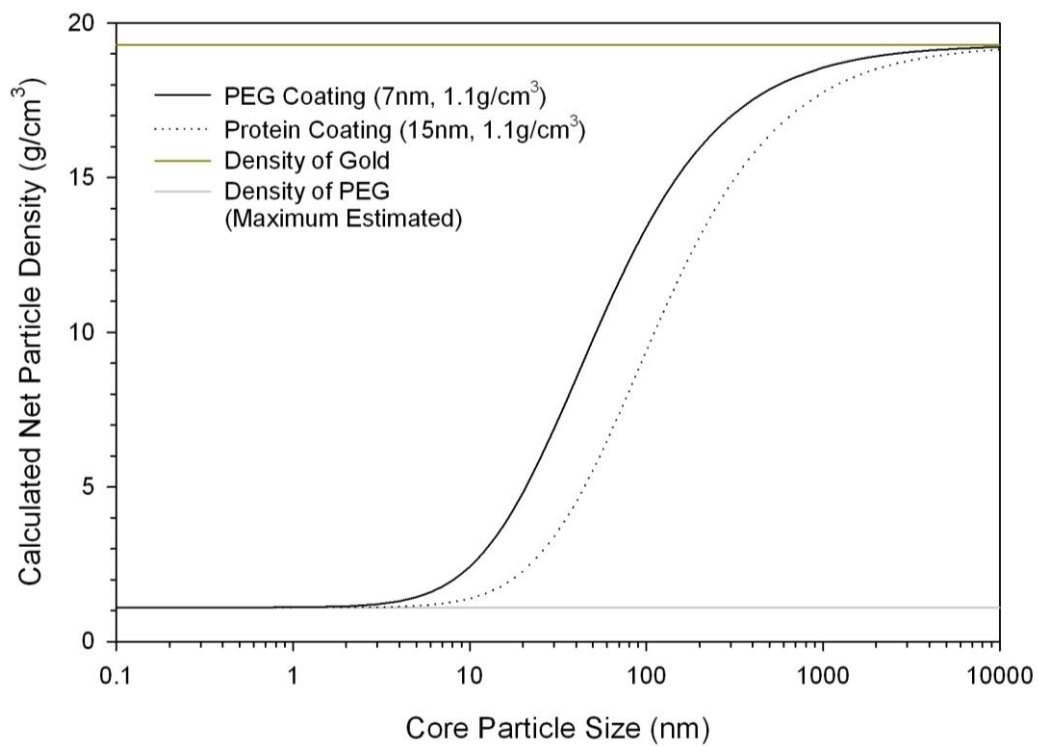
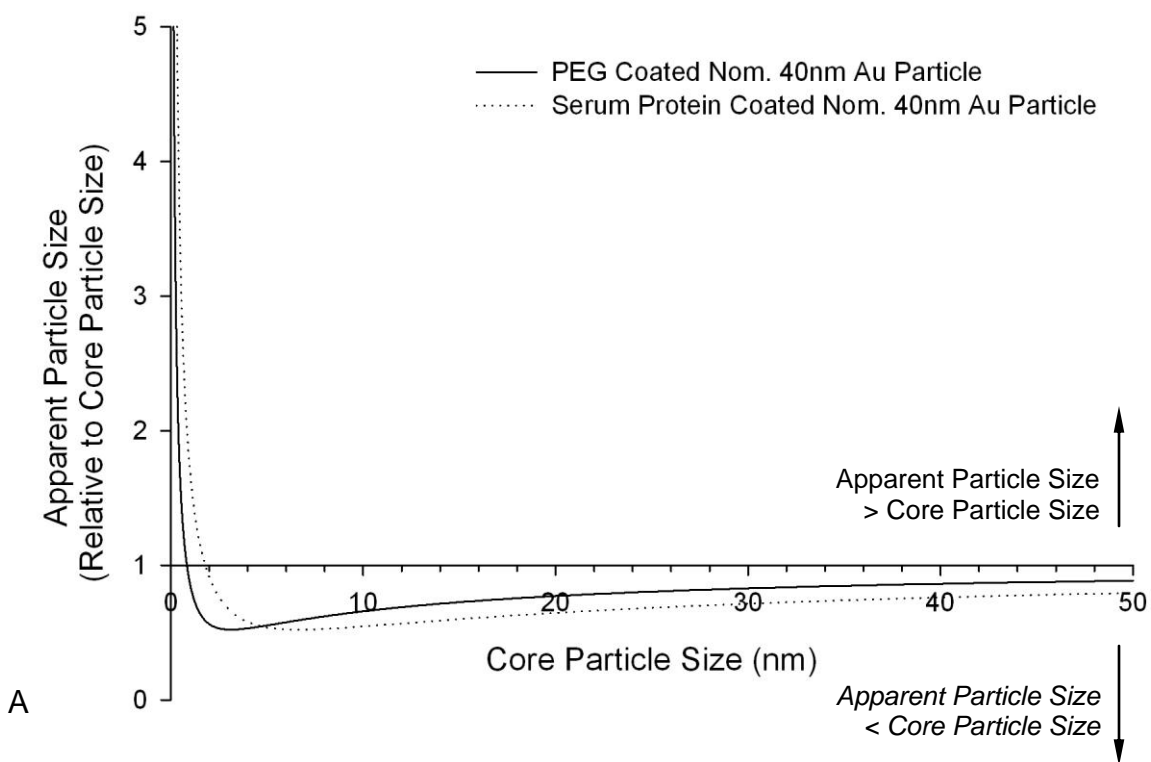
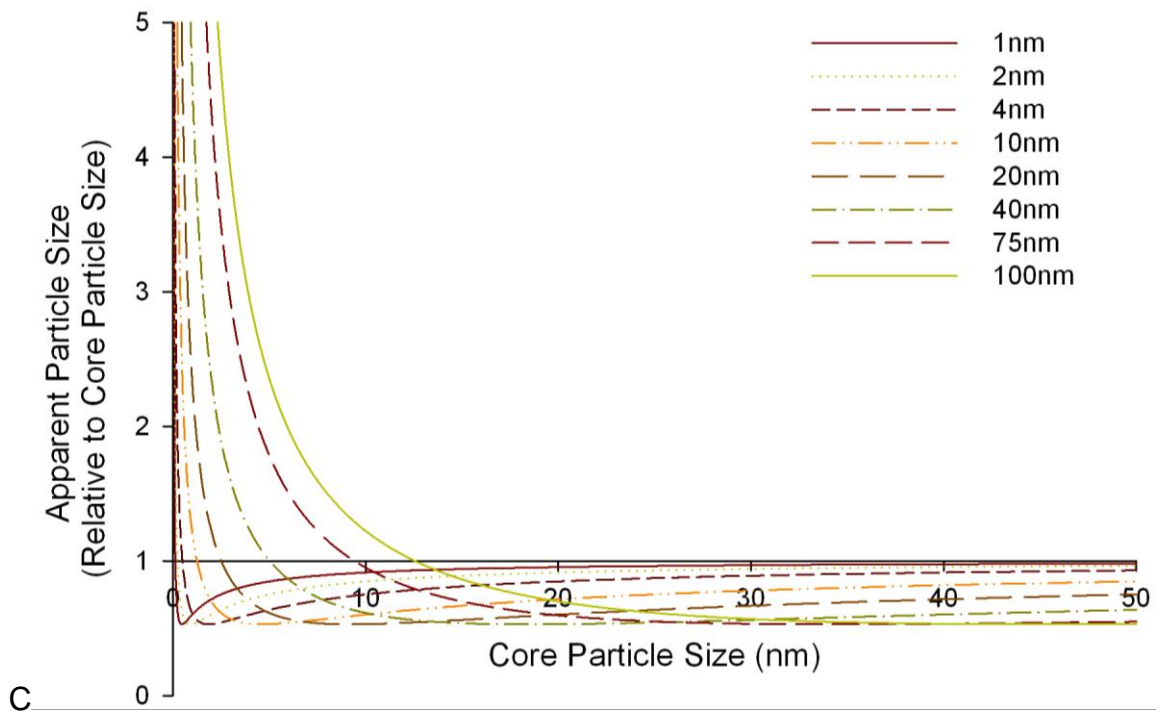
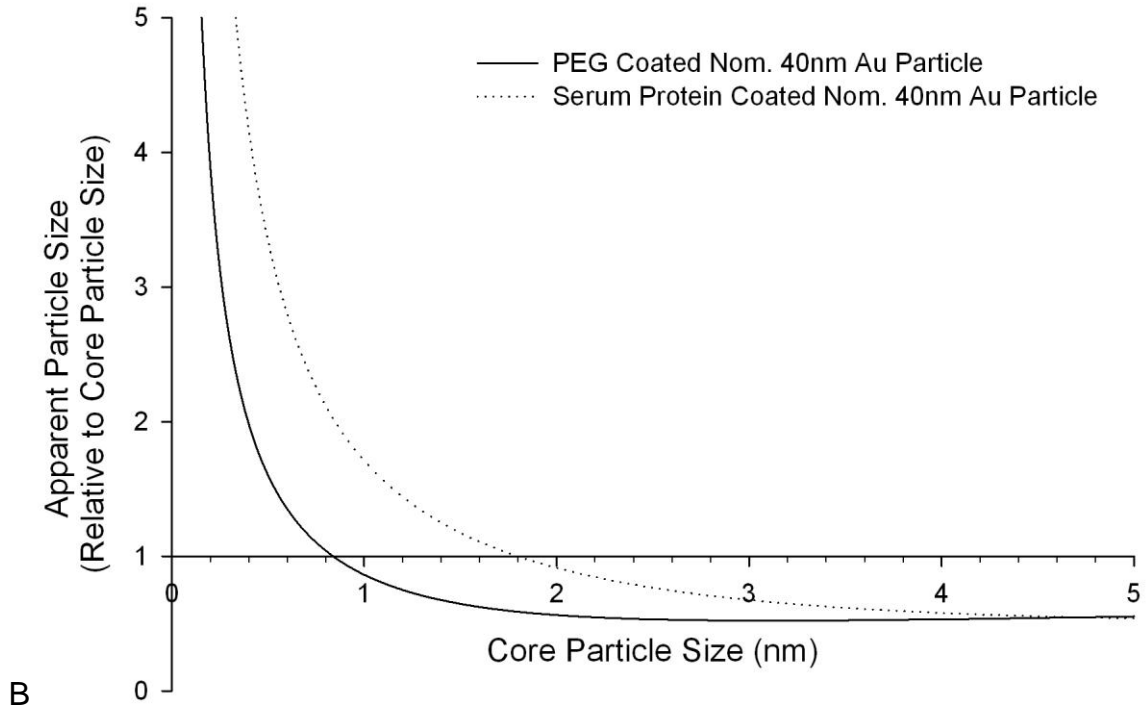


Figure 2-11. Calculated net densities of coated gold particles.

Figure 2-12. Calculated apparent particle size relative to core particle size for various coated gold particles. A) Core particle sizes up to 50nm with PEG and serum protein coatings. B) Detail of sizes up to 5nm with PEG and serum protein coatings. C) Core particle sizes up to 50nm with coating densities of 1.1g/mL and various coating thicknesses. D) Detail of sizes up to 15nm with coating densities of 1.1g/mL and various coating thicknesses. Relative apparent sizes greater than 1 indicate that the coated particle sediments at a velocity higher than the core particle, relative apparent sizes equal to 1 indicate that the coated and uncoated particles sediment at the same velocity, and relative apparent sizes less than 1 indicate that the coated particle sediments at a lower velocity than the core particle. E) Point of sedimentation equivalence (where coated and uncoated particles have identical sedimentation velocities) relative to coating thickness and coating density.





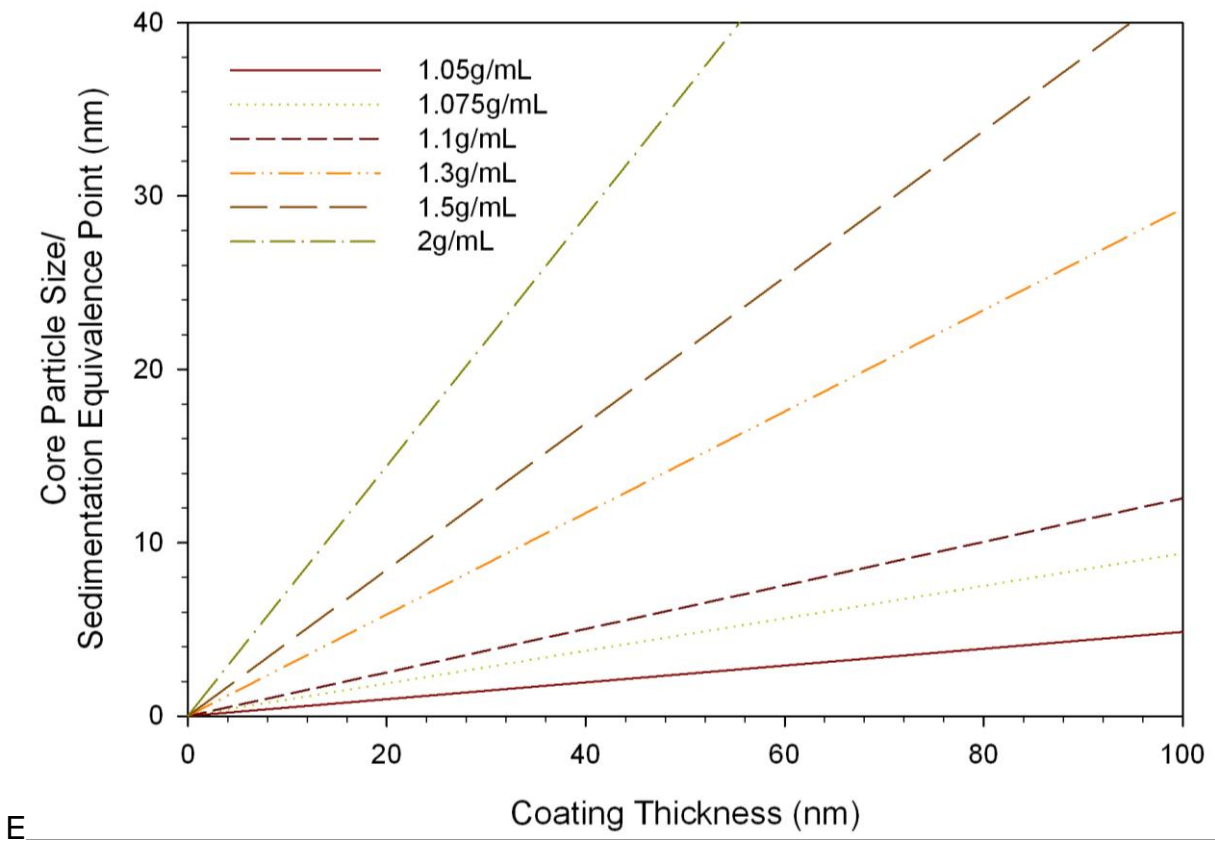
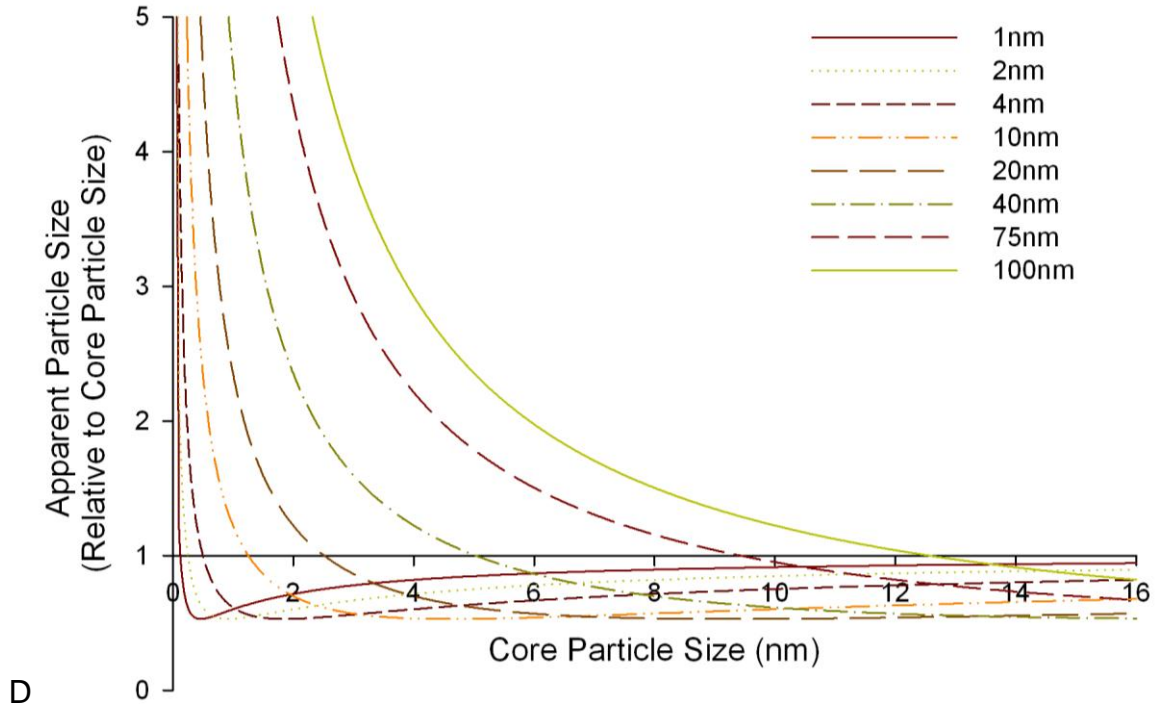
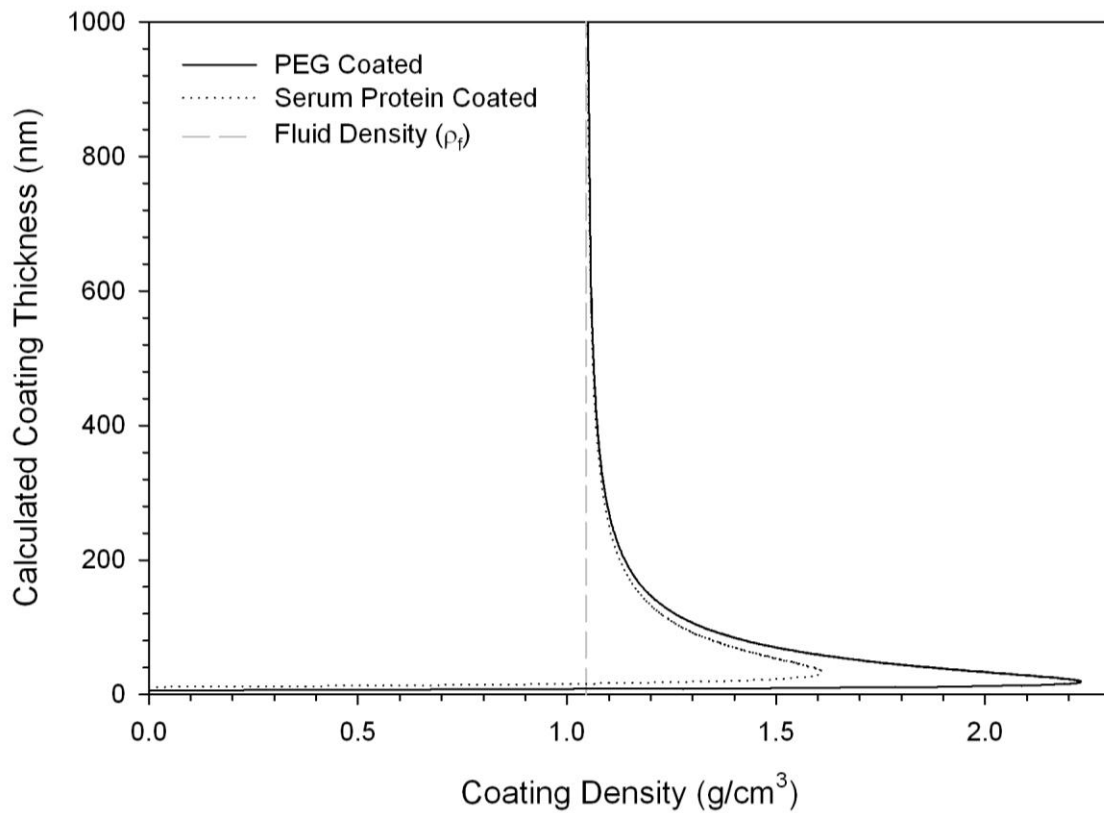
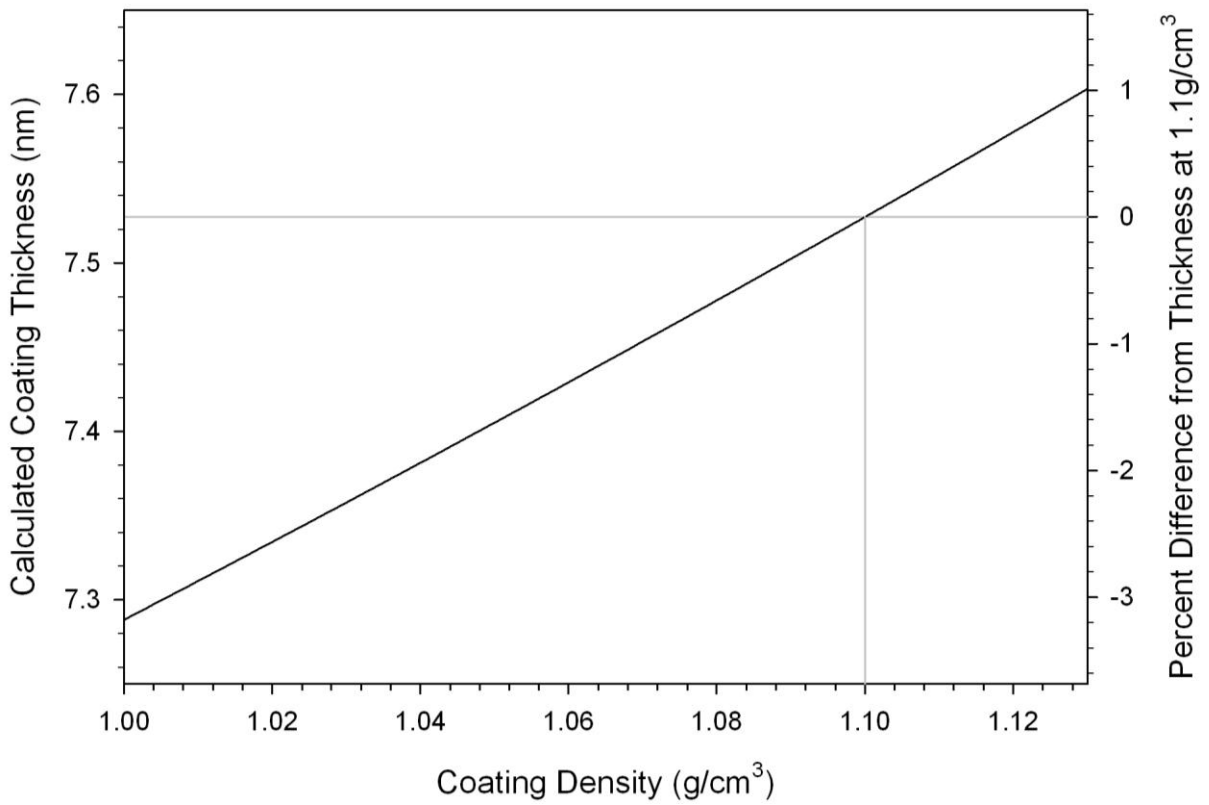
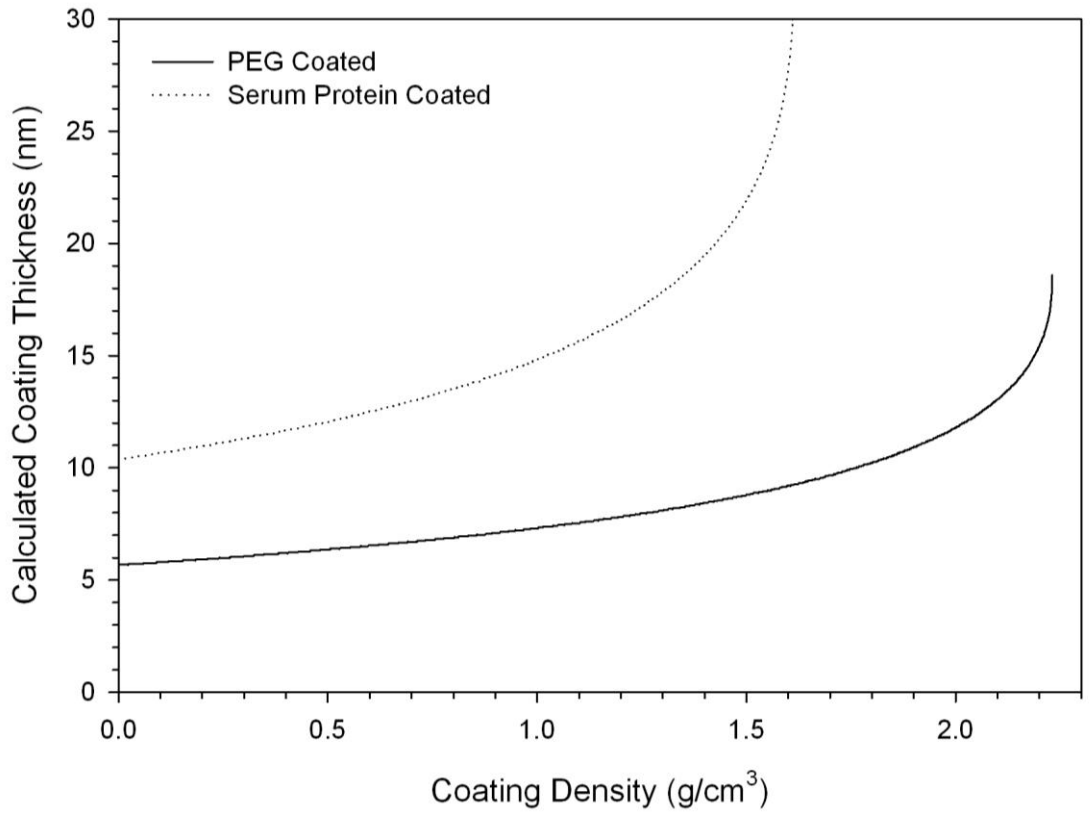
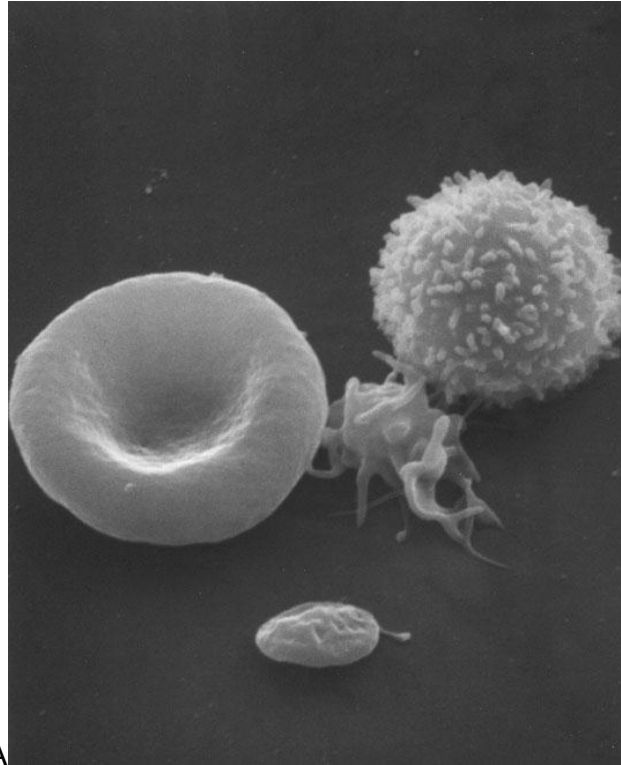


Figure 2-13. Variance of calculated coating thickness with assumed coating density. Calculations were based on measured differences in sedimentation velocities of 40nm gold particles before and after coating with PEG (Reagent 2) or serum proteins. A) Complete solution of the sedimentation equation 2.3 for the specified particles. The curve has a vertical asymptote at the fluid density (ρ_f), allowing for two possible thickness solutions at coating densities greater than the fluid density. B) The first solution for PEG and protein coated particles with coating densities up to approximately 2.23 and 1.16g/cm³ respectively. C) The first solution for densities between 1 and 1.14g/cm³ (density range from de-ionized water to maximum reported density for solid PEG).

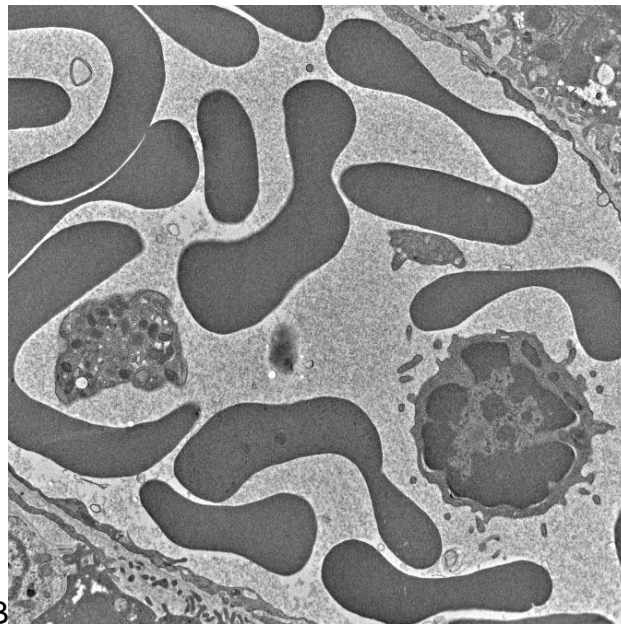


A





A



B

Figure 2-14. Electron micrographs of human blood cells. A) Scanning electron micrograph of human erythrocyte (left), activated platelet (center), unactivated platelet (center bottom), and lymphocyte (right). B) Transmission electron micrograph of blood showing erythrocytes, lymphocytes, and platelets. Images produced by the National Cancer Institute Electron Microscopy Lab⁹⁴.

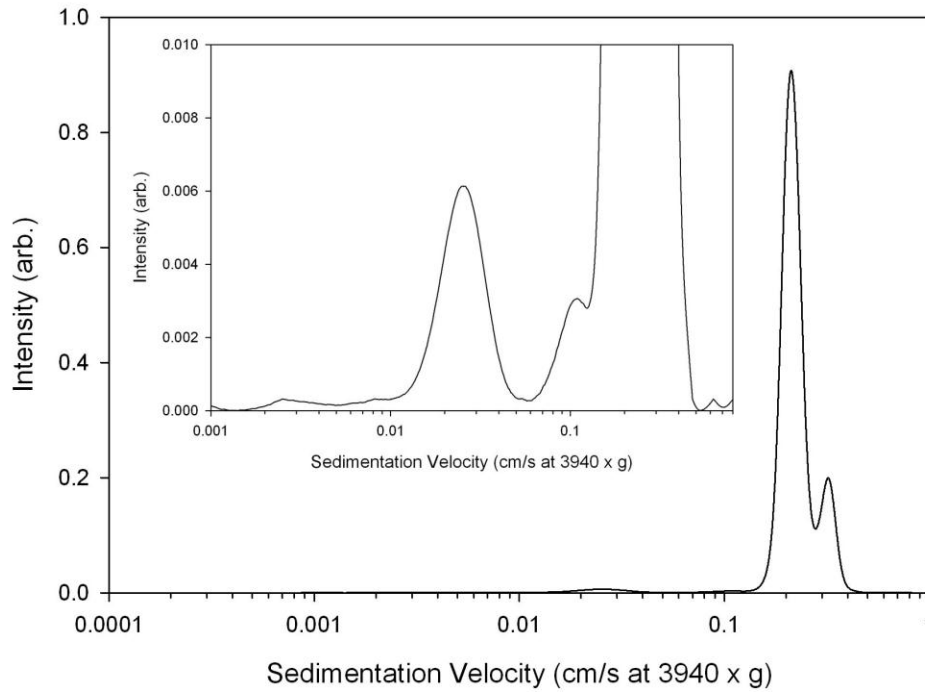


Figure 2-15. Sedimentation velocity distribution of whole blood. The inset plot shows detail of the lower intensity peaks.

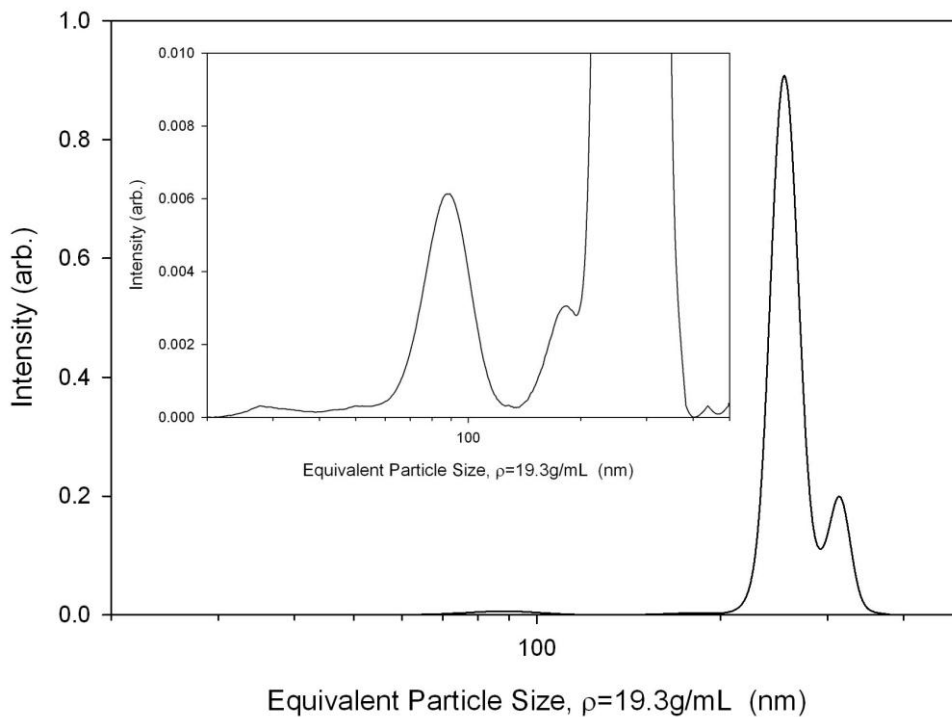


Figure 2-16. Equivalent particle size of whole blood components. Particle density assumed to be that of gold (19.3g/mL). The inset plot shows detail of the lower intensity peaks.

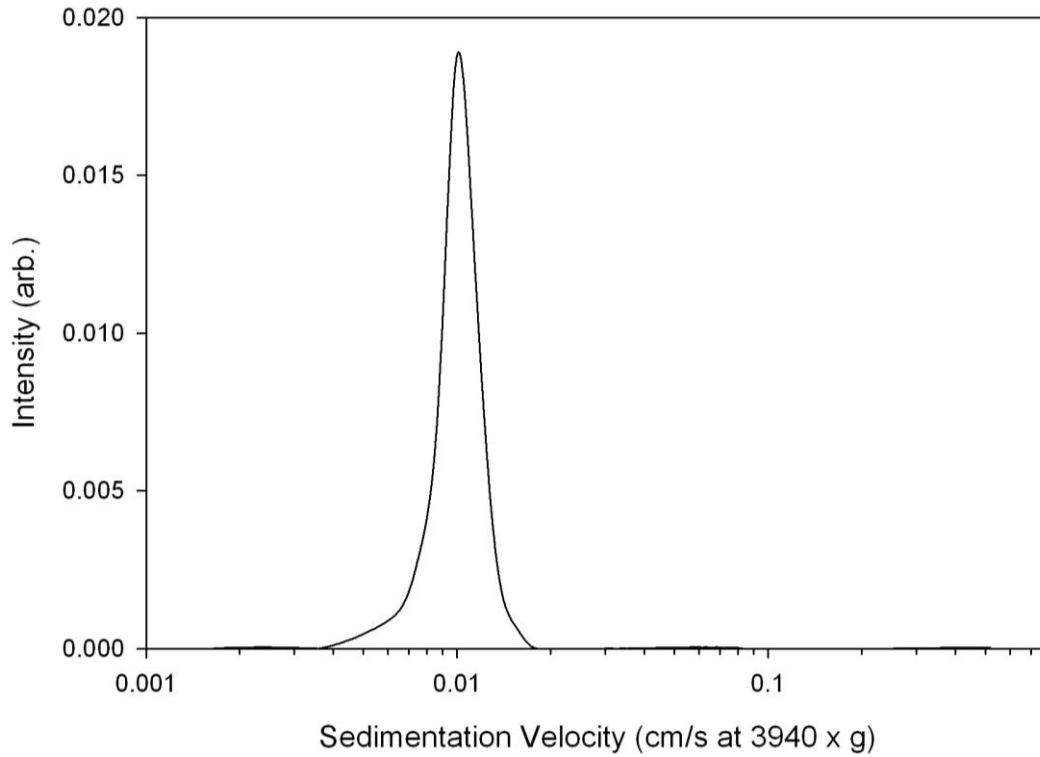


Figure 2-17. Sedimentation velocity distribution of lysed whole blood.

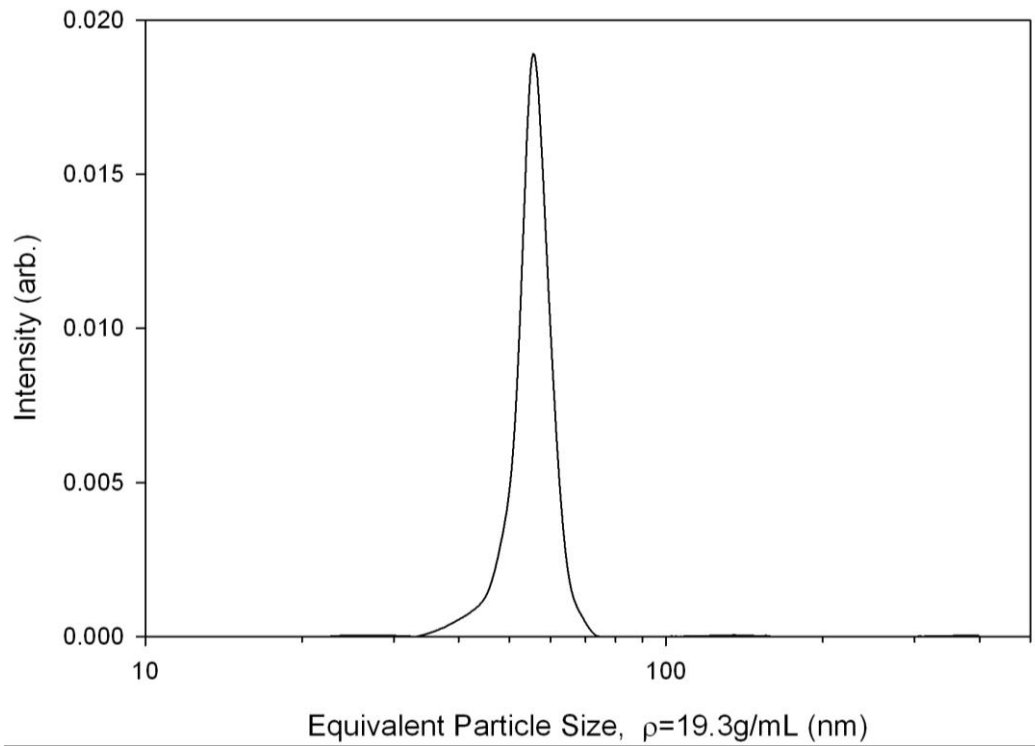


Figure 2-18. Equivalent particle size of lysed whole blood components. Particle density assumed to be that of gold (19.3g/mL).

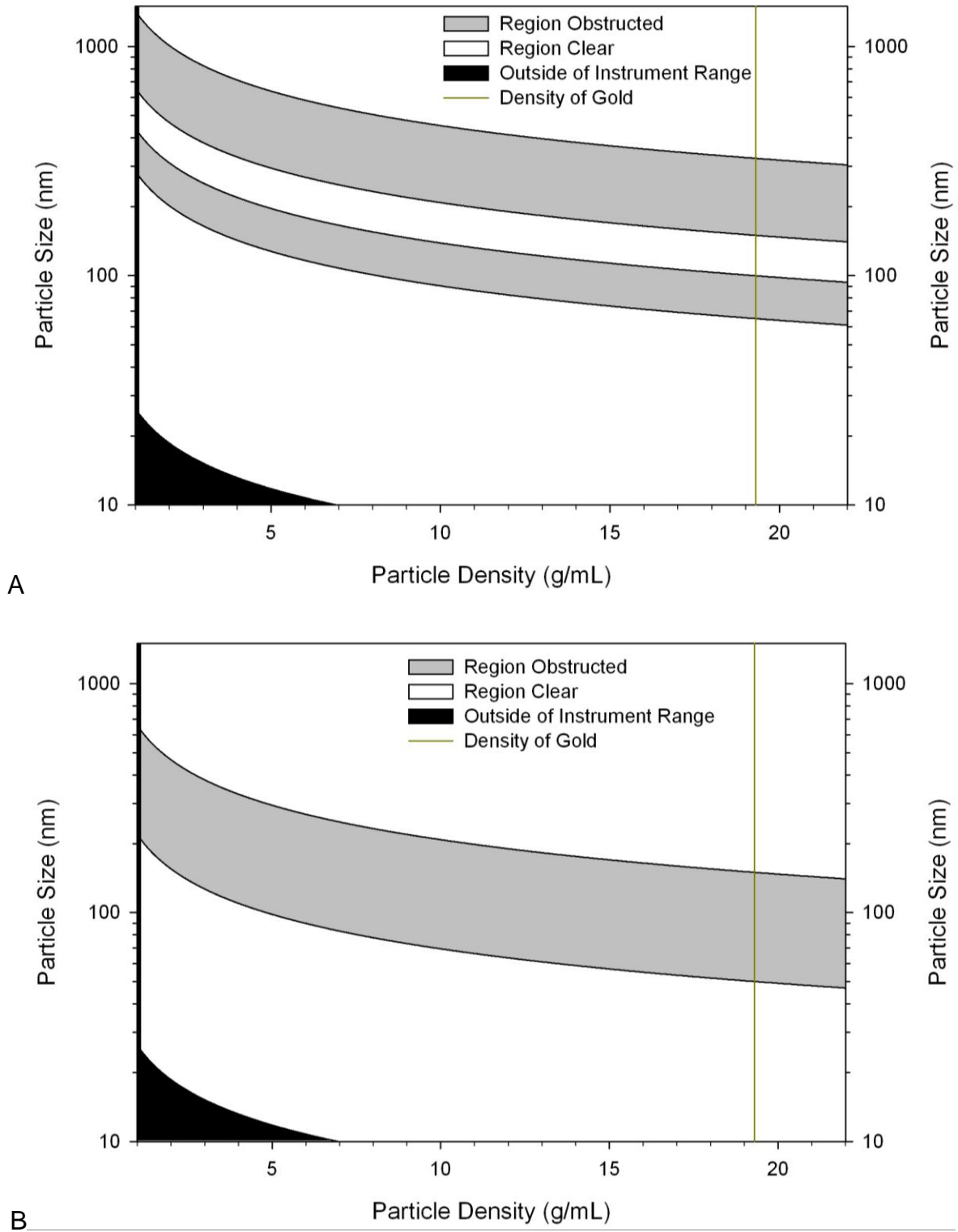
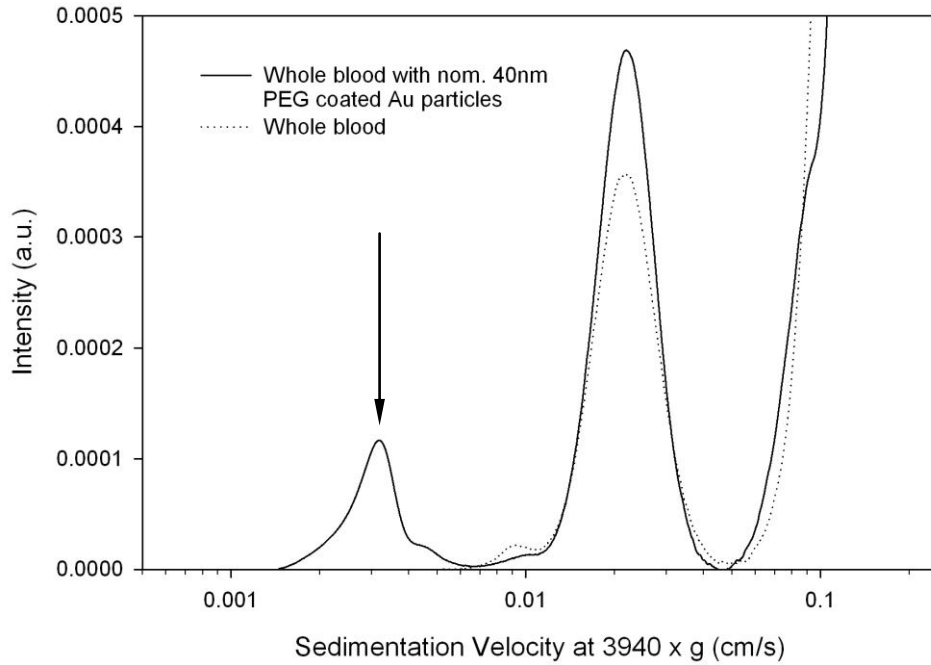
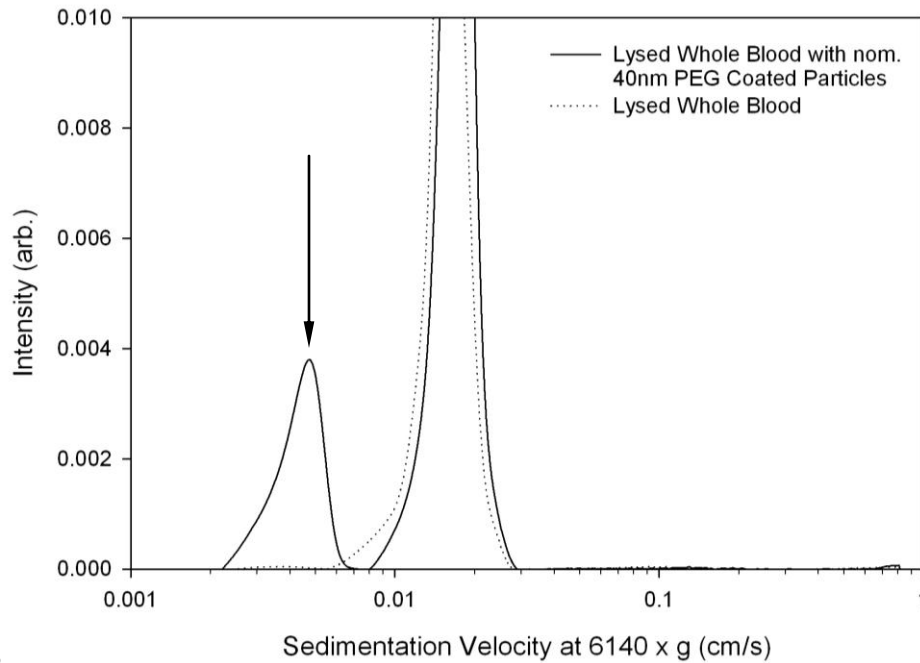


Figure 2-19. Obstruction of analysis range by blood relative to particle density. A) Blood Isotonic, diluted 1:20 in 1x PBS. Analysis performed in an isotonic/buffered gradient. B) Blood lysed 1:20 in deionized water prior to analysis, analysis performed in a non-isotonic gradient.



A



B

Figure 2-20. Sedimentation velocity distribution of blood with PEG coated gold particles. Peaks from gold particles are indicated with an arrow. A) Blood was kept isotonic and analyzed in an isotonic gradient. The peak corresponding to the coated gold particles is evident at approximately 0.003cm/s. The shoulder present on the right side of the particle peak was present in the parent suspension. B) Blood was lysed prior to analysis and analyzed in an isotonic gradient. The peak corresponding to the coated gold particles is evident at approximately 0.004cm/s

Table 2-1. Summary of preparation methods for differential sedimentation analysis of gold particles in whole mouse blood.

Preparation Method	Approximate Region of Applicability for Gold Particles	Primary Use
Isotonic	<65nm	Primary Particles
	100-150nm	Large aggregates
	>325nm	
Lysed	<50nm	Aggregates
	>150nm	Small primary particles

Note that some variability exists between species and other factors such as hydration.

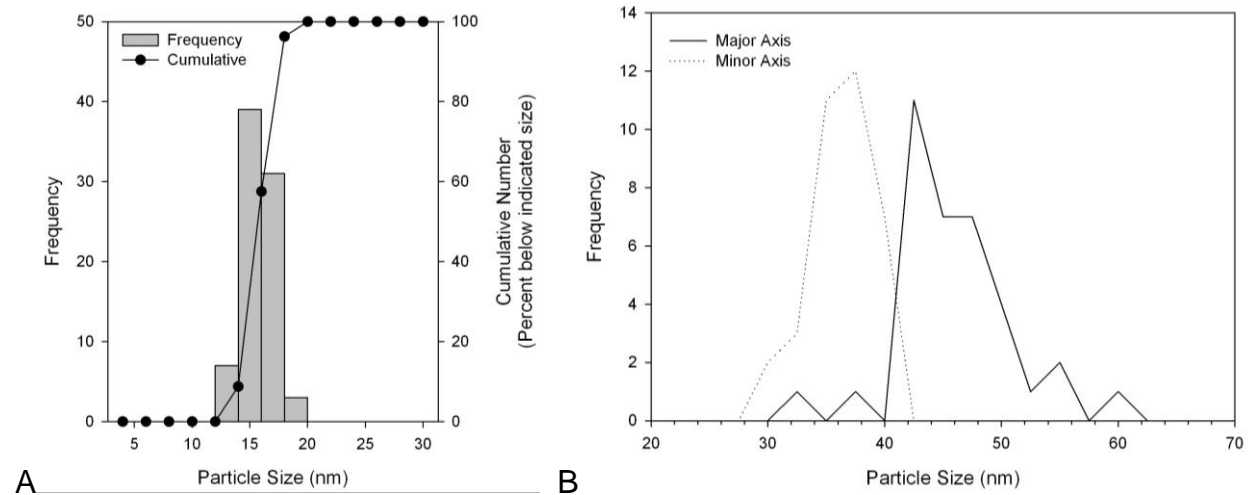


Figure 2-21. TEM image analysis particle size distributions of gold particles prepared by the citrate method. A) Particle size distribution of 15nm particles (n=80). B) Major and minor axis size distributions of nom. 40nm particles (n=35).

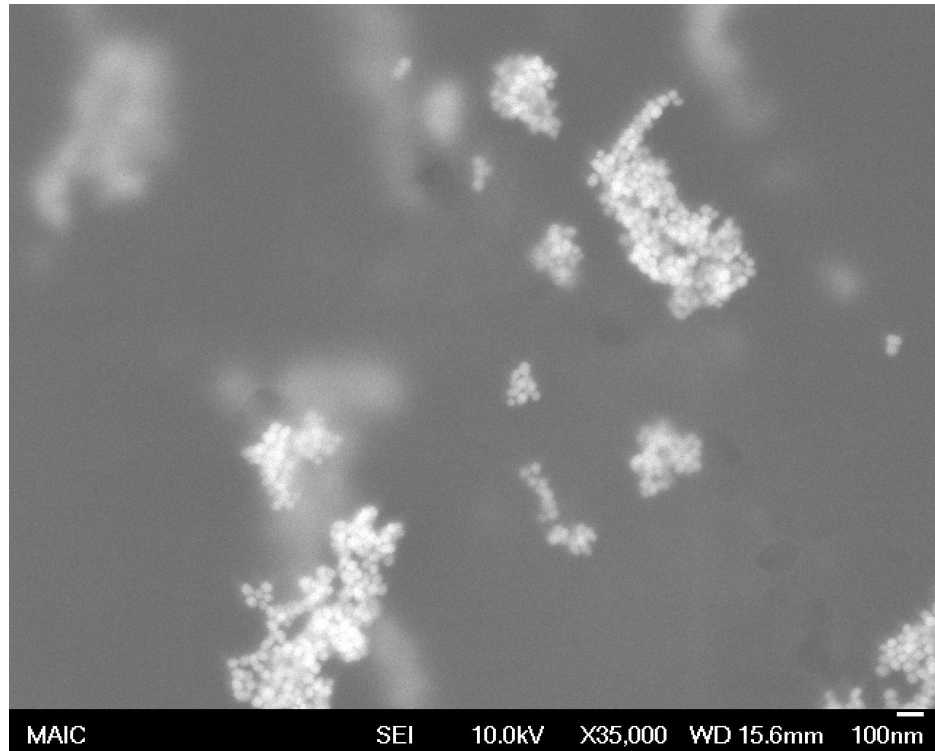


Figure 2-22. Aggregates of uncoated gold particles in mouse gastric fluid. The primary particles composing the aggregates can clearly be seen.

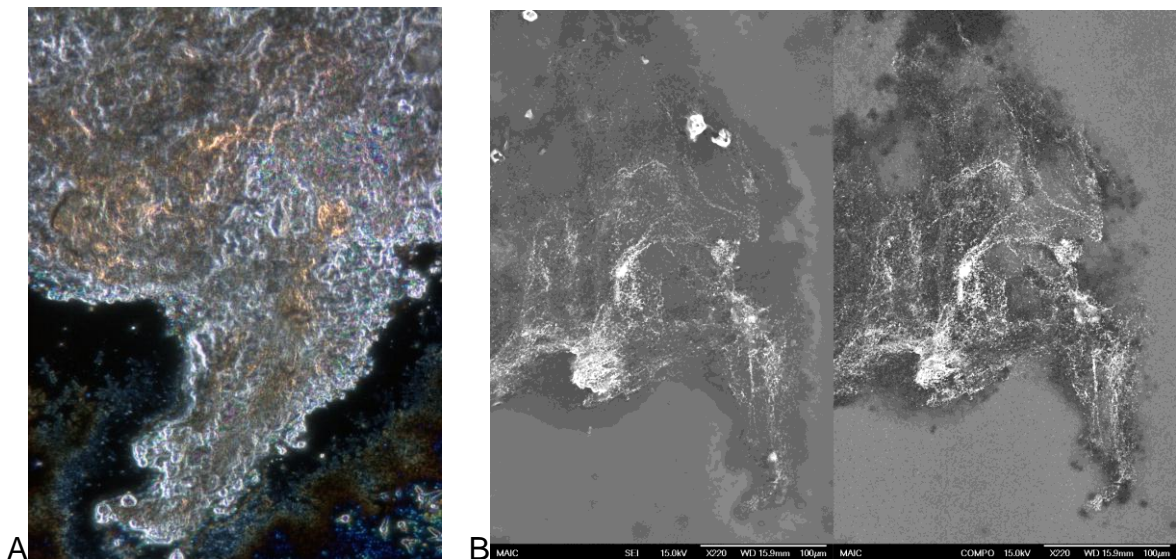


Figure 2-23. Distribution of gold particles in mouse gastric contents. A) Darkfield optical micrograph. B) SE (left) and BSE (right) images of the same area showing concentrations of gold particles. The gold particles appear as yellow reflected light optically and as bright (high Z) regions in SE and BSE images. These complementary images illustrate the differences between each technique.

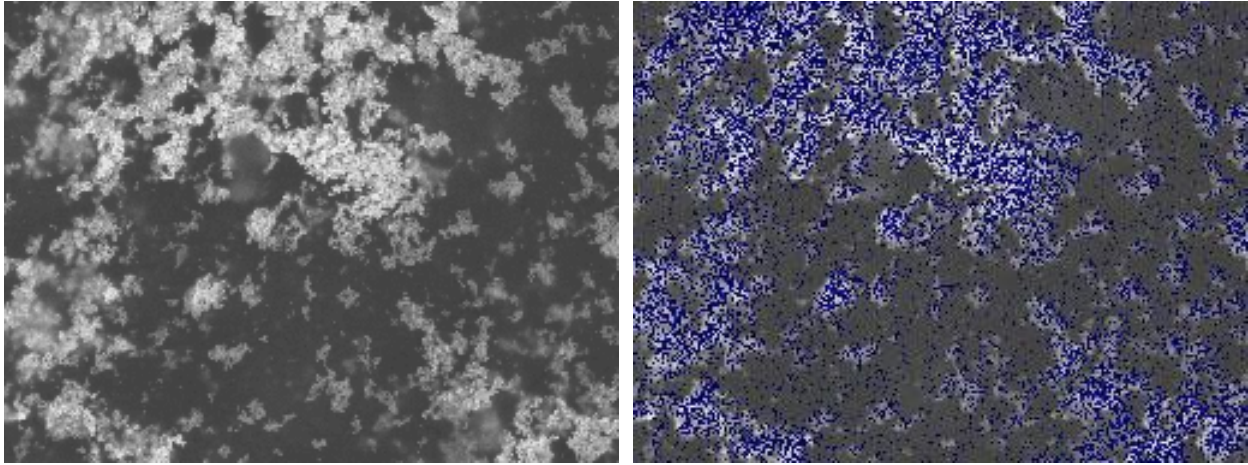


Figure 2-24. Identification of gold particles by EDS mapping. The image on the left shows a SE image of the gold particles in gastric contents, and the image on the right shows an overlay of gold M_{β} characteristic x-ray intensity (blue pixels).

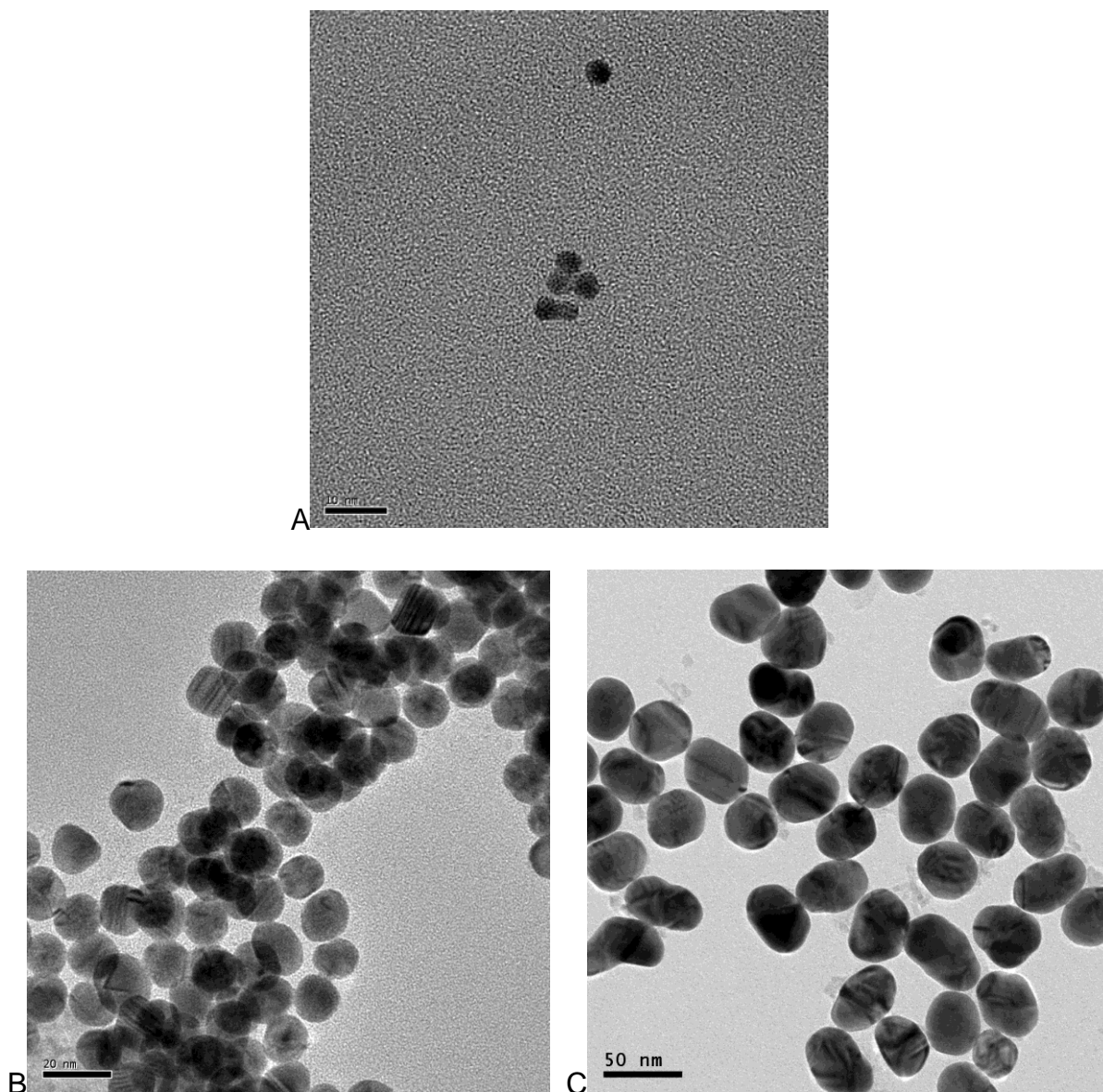


Figure 2-25. Transmission electron micrographs of gold particles as prepared. A) Nom. 3nm gold particles. B) Nom. 15nm gold particles. C) Nom. 40nm gold particles. As the particle size increases, sphericity and monodispersity decrease.

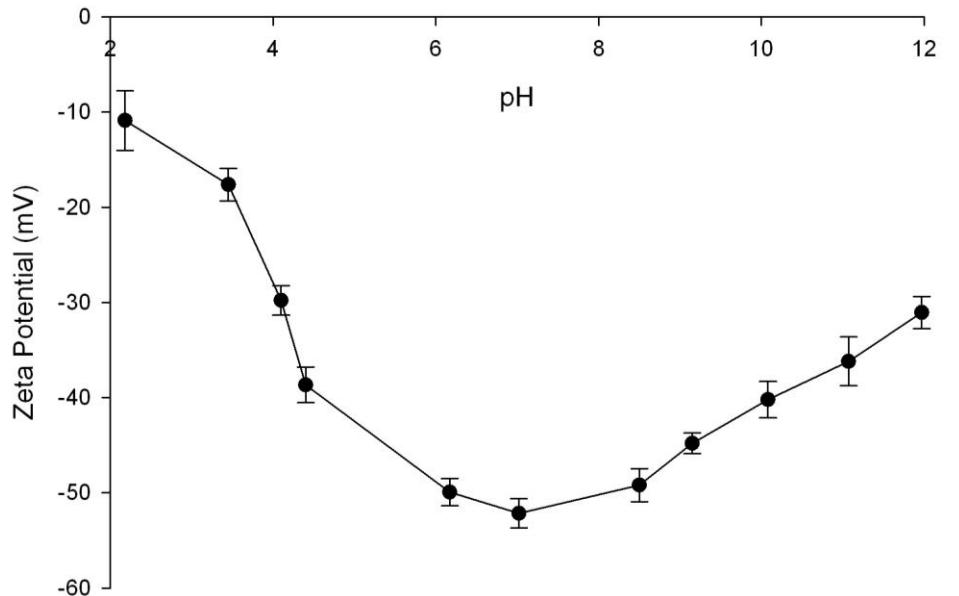


Figure 2-26. Zeta potential titration of nom. 50nm gold particles as determined by DLS. The particles exhibited a negative charge across all pH values tested. pH range was restricted to between 2 and 12 since particles were unstable outside of this range.

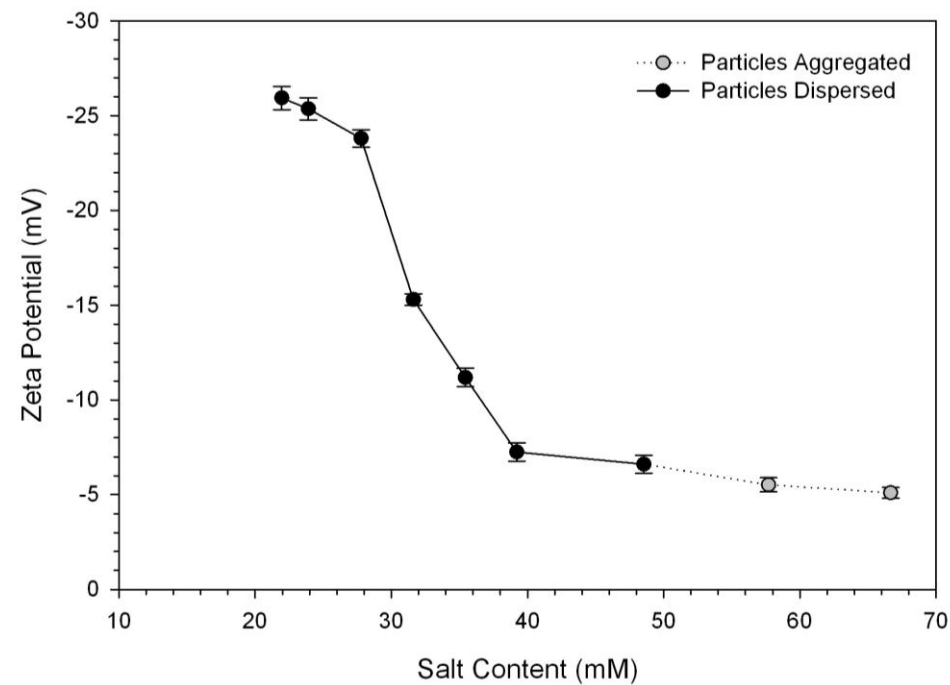


Figure 2-27. Zeta potential of a 50ppm suspension of nom. 40nm gold particles titrated with sodium chloride. Zeta potential neutralization due to charge screening is evident. Though immediate aggregation did not occur until approximately 50ppm, particles may aggregate over time at lower concentrations.



Figure 2-28. Photograph of spherical and monodisperse gold particles ranging in size from approximately 40nm (left) to 100nm (right).

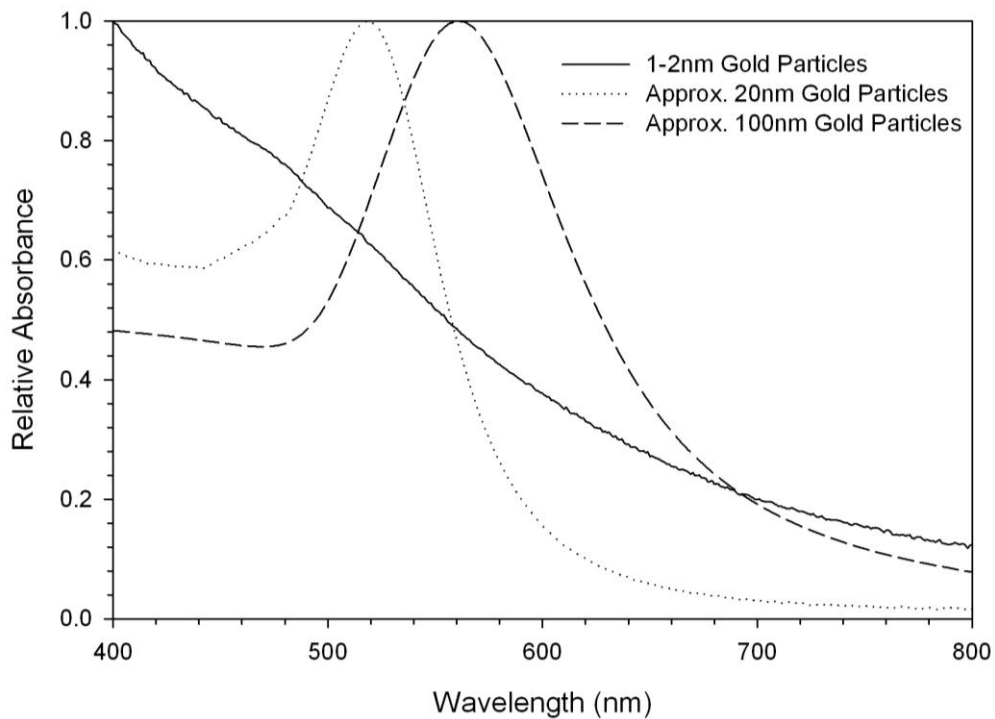


Figure 2-29. Visible absorption spectrum of gold particles at various sizes.

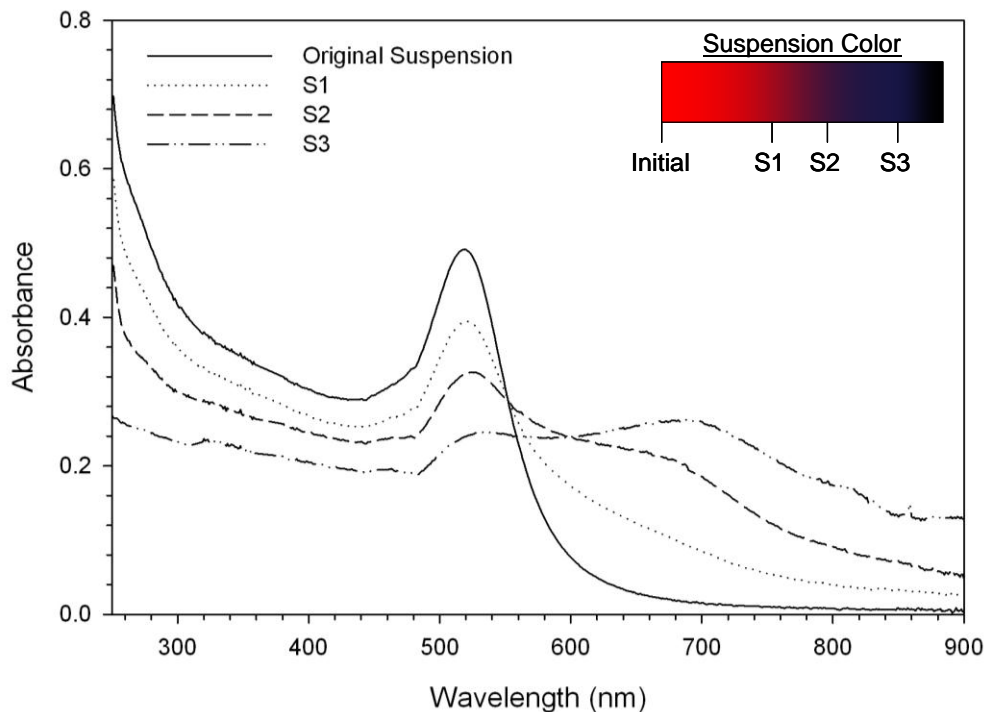


Figure 2-30. UV/Visible absorption spectrum of gold particles with increasing concentration of salt (increasing from S1 to S3). A shift in the optical absorption characteristics of the particles is apparent upon aggregation.

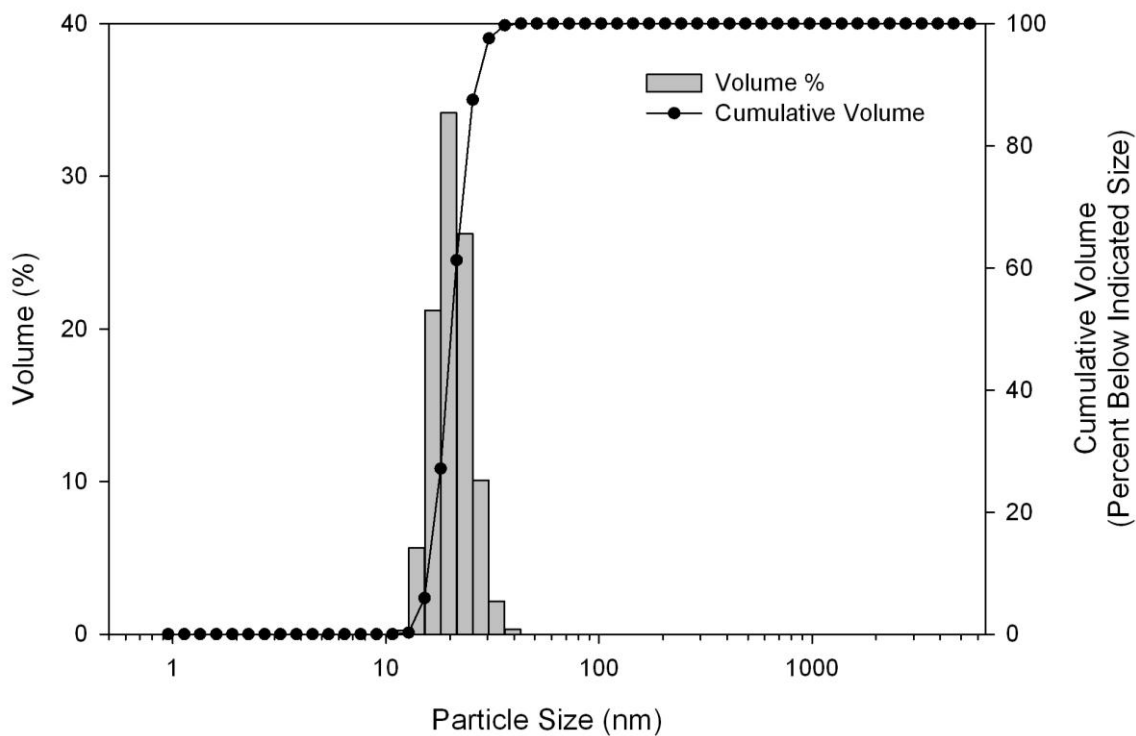


Figure 2-31. Particle size distribution of nominally 20nm gold particles by DLS.

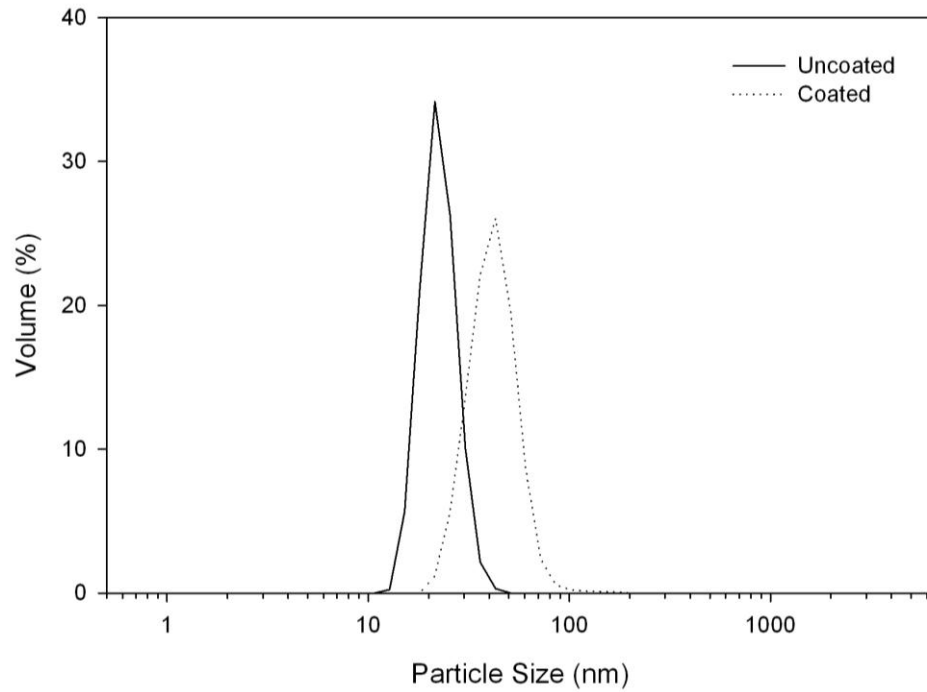


Figure 2-32. DLS particle size distribution of nominally 20nm gold particles before and after coating with PEG. A particle size increase of approximately 20nm can be seen, corresponding to a 10nm coating thickness.

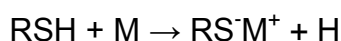
CHAPTER 3 PROPERTIES AND STABILITY OF PEG COATINGS

Adsorption and Desorption on Gold Surfaces

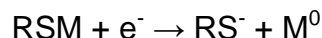
Surface modification of gold surfaces is almost exclusively achieved through a metal to sulfur bond to the surface, though a small number of applications also involve amines, phosphines, and physically adsorbed polymers/biomolecules. Various sulfur containing compounds are capable of forming monolayers on gold surfaces such as: thiols/sulfides, disulfides^{98, 99}, thioethers¹⁰⁰, dithiocarbamates^{101, 102}, thiones^{99, 103, 104}, xanthates¹⁰⁵, etc. These compounds and a plethora of derivatives are widely available for modification of metal surfaces. Bifunctional derivatives are also available if additional conjugation to the coating is desired (coating schemes illustrated in Figure 1-1). Thiol terminated reagents of various types are most frequently used for surface modification, and are generally considered to be the most effective compared to compounds such as disulfides. This is primarily due to issues involving solubility and associated physical adsorption²⁷. Recent work on compounds such as dithiocarbamates¹⁰⁶ and disulfides¹⁰⁷ that result in more than one attachment point to the surface have demonstrated greater stability by certain metrics, though reports sometimes differ^{101, 108}.

Thermodynamic studies on the adsorption and desorption of thiols on gold surfaces have shown that the bond is reasonably strong (~25-50kJ/mol), and desorption at room temperature as a disulfide is not kinetically feasible²⁷. Chemical degradation of the coating material, particularly through oxidation of the sulfur has been shown to cause decay of the coating and will be addressed in a subsequent section¹⁰⁹⁻¹¹². The precise nature of the sulfur-gold bond and the reaction which occurs during formation is

not well known^{27, 28, 113-115} despite decades of research, and is even less well known for particle systems than for planar gold surfaces¹¹⁶. Even concepts such as the fate of the thiol hydrogen after bond formation are debated in literature^{27, 113, 117, 118}. Since functionalities such as disulfides, thioethers, and thiones are capable of forming metal-sulfur bonds, the presence of sulfur bound hydrogen is not necessary for bond formation. The bond structure is often described as a reaction involving charge transfer to the bound metal atoms in which oxidative addition to the metal occurs¹¹⁹⁻¹²¹:



And likely arises from experiments involving electrochemical desorption as measured by cyclic voltametry¹²⁰, in which case the following reaction is generally accepted to occur^{27, 114, 119, 120}:



In addition, that fact that the formation of these monolayers can occur in the gas phase without oxygen to act as an oxidizer and the existence of data suggesting the formation of a charged thiolate from several techniques bolsters this theory^{121, 122}. High resolution XPS analyses of gold surfaces with bound sulfides¹²³ and thiols¹²⁴ indicate no evidence to support the theory that the gold surface is ionized upon reaction to form the thiolate. Other XPS reports show the possibility of a small contribution from gold atoms with shifted binding energies; however this could not be unambiguously separated from effects due to atomic positioning¹²⁵. Use of theoretical models to examine the dipole moments and bonding behavior suggests that the bond nature is primarily covalent with only small dipole moments. This model provide a good explanation for the apparent charge on the thiol, but does not address the lack of binding energy shift on gold in XPS

even when nanoscale particles are used¹¹⁴. Some theories for this suggest that the combined effect of the decreased binding energy of the surface atoms (due solely to positioning) and increased binding energy due to oxidation negate each other since both shifts are similar in magnitude but opposite in sign¹²⁴. Additional high resolution XPS work on extremely small (1-3nm) particles showed certain small binding energy shifts in the peaks corresponding to both the surface and bulk gold atoms^{114, 126}. These observations lead to the development of theories that the observed binding energy differences may involve a potential change in oxidation state, interactions involving photoelectron emission from small particles (known as final state effects), charge transfer involving the core atoms in addition to the surface gold atoms during bond formation, or a combination thereof.¹²⁶⁻¹²⁹ Despite all of this intense analysis, it is clear that this topic is and will continue to be debated in literature. It may be some time before the interactions of sulfur with gold are fully elucidated.

Measurements of Adsorption

Measurement of the surface density of PEG chemisorbed onto gold surfaces has been reported and varies considerably in literature (Table 3-2). Though higher values are occasionally reported, typical values range from under 0.1 molecule/nm² to 5 molecules/nm² (0.2 to 10nm² molecular footprint) as shown in Table 3-2 and Figure 3-1. Measurement of adsorbed PEG density is frequently given only cursory consideration, and assumptions about the behavior of reagents and adsorption processes are commonplace. This specific lack of characterization is not frequently cited in literature¹³⁰, though the lack of nanomaterial characterization in general is often cited and is gaining attention^{131,132}. A brief examination of the methods used to determine the coating density and many of the limitations of the techniques can

illustrate the complexity of these measurements (Table 3-4). These methods can be used for two major analysis schemes: direct measurement of the adsorbed species and depletion adsorption measurements. Though discrimination between adsorbed species and free adsorbate is sometimes possible, direct measurement of an adsorbate surface density almost always involves separation of the coated particles for analysis of the adsorbate concentration on the particle. This technique is not suitable for systems where equilibrium exists between bound and unbound adsorbate; however for systems involving chemisorption (such as gold surfaces and thiol adsorbates), this is less of an issue since chemisorbed species will not readily desorb when the equilibrium adsorbate concentration is decreased. In contrast with direct measurements, depletion measurements involve adding particles to a medium containing a known adsorbate concentration. The adsorbate concentration in the medium after particle removal is measured to determine the quantity adsorbed by the particles. In some cases where both primary chemisorption interactions and secondary interactions (typically weaker physisorption) occur, depletion measurements are sometimes faulted for misleadingly high adsorption densities¹³⁰.

The most common techniques used for quantification of PEG adsorption density are colorimetric methods and gravimetric analysis (such as QCM and TGA). Colorimetric methods are advantageous due to simplicity, specificity for the adsorbate, and frequently sensitivity. However, colorimetric methods are influenced by common interfering compounds/impurities, and their high specificity can be a double-edged sword (as will be detailed later in this section). Gravimetric analysis is advantageous due to its sensitivity to all adsorbed species, and the fact that both total gold mass and

the total coating mass can be measured simultaneously. The major drawbacks involve a comparatively larger sample size, the requirement for thorough cleaning of the particle suspension, and the nonspecific sensitivity to all volatile/combustible species adsorbed. The specifics of adsorption measurements using gravimetry/TGA and certain colorimetric methods will be detailed in later sections.

Another common metric used as an indicator of PEG adsorption is the quantity of PEG required to achieve maximum coating density (saturation). Surface saturation is typically indicated by some type of indirect method, often the elimination of salt induced aggregation as monitored visually or by UV/Visible spectroscopy. Other comparative or qualitative methods such as zeta potential and particle size increase by dynamic light scattering are also encountered. Due to far smaller sampling requirements, comparative techniques are useful in many instances where quantitative techniques are impractical, provided that the data they produce accurately reflects the condition of the coating. Though convenient, the aforementioned techniques are highly susceptible to a variety of common interferences (many of which will be detailed later in this chapter) and often lack the sensitivity required to adequately describe the system of interest.

Most of the aforementioned quantitative techniques require relatively large quantities of concentrated and/or prepared gold suspensions for adsorption measurements. This limitation introduces the next issue involving measurements of adsorption: price. The cost both monetarily and in preparation time can be significant for these measurements due to the material cost and/or synthesis requirements. For example, at current (2012) pricing, commercially produced spherical gold particles cost as much as \$80/mg for small quantities. Gravimetric analysis of one coated sample with

using these particles (assuming a 10mg sample size before cleaning) would cost approximately \$500.

Measurement of specific surface area is another issue that can be both material and time consuming but necessary for accurate adsorption measurements. Surface area analysis of the gold particles by traditional methods such as gas-sorption (BET) is perhaps even more expensive to perform due the vast amounts of dry sample required. For this reason, BET is rarely performed if at all, as single measurements of surface area can reach into the thousands of dollars per sample. The vast majority of surface area measurements or estimates are made based on ensemble particle size analysis (most often DLS) or image analysis assuming spherical and/or monodisperse particles. For spherical and monodisperse particles, these estimates are likely to be close to the actual specific surface area; however many of the particles synthesized (particularly by the ubiquitous citrate reduction method) are non-spherical at certain size ranges. Some consideration has been given to particle shape by at least one group¹³³⁻¹³⁵ for faceting on smaller particles. To illustrate this issue, measurements based on image analysis were performed using techniques capable of taking certain components of particle shape into account (methods are detailed in Appendix A). These methods accounted for differences in specific surface area due to anisotropy as well as the distribution of sizes. A finite element analysis method was the primary method used to estimate specific surface area. An example of how particle anisotropy can cause differences in specific surface area is shown in Table 3-1. In the particles produced by the standard citrate method, particle anisotropy caused the specific surface area to be at least 20% higher than the value determined by assuming spherical monodisperse particles. This number

is expected to increase dramatically as the particle size increases due to increasing anisotropy. For comparison, a suspension of higher sphericity particles of similar size were analyzed and showed little to no difference between the various methods used to determine specific surface area.

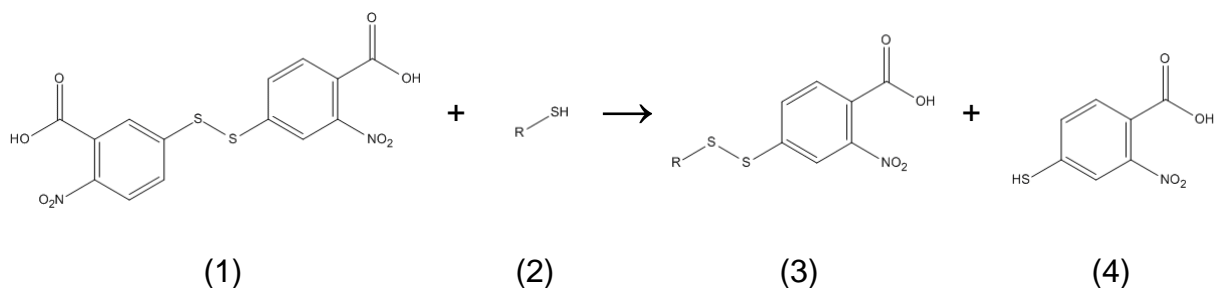
Several common issues involving the behavior of PEG adsorption onto gold particles and measurements of adsorption will be addressed in this section, including:

- Adsorption is assumed to occur with 100% efficiency until saturation is reached.
- Errors in or limitations of measurement techniques frequently overlooked.
- Indirect metrics such as zeta potential neutralization and prevention of salt induced aggregation are frequently used to determine density at surface saturation.
- All excess PEG and synthesis residues are assumed to be removed by centrifugation or dialysis.
- The presence of excess polyethylene glycol in the particle supernatant is frequently overlooked.
- PEG is assumed to readily and/or completely displace many other adsorbed species (or partial displacement is assumed to occur).
- Little to no inactive adsorbates or impurities are assumed to be present in PEG reagents.
- Addition of PEG at a ratio of 4 molecules/nm² is necessary and/or sufficient to fully coat the gold particles.

Colorimetric methods

Colorimetric methods are an attractive quantification technique since they are relatively easy to perform, typically do not require specialized equipment, and can be very sensitive. Colorimetric analysis of thiolated PEG adsorbates can be accomplished using two major schemes: analysis of a label or analysis of a reactive (adsorbing) group. Analyses of labeled PEG reagents are typically performed through a bifunctional PEG molecule, most often a thiol-PEG-amine^{15, 141}. Quantification of PEG concentrations in this case is performed with an assay for amines or attachment of a chromophore or fluorophore to the adsorbate's amine group. This technique is an

indirect method, particularly when the adsorbate of interest is not the amine terminated PEG compound. Additionally, the number and uniformity of the two functionalities on the polymer chain, the availability of the label group, and interfering impurities may impact the measurement quality. It has also been noted in literature that the presence of a label, particularly if a chromophore or fluorophore is attached, may impact the coating density. This technique was not utilized for quantification of PEG density, and will therefore not be detailed here. The second major method involves quantification of the PEG reagent by quantification of the reactive (thiol) binding group. The most prominent method for this purpose involves the use of Ellman's reagent¹⁵⁷, which is a thiol reactive symmetric disulfide (compound 1 below). In the presence of a thiol (compound 2 below), Ellman's reagent cleaves to form an asymmetric disulfide product (product 3 below) and thionitrobenzoic acid (product 4 below) according to the following reaction:



Ellman's reagent has a near UV absorbance band at approximately 324nm, but does not have a significant visible absorption band. The compound is therefore initially colorless to pale yellow. After reaction with a thiol, the principal colored product, a dianion of thionitrobenzoic acid, exhibits a visible absorption at approximately 407nm, and is yellow in color. Quantification is performed with a spectrophotometer at a wavelength of 412nm, where a molar extinction coefficient of $14150 \text{ M}^{-1}\text{cm}^{-1}$ is typical for dilute solutions^{158, 159}. An example of the absorption spectra of the reagent and the

product mixtures with varying concentrations of a thiol can be seen in Figure 3-3. The reagent has poor solubility in water and must be buffered at a slightly alkaline pH for use; however excessively high pH values must be avoided. For all experiments performed in this work, reagent pH control was maintained with a phosphate buffer at a pH of 8 where little variance in extinction coefficient is observed¹⁵⁸. Response curves using cysteine (reference) and the PEG-thiol reagent were performed at each analysis and demonstrated good response uniformity over time. Experimentally determined limits of detection are in the micromolar region under typical conditions.

There are several important considerations when using Ellman's reagent to quantify thiols for adsorption measurements:

- The chemical composition of the sulfur group
- The type of calibration performed.
- The presence of impurities in the reagent

The chemical composition of the sulfur terminal group on the PEG chain is a critical determiner of the assay effectiveness. The terminal thiol group can be oxidized to form disulfides and various other oxidized groups; however the assay only responds to reduced thiols. Although less likely, the presence of thioethers, typically formed when certain synthesis procedures are used, is another assay nonreactive possibility. Though nonreactive to the assay, disulfides and thioethers may still adsorb to gold while the sulfonates will not. These chemical functionalities can impact the results of a depletion type adsorption measurement as outlined in Table 3-5 and Figure 3-2. Common byproducts of synthesis and reagent degradation, such as SO₂ and H₂S are also assay reactive, but may or may not adsorb to the particle surface. The standard selected for these types of measurements is important, and use of the thiolated PEG reagent as a

reference should be done cautiously. Typically, a water soluble thiol containing compound such as cysteine is used for calibration purposes. It is important to compare the assay response of the thiolated PEG to a stable reference material as demonstrated in Figure 3-4. Clear differences between two sources of the same PEG reagent are evident as well as virtually no assay activity after intentional degradation of one reagent. Even though the degraded reagent showed a nearly negligible response to Ellman's reagent, it was still capable of adsorbing to gold surfaces without requiring an inordinate excess of reagent (adsorption maximum achieved at approximately 2-3 times the quantity required when the reagent was fresh as determined by electrophoresis and sedimentation). The influences of these interferences on the adsorption isotherms determined by colorimetric (and fluorimetric) depletion methods are shown in Figure 3-2.

A representative adsorption isotherm of thiolated PEG on nom. 20nm gold particles is shown in Figure 3-5. All isotherms measured demonstrate a classical high affinity shape with no detectable concentration of PEG remaining in solution prior to monolayer formation.

Sedimentation methods

Sedimentation is a useful technique for characterizing the adsorption of PEG onto the surface of gold particles. The theoretical background used for the analysis of applicable coatings was described in detail in chapter two. The presence of a coating adsorbed onto the surface of gold particles significantly changes both the net density and size of gold particles, which in turn alters the sedimentation velocity. For the vast majority of gold particles and coatings of interest, the combination of increased drag (increased size) and decreased net density results in a decrease in sedimentation

velocity relative to the parent particle (Figure 2-12). Variances in the adsorbate surface density result in changes to the adsorbate surface structure, which in turn alter the particle sedimentation velocity. The relationship between coating density and sedimentation velocity relative to a core particle of 20nm are shown in Figure 3-6. The data obtained for these particles (and all others analyzed) demonstrated an exponential decrease in sedimentation velocity until a minimum value was obtained at coating saturation. This translated into an exponential increase in calculated coating thickness until a maximum value was obtained at saturation. One major limitation of this technique is that both the coating thickness and particle (coating) density change simultaneously. This results in a set of possible solutions rather than a discrete point (unless the coating density is precisely known), which is shown as a gray region in Figure 3-6B. For coated nanoscale gold particles with a relatively thin and low density coating, this region of uncertainty is typically small with respect to the computed thickness at an estimated density of 1.1g/cm^3 (Figure 3-6B, Figure 2-13). Another major limitation that can severely decrease the applicability of this technique involves fouling of the gradient with unbound PEG. As previously established, the thiolated PEG demonstrates a very high surface affinity for gold particles (Figure 3-5). When an uncoated or partially coated particle passes through a gradient with even trace quantities of unbound PEG present, some of the PEG adsorbs and alters the sedimentation properties of the particles. The effect of this buildup can be seen in Figure 3-7 where uncoated particles were analyzed after each sample in a series of coated particles. A marked decline in the sedimentation velocity of the uncoated particles occurs immediately following the introduction of a suspension containing a small quantity of unbound PEG. This specific limitation

prevents the analysis of PEG coated particles with incomplete coverage from being analyzed correctly once samples with excess PEG concentrations have been analyzed. Since it can be difficult to establish this prior to analysis, the use of this method is severely limited. One method to monitor gradient fouling is to include an uncoated particle between each coated sample to monitor for any adsorbate buildup in the gradient (as described previously and demonstrated in Figure 3-7). While this limitation presents a roadblock to certain analyses, it also presents an opportunity as a sensitive technique for analyzing trace residual thiol-PEG concentrations.

Sedimentation velocity analysis of coated particles with varying core particle sizes was used to probe whether or not the coating thickness is significantly size dependent. Some reports have shown both theoretical and empirical data for various adsorbates that the sharp radius of curvature in spherical nanomaterials can result in higher coating densities with decreasing particle size¹⁶³. The theoretical cause of this increase is related to the greater available volume for the adsorbate to occupy with increased distance from the surface as well as increased accessibility to the surface atoms. Sedimentation data collected during the course of this work spanned particle sizes from 10nm to 70nm. Data gathered from the particles both before and after coating was used to compute the relative sedimentation velocity of the coated particle, which was then fit to the theoretical curve (Equation 2.3) using least squares with the coating thickness as the independent variable and a fixed coating density of 1.1g/cm^3 (Figure 3-8). A noticeable discontinuity in the curve occurs with particles sizes of 30nm and higher. This was attributed to the decrease in sphericity observed in the standard citrate synthesis method (discussed in chapter 2). Higher sphericity particles with sizes of approximately

30nm and 70nm were also analyzed, and these particles continued to follow the theoretical curve. Calculation of the best fit for high sphericity particles yielded a coating thickness of 6.1nm, while the fit for all particles yielded approximately 7nm. Iterative fitting calculations with both coating size and coating density (bounded by the density of water and the density of solid PEG) as independent variables for the high sphericity particles yielded a better fit at a density of 1.0g/cm^3 and a coating thickness of 6.0nm. Individual calculations of coating thickness showed that the error in these measurements was approximately $\pm 1\text{nm}$ for the high sphericity particles at a coating density of 1.1g/cm^3 . At least over the range of sizes less than 70nm, no statistically significant trend was observed in the coating thickness as a function of the core particle size. Though not shown, differences in coating thickness measured by sedimentation were evident for different reagent sources and particle synthesis chemistries.

Electrophoresis

Electrophoresis can be utilized in a manner similar to sedimentation for characterizing the PEG coating on gold particles. Attachment of an uncharged coating such as PEG to the charged surface of a gold particle can largely neutralize its zeta potential (Figure 3-24). The net effect of electrophoretic mobility and drag on the particle migration when under the influence of an electric field can be indicative of the coating condition. This in turn can be used to characterize (qualitatively at a minimum) the coating applied to gold particles.

The earliest reference to electrophoretic mobility dates back to 1809 where Reuss discovered that charged clay particles migrate under an electric field¹⁶⁴. The first equation to describe this mobility was developed by Helmholtz in the late 1800s¹⁶⁵, and

later modified to include the permittivity in the Smoluchowski equation¹⁶⁶, which is still widely used:

$$\mu = \frac{\varepsilon\varepsilon_0\zeta}{\eta} \quad (3.1)$$

At the time, consideration was not given to the structuring of the ions around the charged particle until Gouy's work several years later^{167, 168}. To address some of shortcomings of the Smoluchowski model (valid for a very thin double layer), a model valid at the opposite extreme in double layer thickness was proposed by Hückel¹⁶⁹:

$$\mu = \frac{2\varepsilon\varepsilon_0\zeta}{3\eta} \quad (3.2)$$

The incorporation of considerations related to ionic structuring (double layer) and the behavior of these ions during electrophoresis is important in modeling the forces acting on a particle during electrophoresis. Like sedimentation, electrophoresis involves a balance of forces, as illustrated in Figure 3-9. The major forces include¹⁷⁰:

- The electrostatic attraction force of the charged particle to the electrode of opposite charge. This is the primary driving force exerted on a charged particle.
- The drag force exerted on the moving particle as it passes through a fluid medium. For spherical particles in laminar flow systems with a low Reynolds number, this can be modeled as Stokes drag.
- The electrophoretic retardation force. This force is generated due to the migration of ions in the electrical double layer with an opposite charge to the particle surface which surrounds the particle. Ions with a charge opposite to the particle surface charge can associate with the particle surface as part of the ionic double layer. These ions then migrate in the opposite direction of the particle, retarding the particle's migration.
- The retardation – relaxation force. This force arises from the distortion of the double layer due to the applied electric field during particle migration, as shown in Figure 3-9. The particle is no longer the center of charge in the local ionic environment.

Though earlier references exist^{164, 171, 172}, the advent of modern electrophoresis is typically attributed to Tiselius and his self-named apparatus from the 1930s¹⁷³.

Electrophoresis remained a relatively unknown technique until the mid 1950s when Oliver Smithies introduced gel electrophoresis based on starch gels¹⁷⁴. Separations of small molecules and proteins using a polyacrylamide gel, which remains widely used today, were first described in 1959 by Ornstein and Davis^{175, 176}. Separations of larger molecules, such as DNA, via agarose gel electrophoresis was not introduced until over a decade later in 1972 by Sharp, Sugden, and Sambrook¹⁷⁷. Gel electrophoresis remains a staple technique to this date for analytical separations of biological macromolecules.

In gel electrophoreses, samples are placed into a gel medium and an electric field is applied across a gel. The aqueous phase in the gel and the solution surrounding the gel slab is typically a buffered electrolyte. The charged molecules in the sample begin to migrate toward the electrode of opposite charge at a rate related to the molecular charge and size, depending on the gel employed. The gel matrix serves to retard the migration of molecules based on size (when sieving gels are used), and also minimize convection and bulk fluid motion during analysis. When electrophoresis is performed within a porous medium such as a gel, additional electrokinetic phenomena occur. Most notably, electroosmosis is induced due to charged surface groups on the gel or porous material. In addition, interactions between the migrating particles with the gel medium are also possible. Electroosmosis occurs when the charged double layer formed on the charged surface of a capillary or porous material begins to migrate due to an applied electric field. The fluid in the capillary or porous material is drawn along with the

migration of the ions in the layer. This results in a plug flow through the porous medium rather than a parabolic flow profile as would be the case for pressure induced flow (minor edge effects do occur). Typically in gel electrophoresis, the charge on the gel is anionic, which results in migration of fluid to the anode.

The addition of an uncharged layer of PEG to the charged surface of the gold particles causes the surface potential to be rapidly masked. This negates the majority of the electrophoretic component of the mobility, leaving the electroosmotic flow to be the primary driver of the observed particle mobility. For the same core particle, differences in the density of the PEG coating result in differences in coating thicknesses (Figure 3-6, Figure 3-23, Figure 3-26) and consequently differences in the distance between the charged surface of the particle and the shear plane (where the electrophoretic mobility/zeta potential is measured). This decrease in distance to the shear plane results in a higher effective charge, which in turn results in increased coulombic attraction to the oppositely charged electrode. In electrophoresis, this ultimately results in observed mobility counter to the electroosmotic migration. An illustration of the origin of this behavior is shown in Figure 3-11. Although this behavior (neglecting electroosmosis) can be observed by dynamic light scattering (Figure 3-24), the ability to time resolve analyses in electrophoresis provides far more precise data. Under these conditions, differences in the electrophoretic mobility (zeta potential) are relatively small, and the variance in measurements made by dynamic light scattering typically exceeds the precision required for this type of analysis.

Electrophoresis was utilized for comparative analysis of PEG coated samples throughout this work. Some of the principal advantages of this technique include: very

small sample requirements, elimination of the issue involving interfering adsorbate buildup in sedimentation (Figure 3-7), simultaneous analysis of multiple samples, the ability to segregate particles based on charge differences, the ability to analyze small particles efficiently, and the ability to time-resolve some analyses. Interpretation of this data must be done with attention given to conditions which may change the particle or coating charge, as these may interfere with the analysis of the property of interest. For this reason, sedimentation is an excellent complementary technique to electrophoresis, as the sedimentation velocity is independent of the particle charge and can be used to confirm the interpretation of electrophoresis results (provided that gradient fouling is not an issue).

The migration of 20nm PEG coated gold particles with varying PEG densities in a 0.7% agarose gel at 100V using a 1x TRIS-acetate-EDTA buffer (TAE) system (pH 8) is shown in Figure 3-10. Note that throughout this work, the sign convention for mobility is positive for migration toward the negative electrode (apparent positive particle charge). A low gel density (0.7-1%) was selected to provide sufficient resistance for separation without excessively retarding particle migration. To verify that adsorption of TAE buffer components were not influencing the migration of the particles, a phosphate buffered saline electrolyte with identical conductivity to the TAE buffer was prepared. Testing of a variety of coated gold particles that spanned the chemistries anticipated for both PEG coating and protein binding analyses under these conditions indicated that the buffer composition did not influence the final result. This confirmed that the primary reason for the migration of coated particles toward the anode was due to electroosmosis rather than interactions of the particle surface with the buffer. Over the range of most coating

densities (>10-20% of maximum), the migration of the particles due to electroosmosis outweighs the electrophoretic mobility of the particles, causing migration toward the anode. Below this coating level, particle migration toward the cathode increases rapidly before the particles begin to aggregate and can no longer enter the gel pores. In order to achieve optimal migration velocity in electrophoresis and adequate surface area for complementary adsorption measurement techniques, particles of 20nm were used in most cases, though larger particle sizes (sizes up to 50nm tested) were easily able to migrate into the gel.

In addition to the capabilities of analyzing the time dependent coating density, electrophoresis is also capable of separating particles of different sizes as illustrated in Figure 3-12 with PEG coated particles. In this case, the differences in charge to size ratio, drag, and resistance due to the gel result in changes to the net mobility. If a more rapid analysis is desired, a charged polymer layer may be added to increase the electrophoretic mobility while maintaining particle stability.

Ultraviolet absorption methods

Most organic compounds and many inorganic compounds strongly absorb in the near ultraviolet region (190-380nm). It is for this reason that many chromatographic techniques, most notably HPLC, utilize UV detectors for sensitive general detection of organics as they elute. UV absorption is primarily driven by lower energy (valence) electron transitions within a molecule. These transitions are pronounced for unsaturated systems in the visible and UV, but are also present in heteroatomic and saturated functionalities at lower wavelengths. This high degree of sensitivity for a broad range of compounds was investigated as a potential means of quantifying and detecting dilute PEG concentrations. The near UV absorption spectrum of un-functionalized hydroxyl-

terminated PEG and the thiolated methoxy PEG used for this study are shown in Figure 3-13. PEG demonstrated very strong absorption at wavelengths under approximately 220nm. Although the absorbance maximum of PEG (and consequently the most sensitive wavelength for quantification) is expected to be around 180-185nm (Table 3-6), a practical limitation of 190nm exists due to the absorption of water. The UV response to varying concentrations of PEG is nonlinear even in dilute concentrations, as shown in Figure 3-15. Over short ranges, particularly at low concentrations, the curve may be linearized with little to no error in measurement. It can be seen from Figure 3-15 that sub-micromolar concentrations of PEG can be measured by this technique, and detection down to 0.5 μ M is possible under ideal conditions. The utility of this technique is restricted by two primary limitations: the presence of background and the fact that absorbances are less unique to each molecule or functionality (unlike vibrational spectroscopic techniques such as IR and Raman). The absorption spectra of some common and potentially interfering compounds are shown in Figure 3-14. The spectral overlap in these samples with PEG (Figure 3-13) necessitates thorough washing of any suspension used to reduce or remove background from the salts used in synthesis. Suspensions can be effectively cleaned of background by centrifugation, dialysis, or diafiltration.

The presence of an unexpected peak at 235nm was observed in all thiolated PEG reagents analyzed. This peak and its intensity relative to the other wavelengths do not correspond with any functionality expected to be found in the specified structure (Table 3-6), and did not exactly match the absorbance maximum of hydrosulfides or sulfides (which occur at 230nm as shown in Figure 3-14).

Adsorption measurements were performed by depletion using UV absorption to quantify the amount of adsorbed PEG. Prior to coating, all particles were thoroughly cleaned of residual salts by diafiltration, which resulted in a minimum theoretical removal efficiency of 99.999%. The background UV absorbance due to trace residuals was analyzed in the cleaned particles for the purpose of background subtraction, and was extremely low. The cleaned suspensions were then mixed with a quantity of thiolated PEG, and the particles removed by centrifugation. The near-UV absorption spectra of the supernatants were then measured, and the equilibrium concentration of PEG determined by comparison to standards as shown in Figure 3-15. Although certain changes in absorption measured by this method tracked with particle size, spectral changes which were inconsistent with a simple decrease in concentration of a pure reagent were observed. The most prominent difference was that the absorption spectra of the supernatants did not exhibit the unknown peak at 235nm as previously observed. To verify that this was not caused by an interaction with trace residuals in the supernatant, a quantity of PEG was added to the cleaned supernatant, supernatant from the particles as prepared, and deionized water. With background subtraction, the absorption spectra of the PEG and supernatant mixtures were identical to the PEG reagent in deionized water (Figure 3-16), indicating that the previously observed decrease in absorbance at 235nm was not generated by interaction with synthesis byproducts. This then indicated that the peak disappearance was due to interactions with the particles. To verify that this phenomenon was not solely related to the type of particles used in this study and that residual small particles were not contaminating the spectrum, a cleaned glass slide was sputter coated with a thin layer of gold and was

allowed to react with an excess quantity of PEG-thiol. The slide was removed after reaction with PEG, and the near-UV absorption spectrum of the remaining solution was analyzed. As with the particles, no absorbance peak at 235nm was present Figure 3-17. These results indicate the possibility of an adsorbing contaminant present in the commercial PEG reagents for two major reasons: The 235nm peak is rapidly removed at PEG concentrations above what is required for surface saturation, and this change only occurs when the PEG reagent is in contact with a gold surface (regardless of type). This behavior represents a severe limitation on the utility of UV absorption for quantitative analysis of PEG adsorption. Although initial adsorption results did track correctly with particle size, the presence of this interference confounds the analysis. For this reason, UV absorption methods were limited to use in detection and qualitative analysis rather than quantitative analysis of PEG concentration. It may still be possible to use this technique provided that this interference can be predicted or eliminated.

Thermogravimetric analysis

Thermogravimetric analysis is a simple but useful technique for characterization of adsorbed PEG densities, particularly because both the particle mass and coating mass can be directly measured. In thermogravimetric analysis, a coated particle sample (dry) is heated until the organic coating burns off while the sample mass is continuously monitored. The mass loss characteristic of PEG decomposition or combustion represents the total coating mass, and the final mass is the uncoated particle mass. The fraction of coating mass loss relative to the total initial particle mass or final particle mass can then be used to calculate the coating density (Figure 3-18). Many modern TGA instruments are equipped with a microbalance, making analysis of milligram size samples typical. It is important though to ensure that the mass change is significant

enough to be reliably quantified by TGA, and Figure 3-18 can be used to estimate the minimum sample quantity with a known mass loss threshold.

The TGA curves for thiolated PEG under inert (nitrogen) and reactive (air) atmospheres are shown in Figure 3-19. Under an inert atmosphere, PEG exhibited a rapid single stage decomposition beginning at approximately 310C. Under an oxidative atmosphere, the onset of decomposition was reduced to approximately 240C and a possible second decomposition stage at approximately 400C with less than 5% of the mass remaining may also occur. Since sodium citrate and other associated synthesis byproducts were anticipated to be the only other significant interfering/background species, sodium citrate dihydrate was also analyzed under the same conditions as shown in Figure 3-20. Sodium citrate dihydrate underwent a multi-step decomposition beginning at approximately 160C with the loss of water and continuing with three other stages at approximately 310C, 430C, and 840C.

Because TGA does not discriminate between coating material and any other volatiles present in the sample (such as water, residual synthesis reagents, residual/unbound PEG, etc.), thorough cleaning and drying of the suspension is necessary to remove these potentially interfering components. Some popular synthesis methods involve the use of phase transfer catalysts¹⁷⁹, which may remain adsorbed to the particle surface post synthesis in a manner similar to CTAB on gold nanorods¹⁸⁰. Competition with or coadsorption of other compounds on the surface of the particles can significantly alter the PEG coating density or increase the quantity of adsorbed impurities on the particles. One key consideration is the molecular weight of these adsorbed impurities. The majority of these potentially interfering adsorbates have a

relatively low molecular weight. Even if the surface density is relatively high, particle surfaces completely saturated with small molecules such as sulfides, thioacetic acid, etc. typically represent an immeasurably small percentage of the total particle mass. Even larger molecules such as CTAB at a relatively high surface density on all but the smallest particles will only represent at most a few percent of the total particle mass (ex. with 4 molecules/nm² density coating on 20nm particles, CTAB would be <3% of the total particle mass). This is beneficial if the sole concern is the larger PEG adsorbate molecule. However, the presence of impurities on the surface may not be reliably detected if the adsorbate molecule is relatively small or a low percentage of the total coating mass. The effects of these impurities, though small at larger particle sizes, can be significant at the sizes of particles typically prepared with phase transfer catalysts or other stabilizing adsorbates (<5nm). A particle coated with the phase transfer catalyst used in one popular method¹⁷⁹ at a surface density of 4 molecules/nm² on 3nm particles would represent nearly 25% of the particle mass. Although these impurities themselves may not be easily detected and quantified by TGA in some cases, the effects of the impurities on the coating density can be measured in certain circumstances as shown in Table 3-7. Serial adsorption of impurities such as CTAB results in higher mass losses when added after the formation of the PEG coating, indicating the adsorption of a small quantity of CTAB. If the presence of these compounds were not known beforehand or were overlooked, this data would be misinterpreted as higher levels of PEG adsorption. In the opposite case where CTAB is added to gold particles first, nearly complete elimination of PEG binding occurs, though a significant mass loss is still observed.

The presence of inorganic salts and other nonvolatile and noncombustible compounds present another potential interference by artificially inflating the final mass of the sample, which is taken to be the total mass of gold in the calculation of surface density. This is less of an issue since other techniques can be used to correctly determine the quantity of gold used in the experiment (such as ICP or AA).

The surface density of coated gold particles was determined by TGA using the aforementioned procedures. Samples were thoroughly washed by diafiltration with a minimum 99.991% calculated removal efficiency for soluble residues. For suspension samples containing higher concentrations of impurities in the medium, additional washing was employed to minimize interference from these species (minimum theoretical removal rate was 99.9998%). In most of these cases, samples of the diafiltration permeate (volume equivalent to the volume of particle concentrate) was also analyzed to determine the mass of any remaining unbound adsorbate. These washed samples were then oven dried in a crucible prior to analysis to remove excess moisture. After analysis, the mass change relative to the particle mass (a representative example is shown in Figure 3-21) was used to calculate the coating density of the particles as shown in Figure 3-18. Analysis of the uncoated particles (Figure 3-22) showed no significant mass change over the entire temperature range, indicating that the cleaning procedure was effective at removing interfering concentrations of impurities. Samples of the permeate showed little to no mass loss (0.005mg loss observed in only one case and represented 0.1% of the coated particle mass), also indicating that the cleaning process was effective. Little to no mass loss observed prior to combustion of the coating confirmed that the suspension samples were adequately dried prior to analysis.

Other measurements

Aside from the aforementioned qualitative and quantitative measurements of adsorption, measures of particle charge and size by dynamic light scattering and imaging of the coating by TEM were also performed.

As indicated by the change in sedimentation velocity and the accompanying coating thickness calculations, the coating thickness increases exponentially with increasing adsorbate concentration until a maximum is reached. Unlike sedimentation where the coating thickness is dependent on density (among other factors), mean migration due to Brownian motion is density independent. In a trend similar to sedimentation, the particle size measured by DLS increased exponentially until a maximum value was reached (Figure 3-23). The measured values of coating thicknesses obtained by DLS are expected to be slightly higher than sedimentation since DLS measures the hydrodynamic radius at relatively low shear. By contrast, thickness measured by sedimentation involves the use of a hard sphere equivalent coating thickness for calculation purposes. Neutralization of the electrophoretic mobility (zeta potential) due to incorporation of an uncharged polymer layer is another phenomenon that occurs on coating, as discussed previously (Figure 3-11). Aside from single measurements of PEG coating thickness increase, DLS was not used in this work as a primary means of quantifying coating thickness or qualifying coating condition. The typical variance in DLS measurements presents a significant limitation to its use in this capacity, though DLS is a useful technique for providing density independent sizing data.

Transmission electron microscopy was used to image the PEG coating on the particles. The thin, low density PEG coating does not provide significant brightfield

contrast, so a negative staining technique was used to improve contrast. Negative staining involves treatment of a sample with heavy metal ions that form a dark background film. Since the stain does not significantly penetrate or adhere to the PEG coating, the coating appears bright in contrast to the darkened background. Samples of uncoated and PEG coated particles were provided to Kerry Siebein for staining and imaging. Images of the particles before and after coating are shown in Figure 3-25. A light colored halo, present only in the coated sample, can be seen around the particles in Figure 3-25B. The dimensions of the coating (dried) range up to 4nm in thickness, and some heterogeneity in thickness and contrast within the coating were observed.

Surface Conformation

Surface conformation of the polymer coating is one of the determining factors in particle stability and resistance to protein adsorption. The desired structure of the adsorbate on the surface is a densely packed end-grafted polymer layer to provide steric repulsion of other particles and biological macromolecules, though some argue that a less dense coating may be beneficial¹³⁰. The final PEG conformation is a function of the surface density, adsorbate size and structure, and the particle radius of curvature.

The adsorbate structure on the particles surface was determined by combining the aforementioned adsorption and coating thickness measurements. Assuming radial symmetry, the adsorption density was used to determine the adsorbate footprint and sedimentation analysis to determine the coating thickness. These results are illustrated in Figure 3-26 for spherical gold particles of approximately 20nm in size. Figure 3-26 clearly shows the transition of the coating to a dense, brush type conformation as the adsorbate concentration is increased to saturation. At low adsorbate concentrations, the data indicates that the polymer exists in a 'mushroom' type conformation. Additional

adsorption decreases the available volume for the polymer molecules to occupy, driving the polymer chains to extend farther from the surface to accommodate additional adsorbate.

Preparation and Properties of PEG Coated Particles

Coating gold surfaces with thiol monolayers is a relatively straightforward process since adsorbates rapidly bind to the surface with no special preparation. This behavior remains the same when the surface becomes a particle in suspension; however special consideration must be given to preserve the stability of the suspension during this process. Although the formation of the thiol to gold bond occurs almost immediately upon mixing (resulting in dense coverage of the surface)²⁷, it may be advisable to allow the coating to equilibrate for several hours to one day with excess reagent prior to use, as rearrangement of thiols during competitive adsorption occurs over the course of hours to one day (data not shown). Conventional wisdom involving the formation of self assembled alkanethiol monolayers suggests 12-18h for monolayer formation to maximize reproducibility²⁷. Early work involving self-assembled alkanethiol monolayers¹⁸¹ indicated that the initial formation of the thiol based monolayer occurred extremely rapidly; however small changes were observed up to several days after coating. It is important to note that these layers differ considerably from the polymeric systems of interest in this work, as alkanethiol monolayers form highly ordered layers on planar substrates while the polymers and the particle surface curvature limit the ability of the adsorbate from forming such structures^{27, 182, 183}.

As indicated by stability observations recorded when adsorption isotherms were measured, particles become unstable at sufficiently low PEG concentrations using as-prepared suspensions (typically less than 0.1 molecules/nm²). The addition of sub-

optimal concentrations of PEG results in charge neutralization and/or charge patching on the particle surface, rendering the particles' native electrostatic repulsion ineffective before they become sterically stabilized. Residual salts present in the medium from synthesis provide an additional driving force through charge screening. It is therefore important that the coating is applied in a manner involving rapid mixing with addition of particles to PEG reagent in order to minimize aggregation on mixing. Reversible aggregation on mixing was observed in some limited cases where, although the quantity of PEG reagent used was well in excess of the minimum requirement for surface saturation, slow mixing resulted in aggregation (much of which was reversible) as seen in Figure 3-27. With sufficient reagent concentration and vigorous mixing, the water soluble non-ionic PEG easily disperses in the particle suspension and is capable of sterically stabilizing the particles without causing aggregation. Another potential point of concern at low PEG concentration is an apparent hydrophobization of the suspension. At concentrations below the point of surface saturation, the particles exhibit an apparent hydrophobic nature as indicated by partitioning at the air-liquid and liquid-container interfaces (in hydrophobic polymer containers). Apparent partitioning at the air-liquid interface was also observed when PEG coated particles were placed in saline solutions. This behavior can be observed as a reflective 'sheen' on the surface as well as a red colored residue on containers as shown in Figure 3-28, and has been reported at least once in literature¹⁵⁴ for mixed monolayer particles with a partial PEG coating. Hydrophobization of a particle surface can lead to aggregation and more rapid accumulation of opsonins via interaction with the hydrophobic regions of plasma proteins, and therefore is considered to be a potential cause of RES clearance¹⁸⁴.

Adhesion of coated particles to glass containers was also observed under certain circumstances (Appendix C).

Susceptibility of the coated particles to aggregation has often been used as an indicator of particle stability, coating effectiveness, and adsorption density^{144, 152}. Many of these references assert that salt induced aggregation occurs at concentrations immediately below the point at which adsorption is maximized; however this is typically not the case as shown in Figure 3-29. Particles are effectively stabilized by steric repulsion well before surface saturation is reached. Using this assumption as a means of determining the quantity of PEG required to stabilize a gold suspension can lead to incorrect (usually low) coating densities. The stability of particles in a high ionic strength medium is an important parameter to consider when suspension stability after degradation of the surface coating is a concern.

One major and often overlooked consideration involving PEG coated gold particles is the quantity of unbound PEG remaining in the suspension after preparation. Experiments involving coating degradation and protein binding can be severely impacted by the presence of even small quantities of unbound PEG in the suspension medium, as will be discussed in subsequent sections. Comparisons made between *in vitro* and *in vivo* behaviors may differ due to the PEG being 'contained' *in vitro*. Excess PEG introduced with particles *in vivo* may be diluted and/or cleared, accumulated, or bound/chemically altered. Removal of the excess PEG is most efficiently performed by dialysis or (preferably) diafiltration. Centrifugation is a commonly used technique; however the possibility of pelleting particles into a mass which can no longer be dispersed represents a significant avenue for loss during cleaning and concentration.

There is a long-held belief by many that PEG and other adsorbates bound to surfaces by the thiol-gold bond are strong and resist desorption and place exchange reactions¹³⁸. Reports of surface rearrangement on planar alkanethiol monolayers²⁷ and place-exchange reactions involving alkanethiol monolayers on both particles^{143, 185, 186} and planar surfaces^{27, 121, 187} exist in the presence of excess adsorbate. The possibility that this surface rearrangement behavior could extend to exchanges between individual particles was investigated. To determine whether or not inter-particle exchange of thiolated PEG was possible, a suspension of nom. 20nm coated gold particles (Reagent 1) was thoroughly cleaned of excess (unbound) PEG by five rounds of centrifugal diafiltration, resulting in a theoretical removal of 99.99999994% of soluble impurities. A small quantity of uncoated 45nm gold particles was added to this suspension (final concentration was approximately 10% of the concentration of 20nm particles by mass). Along with the uncoated particles, this mixture was analyzed by differential sedimentation to determine whether or not any shifts in the sedimentation velocity occurred (indicating changes in the coating density). For control purposes, samples of the PEG coated particles without the presence of 45nm particles were also prepared. Smaller coated particles were selected to provide ample quantities of PEG, while larger uncoated particles in smaller quantities were selected to maximize detection of any exchange of active adsorbates. Initial measurements of the mixture showed no shift in the larger particles, indicating that no significant quantities of unbound PEG remained in the coated sample (Figure 3-30, Figure 3-31). The mixture was placed in the oven at 37C and analyzed less than 24h after preparation. The results at the first time point showed a surprisingly large shift in the size of the uncoated particles after incubation,

indicating that significant exchange of coating from the smaller coated particles to the larger particles occurred (Figure 3-30). The sedimentation velocity of the originally uncoated particles was 95% of the same particle when fully coated. Analysis of samples incubated without uncoated particles showed that the PEG coated particles in deionized water release active PEG molecules regardless of whether or not uncoated particles were present (Figure 3-32). The quantity of PEG released by the sample incubated without uncoated particles was less than those incubated with uncoated particles as evidenced by a smaller sedimentation velocity shift. It is difficult to determine whether or not the PEG released by the particles was initially bound to the surface or just weakly associated, though initial measurements showed no detectable levels of PEG release. To verify that this effect was not related to reagent purity issues (discussed extensively in the next section), the same analysis was performed on the purified reagent, and showed the same result as the as-received reagent (Figure 3-33). Finally, to eliminate potential sources of interference due to interactions of the small coated particles with the larger uncoated particles, samples of particles incubated with and without particles were centrifuged to remove all particles. The uncoated particles were then added to the supernatant and analyzed. The results from this experiment showed significant shifting of the sedimentation velocity as was the case when both particles were present (Figure 3-34). Analysis of a sample stored under refrigeration at 4C showed significantly lower levels of released PEG than the samples at elevated temperatures, indicating that the behavior was temperature dependent (Figure 3-32).

Reagent Purity

Reagent purity is an often overlooked but critical parameter that plays a role in the quality and protein resistance of PEG coatings. The quality of the reagent and presence

of synthesis or degradation byproducts can impact both coating effectiveness and protein resistance characteristics of the particles. The most common mechanisms by which a thiolated PEG compound will degrade include:

- Formation of a disulfide via oxidation (adsorbing).
- Oxidation of the thiol to a sulfoxy group (non-adsorbing).
- Thermal, oxidative, or UV degradation of the polymer.

Some of these issues can be mitigated by storage of the reagents in a cold, dark, sealed container. Though the condition of the thiol terminal group is the easiest to oxidize and the object of most concern, the PEG chain can be degraded even at relatively low temperatures of 30-40C¹⁸⁸. Cold storage of PEG reagents can prolong the reagent's usable lifetime considerably, and preparation of a fresh reagent stock solution for each use will minimize the opportunity for oxidation. Observed rates of degradation (as loss of reduced thiol activity) on storage were generally constant at 4.6%/day at 65C, 0.87%/day at 37C, 0.5-0.6%/day under ambient conditions, and $\leq 0.38\%$ /day at 4C with a starting concentration of 0.1mM (Figure 3-35). Regardless of storage conditions, the quality of the reagent is source dependent, as seen in Figure 3-41. The quantity of reagent required to achieve a complete coating is one potential indicator of the fraction of active groups on the polymer. Degradation of the reagent by oxidation or other means reduces the fraction of active groups present in the reagent. Figure 3-41 shows the effects of this type of degradation, where Reagent 1 after degradation required over three times the initial concentration to achieve saturation than the same reagent as-received. Differences were also observed when the suspension was cleaned, where the particles coated using Reagent 1 showed a small difference in sedimentation velocity and electrophoretic mobility, indicating possible coating loss. The mobility of particles

coated using Reagent 1 decreased by approximately 4-7% (Figure 3-48) while particles coated using Reagent 2 decreased 0-1.7% (this difference was not statistically significant in most cases) after cleaning. It is difficult to say whether or not this was related to degradation of the coating or some type of reversible association of adsorbate with the surface. Additionally, the sedimentation velocity change and electrophoretic mobility of the particles as prepared differed by reagent, indicating differences in coating as prepared. When directly compared, the mobility of particles coated with Reagent 1 was approximately 90% of the value measured for the same particles coated with Reagent 2, suggesting that the coating density was not as high. This observation was supported by the direct comparison of coating densities using TGA, where the coating density achieved using Reagent 1 was significantly lower than Reagent 2 (Table 3-7). It is important to note, though, that the thorough cleaning required for gravimetric analysis of the coating density may have introduced artifacts in the TGA measurements if the coating degraded during this process (discussed previously). The calculated coating thickness based on sedimentation data was approximately $10\text{nm} \pm 0.7\text{nm}$ for Reagent 1 as opposed to the value of $6\text{nm} \pm 1\text{nm}$ for Reagent 2. It is possible that the differences in the polymer molecular weight distribution are responsible for this change, though both reagents were nominally 5kDa.

UV absorption spectra of the PEG reagents in water yielded useful information on potential contaminants. An unexpected peak was observed in all PEG reagents tested, including those used in this study, at approximately 235nm. This was briefly discussed previously and shown in Figure 3-13 and Figure 3-37. Although the PEG reagent was exposed to particles in at least a two fold excess, this unexpected peak disappeared

when exposed to gold particles (Figure 3-16) and surfaces (Figure 3-17). Interactions with components of the supernatant were ruled out as a potential cause of this disappearance (Figure 3-16), as were interactions with the specific type of particles used (Figure 3-17). This behavior suggests a potential adsorbing impurity present in the PEG reagents. Some possible impurities that could account for this behavior include the compounds used to thiolate the PEG polymer, such as inorganic sulfides, thioacetate, and thiourea. The near UV absorption spectra of these pure compounds in water are shown in Figure 3-36. Of these compounds, the only one which bears any similarity to the absorption curves observed in the thiolated PEG reagents is thiourea. To verify the hypothesis that an adsorbing impurity was present, a PEG solution (Reagent 2) was dialyzed using a 3kDa MWCO membrane to separate the larger PEG molecules (5kDa) and smaller potentially interfering compounds. The UV absorption spectra of the permeate, retentate, and an aliquot of the parent solution were then analyzed. The relative spectra of these solutions are shown in Figure 3-37. It can clearly be seen that the component responsible for the absorbance peak at 235nm is depleted from the retentate and enriched in the permeate. The absorption spectrum of the retentate is a near exact match to thiourea. To further demonstrate that the permeate fraction did not contain an appreciable concentration of thiolated PEG, the PEG reagent (as received), the permeate, and the retentate were added to a suspension of gold particles to determine whether or not each was capable of stabilizing the suspension. Both the parent PEG reagent and the retentate were able to fully stabilize the particles; however the permeate caused immediate aggregation of the suspension (Figure 3-38). This behavior is consistent with the behavior of a small molecule which is incapable of

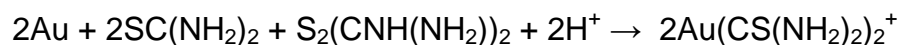
sterically stabilizing the particles and causes charge neutralization. To estimate the quantity of thiourea in the PEG reagent, the absorbance of the permeate at 236nm was compared to a standard curve for thiourea (Figure 3-39). This showed that the commercial reagents contained as much as 2100ppm (13.7 mol%, 0.21 mass%) of the impurity thiourea. The sulfur content of the reagent, permeate, and retentate were analyzed in a separate experiment using ICP-AES and Ellman's Assay for sulfur content as S and as thiol respectively. Initial ICP measurements showed that the reagents contained 8.9% more sulfur than theoretically calculated (Table 3-9); however measurements of sulfur as a reduced thiol in these polymers was considerably lower at 75-80% of theoretical (Figure 3-4). Analysis of the sulfur content in the permeate showed that 21.2% of the initial sulfur content in the reagent passed through the dialysis membrane. The measured sulfur content (as thiol) in the permeate, however, was extremely low at 1.4% of the initial value, indicating that the sulfur in the permeate was primarily an impurity (such as thiourea), inorganic sulfur compound (such as sulfate), a non-thiol organic (such as a disulfide or sulfoxy compound), or a combination thereof. Thiourea alone generates only a weak response from Ellman's Assay. Experimentally determined response curves showed that the sensitivity to thiourea was approximately 5000x less than thiol standards such as cysteine. Assuming that thiourea did not interfere with the assay chemistry (experimentally verified for the reagents used), this is likely due to the fact that the thione tautomeric form of thiourea is preferred in solution. References confirm that this is indeed the case¹⁸⁹⁻¹⁹¹. The sulfur content of the PEG in the retentate was calculated to contain 84.7% of the theoretical sulfur content and 98.8% of the initial thiol content. Deconvolution of the previously obtained UV spectra of

the permeate assuming that thiourea was a primary impurity revealed the spectrum of the remaining compounds in the permeate (Figure 3-42). Careful concentration of the permeate and subsequent dispersive Raman spectroscopic analysis showed that some of the PEG passed through the 3kDa dialysis membrane. To remedy this, a dialysis membrane with a MWCO range of 100-500Da was used for a second round of separation. This membrane retained a higher fraction of PEG, which is particularly evident in the UV absorption spectrum of the permeate at lower wavelengths (Figure 3-40). To verify that the unknown compound was thiourea, HPLC was performed on the permeate from the 100-500Da dialysis. The retention times of the unknown impurity and thiourea were identical (Figure 3-44). UV absorption spectra of separated compounds as they eluted showed the characteristic absorption behavior of thiourea. Although Raman and FTIR spectra of these compounds were obtained initially, these techniques are not sensitive enough to the impurities when in such a low mass fraction. UV absorption on the other hand is far more sensitive, but lacks the detail of the vibrational spectroscopic techniques. UV absorption is a useful technique as a screening test to identify and potentially estimate the concentration of certain impurities.

The fact that this impurity was present in all reagents tested from several manufacturers and lots indicates that this is more of a systemic problem rather than an isolated case (Figure 3-13). The presence of this impurity would explain the higher than expected concentration of sulfur in the reagents as determined by ICP-AES (Table 3-9) and certain anomalous shifts in mobility observed during timed coating stability analyses. Throughout this work, the reagent was used as-received, since the PEG

reagents are typically used without purification in literature. For most major topics, both purified and as-received reagents were tested.

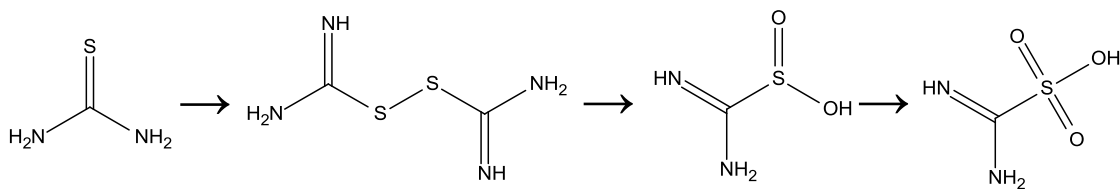
Unique to thiourea among the previously listed thiolation compounds is its ability to dissolve gold via formation of a bicoordinate Au(I) complex (Figure 3-38B). This process has seen considerable use in commercial mining operations for leaching of precious metals as a safer and often more efficient method of gold extraction than cyanide. The chemistry of this reaction is thought to proceed via the formation of formamidine disulfide from thiourea¹⁹² in the presence of an oxidant (including dissolved oxygen¹⁹³), which subsequently oxidizes the metallic gold while cleaving to form the bicoordinate complex as shown in the following reaction:



Since hydrogen ions are consumed in this process, an acidic environment is preferred. Under ambient conditions with no external oxidizer (aside from dissolved oxygen), this reaction is slow and requires days for complete dissolution to occur (Figure 3-38B), which is consistent with literature observations on ore refining¹⁹⁴. It may also be possible for this process to act upon the gold-sulfur bond used to attach PEG to the surface of gold particles. Although washing can be performed, this compound chemisorbs to the particle surface, as shown previously by the disappearance of the UV peak at 236nm (Figure 3-16, Figure 3-17). The adsorption isotherm of pure thiourea on gold particles was measured to determine the maximum capacity of gold particles to adsorb thiourea. The adsorption isotherm, determined by near UV absorption, showed that the gold particles adsorb thiourea with a relatively high surface density of approximately 14 molecules/nm² on nom. 20nm gold particles (Figure 3-47).

Preparation of PEG coated particles most often involves the addition of excess quantities of thiolated PEG to ensure a complete coating. This type of preparation can lead to variable concentrations of thiourea on the surface and potentially differences in the PEG coating density due to competitive adsorption. Like many other adsorbing small molecules, thiourea can displace adsorbed PEG on gold surfaces. Small strongly adsorbing molecules have the ability to easily penetrate the PEG layer and can outcompete the larger molecules for surface area (due to higher adsorbate flux and lack of steric interactions with the remaining coating). While this seems to be a solely deleterious effect, it may be beneficial under certain circumstances. The presence of a mixed monolayer composed of the large PEG molecules and smaller thiourea molecules may act to resist additional competitive desorption by coating as much accessible surface with adsorbate as possible, provided that the competing adsorbate is not present in extremely high concentrations.

Thiourea has well known antioxidant properties¹⁹⁵⁻¹⁹⁸, which result from the conversion to formamidine sulfinic acid (also known as thiox or thiourea dioxide) in the presence of an oxidizer. Formamidine sulfinic acid can be generated both through industrial oxidation processes¹⁹⁹ as well as metabolism of thiourea *in vivo*¹⁹⁸. This compound is also a reducing agent, which can be oxidized to the sulfonic acid²⁰⁰ form as described below:



The final products formed upon oxidation of thiourea are highly dependent on solution pH and oxidant strength and concentration, with various compounds such as H₂S, elemental sulfur, cyanamide, sulfates, carbon dioxide, and ammonia formed upon oxidation^{199, 201} in addition to the formamidine disulfide, sulfinic, sulfenic, and sulfonic acid products. Under aqueous conditions at elevated temperature, rearrangement of thiourea to ammonium thiocyanate has been described for some time²⁰². This behavior also occurs in the solid state at elevated temperatures¹⁹⁸.

PEG Coating Stability

The primary theorized mechanism of coating degradation in deionized water is related to oxidation of the sulfur binding group leading to desorption. Oxidation can arise from a variety of sources, such as ambient or dissolved oxygen, UV, and electrochemical sources. These sources ultimately result in oxidation of the thiol to sulfinate and sulfonate groups (possibly via a disulfide), which are no longer capable of adsorbing to gold surfaces. The presence of these products have been identified on numerous occasions by MS, vibrational spectroscopy (FTIR and Raman), and XPS¹⁰⁹⁻¹¹² after oxidation of thiol based monolayer coatings. The exact role that oxygen plays and its ability to oxidize coatings on gold are disputed in literature. Some reports show that degradation under ambient conditions is possible under a variety of circumstances. References indicate that thiol coupled coatings on most coinage metals may only last for one week under ambient conditions^{109, 203}, which challenges the long held belief by some that thiol based monolayers are highly stable under ambient conditions^{109, 204}. Studies performed to identify the mechanism of oxidation indicated that the primary oxidant which results in rapid coating degradation is ozone, and that even in the presence of pure oxygen, coating degradation is minimal²⁰⁴. Other reports indicate that

exposure to UV light in the presence of oxygen is sufficient to remove thiol based coatings, and it was hypothesized that ozone generated during this process was the cause of oxidation. Later work using lower energy “ozone free” UV lamps indicated that this was not the case¹¹¹. Another study found that samples stored in sealed containers showed little degradation compared to open containers under the same conditions and regardless of exposure to ambient light¹⁰⁹.

In most of the previous cases, the behaviors of these thiol based monolayer coatings were analyzed in a dry state or with limited availability of moisture. Though data is limited on their behavior in solutions, it is believed by some that the stability of thiol based monolayer coatings is higher when immersed in a solution than in air²⁰⁴. Studies of alkanethiol monolayers on planar surfaces in phosphate buffer and media show that the surface is compromised over the course of a week to several weeks rather than days^{205, 206} while studies using cell adhesion as a metric showed apparent degradation over the course of one week²⁰⁷. Regardless, little information is available on the time dependent stability of thiol based coatings *in vitro*^{205, 206} and the behavior of similar coatings on particles (under any condition)²⁰⁸.

Since most of the aforementioned studies focus on planar gold surfaces rather than particles (which differ in surface chemistry and physical structure) and with smaller alkanethiols or substituted alkanethiols rather than polymers, it is important to study the behavior of polymer coated particle systems. Information from studies on planar gold surfaces suggest the potential for differences in the behavior and stability of coatings on particles. Certain studies report that coated gold surfaces which are polycrystalline exhibit dramatically higher rates of monolayer degradation as the grain size

decreases¹¹², with degradation occurring over the course of hours to days for smaller grain samples and weeks for higher grain size samples. Gold particles, such as those used in this study, are polycrystalline and exhibit a multiply twinned structure (usually 5 planes) and are themselves small 'grains'. Dramatic differences in susceptibility to oxidation based on the type of adsorbate have also been noted in literature¹¹¹. Reports on certain types of particles have suggested a relationship between residual halide ion content (residual bromide from particle synthesis) and degradation of thiol based monolayer coatings as well as dissolution of the particles themselves under ambient conditions²⁰⁸. Taken together, these facts illustrate some of the complexities which may be present on particle based systems.

Coating Stability Kinetics

The time dependent coating stability of gold particles was evaluated using 20nm gold particles in deionized water and incubated at body temperature. Suspension samples were treated with excess thiolated PEG and purified by diafiltration (resulting in a minimum theoretical removal rate of 99.998% of unbound PEG and residual salts) prior to being incubated for a period of time at 37C. The condition of the coating was evaluated by electrophoresis relative to control suspensions of known coating density prepared at the time of analysis. These standards were selected at specific points that would fully describe the shape of the adsorption isotherm, and were compared to a complete adsorption isotherm to ensure that the curve was accurately described. All experiments were repeated at least twice with similar results observed each time. Differences were noted between sources of PEG reagents, as noted in Figure 3-48. The reagent shown in Figure 3-48A/B showed a loss of approximately 50% beginning after

approximately 1.5h. This behavior was not observed in the reagent shown in Figure 3-48C/D, which required approximately 24h for 50% of the coating to degrade.

The exponential rise to a maximum migration velocity observed in electrophoresis can be sensitive to data variance when the coating density is at or near saturation (since the slope of the curve is extremely low at this point). To account for these variations and provide a better model of the degradation behavior, the following process was used to model and fit the mobility data. The relationship between migration velocity and coating density can be modeled using a three parameter exponential:

$$\Gamma = \frac{-1}{b} \ln \left(\frac{v_o - v}{a} + 1 \right) \quad (3.3)$$

Where Γ is the surface density, a, b, and v_o are constants, and v is the migration velocity. Since the measured time dependent mobility must 'pass through' this curve as the coating degrades, the relationship between mobility and time can be substituted to determine the time dependent coating density. The migration velocity can be parameterized in terms of incubation time using the following relationship:

$$v(t) = v_{o1} + c(1 - e^{dt}) \quad (3.4)$$

Where $v(t)$ is the time dependent migration velocity, c, d, and v_{o1} are constants, and t is incubation time. The combination of these equations was used to fit the time dependent degradation behavior of the PEG coated particles shown in Figure 3-48D.

Factors Affecting Coating Stability

In the previous sections, various factors such as oxidation were discussed as potential sources of coating degradation. Since one of the primary uses of PEG coated gold particles is for *in vivo* applications, particles were expected to be exposed to a

variety of compounds which may mediate the rate of degradation. To screen some of these compounds which may affect the rate and mechanism of coating degradation, samples of particles were exposed to a variety of different compounds and conditions to determine which factors had the greatest effect on the degradation of PEG coated gold particles. Compounds such as oxidizers, antioxidants, small thiol molecules, salts, and biomolecules were of particular interest. These samples and the properties of the selected compounds anticipated to affect coating stability are summarized in Table 3-11. Coated suspension samples (500ppm as gold) were cleaned of excess thiolated PEG and residual salts by centrifugal diafiltration (theoretical rate of removal was 99.9998% of residual PEG and solutes) before being aliquoted into the various solutions listed in Table 3-11. The final concentration of each listed compound was 1mM after addition of the gold suspension with the exception of the PBS, saline, plasma, and plasma small molecules. The particles were incubated at 37C and analyzed qualitatively and by electrophoresis on a daily basis.

The results of these experiments indicated that the two most effective mechanisms of coating degradation include oxidation and competitive desorption due to other sulfur compounds. Samples exposed to oxidants such as peroxide and iron chloride and competing adsorbates such as mercaptoethanol and thiourea degraded at the most rapid rate. Additional experiments using hydrogen peroxide indicated that the oxidative desorption of thiolated PEG occurred immediately and close to stoichiometrically. Separate experiments were performed to identify the rate and influence of mixing order on the competitive adsorption process. Various water soluble small thiol compounds were added either with or after the PEG reagent (purified prior to use) in concentrations

similar to the concentration of thiourea found in the PEG reagent as received. The timing of addition had a significant effect on the coating of the particles initially (as measured by sedimentation and electrophoresis within the first hour to two hours after mixing). Subsequent measurements performed after the samples were allowed to stand for approximately 12h were virtually indistinguishable for pairs of samples exposed to the same small thiol, indicating that rearrangement/equilibration of the adsorbates occurred within hours after mixing. The presence of the strong reducing agent sodium borohydride also resulted in rapid degradation of the coating, though not nearly as rapidly as the oxidants and competing adsorbates at similar concentrations. The ability of sodium borohydride to rapidly (in minutes) remove thiol based self-assembled monolayers has been recently reported in literature at high concentrations²⁰⁹.

Initial experiments with the pure compounds listed in Table 3-11 resulted in rapid degradation of the acidic samples (ascorbic acid, TCEP, uric acid). The influence of pH (discussed later) was anticipated to be a factor, but was not the property of interest in these experiments. For this reason, a separate set of experiments was performed with all solutions buffered to physiological pH with phosphate. This resulted in a significant extension in the lifetime of the coating, and eliminated the rapid degradation of acidic samples. Due to its low solubility at neutral to basic pH and in the presence of phosphate, the sample containing iron was not considered for this test. All samples were analyzed at varying intervals over the course of several weeks by electrophoresis. Degradation rates for the samples which exhibited the most rapid loss of coating were similar to the non-buffered samples. Samples containing competing adsorbates (mercaptoethanol and thiourea) and oxidants (hydrogen peroxide) aggregated in less

than 24h. Suspension aggregation is only possible when removal of the PEG coating is nearly complete, leaving the particles susceptible to charge screening. The times until aggregation of the particles or near complete loss of coating (approximately 80-90% removal of the coating) for the samples which aggregated most rapidly are listed in Table 3-12. For those samples which did not rapidly degrade, the relative mobilities are shown in Figure 3-48 after approximately 3 weeks of incubation at 37C. The results in Figure 3-48 and Table 3-12 show that mild reducing agents can extend the lifetime of the coating provided that they are not strong enough to desorb the PEG coating, as in the case of borohydride. The small molecules present in plasma also contain many species which can act as mild reducing agents, though the complexity of this mixture makes determining a single cause of coating life enhancement difficult to determine.

Dissolved gases

The presence of dissolved gases, particularly dissolved oxygen, are a strong and easily overlooked source of chemical PEG degradation. As previously discussed, oxidizers are among of the most effective means of degrading the sulfur-gold bond on the surface of these particles. Dissolved oxygen content in water equilibrated with air at STP is approximately 8.2ppm^{210, 211} (Figure 3-50). To determine the effects of dissolved gases on coating degradation, several samples were prepared with gold particles exposed to various media with or without dissolved gases. A summary of the samples prepared are listed in Table 3-13. The two media used in this study were de-ionized water that was either degassed or equilibrated with ambient gases (referred to as “degassed” and “equilibrated” respectively). All handling of degassed water and suspensions was performed under an inert atmosphere and stored in sealed containers. A suspension of 20nm gold particles was prepared and coated with excess PEG-thiol.

This suspension was then purified by three rounds of centrifugal diafiltration with a 100kDa membrane, resulting in an estimated minimum 99.998% removal of excess PEG. The resulting suspension was concentrated to 50-60 μ L and was split into two aliquots. One aliquot of concentrate was added to degassed and equilibrated water at a volume ratio of 80:1. These parent suspensions were then aliquoted into smaller samples which were sealed and dispersed to their various environments. Samples were allowed to stand undisturbed for five days before being analyzed by gel electrophoresis.

The electrophoresis results are detailed in Figure 3-51. Compared to the standard, little change was observed in the samples under ambient conditions over 5 days, indicating that at least over the short term, the presence of ambient lighting does not severely affect the PEG coating density. Both samples incubated at body temperature showed significantly higher levels of coating degradation than their room temperature counterparts, indicating that degradation kinetics are a significant factor (the kinetics of coating degradation will be detailed in the next section). Most notably, the samples prepared with degassed water showed dramatically lower levels of coating degradation than similar samples prepared with air equilibrated water. Over a five day period in fully equilibrated water, the coatings on samples incubated at body temperature were almost completely removed. These samples demonstrated rapid cathodic mobility with little to no aggregation, indicating that a small amount of PEG remained on the surface.

The contribution from the individual gases in air and certain gas mixtures was also investigated. The potential gases and mixtures of interest included: oxygen, nitrogen, carbon dioxide and oxygen, and air. The contributions of oxygen and carbon dioxide were of particular interest since these gases could contribute to oxidation and pH

change respectively while other gasses (N_2) are inert. There is a relationship between the solubility of dissolved oxygen and the presence of other solutes and dissolved gasses in water. Typically the presence of other solutes and dissolved gases cause a reduction in the solubility of oxygen by a salting-out phenomena. The nature of the salt or dissolved gas is an important determinant of the final dissolved oxygen content²¹². For example, the quantity of dissolved oxygen is lower when air is dissolved in water than when pure oxygen is dissolved in water. However, the proportion of dissolved oxygen relative to other dissolved gases (principally nitrogen) is higher than its proportion in air due to a higher affinity for oxygen over nitrogen. The result of this behavior was observed when the degradation rates of PEG coatings were compared in degassed water sparged with pure oxygen vs. water sparged with air (Figure 3-52).

The individual contributions of dissolved gases to the degradation of PEG coating were investigated by exposing PEG coated gold particles to media saturated in each of the aforementioned gases and mixtures. For each of the aforementioned gases and mixtures, a quantity of degassed water was aliquoted into separate containers and sealed. These containers were then vigorously sparged with the selected gases or mixtures to produce a saturated solution. Small quantities were withdrawn from each container and combined with cleaned and concentrated gold particles. These suspension samples were then sealed and placed in an oven at 37C for five days prior to analysis by electrophoresis. The results of this experiment are shown in Figure 3-52. As observed previously, the deoxygenated sample showed a relatively small to moderate amount of coating degradation. The nitrogen sparged sample showed the next lowest level of degradation. Although significantly different from the control and

degassed sample, the difference can not be completely attributed to the influence of nitrogen alone. Industrial grade nitrogen gas such as the type used to sparge this sample, may contain up to several thousand ppm of oxygen²¹³, and additional sample handling stages increase the possibility of leaks. The samples showing the highest level of degradation were those which contained large quantities of dissolved oxygen: oxygen sparged, and mixed oxygen and CO₂ sparged samples. The presence of dissolved CO₂ in addition to oxygen caused a small increase in the rate of coating degradation compared to oxygen sparged only. The presence of large quantities of CO₂ can decrease the pH, potentially accelerating degradation. An important fact validated in this test is that changes in degradation due to handling during the degassing procedure did not introduce any major interference in the rates of degradation. Removal of oxygen (or air) and subsequent replacement caused the degradation rates to accelerate back to the rates previously observed in air equilibrated water.

In summary, the presence of dissolved gases contributes greatly to the rate of degradation of the PEG coating. Oxygen is a particular concern, and has the largest single impact on coating degradation. Carbon dioxide, thought not as damaging as oxygen, mildly accelerated the rate of degradation when combined with oxygen.

Thermal stability

In the previous section, some evidence was presented that the degradation rate of PEG coatings are significantly impacted by temperature and dissolved oxygen. As shown in Figure 3-51, the relatively small difference in temperature between ambient temperature and body temperature resulted in significantly different degradation rates, particularly when dissolved oxygen was present. Literature reports indicate that thiol based coatings thermally desorb from gold at temperatures varying from below room

temperature²¹⁴ to approximately 250C^{120, 122, 215}. With desorption often occurring near or above ~100C, this point is often given as the maximum stable temperature^{114, 120, 215} of thiol based coatings.

To further probe interactions between temperature and dissolved oxygen content, cleaned and concentrated particles were prepared and added to either air equilibrated water or degassed water as described in the previous section. These pairs of suspensions were sealed and placed in dark, temperature controlled convection ovens at 30, 37, 45, 55, and 65C as well as a refrigerator at 4C and ambient temperature (22C, protected from ambient light). Samples were drawn at various time intervals (initially withdrawn at 24h intervals) and analyzed by electrophoresis relative to a control sample with excess PEG. The time and temperature dependent particle mobility relative to the control particles are presented in Figure 3-53. These mobilities were correlated to PEG coating density using set of calibration samples with known quantities of PEG added to the parent suspension. Data from this work matched replicate experiments as well as several single point measurements performed for other purposes.

It can be clearly seen from these curves that the temperature and presence of dissolved oxygen play a critical role in the stability of the PEG coating. At temperatures above body temperature, samples with dissolved oxygen degraded at approximately twice the rate of the corresponding degassed samples (Figure 3-54). The change in temperature from room temperature to body temperature provides an even more dramatic increase in rate of degradation, with an 8 to 15 fold increase in degradation rate in equilibrated and degassed media respectively. No significant degradation was observed in the samples kept under refrigeration, and extrapolation of the curves in

Figure 3-54 indicates that the coating is likely to remain stable for a considerable amount of time. Analysis of samples stored under refrigeration in the presence of dissolved oxygen over 8 months after preparation showed virtually no detectable levels of coating degradation (mobility was 99.3% of the same particles with excess PEG). PEG coated gold particles, therefore, are best stored under refrigeration if they can not be used immediately. If long-term storage is necessary, refrigerated storage of the particles with the addition of excess PEG would be advisable to maintain long term coating integrity.

Effects of reagent impurities

In a previous section on reagent purity, the presence of the potentially concerning impurity thiourea was detected in all reagents tested. It was noted that this compound can adsorb to gold surfaces (Figure 3-16, Figure 3-17, Figure 3-47) in significant quantities (Figure 3-47), alter the surface chemistry and decrease charge, has the ability to dissolve gold (Figure 3-38B), may take part in oxidation processes (Figure 3-43), and can competitively adsorb with thiolated PEG (Figure 3-46). All of these features present potential mechanisms of degradation, many of which are dependent on dissolved oxygen and pH. To determine what (if any) a role thiourea plays on the rate of coating degradation, several comparative sets of samples were prepared for analysis as summarized in Table 3-14. Though previous analyses indicated that almost all of the active thiol components in the reagents were present in the retained fraction after dialysis, samples coated with cleaned PEG were exposed to a higher initial concentration of PEG reagent to ensure that any loss during dialysis was accounted for. Analysis of the coated particles was performed in a manner similar to the method described in previous sections. The qualitative stability at elevated temperature (65C),

and under ambient conditions in the presence of thiourea, mercaptoethanol, and iron (III) ions was also examined.

The results of both qualitative and quantitative tests indicated that the presence of thiourea was a key factor in the stability of the particles. In all cases, purification of the reagent significantly increased the sensitivity of the coated particles to sources of degradation, such as oxidizers and competitive adsorbates. The qualitative tests all showed a higher degree of sensitivity in the uncoated particles as indicated by aggregation of the suspension. Suspensions coated using the purified reagent degraded at a faster rate than the uncoated particles, as indicated by the mobility data in Figure 3-55. Although previous analyses indicated that the PEG coating density was slightly higher in the cleaned samples, this did not translate into greater final stability, indicating that thiourea plays a role in stabilizing the coating. Importantly, this increase in the rate of degradation was reversed upon addition of thiourea to the purified suspension in concentrations similar to those present in the impure reagent, confirming that this change of stability was related to the presence of thiourea in the raw reagent. Addition of thiourea in high concentrations to the coated particles (greater than ~100x the concentration present in the PEG reagent tested), on the other hand, had the opposite effect on the suspension. In this case, the suspension was rapidly destabilized at a rate dependent on the initial concentration of thiourea. These effects are likely due to competitive desorption of the PEG and/or chemical degradation of the particles at the higher concentrations of thiourea. Since the suspensions were purified of unbound PEG (and unbound thiourea in the case of the raw reagent) prior to addition of excess thiourea, there was no excess PEG present to drive re-adsorption.

Salt and solute effects

In several previous experiments, the presence of salts (in the form of phosphate buffered saline) lead to an unexpected decrease in the rate of coating degradation. Separate experiments were therefore performed to identify whether or not there was a relationship between the type and concentration of salt and the rate of degradation. Particles were placed into 100mM solutions of the following salts and compared to particles in deionized water alone at 37C: LiCl, NaCl, KCl, KBr, CaCl₂, NH₄F, NaF, NaNO₃, Na₂SO₄, NaHCO₃, Na₂HPO₄, Na₃Citrate, glycerin, and unfunctionalized PEG (added at a concentration (w/v) equivalent to glycerin due to the large molecular weight difference). The trends in the degradation rates indicated that many polyvalent anions, nitrate, and fluoride ions degraded more rapidly than the monovalent halide samples tested. The following general trends in the rates of degradation were observed in the tested ions: most polyvalent anions \geq Chloride/Fluoride, $\text{Li}^+ \approx \text{Na}^+ > \text{K}^+ > \text{Ca}^{2+}$ ions for chloride salts, and $\text{NH}_4^+ > \text{Na}^+$ for fluoride salts, $\text{F}^- > \text{Cl}^-$ for sodium salts, and $\text{Cl}^- > \text{Br}^-$ for potassium salts. Although these trends were noted repeatedly, the rates of degradation were similar for similar classes of salts. Monovalent halide salts (with the exception of ammonium and fluoride salts), for example, all degraded at similar rates while sodium salts of most polyvalent anions degraded at a slightly more rapid rate. The results also showed that nonionic solutes degraded at a markedly higher rate than all other ionic solutes, with rates of degradation similar to or slightly longer than the coated particles in deionized water alone. Of the tested ionic solutes, the highest rate of degradation was observed in the ammonium fluoride and sodium nitrate samples.

Several potential interactions were considered for to explain this behavior:

- Solute effects on dissolved oxygen content.

- Solute effects on the PEG coating.
- Interactions of ions with the particle surface chemistry.

The first of these three interactions addressed were solute effects on the dissolved oxygen content. The solubility of dissolved oxygen in aqueous solutions is highly dependent on the type and quantity of solutes present²¹⁰⁻²¹². Typically, highly charged ions have the most pronounced effect on dissolved oxygen, and would therefore have the greatest effect on the dissolved oxygen content. Literature reported values for the effects of salts on dissolved oxygen content are often given in terms of their salt effect parameter²¹², which is indirectly related to the solubility of dissolved oxygen in water (i.e. a higher salt effect parameter indicates lower oxygen solubility for salts of the same concentration). Some of the literature reported values for various salts are shown in Table 3-15. From this table, we can see that certain extreme cases (namely NH_4F) are consistent with the trends observed experimentally; however this hypothesis does not follow the predicted trends when the polyvalent ions are considered. Though these ions would have the largest effect on the dissolved oxygen content, they in many cases exhibited slightly higher rates of degradation. In addition, even though the degradation rate of NH_4F was rapid, it still did not degrade as rapidly as the coated particles in deionized water. The samples containing NH_4F , glycerin, and PEG (unfunctionalized) were expected to degrade most rapidly due to their poor effectiveness at salting out oxygen. Both the ammonium and fluoride ions are weak monovalent acids/bases, and contribute less to the ionic environment compared to the 1A and polyvalent ions²¹². The glycerin and PEG (unfunctionalized) have no charged functionalities, and do not contribute at all. Overall though, at the concentrations used in these experiments, the calculated decrease in dissolved oxygen content due to salts would be relatively small

(maximum of 15% decrease in dissolved oxygen content). Although the solute interactions on oxygen are obviously not the sole factor causing the extension of the coating lifetime, they are present and may be a contributing factor in a more complex system.

The second interaction involves solute effects on the PEG coating. In the same way that the oxygen may be salted out or salted in with various solutes, the solution properties of PEG are influenced by the presence and type of salt in solution²¹⁶⁻²¹⁸. The primary mechanism of stability would involve a salting-out type of interaction to produce a more cohesive interfacial layer. Many of the general properties of solutes which govern the efficiency of salting out oxygen also hold true generally for other nonionic solutes such as PEG. PEG is somewhat different, though, in its ability to interact with metal cations in solution²¹⁶. Extensive data collections on the effects of salt on the solubility of PEG exist²¹⁷; however, as with dissolved oxygen, the observed rates of degradation did not precisely follow these predicted trends. This by no means rules out the possibility of interactions with salts, as the effects of salts on the PEG coating can be observed qualitatively (Figure 3-28), and certain 'extreme' cases seem to follow the trend (ex. NH_4F , glycerin, and PEG). Interestingly, the ability of PEG to bind certain metal cations was consistent with certain trends observed experimentally (1A metal chlorides for example), though lack of a more complete data set on cation binding prevents any relationships from being drawn.

The final possibility is the interaction of the salts with the surface and/or linkage chemistry. The sample containing NaNO_3 exhibited a rate of degradation higher than most other salts, which is not surprising given that oxidizers are one of the most

effective sources of chemical coating degradation. Although it is an oxidizer, the degradation rate was slower than the same particles in deionized water. The pH of the solution is another factor which plays a role in the degradation rates of particles, and will be discussed in the next section. Though the pH of most salt solutions tested were at or close to neutral, certain samples such as nitrate had a pH of approximately 5-6, which likely contributed to the rate of degradation. The mild acidity of this sample is likely related to the presence of acidic degradation products of the nitrate anion. Gold ions have the ability to form complexes with various anions in solution, which may mediate interactions with the adsorbed thiol. This may play a role for certain anions (such as the halides), but ions such as sulfate, phosphate, and carbonate are not known to form complexes with gold.

To both verify that the presence of salts were a factor and determine the concentration range over which these effects were manifested, the concentration dependence of the coating stability for suspensions with sodium chloride was examined. Suspension samples with sodium chloride concentrations ranging from 0.5nM to 3M (due to solubility limit) were prepared in order of magnitude intervals. The results, shown in Figure 3-57, demonstrated a concentration dependent rate of degradation at 37C for a 500ppm suspension of nom. 20nm gold particles. The concentration required to significantly enhance stability over deionized water was approximately 1mM.

In summary, the presence, type, and concentration of solutes in the suspending medium with PEG coated particles can significantly increase the stability of the coating. Coating stability increased with the concentration of salt, and suspensions (500ppm, nom. 20nm) containing mM and higher concentrations had higher stability than the

same particles in deionized water. Three potential mechanisms were considered to explain this phenomenon: salting out of oxygen, solute effects on the polymer, and effects on the particle surface and thiol bond chemistry. Of these three, the evidence presented best supports the second possibility: solute effects on the polymer. At the salt concentrations used, the effects on dissolved oxygen concentration would be small (typically < 10%), making this a less likely possibility. The behavior of samples containing nonionic solutes and certain salts which are less effective at salting out PEG as well as the somewhat nonspecific nature of the stability increase suggest that this may be a salting-out phenomenon. These observations also decrease the likelihood that the salts are somehow influencing the surface chemistry directly (though there is no direct evidence to refute this possibility completely). Finally, qualitative observation of these particles shows that salts have an effect on the apparent particle hydrophobicity (Figure 3-28A), which is mediated by the PEG layer and solvent effects. The effect of solutes on the coating stability is an important and potentially confounding factor in the study of these coatings. In many instances, it is difficult to separate an effect of interest and the effects of salts and solutes as the two are fundamentally linked (pH for example). Confounding interferences can occur if salts are released into the sample from an unexpected source, as discussed in Appendix C.

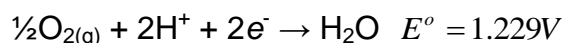
pH

Previously, all experiments focused solely on the behavior of the PEG coating on gold particles at approximately neutral pH or in deionized water. The potential effects of pH on the coating lifetime in several previous experiments were noted. Since many organic oxidation reactions are ultimately dependent on the conversion of covalently bound hydrogen to hydrogen ions, the solution pH can play a role in the promotion or

retardation of an oxidation reaction. Half reactions for the oxidation of an alkane thiol to a disulfide and sulfonate are shown below:



Additionally, media with extremes in either acidity or basicity can directly damage the polymer, linkage chemistry, the particle itself, or a combination thereof. pH affects the ability of dissolved oxygen to take part in oxidation of organic species. This is can be seen in the following reduction half reaction for oxygen:



The oxidative strength of dissolved oxygen decreases with pH as described by the Nernst Equation:

$$E^\circ = 1.229 - 0.059 \text{ pH}$$

This reduction potential is also dependent (to a small extent) on temperature, with a temperature coefficient of $-0.846 \text{ mV/K}^{219}$.

Though the pH of the blood (and many other compartments of the body) remains relatively constant at 7.4 for healthy individuals²²⁰, the pH in other compartments such as the stomach (pH 1-3.5²²¹), lysosomes (pH ~ 5 ²²²), and intestines (pH ~ 8 ²²³) vary considerably. To address the relationship between the degradation rate of PEG coatings and pH, a cleaned suspension of PEG coated gold particles was concentrated and added to 100mM phosphate solutions ranging in pH from 1.5 to 12. Since the presence of chelating species can aid in dissolution of gold, pH adjustments were initially made with a non-complexing phosphoric acid/phosphate system to avoid interferences based on dissolution and/or chelation. The particles were added to these

solutions such that the final concentration (as gold) was approximately 500ppm. These samples were then placed into a temperature controlled convection oven at 37C and analyzed at daily intervals by electrophoresis and at select points by sedimentation. Coating degradation occurred most rapidly in acidic environments; however this rate of degradation over the range tested was significantly slower than the particles in deionized water alone. This behavior is likely related to the solute effects described in the previous section. A sharp cutoff was observed at a pH of approximately 6, below which degradation occurred at the highest rates and above which degradation occurred slowly. It is difficult to say whether or not this effect is related solely to pH, ionic strength, or a combination thereof since the ionic strength of the system is dictated by the desired pH. The general trend observed is predictable in that the oxidizing power of dissolved oxygen is highest at the lowest pH values. Similar behavior was observed with other systems such as Carbonate/HCl where the salt content would be higher at the lowest pH point (selected to account for differences due to salt content when phosphoric was used previously). A separate analysis of particles coated with purified PEG showed similar results to the as received reagent, indicating that interactions between adsorbed thiourea and solution pH are not a major contributor to the pH dependent degradation behavior.

Chapter Summary

Characterization of PEG coatings is given only cursory attention in literature¹³⁰, and values for PEG surface density vary widely (Table 3-2). Accurate measurements of surface density are an indicator of the quality of the PEG coating. The techniques used for characterization of coating surface density are susceptible to a variety of common interferences (Table 3-4), which are a likely contributing factor to the variability in

reported coating thickness. Some of the common errors include: errors due to specific surface area estimation - which are frequently related to particle shape non-uniformity and assumptions about the particle size distribution (Table 3-1), presence of impurities on the surface (Table 3-7), presence of impurities in and/or condition of the PEG reagent (Figure 3-2, Figure 3-4, Figure 3-5, Figure 3-37, Figure 3-38, Figure 3-41). Some frequently used indirect techniques, such as those based on salt induced aggregation (Figure 3-29) and zeta potential neutralization (Figure 3-24), are ineffective for characterization of PEG surface density. The surface density of a particle coated with 5kDa thiol terminated methoxy-PEG is approximately 1 molecule/nm². Agreement between several techniques was achieved with careful experimental work and attention to potential sources of error. Variability due to particle shape and size distribution is a significant concern, and can change these measurements by up to ± 0.2 molecules/nm² (observed) when particles are assumed to be spherical. The polymer coating adopts the predicted brush type conformation as coating approaches maximum density (Figure 3-26). The thickness of the PEG coating is 6-10nm based on the measurement technique. The hydrodynamic radius of a PEG coated particle as determined by DLS is typically 20nm larger than the uncoated particle (Figure 2-31). Sedimentation based methods typically result in a smaller coating thickness of 6nm \pm 1nm as the technique is based on a hard sphere approximation (Figure 3-6). This coating thickness does not vary significantly based on size of the core particle over the range tested; however poor particle sphericity can impact the measured coating density (Figure 3-8). The value determined by sedimentation also varies based on the reagent source, with values as high as 10nm \pm 0.7nm calculated for one reagent (Reagent 1). Sedimentation and

electrophoresis (presumably also other chromatographic type techniques) are both useful and sensitive methods for characterization of the coating condition.

The presence of unbound PEG reagent in a coated particle suspension is often overlooked and can considerably retard coating degradation, even in small concentrations. The factors which most significantly affect the coating stability in deionized water are dissolved oxygen and temperature. The presence of dissolved oxygen significantly increases the rate of coating degradation (Figure 3-51). Temperature also accelerates coating degradation (Figure 3-54). Even the relatively small increase in temperature from room temperature (22C) to body temperature (37C) can cause a decrease the coating lifespan by over one order of magnitude (time to ~90% coating removal is 3 days for body temperature and approximately 60 days for room temperature (22C) when dissolved oxygen is present (Figure 3-54). Storage of coated particles under refrigeration greatly extends the coating lifetime. The presence of strong oxidizers (such as peroxide) causes an immediate loss of coating via oxidation of the thiol. The presence of weaker oxidizers and competing adsorbates cause a slower degradation of the coating which typically occurs over the course of hours (at millimolar concentrations with a cleaned 500ppm suspension of coated 20nm particles). The presence of salts in the medium can cause apparent hydrophobization, making the particles more adhesive to their surroundings (Figure 3-28, Figure 3-28). The presence of non-reactive salts in the suspension typically increases the stability of the gold particles relative to their behavior in deionized water. The magnitude of this effect was dependent on the type and concentration of salt. The hypothesized cause of this behavior is a salting-out phenomenon of the PEG which would result in a more cohesive

interfacial layer. The environment pH can impact the stability of the PEG coating, with acidic conditions demonstrating the highest rate of decay at pH values below approximately 6. Higher stability was also observed at pH values ranging from 10-12. Several buffering systems were tested and produced similar results. The types of ions in solution change as a function of pH, and it is difficult to separate effects caused by changes in the ionic environment from pH dependent effects.

All thiolated PEG reagents tested were contaminated with synthesis precursors/byproducts (Figure 3-37). The primary contaminant was identified as thiourea, and was found in all reagents tested. The concentration of thiourea in the PEG reagent (Reagent 2) was determined to be approximately 2100ppm (13.7mol%). Impurities were detected and quantified by near-UV absorption spectroscopy. Composition of the impurity was confirmed by HPLC (Figure 3-44). The presence of these impurities can interfere with analytical techniques by providing a false positive response in ICP and other methods. The impurities can also act to dissolve the particles by complexation in the presence of dissolved oxygen or other oxidants (Figure 3-38). Thiourea has the ability to adsorb to gold and therefore competes with PEG for available surface area during adsorption. Removal of thiourea from the reagent caused a small increase in surface density as identified by a variety of techniques (Figure 3-45, Figure 3-46). Replacement of thiourea in the purified reagent reversed the effects observed upon cleaning, and addition of excess thiourea caused the observed effects to increase in magnitude (Figure 3-46). Additional increases in thiourea concentration caused the particles to lose coating and aggregate over the course of several hours. Comparison of the susceptibility of particles coated with both purified and as received

reagents to various sources of degradation showed that the particles coated with the purified reagent were more susceptible to sources of damage such as oxidizers and competing adsorbates. The stability of the particles in deionized water was also lower for particles coated with the purified reagent.

Table 3-1. Differences in estimated specific surface area values for gold particles.

Particle Type/Size	Size By DLS ^a	TEM/ Image Analysis Size ^b	Specific Surface Area by DLS (Including Distribution) ^c	Specific Surface Area (Spherical, TEM) ^d	Specific Surface Area (Anisotropic, TEM) ^e
High Sphericity nom. 40nm Au	41	44.4 ±2.9nm	7.58 m ² /g (7.81 m ² /g)	7.30 m ² /g	7.73 m ² /g
Standard Citrate 40nm Au	44	45.2 ±4.9nm	7.1 m ² /g (7.7 m ² /g)	6.96 m ² /g	8.39 m ² /g

Notes:

^a Mean number.

^b Mean number using maximum Feret's diameter

^c Specific surface area calculated by DLS mean particle size assuming spherical monodisperse particles. Values in parentheses are specific surface areas calculated using the numerical distribution of spherical particles as measured by DLS.

^d Mean specific surface area calculated by image analysis of TEM micrographs assuming spherical particles.

^e Specific surface area calculated using image analysis of TEM micrographs and the finite element method described in Appendix A.

Table 3-2. Literature reported adsorption densities of PEG on gold surfaces.

Reference	PEG Type	Particle Size and Type	Characterization Method	Surface Density (nm ⁻²)
Takae et al. (2005) ⁹⁸	(6kDa acetal-PEG-S) ₂	20nm spherical	TGA	0.41 ^a
Manson et al. (2011) ¹³⁶	5kDa thiolated methoxy-PEG	17.9nm spherical	TGA	1.13
Karunamuni (2011) ¹³⁷	5kDa thiolated methoxy-PEG	14nm spherical	Assumed/Minimization of zeta potential	4
Wuelfing et al. (1998) ¹³⁸	5kDa thiolated methoxy-PEG	2.8nm spherical ^b	TGA	2.86
Walkey et al. (2012) ¹³⁹	5kDa thiolated methoxy-PEG	15, 30, 60, and 90nm spherical	Colorimetric assay for free thiols	Approximately 3.5, 2.6, 1.7, and 1.3 respectively
Corbierre et al. (2004) ¹³⁴	2.1kDa thiolated methoxy-PEG	3.8nm spherical	TGA	0.98 ^c / 1.2 ^d
		Planar surface	Elipsometry	0.9 ^e
Corbierre et al. (2001, 2004, 2005) ¹³³⁻¹³⁵	2.1kDa thiolated methoxy-PEG	3.6nm spherical	TGA	1.15 ^c / 2.0 ^d
Zhang et al. (2009) ¹⁴⁰	5kDa thiolated methoxy-PEG	20 and 50nm spherical	Not specified.	4-5
Xia et al. (2012) ¹⁴¹	5kDa thiolated amine-PEG	42nm spherical	Colorimetric and fluorimetric amine assays	1.63
Bell (2009) ¹⁴²	5kDa thiolated methoxy-PEG	5-250nm spherical	NMR	3000-2.03 x10 ⁵
			ICP	5.15x10 ⁴ – 3.65 x10 ⁷
Tsai et al. (2010) ¹⁴³	5kDa thiolated methoxy-PEG	30nm spherical	ES-DMA/DLS ^f	Values <0.6 reported ^g
Qian et al. (2008) ¹⁴⁴	5kDa thiolated methoxy-PEG	60nm Spherical	Salt induced aggregation ^h	2.86
Von matlzahn et al. (2009) ¹⁵	5kDa thiolated-PEG-amine	12.7x47nm nanorod	SPDP amine assay	10.0-10.67 ⁱ

Table 3-2. Continued

Reference	PEG Type	Particle Size and Type	Characterization Method	Surface Density (nm ⁻²)
Levin et al. (2006) ¹⁴⁵	2kDa pMA-PEG-Fluorescein	107nm gold coated silica nanoshell	Raman Spectroscopy (SERS)	0.28 ^j
	5kDa pMA-PEG-Fluorescein			0.093 ^j
Akiyama (2009) ¹⁴⁶	5kDa thiolated methoxy-PEG	9x55nm nanorod	Elemental analysis ¹⁴⁷	Values <0.59-0.6 reported ^{i,k}
Oh et al. (2010) ¹⁴⁸	600Da TA-PEG-Maleimide	10 and 15nm spherical	CY5-Peptide attachment to maleimide	0.74-0.094
Unsworth et al.(2005) ¹⁴⁹	5kDa ^l thiolated methoxy-PEG	Planar surface	Elipsometry ^m	0.12-0.30
			Neutron Reflectometry	0.23±0.07
Kim et al. (2007) ⁶⁴	5kDa thiolated methoxy-PEG	31nm spherical	TGA	0.57
Maccarini et al. (2010) ¹⁵⁰	2kDa thiolated methoxy-PEG	4.9nm spherical ^b	TGA	7.0-7.9 ⁿ
Sebby et al. (2010) ¹⁵¹	5kDa thiolated methoxy-PEG	30nm spherical	Mass loss after heating (QCM)	0.77 ^o
Ansari (2008) ¹⁵²	5kDa thiolated methoxy-PEG	Approximately 60nm spherical	Salt induced aggregation ^h	2.63
Choi et al. (2011) ¹⁵³	Unspecified thiolated methoxy-PEG	20-80nm spherical	Calculated ^p	0.2-0.4 ^p
Larson-Smith et al. (2011) ¹⁵⁴	10kDa thiolated methoxy-PEG	12nm Spherical	TGA	Values up to 1.64 (measured) and 1.8 (extrapolated) reported. ^q
Larson-Smith et al. (2012) ¹⁵⁵	10kDa thiolated methoxy-PEG	36nm Spherical	TGA	2.0±0.3
Doane, et al. (2010) ¹⁵⁶	2kDa thiolated methoxy-PEG	5.7nm spherical ^b	TGA	2.38 ^r

Notes:

^a Density of individual 6kDa PEG chains, not the disulfide.

^b The parent particles were synthesized according a method¹⁷⁹ which involves the use of a phase transfer catalyst.

^c Calculated assuming truncated octahedral particle shape.

^d Calculated assuming spherical particle shape.

^e Calculated from thickness with an assumed bulk density (dry) of 1.21g/cm³.

^f Calculated from a measured size change on coating with an estimated PEG size (random coil).

^g It is unclear whether or not surface saturation is reached at the highest dosed PEG reagent concentration in this reference, though the shape of the curve shown suggests that this may be the case.

^h Minimum amount of PEG required to prevent salt induced aggregation assuming adsorption of all added PEG.

ⁱ Coating density may vary due to curvature on nanorod ends. The range of values reported covers perfectly cylindrical nanorods to nanorods with end curvature equivalent to the nanorod diameter. Electron micrographs show that the particle shape lies somewhere between these two extremes. These values were calculated from the particle dimensions and mean number of PEG molecules per particle, which were provided in the reference.

^j Error in measurement ~50%.

^k It is unclear based on the data presented whether or not surface saturation has been achieved. The quantities of added PEG reagent are extremely high; however only a small fraction of the quantity added was actually adsorbed (values between 0.059% and 1.75% were shown). This is uncharacteristic of a quality reagent on a clean gold surface, and may be related to the presence of an adsorbed CTAB layer on the particle surface.

^l Adsorption densities for 750Da and 2kDa were also provided and are: 0.4-0.7 and 0.33-0.58nm⁻² respectively for elipsometry measurements, and 1.18±0.9 and 0.82±0.02nm⁻² respectively for neutron reflectometry measurements.

^m Calculated from thickness with an assumed bulk density (dry) of 1.0g/cm³.

ⁿ The range of densities provided by the authors is based on calculation of particle surface area (using TEM image analysis) by the size of the inscribed and circumscribed circle of each particle. Since the particles were faceted and TEM imaging would not provide adequate characterization of the shape, the authors used this range of values to characterize the range of possible specific surface areas. The variance associated with these densities was: -32% to +91% for the smaller and -30 to +73% for the larger numbers.

^o Error is +0.48nm⁻² (62%) and -0.21nm⁻² (27%) from the value presented.

^p Calculated from literature reported values^{98, 163}. The authors indicate that this is a rough estimate.

^q The authors did not determine whether or not full saturation was achieved, and evidence presented in this reference suggests that complete surface saturation is not likely at the highest dosed PEG concentration (as measured by TGA).

^r TGA curve showed an apparent multi-step decomposition, which is uncharacteristic of PEG coated particles that are effectively cleaned of residues/other bound adsorbates.

The authors claim that a certain fraction of PEG was 'loosely bound' (as determined by TGA); however no supporting information was given on how the authors differentiated between 'loosely' bound, bound, and unbound PEG via TGA. Neglecting this 'loosely' bound fraction, the surface density was 1.9nm^{-2} . Analysis performed in this dissertation and many other works show that the mass loss curve does not differ significantly between pure PEG and PEG adsorbed to a particle surface for clean PEG coated particles. Since PEG of this molecular weight is nonvolatile prior to combustion under typical ramp rates and conditions, there is no reliable mechanism for differentiating between binding states of the polymer. Given that the method used to synthesize the particles involved a phase transfer catalyst, there is a high likelihood that some of this compound remained adsorbed to the particle surface and may have contributed to the TGA curve.

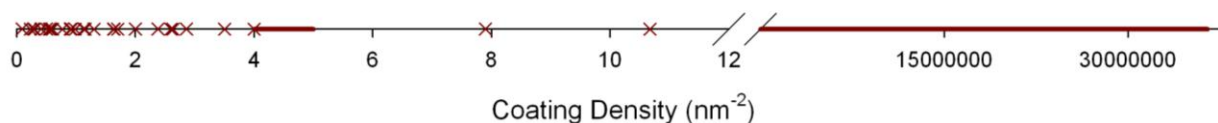


Figure 3-1. Frequency of literature reported PEG coating densities on gold particles.

Table 3-3. Summary of selected methods used for quantitative determination of coating density.

Characterization Method	Direct/ Depletion [†]	Mechanism of Measurement	Potential Interferences	Benefits	Drawbacks
TGA/ Gravimetry/ QCM	Yes/No*	Difference in mass on combustion (or on adsorption in the case of QCM) of organic coating to yield mass of coating material.	Presence of volatile or combustible impurities. Presence of nonvolatile/noncombustible impurities (ex. residual salts, etc.). Cleaning process/time required for cleaning of particles. Incomplete combustion (less likely)	Both total particle and coating mass measured. Direct measurement of coating mass.	Sensitive to any volatile or combustible compound present; requires extensive sample cleaning to reduce background (some strongly bound impurities can't be removed without impacting the coating of interest). Coating degradation during cleaning may result in artificially low density. Presence of nonvolatile impurities will result in an artificially high uncoated particle mass (can be mitigated with a secondary technique such as ICP). May require significant amounts of suspension. Samples must be dried for analysis.
Colorimetric Assays for binding group	No/Yes	Reaction with active (binding) group to produce a colored product.	Interfering impurities, Background absorbance. See also Table 3-5.	Sensitive only to active group. Sensitive to low analyte concentrations.	Impurities or degradation of adsorbate can cause measurement errors. See also Table 3-5.

Table 3-3. Continued

Characterization Method	Direct/ Depletion [†]	Mechanism of Measurement	Potential Interferences	Benefits	Drawbacks
Colorimetric assays for bifunctional or labeled PEG	Yes*/Yes	Reaction with a non-binding label on the adsorbate to produce a colored compound.	Interfering impurities, label and binding group not applied to adsorbate in a uniform manner. Label not available. Background absorbance. See also Table 3-5.	Can be used for both direct and depletion methods under certain circumstances.	Indirect measurement unless the adsorbate of interest is the bifunctional/labeled compound. Assumes that the label and active groups are available and applied uniformly to all adsorbate molecules. Impurities or degradation of adsorbate can cause measurement errors. Presence of label known in certain circumstances to cause differences in coating structure and density. Excess adsorbate must be thoroughly removed for direct measurements (if direct measurement is possible).
UV Absorption	No/Yes	Adsorbate absorbs in the near UV range.	Presence of other species with similar absorbances.	High sensitivity, direct measurement of sample.	Requires extensive cleaning to reduce background initially. Most absorbances are broad and not particularly unique to a bond or functionality. Many potential interferences.

Table 3-3. Continued

Characterization Method	Direct/ Depletion [†]	Mechanism of Measurement	Potential Interferences	Benefits	Drawbacks
Labeled PEGs	Yes*/Yes	Measurement of label (ex. fluorescent tag) concentration.	Label not applied uniformly to adsorbate. Fluorescence quenching in direct measurements.	Direct measurement of adsorbate.	Indirect measurement: presence of label known to cause differences in coating structure and density.
TOC	No*/Yes	Measurement of carbon in the adsorbate.	Presence of other carbon containing compounds. Presence of interfering species.	Direct measurement of sample.	Requires extensive cleaning to reduce background. Requires large samples, particularly for low carbon concentrations.
Chromatographic Techniques (ex. HPLC)	No/Yes	Direct measurement of adsorbate concentration.	Inactive adsorbates which are not separable from active adsorbates.	Selective only to compound of interest.	May be sensitive to inactive and/or degraded adsorbates
Raman/FTIR	Yes*/Yes*	Measurement of relevant vibrational modes.	Impurities with similar chemistry or vibrational modes.	Direct detection of relevant bonds.	Typically not quantitative. Samples must be dried for FTIR. Sensitivity may be an issue in some cases.

Table 3-3. Continued

Characterization Method	Direct/ Depletion [†]	Mechanism of Measurement	Potential Interferences	Benefits	Drawbacks
ICP	Yes*/Yes	Measurement of label or active group concentration.	Impurities containing the same element as the label/ reactive group. Labels not applied uniformly to adsorbate.	Sensitivity, direct measurement. Both particle concentration and binding group concentration can be measured in direct methods.	Low sensitivity of some ICP systems to active group. Direct measurement requires careful digestion.
DLS/DMA/ Optical tracking	Yes/No	Measurement of size change on coating used to compute density with an assumed adsorbate size.	Poor size resolution, aggregation.	Small sample size.	Very indirect measurement method. Relies on assumptions and/or models of adsorbate structure on surface. Changes in adsorbate structure can not always be accounted for. Sensitive to aggregation. Resolution of DLS not always adequate.

Note that these analyses are assumed to be performed with clean particles in DI water or in the presence of the synthesis products, not with biomolecules or other impurities.

*This is the typical condition, and may not be true, applicable, or appropriate under all circumstances.

[†] Direct measurement is defined as direct measurement of adsorbed species concentration on the particles. Depletion measurement is defined as the measurement of adsorption by depletion of a known starting adsorbate concentration.

Table 3-4. Summary of selected methods used for qualitative analysis of coating density.

Characterization Method	Direct/ Depletion [†]	Mechanism of Measurement	Potential Interferences	Benefits	Drawbacks
Analytical ultracentrifugation	Yes/No	Sedimentation velocity dependent on PEG coating density.	Unbound adsorbate in gradient for static systems (Figure 3-7). Shearing/length of analysis time.	May be made quantitative if compared to standards. Little to no sample preparation typically needed. Relatively fast for large particle sizes.	Unbound adsorbate accumulates in the gradient and can adsorb to subsequent samples, causing an artificially high and variable adsorption density. (Figure 3-7). This limits the technique to only thoroughly cleaned samples. Can be time consuming.
Capillary hydrodynamic fractionation, Capillary electrophoresis, Gel electrophoresis, Field flow fractionation.	Yes/No	Migration velocity/ elution time dependent on PEG coating density.	Excess adsorbate in eluent/medium (typically not an issue). Length of analysis time.	Fluid movement typically carries away potentially interfering compounds. Can run multiple samples simultaneously in some cases. Can be made quantitative if compared to standards. Sensitivity. Little to no sample preparation typically needed.	Time consuming. Precise reproducibility of migration velocity between analysis sets can be an issue under certain circumstances. Gel limits maximum effective particle size.

Table 3-4. Continued

Characterization Method	Direct/ Depletion [†]	Mechanism of Measurement	Potential Interferences	Benefits	Drawbacks
XPS	Yes/No	Measurement of relevant Au-S bond energy intensities.	Impurities with similar chemistry. Dry/vacuum environment. Particle geometry.	Direct detection of the surface bound adsorbate. Binding energy measurement can reveal detailed chemical information.	Sample manipulation required for analysis (drying, UHV conditions).
Raman/FTIR	Yes*/Yes*	Measurement of relevant vibrational modes.	Impurities with similar chemistry or vibrational modes.	Direct detection of relevant bonds.	Samples must be dry for FTIR. Poor sensitivity in some circumstances.
DLS/DMA/Optical tracking	Yes/No	Size change on coating. Zeta potential change on coating.	Poor resolution, sensitive to aggregation.	Small sample size.	Poor resolution. Size increase and zeta potential frequently maximized before coating density is. Sensitive to aggregation.

* This is the typical condition, and may not be true, applicable, or appropriate under all circumstances.

[†] Direct measurement is defined as direct analysis of adsorbed species on the particles. Depletion measurement is defined as the measurement of adsorption by depletion of a known initial adsorbate concentration.

Table 3-5. Effects of interferences in colorimetric and fluorimetric assays when used to determine adsorption density by the depletion method. Examples given are specific to the thiol colorimetric assay using Ellman's reagent and involve the use of a calibration curve based on the thiolated PEG reagent rather than a secondary source.

Impurity is:	Adsorbing	Non Adsorbing
Reactive to Assay	<p>Ideal condition for adsorbate of interest. Undesirable impurities will result in an artificially high or low adsorption density (dependent on affinity and adsorbate size).</p> <p>Ex. impurity thiols, $S^{2-119, 123}$, HS^{-119}, and H_2S^{162}</p>	<p>False positive or negative response. Apparent equilibrium concentration higher than actual. Shape of adsorption isotherm altered, saturation never achieved.</p> <p>Ex. SO_2^{160}, HCN^{160}, $SO_3^{2-, 161}$. are assay reactive but may not adsorb to gold surfaces.</p>
Non-reactive to Assay	<p>Artificially low response for adsorption (dependent on affinity). Assay does not account for depletion of all species. If the only impurity is adsorbing/non-reactive and does not compete with the primary adsorbate, the calibration curve may account for adsorption of this compound.</p> <p>Ex. Disulfides, thioethers</p>	<p>Artificially high response for adsorption. Calibration curve accounts for the prepared concentration, not the 'active' concentration.</p> <p>Ex. PEG (unfunctionalized), sulfonates</p>

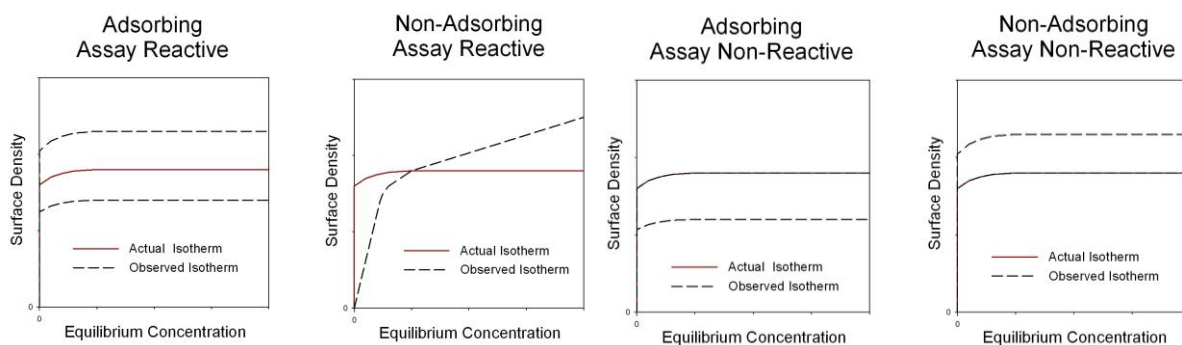


Figure 3-2. Typical effects of impurities listed in Table 3-5 for a high affinity adsorption isotherm.

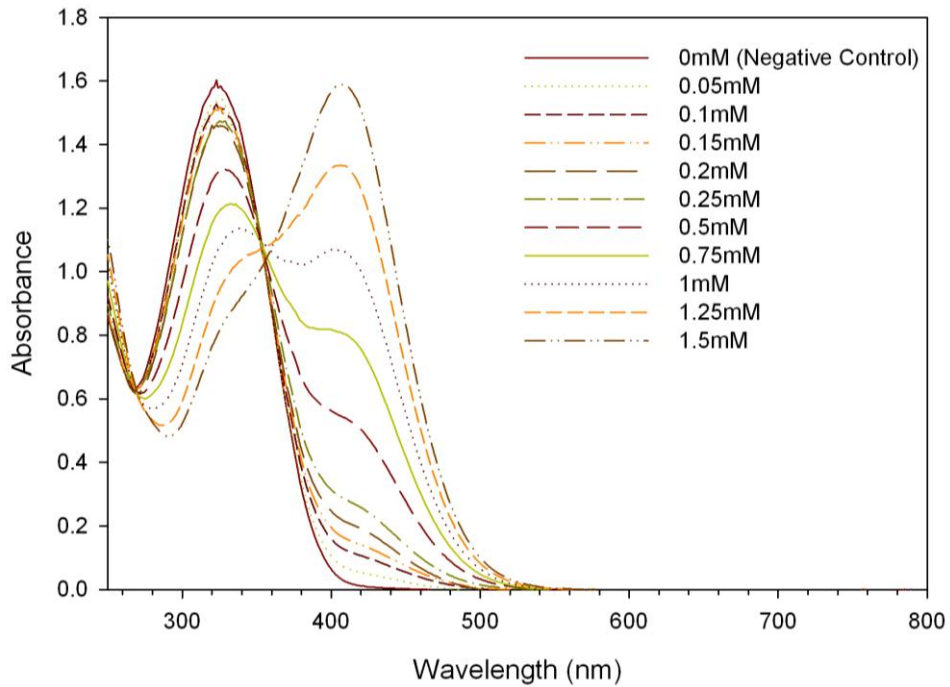


Figure 3-3. UV/Visible absorption spectrum of Ellman's Reagent with various concentrations of mercaptoethanol. The unreacted reagent exhibits a UV absorbance at approximately 324nm, and the colored product exhibits a visible absorbance at approximately 407nm.

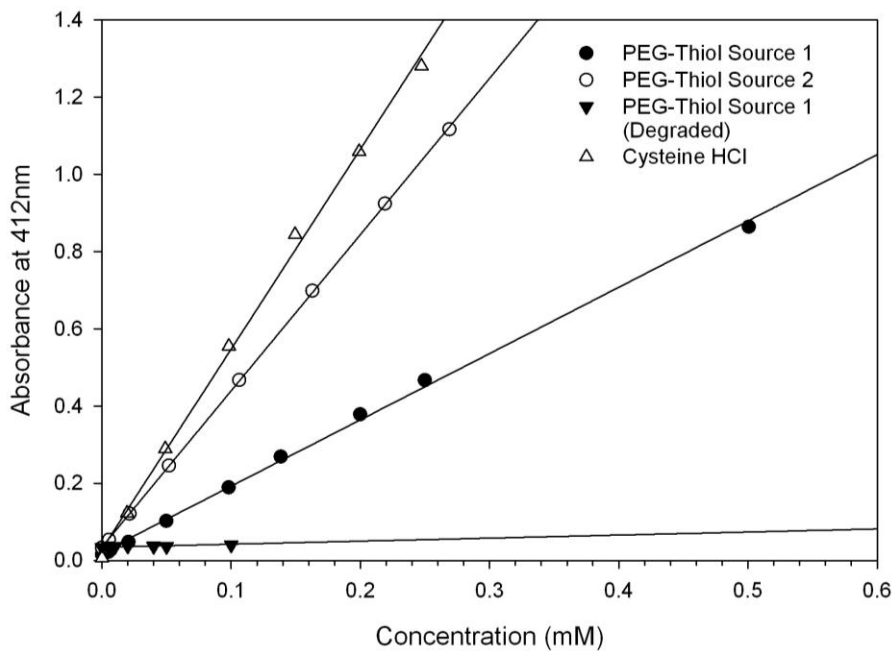


Figure 3-4. Comparison of response curves for two 5kDa PEG-thiol reagents from two sources to a cysteine standard using Ellman's Reagent.

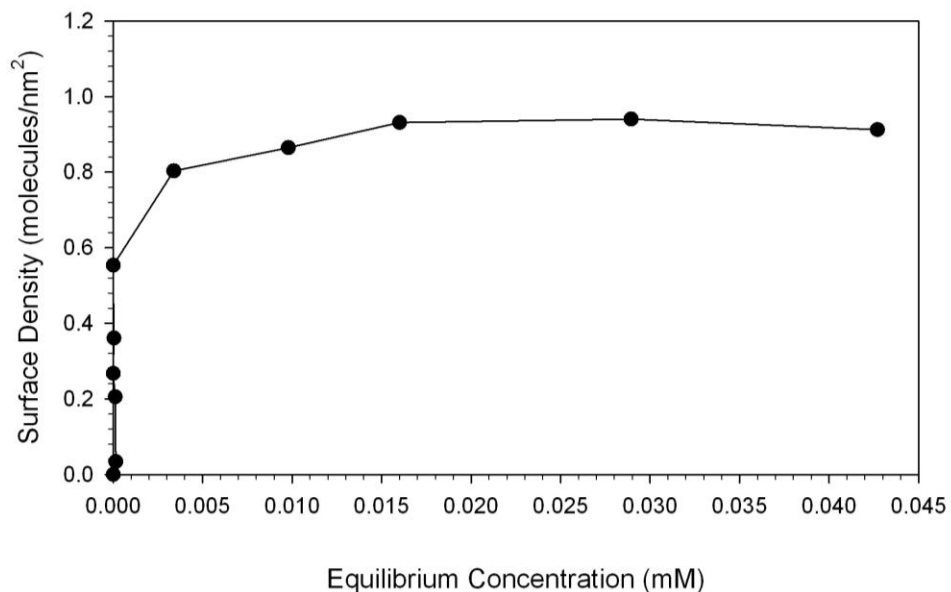


Figure 3-5. Adsorption isotherm of thiol-PEG to the surface of nominally 20nm gold particles. The equilibrium adsorption density observed here and measured by TGA on the same suspension differed by only 2.2%. The point at which adsorption was maximized was confirmed with sedimentation, dynamic light scattering, and electrophoresis measurements.

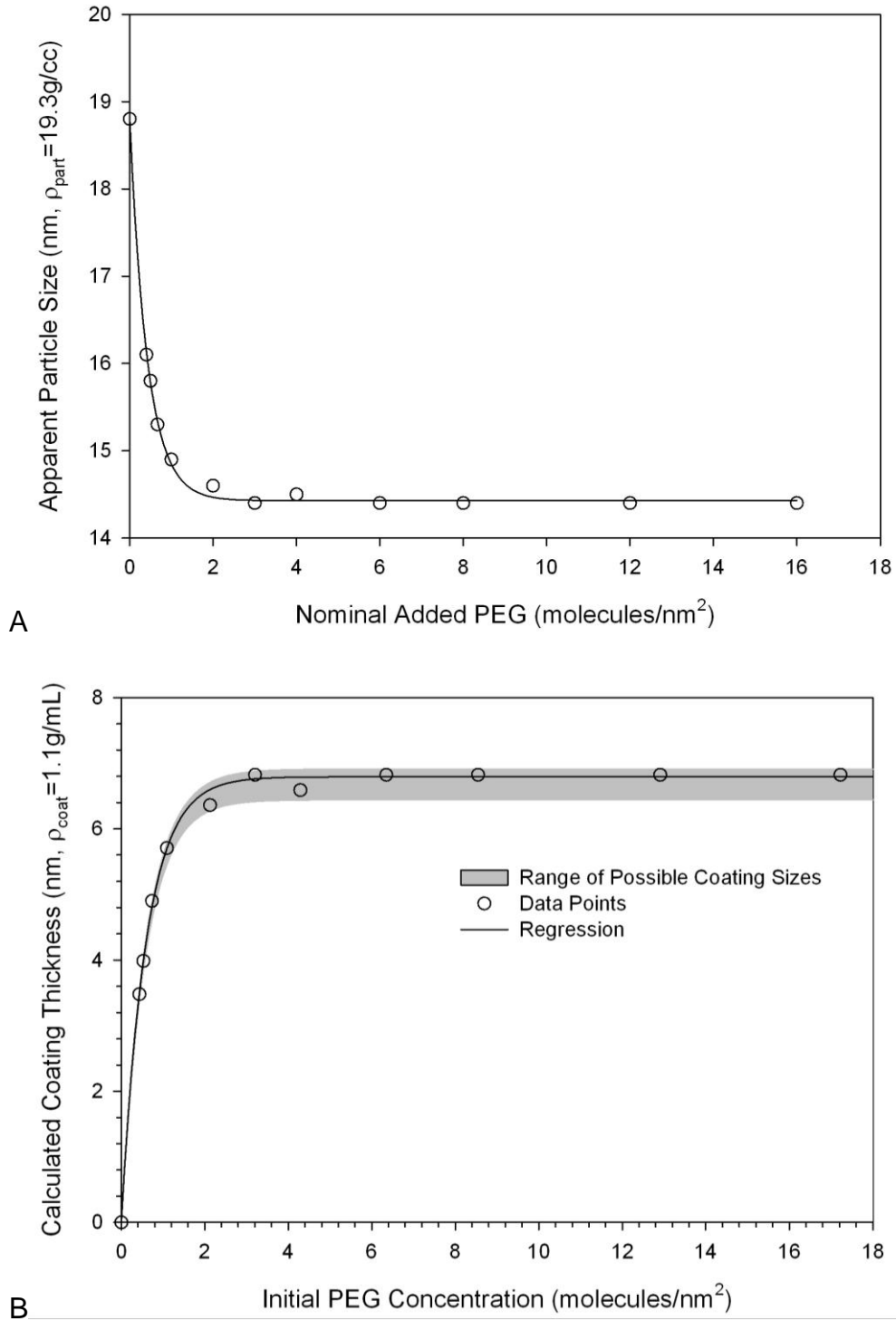


Figure 3-6. Sedimentation velocity and calculated coating thickness for various concentrations of PEG. The core particle size was measured at approximately 20nm. Differences in the assumed density may affect the calculated coating thickness by a maximum of +1.7% and -5.1% of the stated value over the entire range of possible solutions is shown in gray.

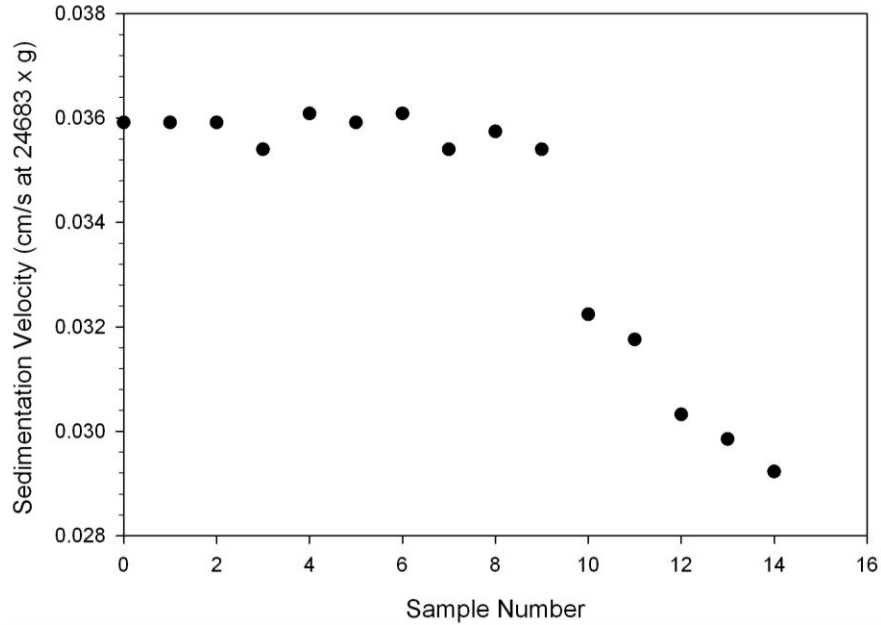


Figure 3-7. Effects of gradient contamination with excess PEG on analyzed particle size. Uncoated particles were analyzed after each coated sample to determine the level of gradient contamination. Uncoated particles will readily bind with excess PEG in the gradient resulting in a decrease in apparent size and sedimentation velocity. Samples 1-9 were thoroughly cleaned of excess PEG while samples 10-14 contained small quantities of excess (unbound) PEG. A significant and continuous decline in sedimentation velocity occurred immediately following the samples with trace quantities of excess PEG.

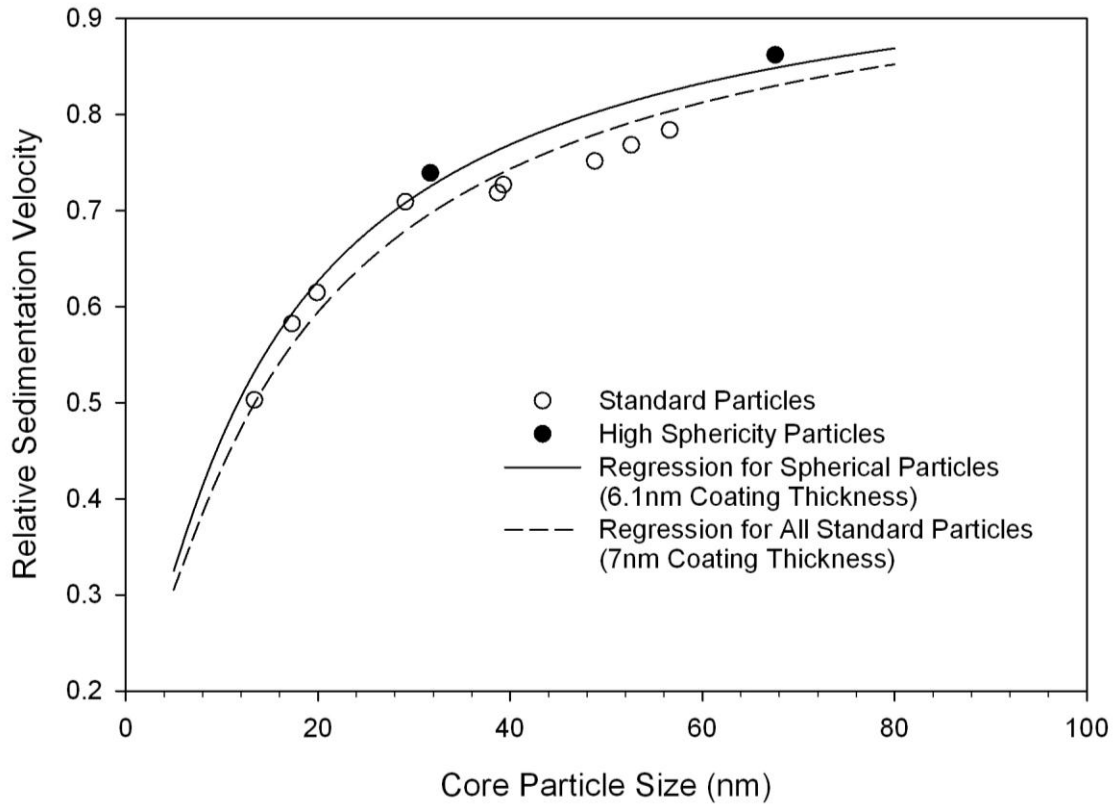


Figure 3-8. Measured relative sedimentation velocity vs. core particle size for PEG coated gold particles. The relative sedimentation velocity data was fitted to the theoretical curve (Equation 2.3) with an assumed coating density of 1.1g/cm^3 . The best fit for the high sphericity particles occurred at a thickness of 6.1nm, and for all particles at 7.0nm. Note that at particle sizes above approximately 30nm, the sphericity of the standard particles declines, resulting in a discontinuity in the curve.

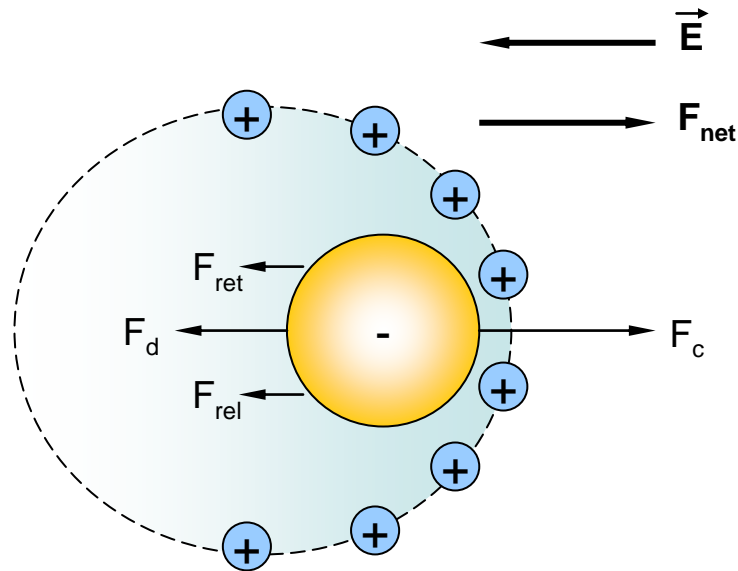


Figure 3-9. Diagram of a charged particle migrating under an applied electric field. \vec{E} is the applied electric field, F_{net} is the net force on the particle, F_c is the coulombic force, F_{ret} is the electrophoretic retardation force, F_d is the drag force, F_{rel} is the electrophoretic retardation – relaxation force.

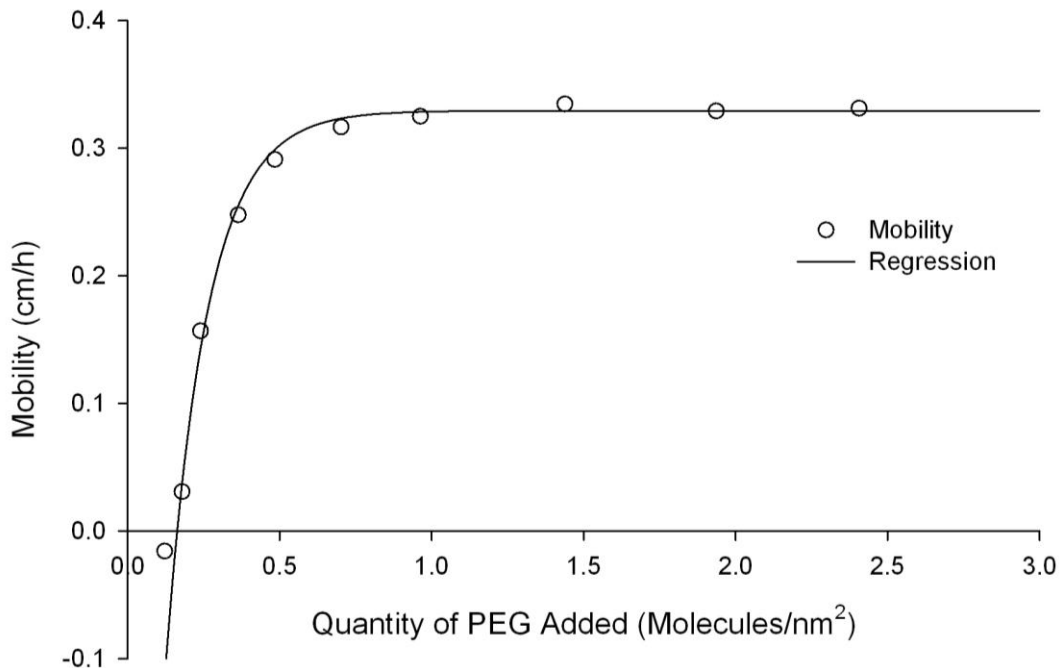


Figure 3-10. Mobility of nom. 20nm PEG coated particles with increasing PEG density. Note that the mobility sign convention used throughout this work is positive for migration to the anode (apparent positive particle charge).

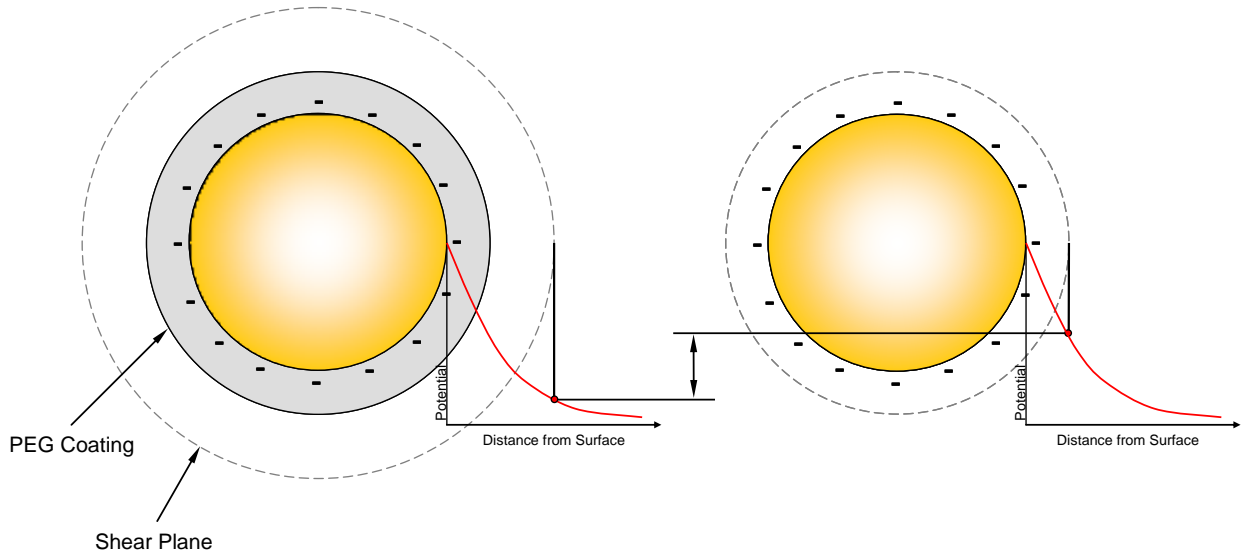


Figure 3-11. Schematic showing the relationship between electrophoretic mobility and PEG coating density. The potential difference between a PEG coated particle (left) and an uncoated particle (right) is indicated by the double arrow in the center. As the PEG coating decreases in density, its coating thickness also decreases (Figure 3-6, Figure 3-23, Figure 3-26). This causes the shear plane to shift closer to the particle surface which in turn results in a higher electrophoretic mobility (zeta potential).

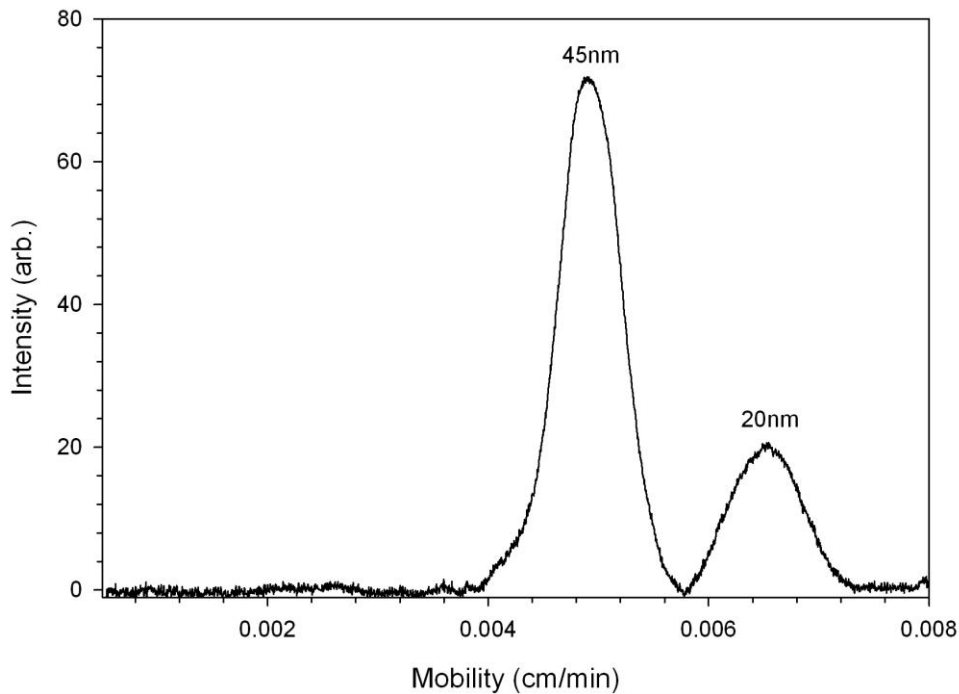


Figure 3-12. Separation of PEG coated nom. 20 and 45nm gold particles by electrophoresis. The 45nm particles were added in a significantly higher concentration.

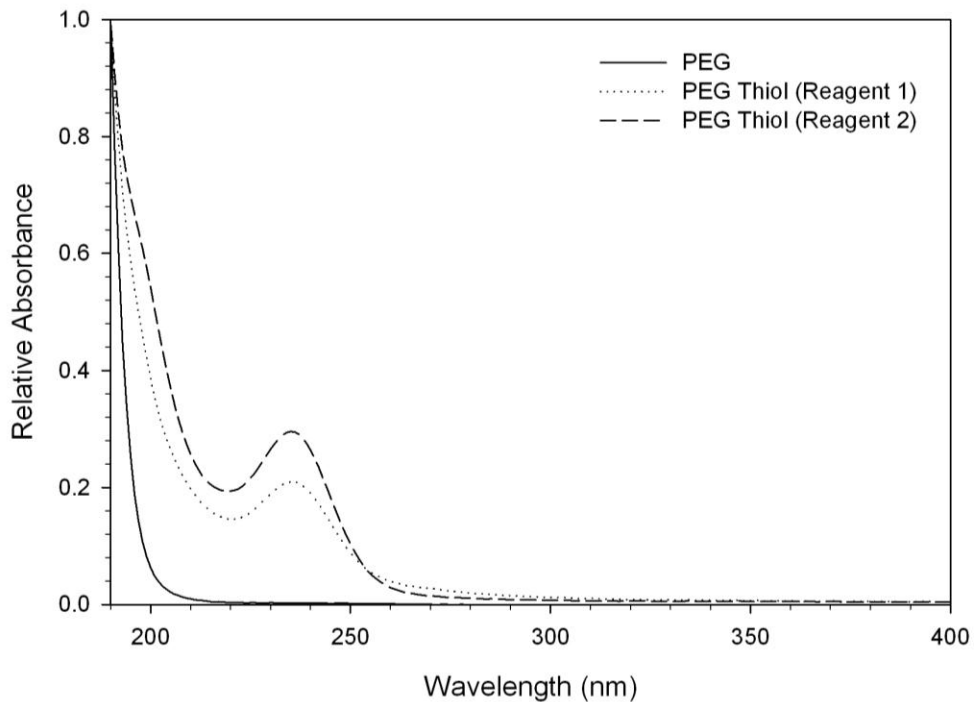


Figure 3-13. Near ultraviolet absorption spectra of PEG (hydroxyl terminated) and thiol functionalized methoxy PEGs in water.

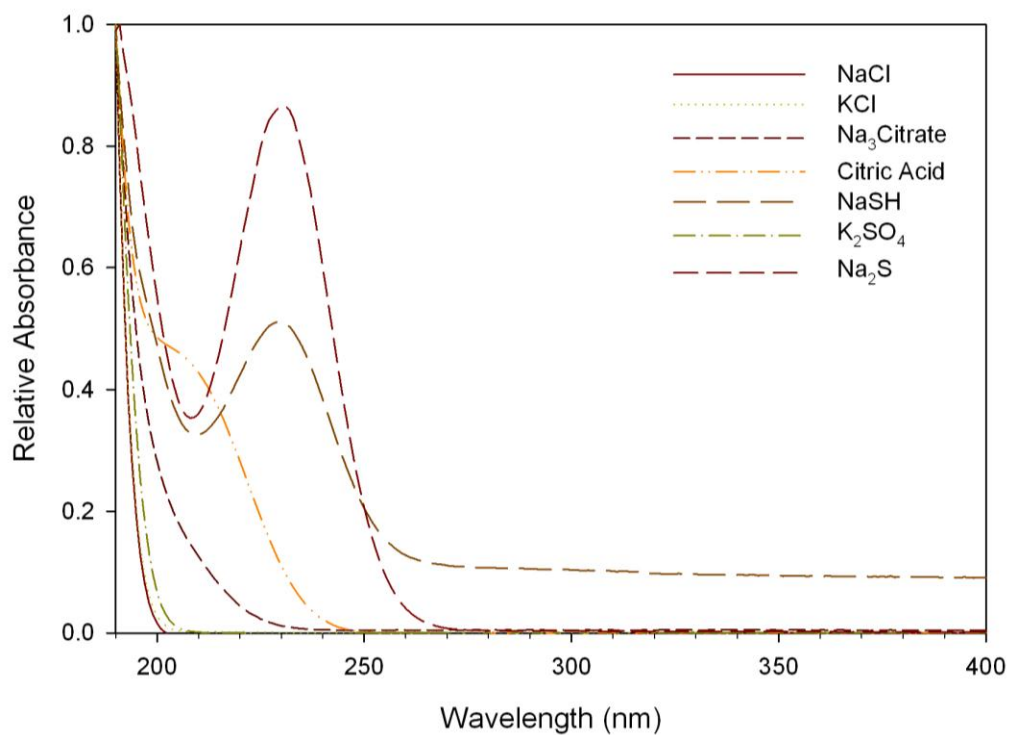


Figure 3-14. Near ultraviolet absorption spectra of selected compounds in water. Note that the curves for NaCl and KCl are superimposed.

Table 3-6. Typical UV absorption range for selected organic functionalities. Adapted from Schirmer¹⁷⁸.

Bond	Typical wavelength range (nm)	Typical molar extinction coefficient ($\text{l mol}^{-1} \text{cm}^{-1}$)
ROR	180-185	3000
RSH	170-175 190-200	300 1500
RSSR	250	400
ROH	180-185	500
RSR	210-215 235-240	1200 100
RCO ₂ H	195-210	20-100

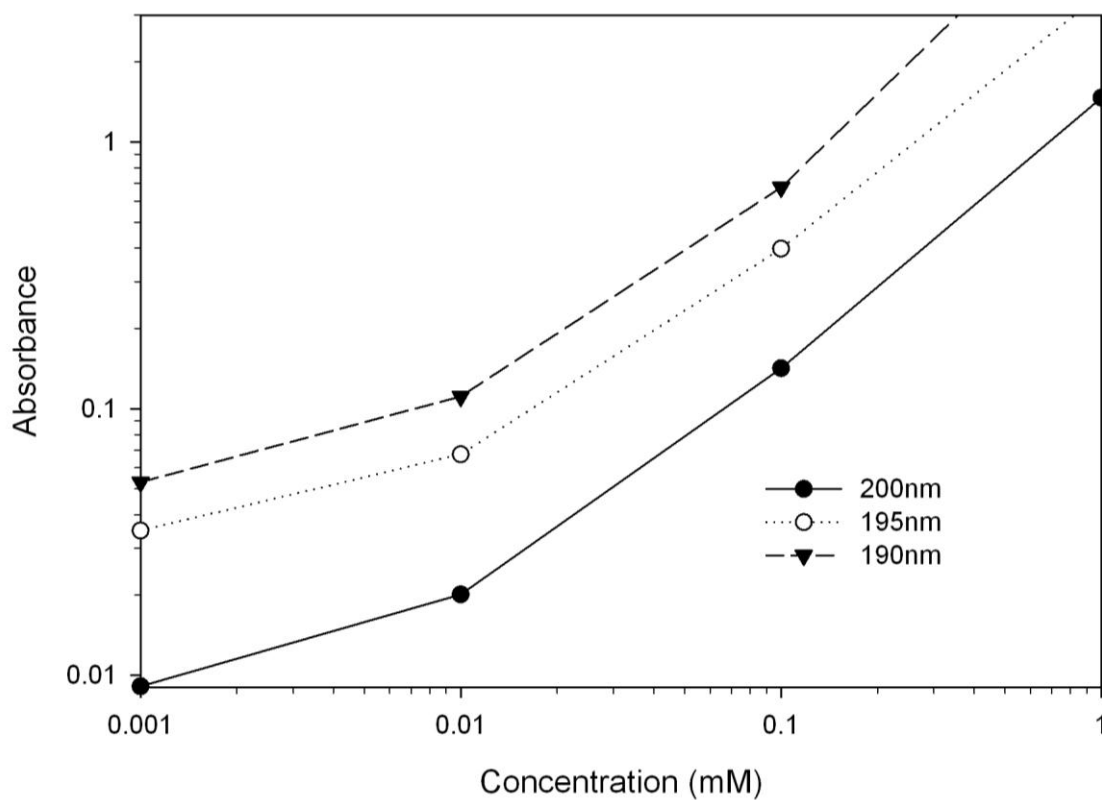


Figure 3-15. UV response curves for thiolated PEG at various wavelengths.

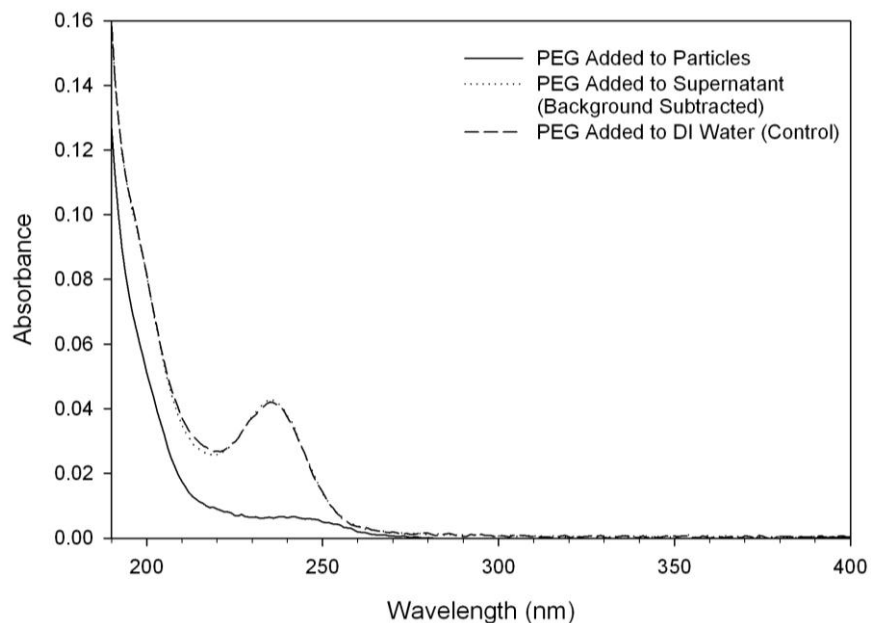


Figure 3-16. Near UV absorption curves of thiolated PEG mixed with deionized water and particle supernatant. The absorption curve of the supernatant recovered after addition of PEG to a suspension of gold particles is included for reference. Note that the absorption curves of PEG added to deionized water and particle supernatant are superimposed.

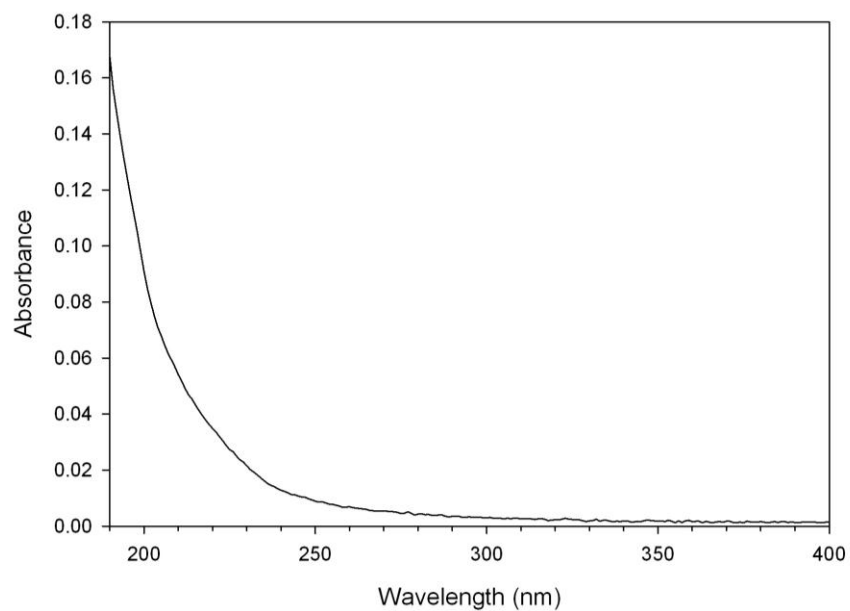


Figure 3-17. Near UV absorption curve of thiolated PEG after exposure to a gold sputter coated glass slide. Note that the absorbance peak at 235nm is not present after exposure.

Table 3-7. Apparent coating densities for various gold particles as measured by TGA. Sets of particles with identical nominal particle sizes were from the same initial batch of particles.

Nominal Particle Size	Particle/Coating Details	Apparent Coating Density (molecules nm ⁻²) ^a
20nm	Uncoated	None Detected
20nm	5kDa PEG ^b coated	0.88
20nm	5kDa PEG ^c coated	0.43
13.8nm	5kDa PEG ^b coated	1.06
13.8nm	5kDa PEG ^b coated with CTAB serially adsorbed ^d	1.21
13.8nm	CTAB coated gold particles with 5kDa PEG ^b serially adsorbed ^e	0.89 ^f

Notes:

^aCoating density assuming adsorption of 5kDa thiolated PEG.

^b Reagent 2.

^c Reagent 1.

^d CTAB was added to PEG coated particles, allowing the CTAB to adsorb after the PEG coating was formed.

^e PEG was added to CTAB coated particles, allowing the PEG to adsorb after the CTAB coating was formed.

^f No mass loss characteristic of PEG decomposition was observed, only mass losses characteristic of CTAB decomposition were observed. Mass losses due to PEG combustion were either not present, or not obvious/separable from the remaining curve.

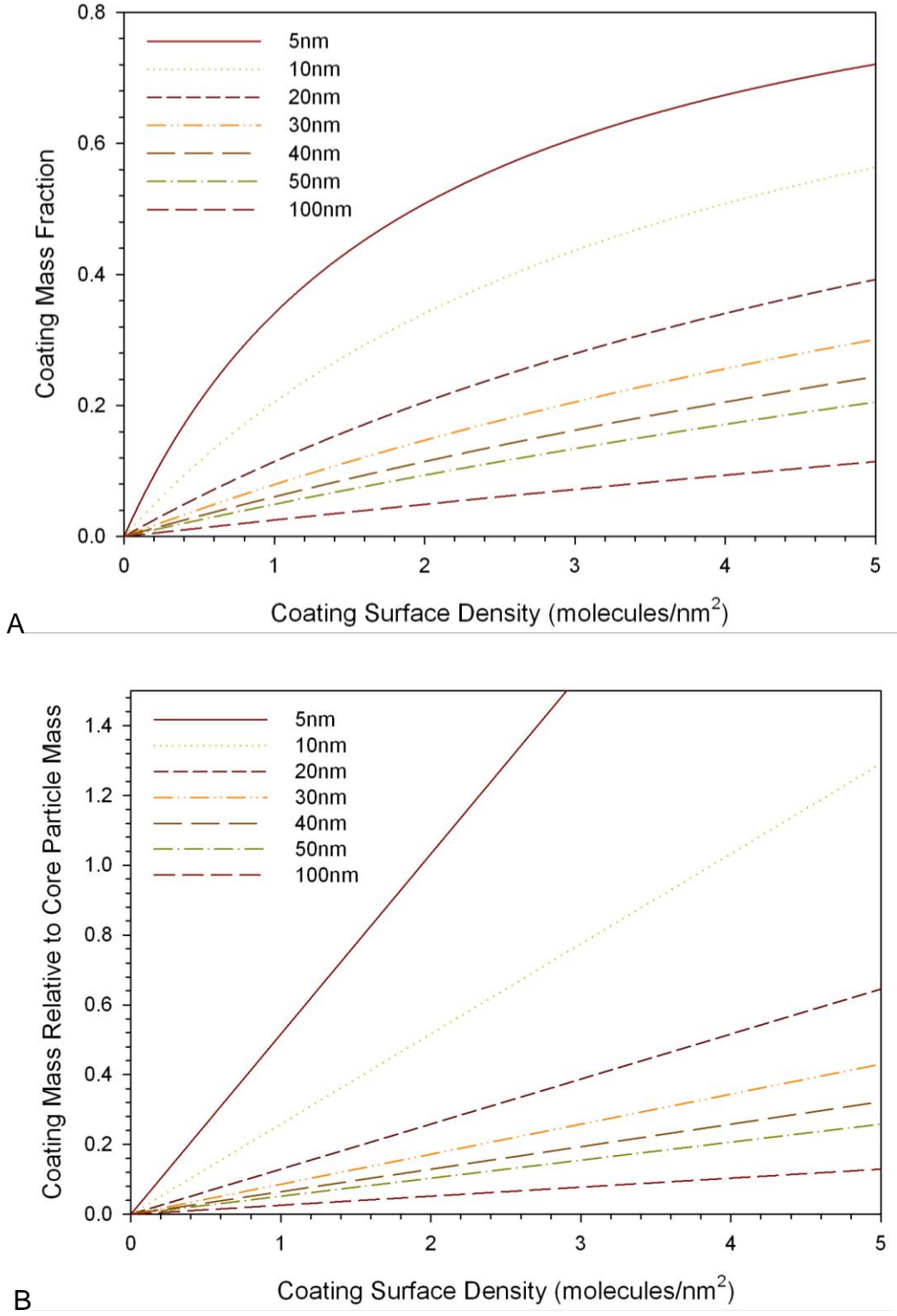


Figure 3-18. Coating mass relative to total particle and core particle mass as a function of coating surface density for various core sizes. A) Coating mass relative to total (coated) particle mass. B) Coating mass relative to core particle mass. Adsorbate is 5kDa thiolated methoxy PEG on gold core particles.

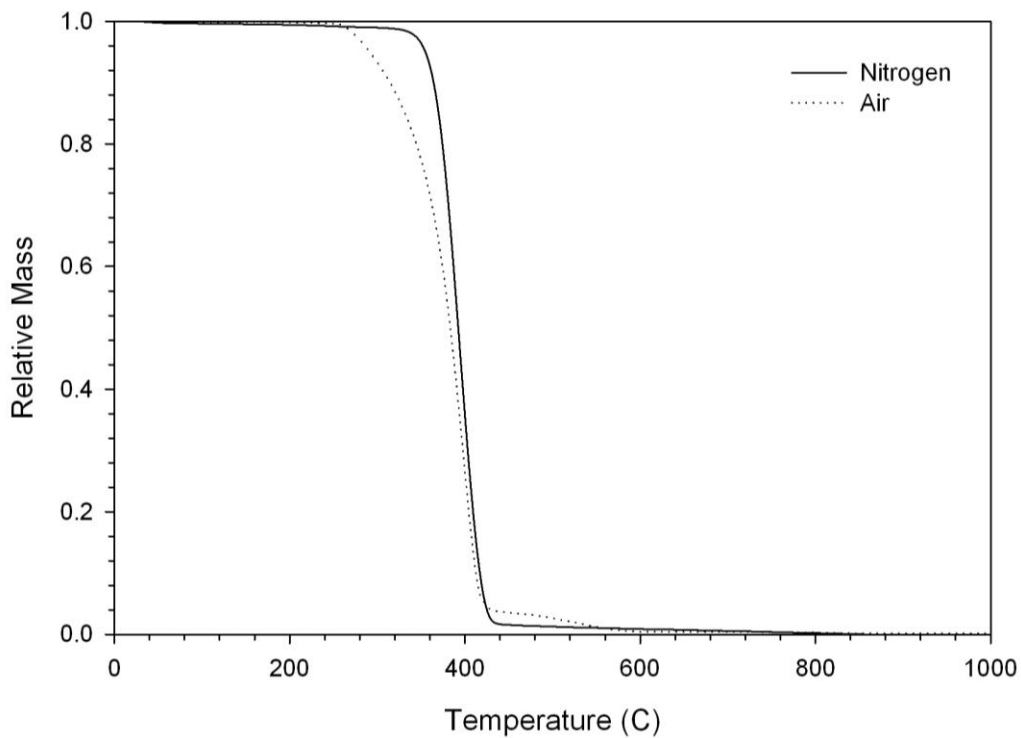


Figure 3-19. TGA curves of thiolated PEG (Reagent 2) up to 1000C under inert (N₂) and reactive (Air) atmospheres.

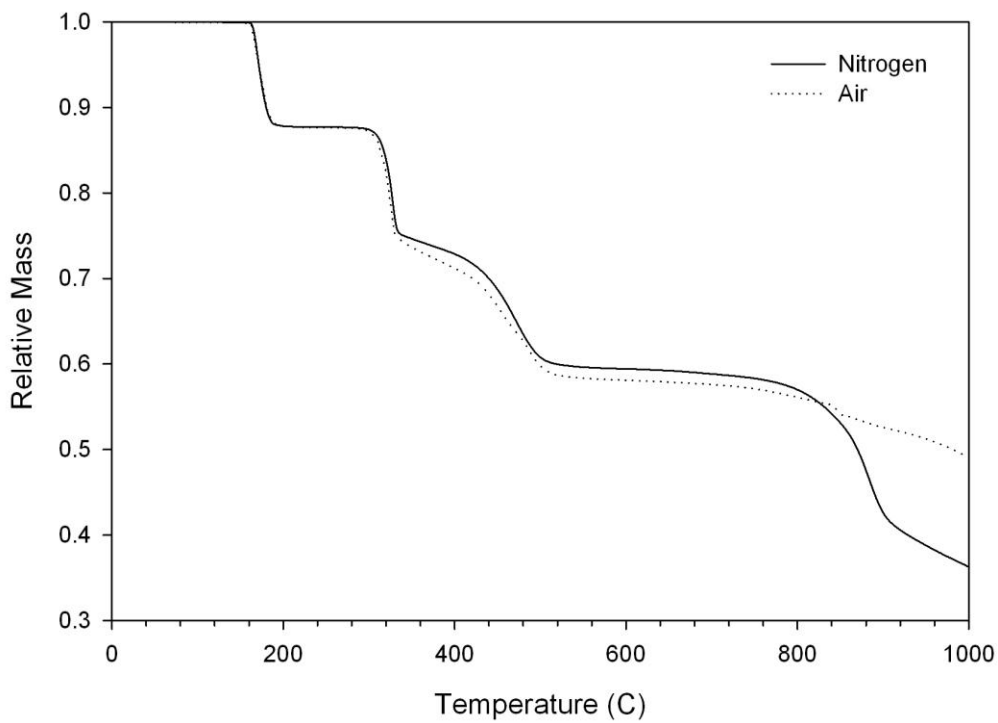


Figure 3-20. TGA curves for sodium citrate dihydrate up to 1000C under inert (N₂) and reactive (Air) atmospheres.

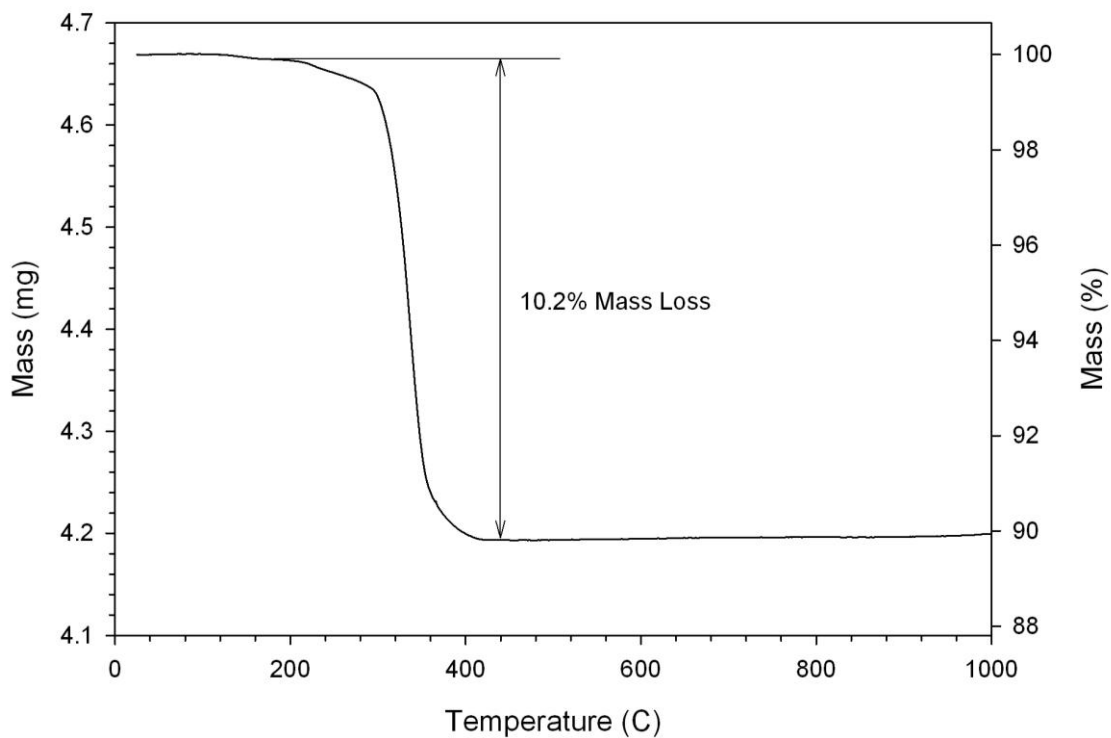


Figure 3-21. TGA curve of coated nom. 20nm PEG coated (Reagent 2) gold particles under an oxidative atmosphere.

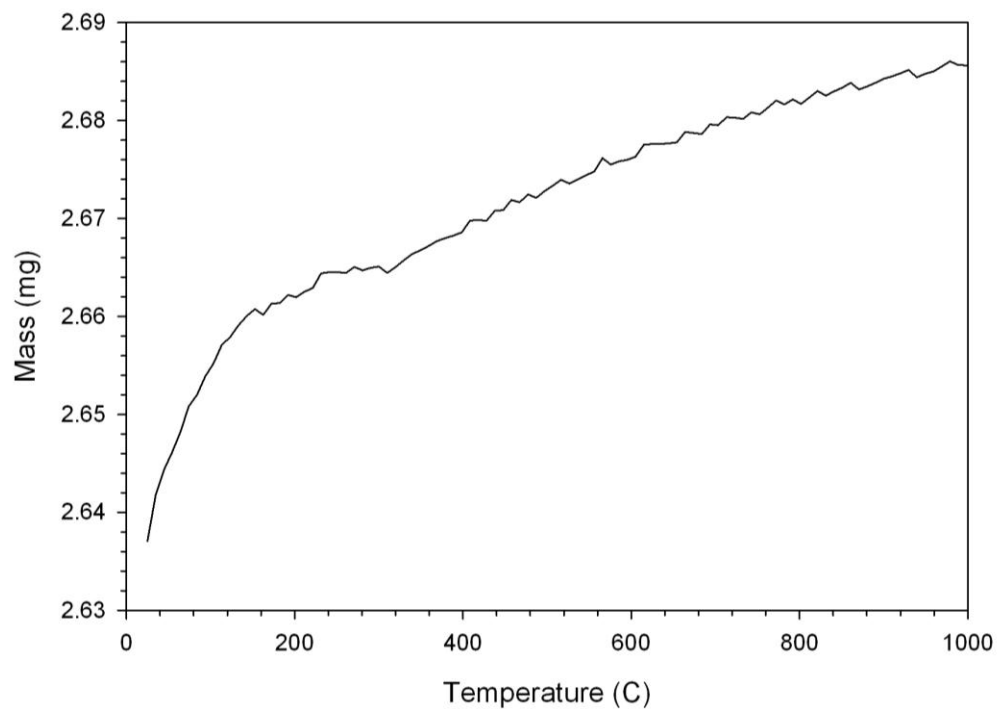


Figure 3-22. TGA curve of uncoated nom. 20nm gold particles under an oxidative atmosphere. No significant mass change was observed.

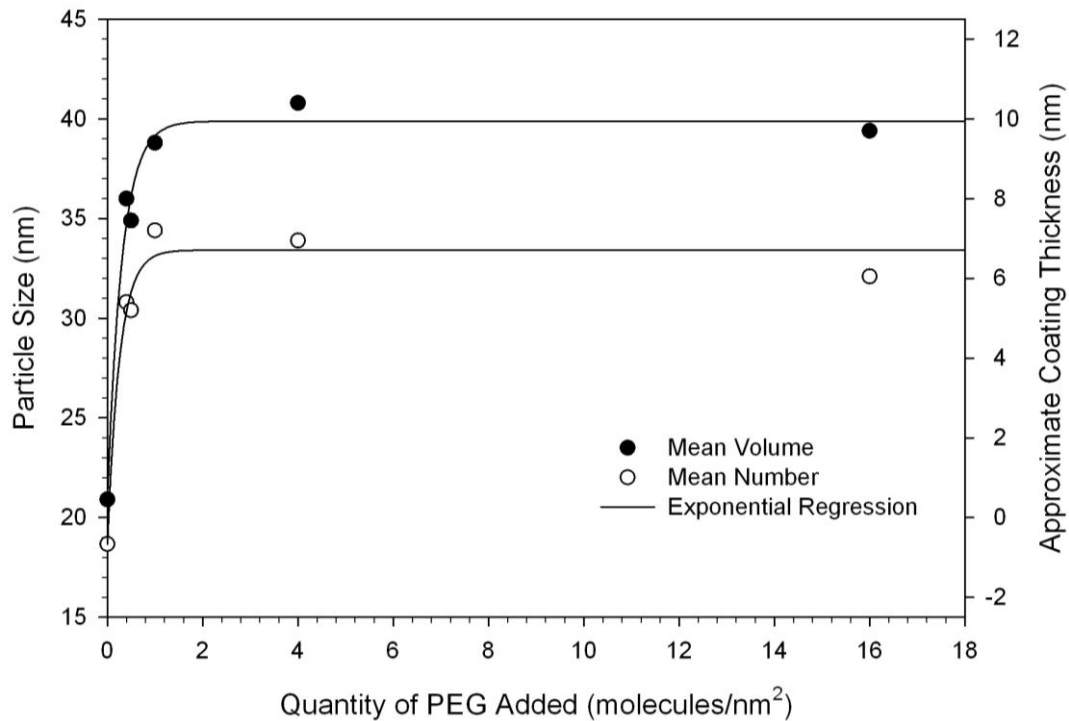


Figure 3-23. Particle size increase of nom. 20nm gold particles on coating with PEG as determined by DLS.

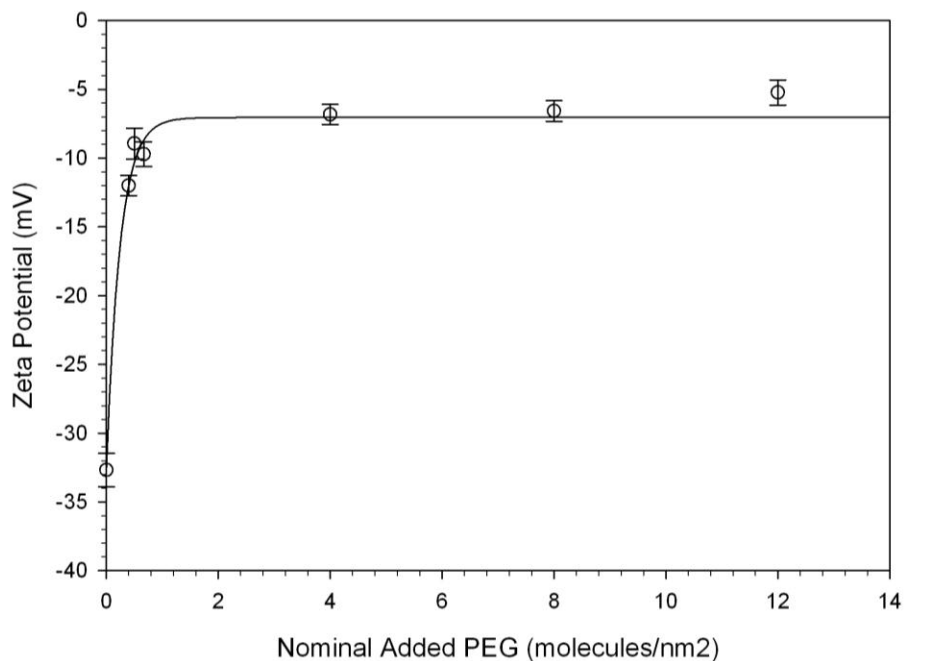


Figure 3-24. Zeta potential neutralization of nom. 20nm gold particles on coating with PEG (as determined by DLS). Error bars indicate duplicate measurements of each data point.

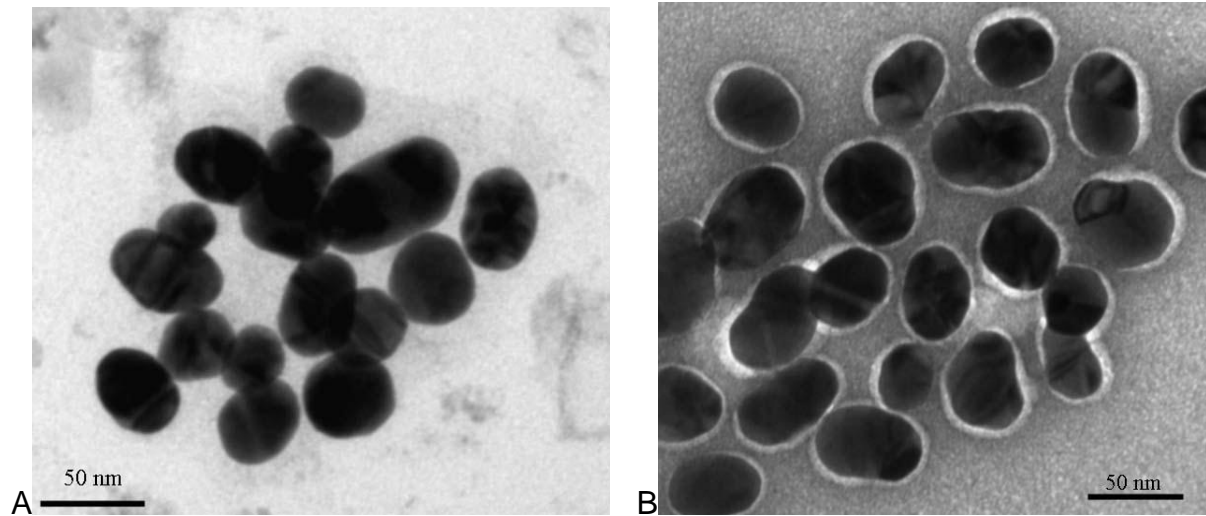


Figure 3-25. TEM images of negatively stained nom. 40nm PEG coated and uncoated gold particles. A) Uncoated particles. B) PEG coated particles. The light (unstained) PEG coating can be clearly seen surrounding the coated particles. Particles imaged by Kerry Siebein.

Table 3-8. Summary of common misconceptions regarding adsorption measurements of PEG coatings of gold particles.

Misconception	Comment
Elimination of salt induced aggregation is an effective means of determining maximum surface coverage.	Salt induced aggregation is eliminated long before surface coverage is maximized. It is not particularly useful in determining adsorption density at saturation, but may be used at lower adsorbate concentrations as a qualitative indicator of coating condition or suspension stability.
Minimization or neutralization of zeta potential is an effective means of determining maximum surface coverage.	Zeta potential is frequently neutralized long before surface coverage is maximized.
Adsorption of PEG occurs with 100% efficiency.	Degradation or poor reagent quality may significantly reduce the adsorption efficiency and leave non-adsorbing PEG in the medium.
Adding PEG at a ratio of 4 molecules per nm ² is necessary and/or sufficient for maximum surface coverage.	The initial ratio of PEG to surface area is largely dependent on the quality and properties of the PEG reagent used and can vary considerably (both higher and lower).
The presence of excess PEG in the suspension medium is often overlooked	Excess PEG present in the suspension medium is one of the key factors that delays onset of PEG coating degradation, even at low levels.

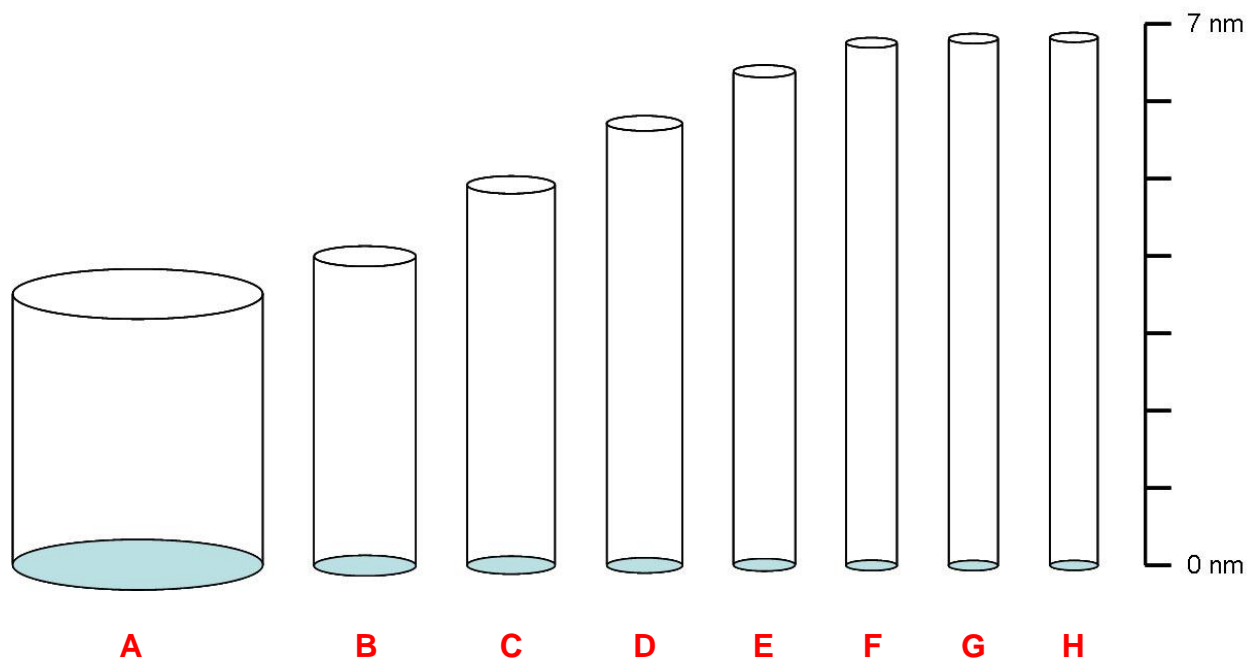
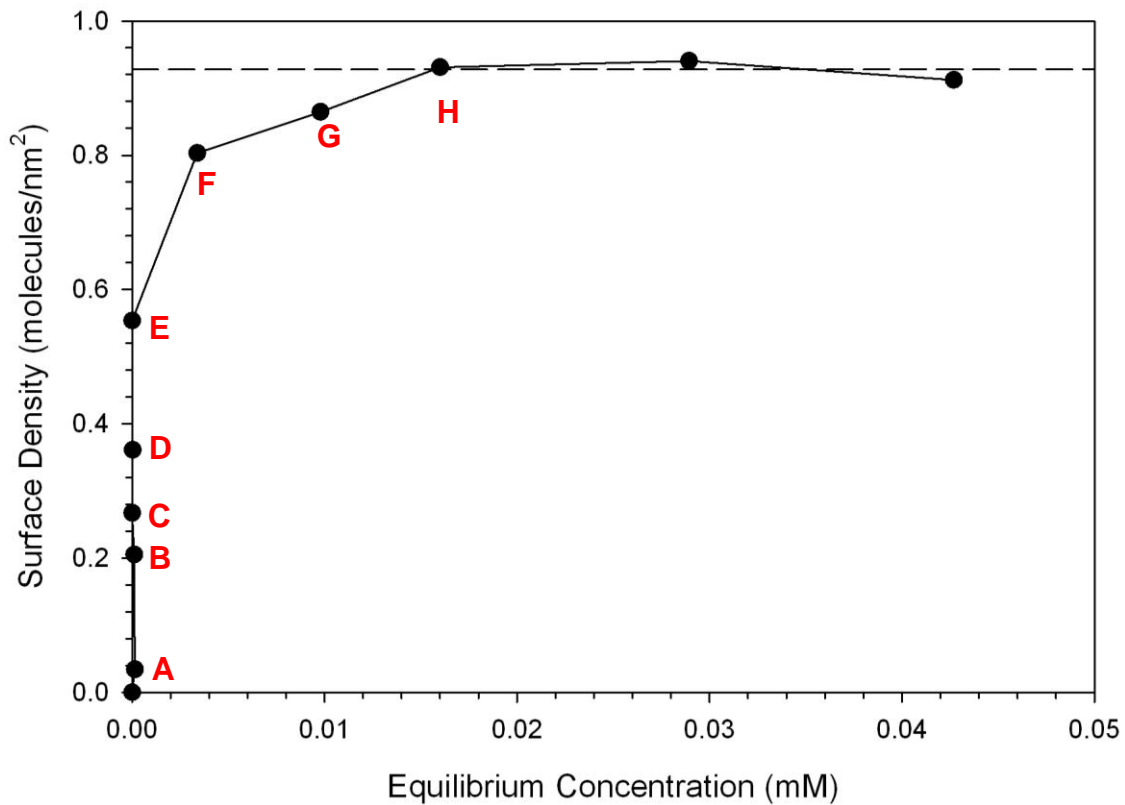


Figure 3-26. Illustration of the adsorbate surface structure with increasing coating density. Adsorbate footprint calculated from the adsorption isotherm assuming a circular footprint, and the height calculated from sedimentation data (as shown in Figure 3-6).

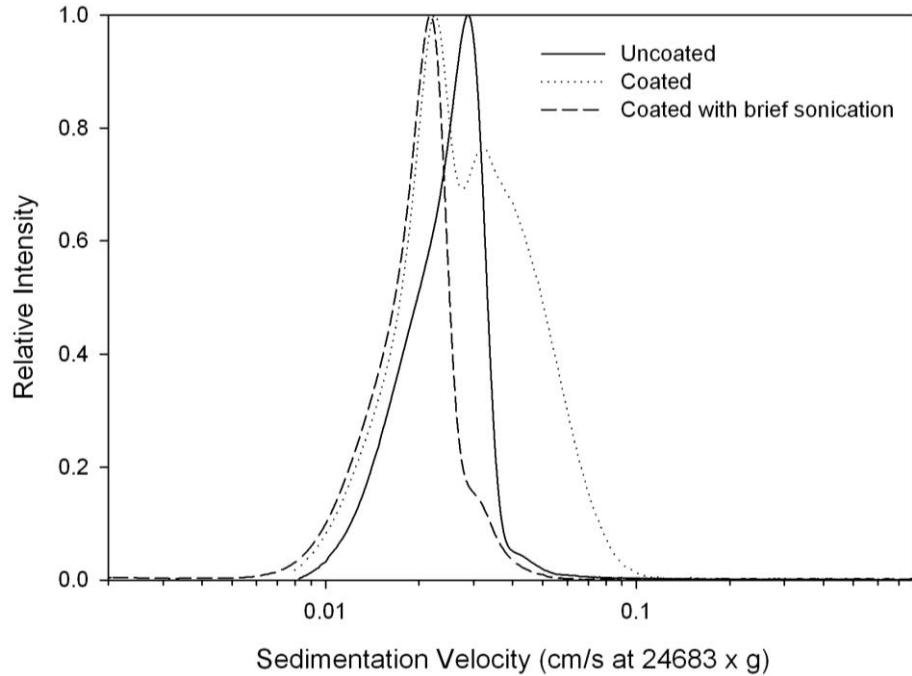


Figure 3-27. Sedimentation velocity distributions at different points during PEG coating (Reagent 1) with a large mixing volume. Reversible aggregation was observed initially and was eliminated with brief low intensity sonication. Aggregation did not recur after the initial sonication treatment.

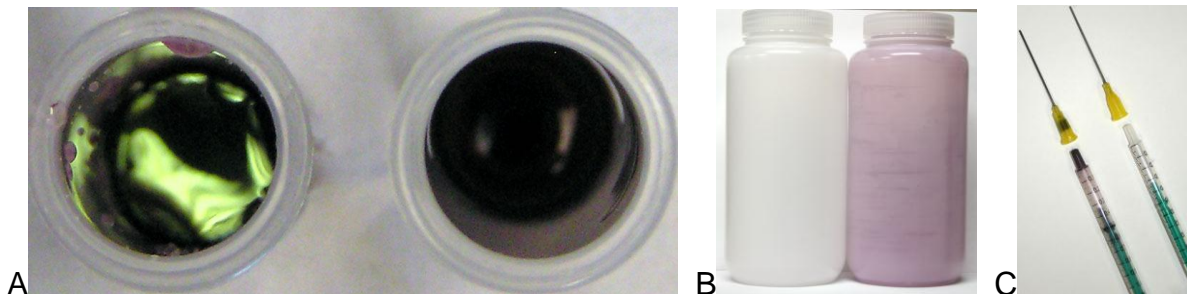


Figure 3-28. Apparent hydrophobicity exhibited by gold particles in salt solutions and when coated with sub-optimal coating densities. A) Apparent partitioning at the air-liquid interface in the form of a reflective surface layer. Left container has a cleaned suspension concentrate added to concentrated NaCl, right container has the same cleaned concentrate added to deionized water. B) Adhesion to the liquid-container interface in a hydrophobic polypropylene container at sub-optimal coating density. The container on the left is a clean container, while the container on the right was exposed to coated gold particles. Uncoated particles do not readily adhere to the polypropylene containers provided that they are stable. C) Syringe used to dispense PEG coated particles at high salinity (left) and a clean syringe (right).

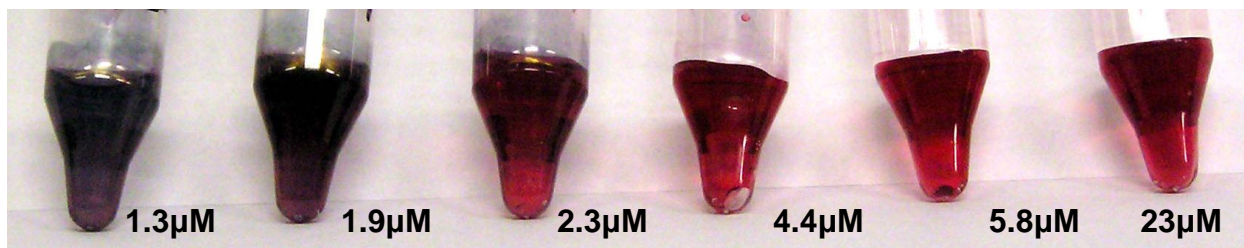


Figure 3-29. Salt induced aggregation of particles with sub-optimal PEG coatings. Aggregation is apparent in samples with $2.3\mu\text{M}$ or less initial PEG concentration. All particles were initially dispersed prior to addition of salt. PEG coating density was maximized at an initial PEG-thiol concentration between 11 and $15\mu\text{M}$ for these particles, however salt induced aggregation was eliminated at a concentration between 2.3 and $4.4\mu\text{M}$

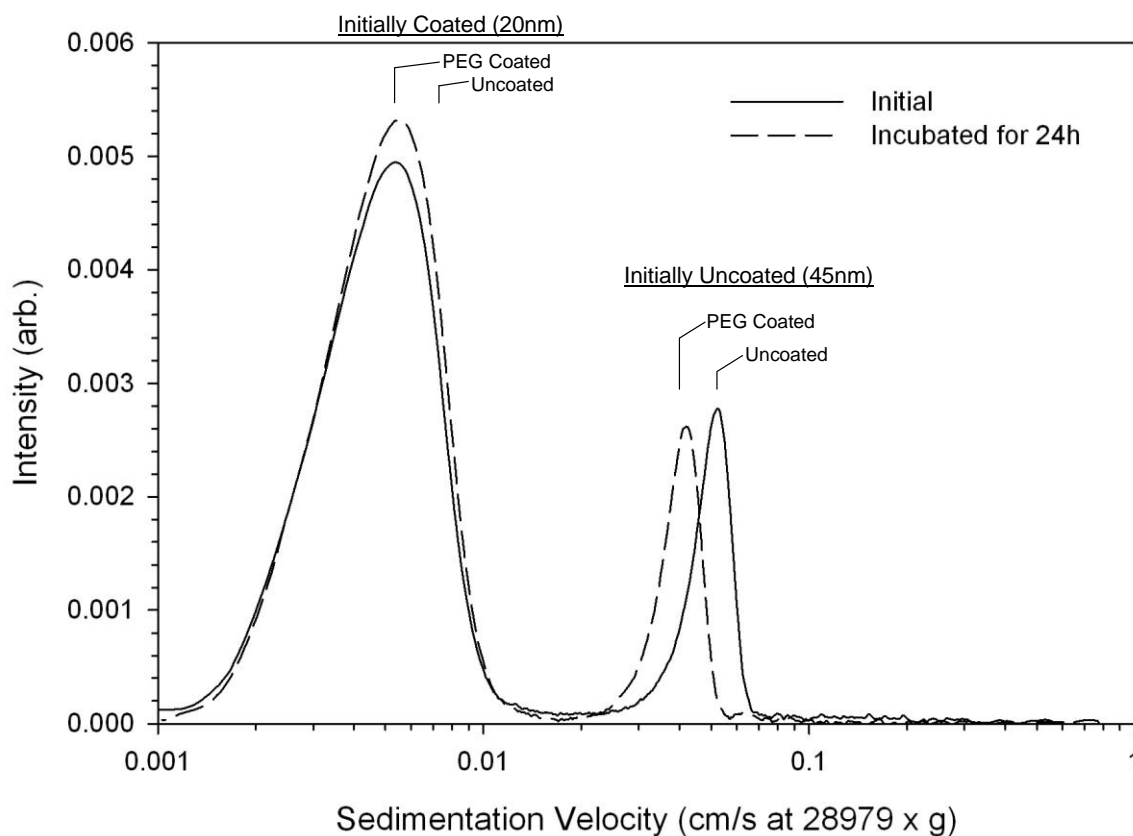


Figure 3-30. Sedimentation velocity distributions of mixed nom. 20nm PEG coated and nom. 45nm uncoated particles after incubation at 37C for approximately 24h . Migration of PEG from the smaller 20nm particles can be seen in the decreased sedimentation velocity of the 45nm peak. No shift in sedimentation velocity was observed immediately after mixing. Sedimentation velocities of fully PEG coated and uncoated particles are indicated.

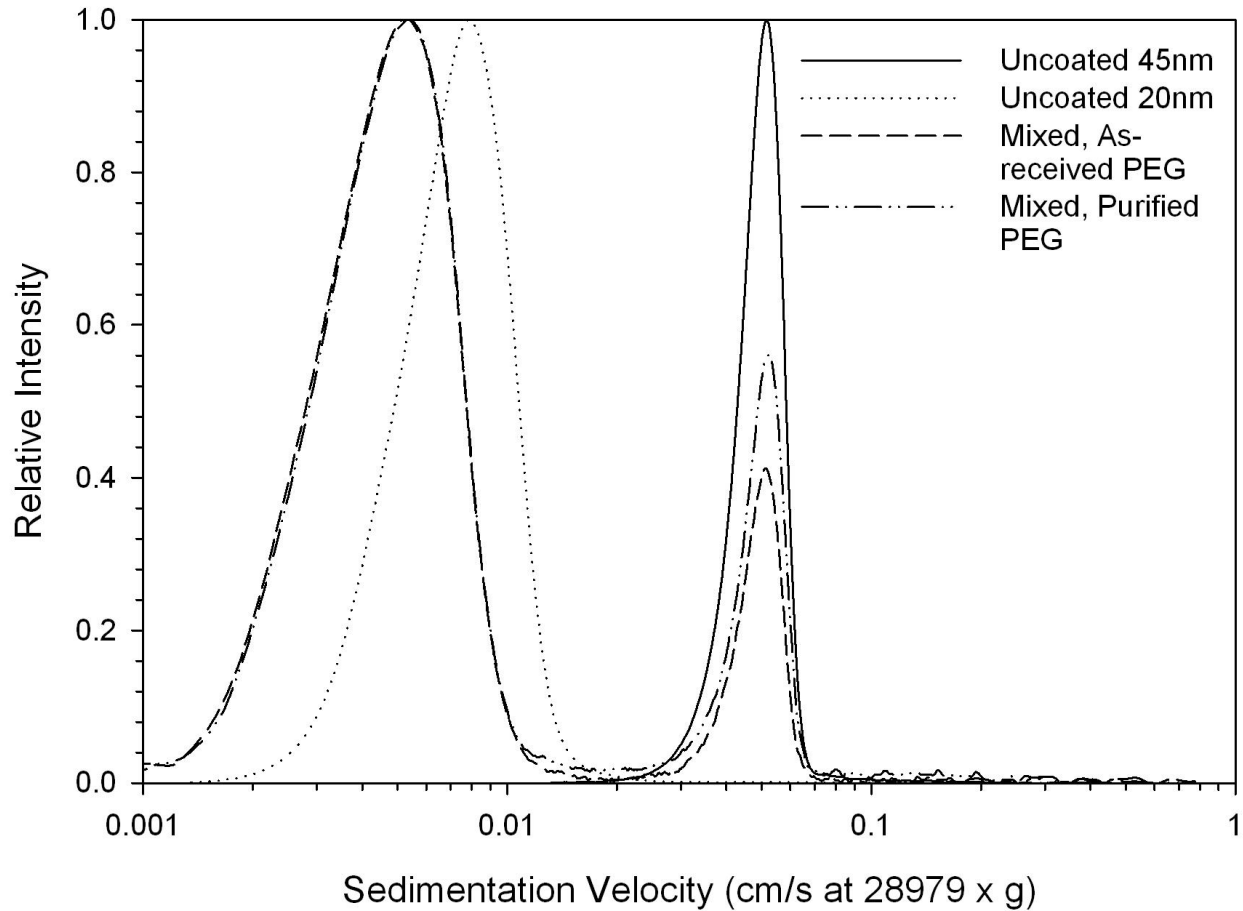


Figure 3-31. Sedimentation velocity distributions of mixed nom. 20nm PEG coated (Reagent 2) and nom. 45nm uncoated particles initially. Note that the sedimentation velocities of the nom. 45nm particles (at approximately 0.05cm/s) are identical initially, indicating that no unbound PEG remained in solution after cleaning.

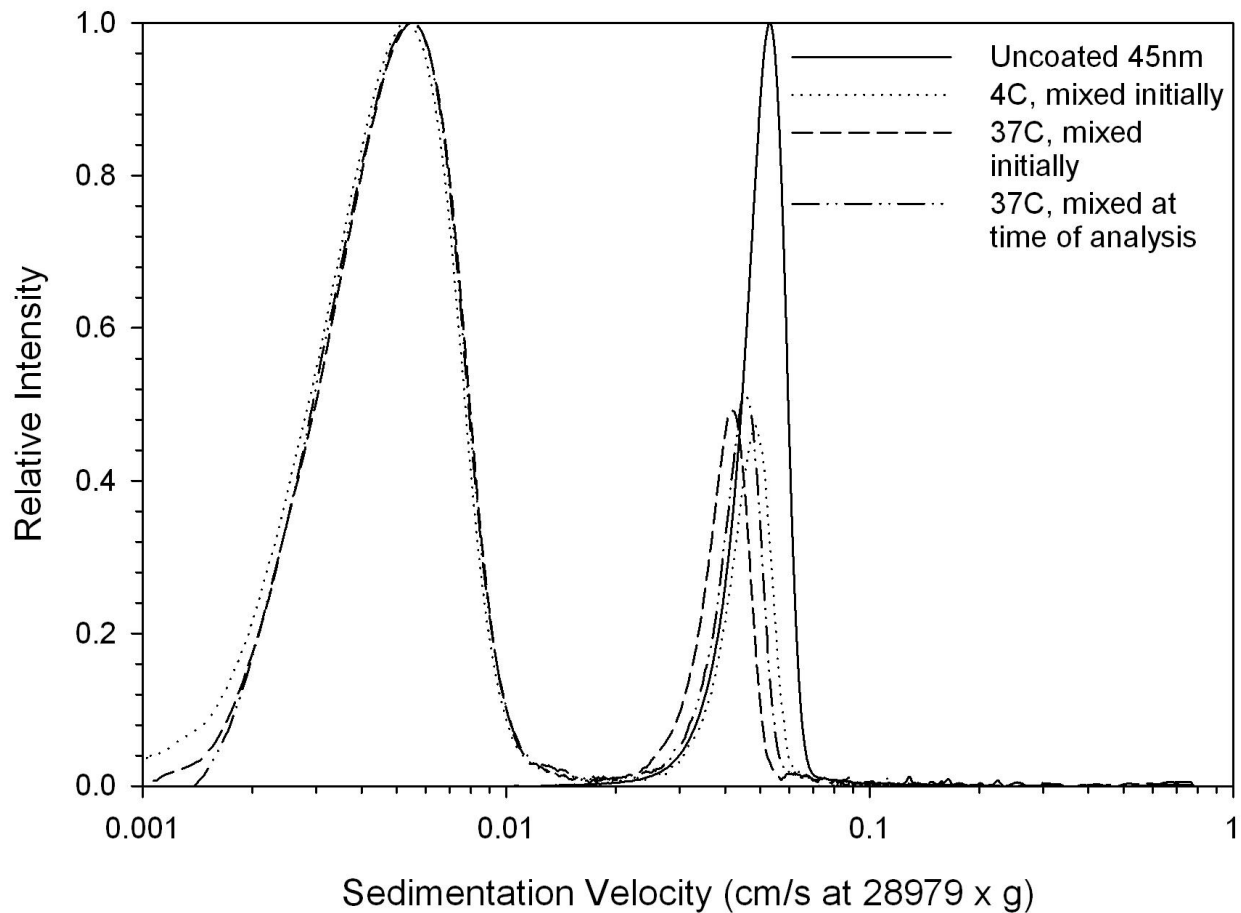


Figure 3-32. Sedimentation velocity distributions of mixed nom. 20nm PEG coated (Reagent 2 as received) and nom. 45nm uncoated particles after 24h under various conditions. The observed shifts in the 45nm particle sedimentation velocity were (in order of increasing shift/apparent PEG coating density): 37C with uncoated particles mixed initially > 37C with uncoated particles mixed just before analysis > 4C with uncoated particles mixed initially.

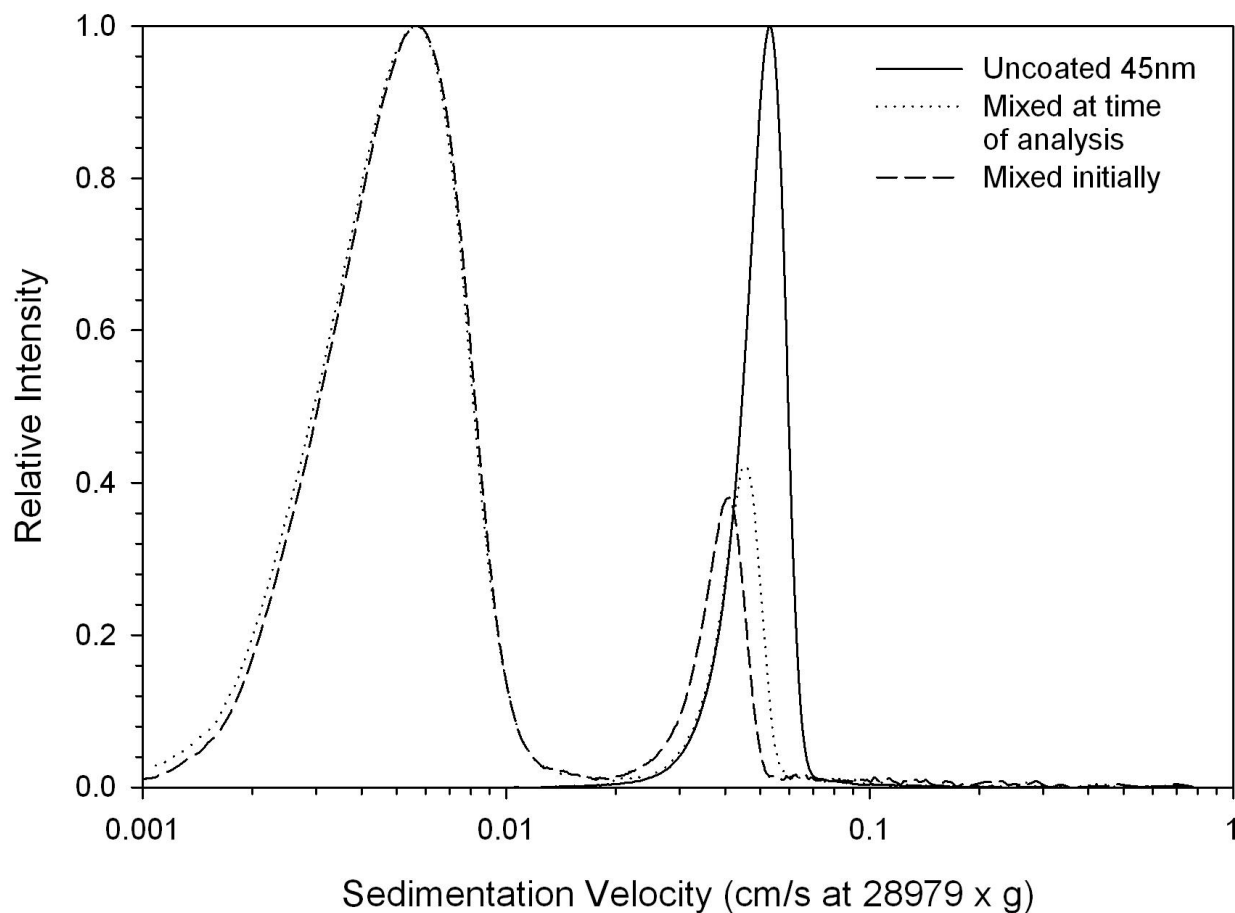


Figure 3-33. Sedimentation velocity distributions of mixed nom. 20nm PEG coated (Reagent 2 purified) and nom. 45nm uncoated particles after 24h at 37C. The shift observed in the nom. 45nm particles was higher in the sample where particles were added initially than those where the particles were added just before analysis.

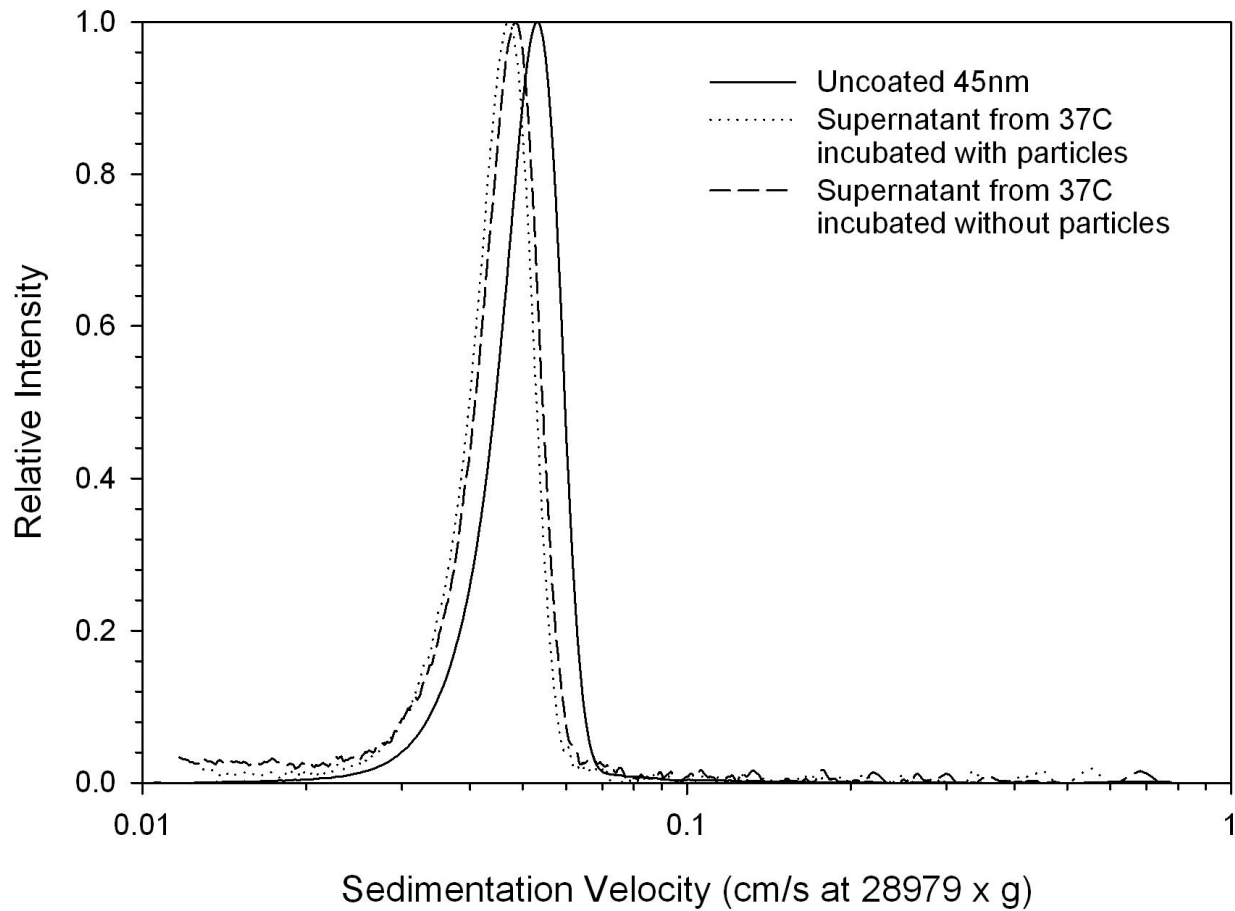


Figure 3-34. Sedimentation velocity distributions of nom. 45nm particles added to supernatants from PEG coated (Reagent 2 as received) nom. 20nm particles after 24h at 37C.

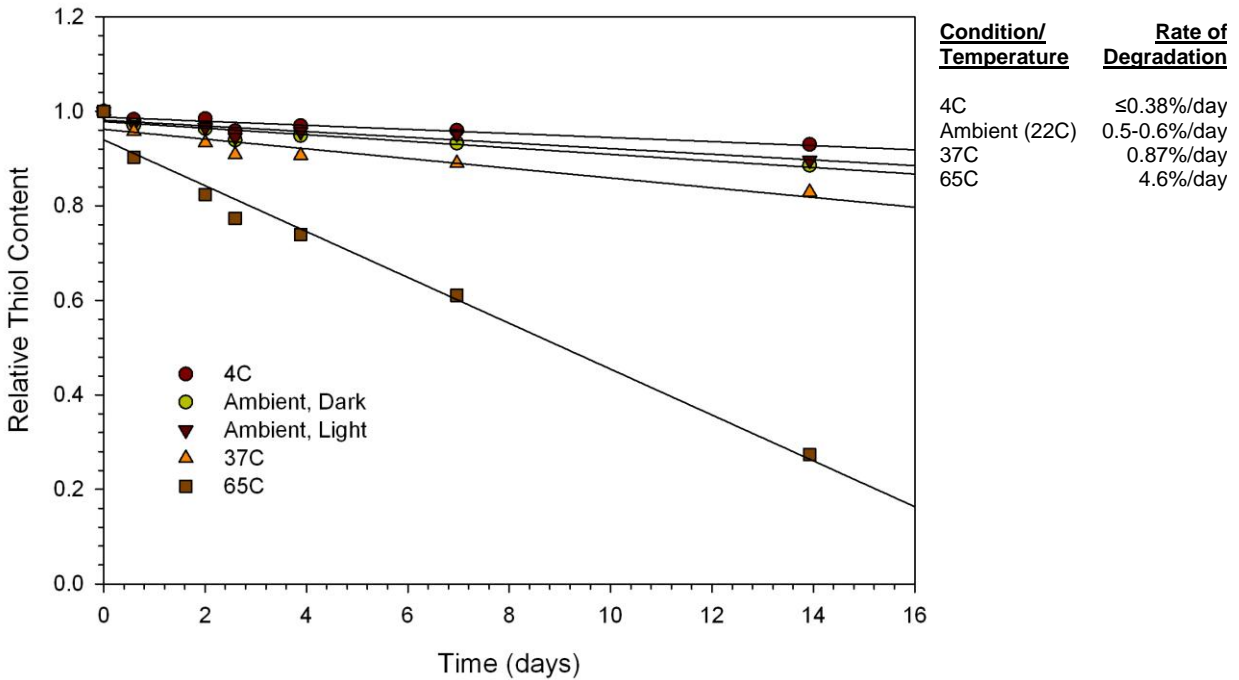


Figure 3-35. Rate of thiol activity loss in PEG-thiol solutions (0.1mM Reagent 2) based on storage condition. The rates of degradation in % of thiol activity per day are shown to the right of the plot.

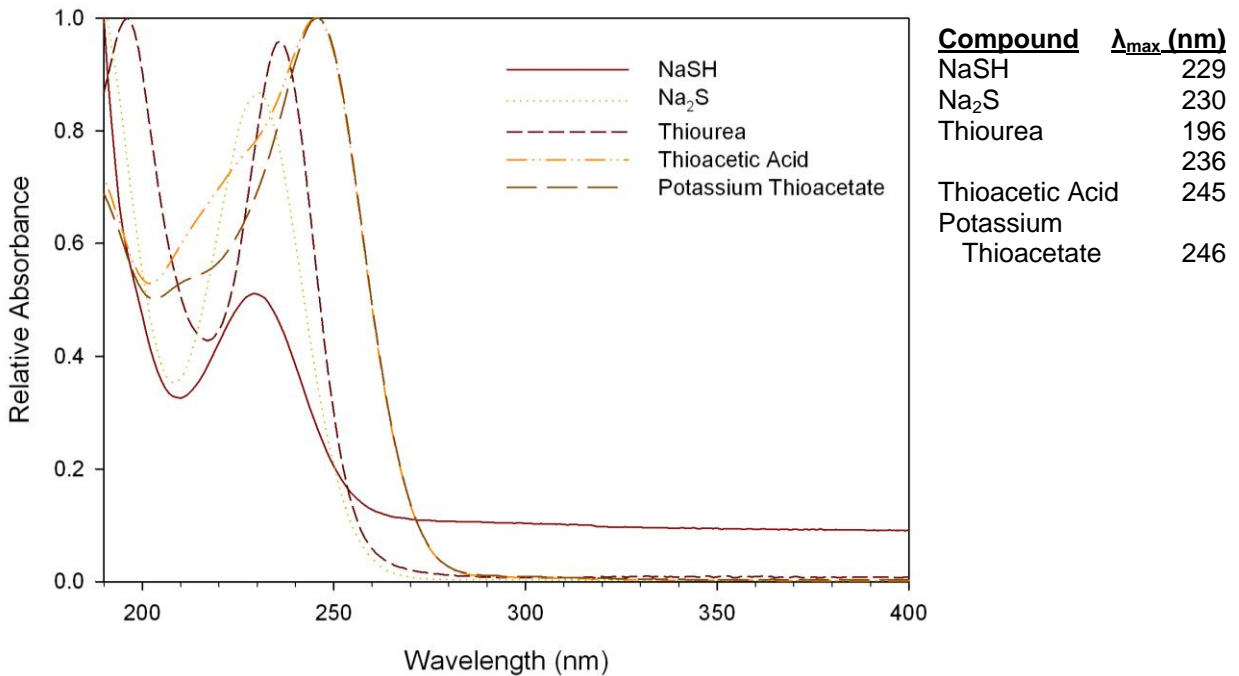


Figure 3-36. Near UV absorption spectra of aqueous solutions of selected compounds used for thiolation. Absorbance maxima are shown on the right for these compounds.

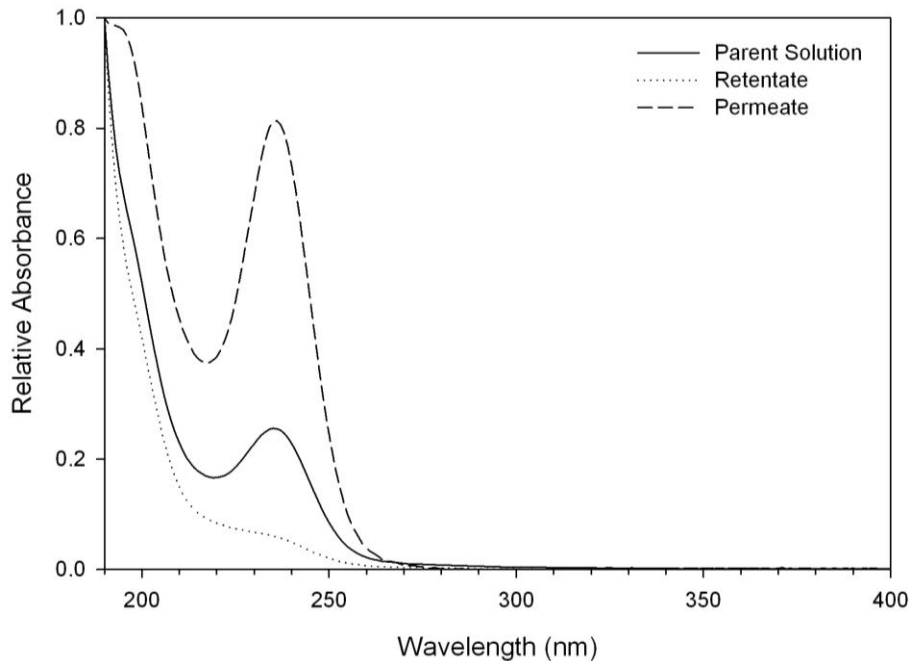


Figure 3-37. Near UV absorption spectra of aqueous solutions of thiolated PEG (as received), dialysis permeate, and retentate of the thiolated PEG compound (3kDa MWCO). Note the enrichment of the compound with absorbance at 236nm in the permeate and corresponding depletion in the retentate.

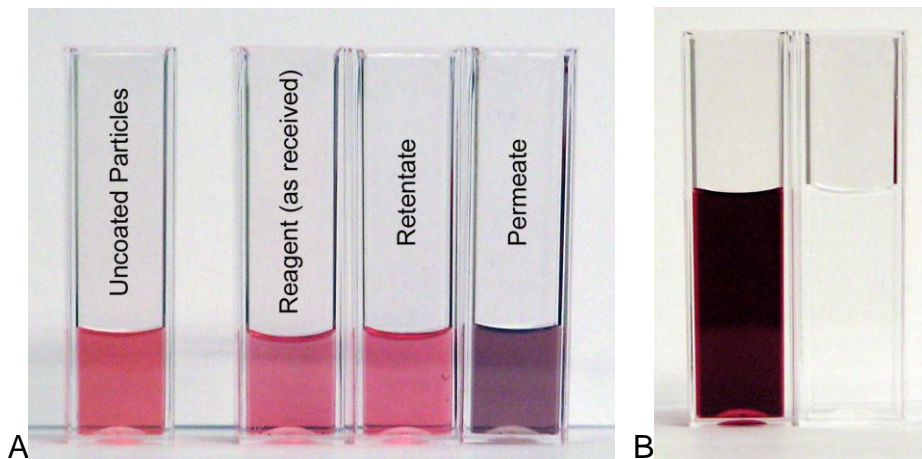


Figure 3-38. Images of a gold suspension before and after exposure to the PEG reagent (Reagent 2 as received), dialysis permeate, retentate, and thiourea. A) Gold suspension before and after exposure to the PEG reagent (as received), dialysis permeate, and retentate. The PEG reagent and dialysis retentate were able to effectively stabilize the gold suspension; however the permeate caused immediate destabilization of the suspension as indicated by a color change. B) Dissolution of nom. 20 nm uncoated gold particles with thiourea under ambient conditions (dissolution confirmed by ICP). Suspension of gold before (left) and after (right) treatment with thiourea.

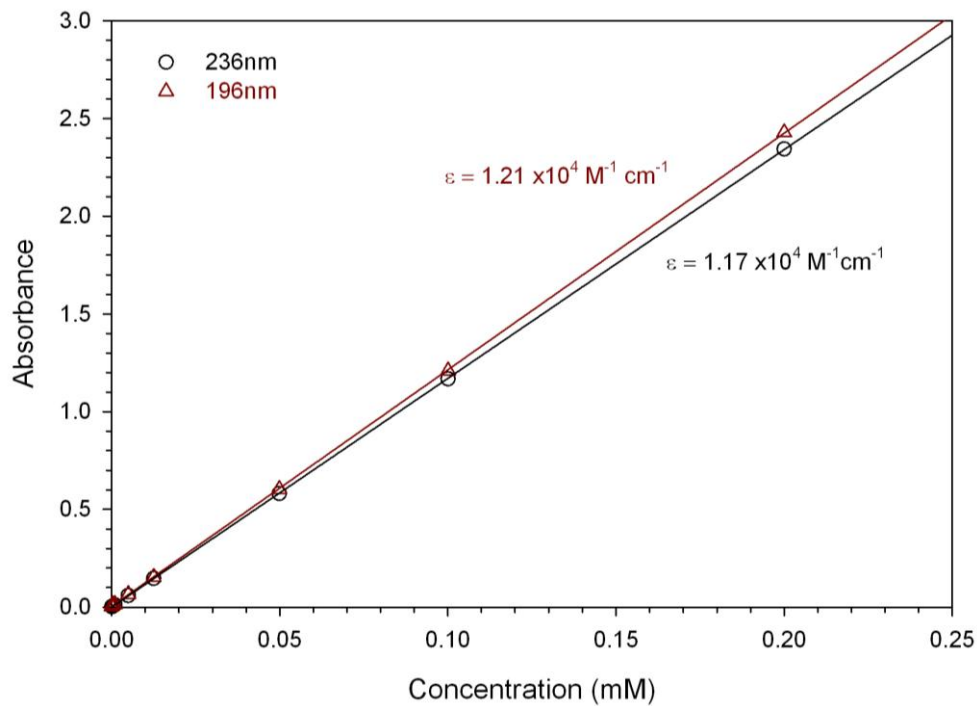


Figure 3-39. UV response curves of thiourea at concentrations below 0.2mM. The molar extinction coefficients at the two absorbance maxima of 196nm and 236nm are shown. Experimentally determined limits of detection are in the μM region. Note that the ratio of the two peaks is not constant at lower concentrations (Figure B-1, Figure B-2), though the peak at 236nm maintains linearity across the entire range.

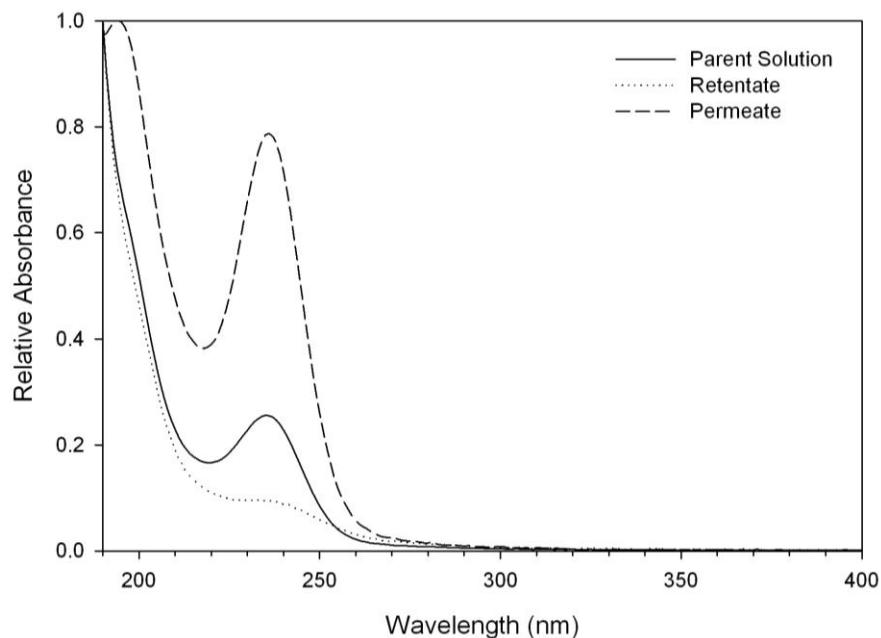


Figure 3-40. Near UV absorption spectra of aqueous solutions of thiolated PEG (Reagent 2 as received), dialysis permeate, and retentate of the thiolated PEG compound (100-500Da MWCO). Note the higher separation efficiency (particularly at lower wavelengths) compared to the 3kDa membrane (Figure 3-37).

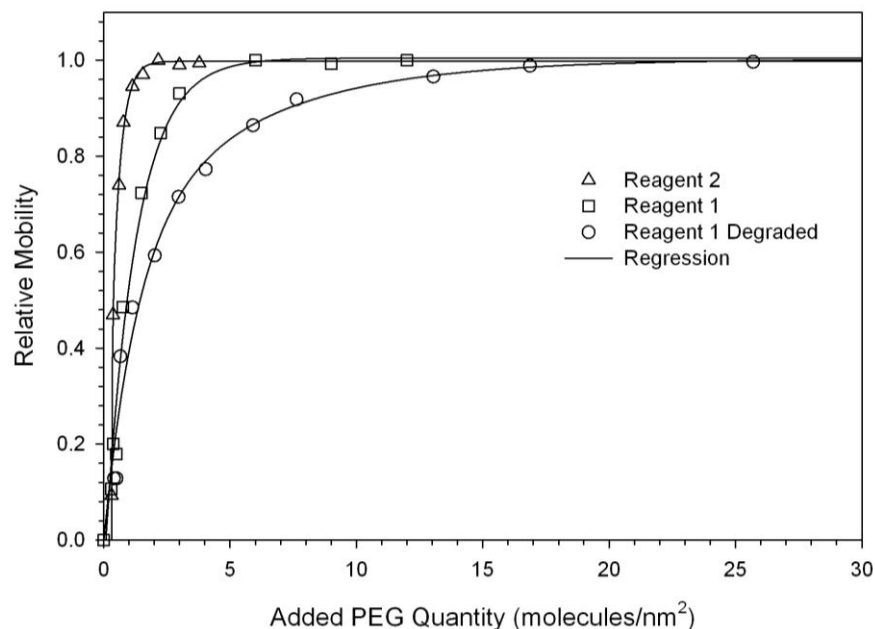


Figure 3-41. Relative mobility of PEG coated nom. 20nm gold particles with increasing concentration of thiolated PEG. Note the differences in concentration required to achieve maximum surface coverage: approximately 2nm^{-2} for reagent 2, 5nm^{-2} for reagent 1, and 16nm^{-2} for reagent 1 after degradation.

Table 3-9. Sulfur content of thiolated PEG reagents as determined by ICP.

Reagent	PEG Concentration (mM)	Expected S Concentration (ppm)	Measured S Concentration (ppm/mM)	Percent Difference
Reagent 1	1	32.064	32.76 ±0.74%	+2.2%
Reagent 1 (Degraded)	0.999	32.039	23 / 0.72 ±1.1%	-28.2%
Reagent 2	0.995	31.906	34.75 / 1.084 ±1.5%	+8.91

Table 3-10. Sulfur and thiol content of dialysis permeate and retentate (Reagent 2).

Solution	Expected S Concentration (ppm/mM) ^a	Measured S Concentration (ppm/mM) ^b	Thiol Content (mM) ^c	% of Initial S Content (as S / as thiol)	% of Theoretical (as S) ^a
Reagent (As received)	32.064 / 1	34.230 / 1.068 ±1.3%	0.80	100% / 100%	106.8%
Dialysis Permeate	N/A (none for pure reagent)	7.075 / 0.22 ±5.1%	0.011 ^d	21.2% / 1.37% ^d	22.1%
Dialysis Retentate	N/A (complete retention for pure reagent)	27.15 / 0.847 ^e	0.79	79.3% ^e / 98.8%	84.7%

Notes:

^a Assuming a pure 5kDa thiol terminated methoxy PEG compound.

^b Analyzed by ICP.

^c Analyzed by Ellman's Assay using a cysteine standard.

^d Ellman's Assay has extremely poor sensitivity to thiourea, with a response at least 5000 times lower than cysteine. References¹⁸⁹⁻¹⁹¹ indicate that the preferred tautomeric form is not a thiol (SC(NH₂)₂ is preferred over HSCNH₂NH). At the indicated concentration, the contribution from thiourea is expected to be infinitesimally small.

^e Not measured directly – calculated by subtraction of permeate sulfur concentration from initial concentration. Since equilibration of permeate and retentate concentration occurs during dialysis and both the permeate and retentate were to be collected for analysis, the dialysis retentate still contains a certain concentration of the components present in the permeate. For this reason the concentration was calculated by subtraction so that the data would reflect the sulfur content of only the retained fraction rather than a combination of the retained molecules and the equilibrium concentration of permeate molecules.

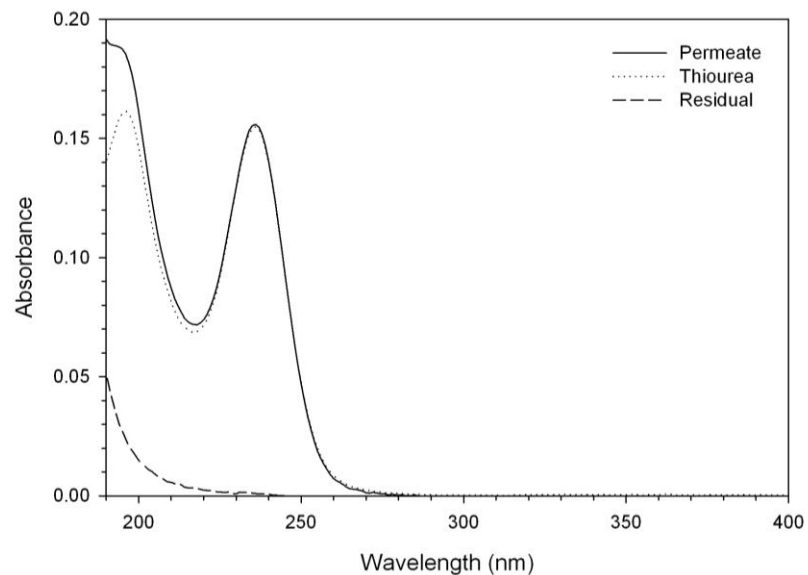


Figure 3-42. Deconvolution of the UV absorption spectrum of the dialysis permeate (from Figure 3-37). Thiourea was assumed to be the principal component.

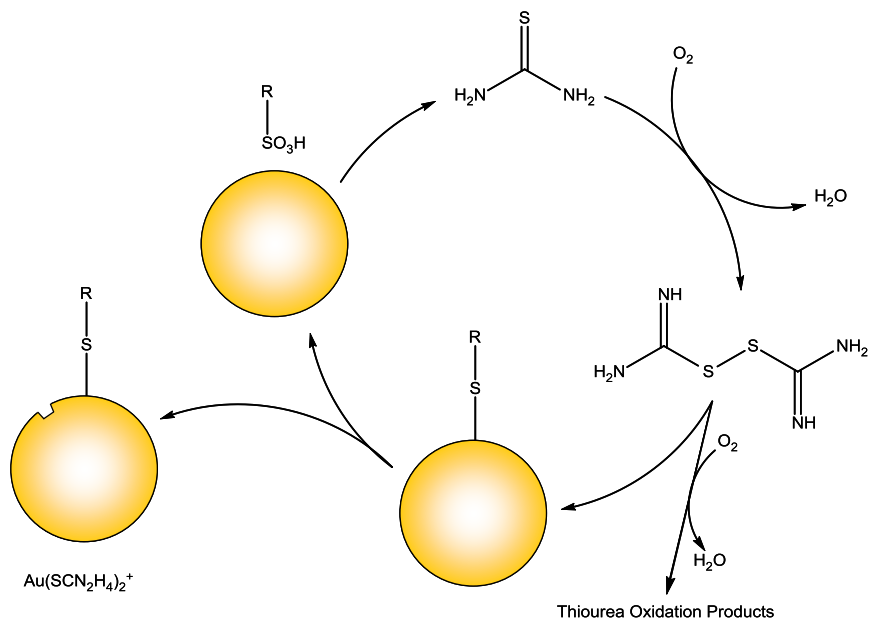


Figure 3-43. Potential thiourea mediated oxidation processes.

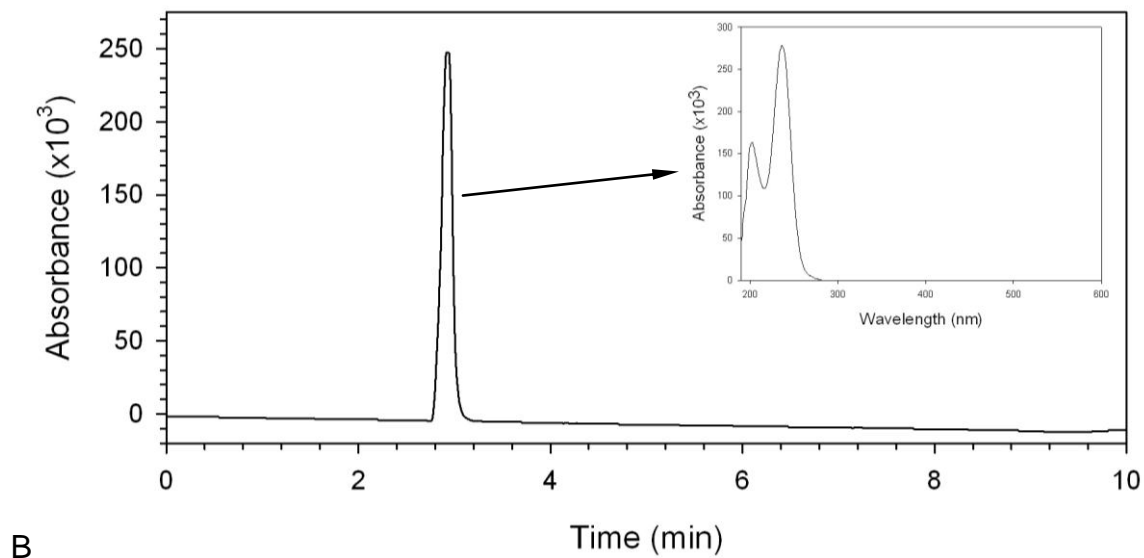
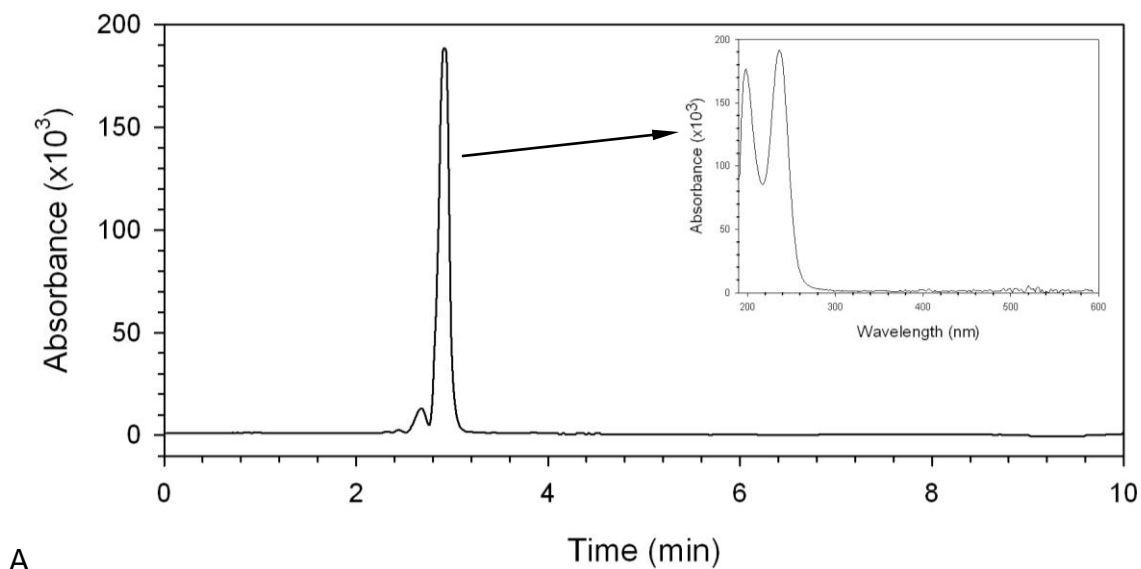


Figure 3-44. Chromatograms of A) dialysis permeate (100-500Da) and B) pure thiourea. Note that the retention times for pure thiourea and the primary component in the permeate are identical. The optical absorption spectra of these compounds show the characteristic absorption behavior of thiourea.

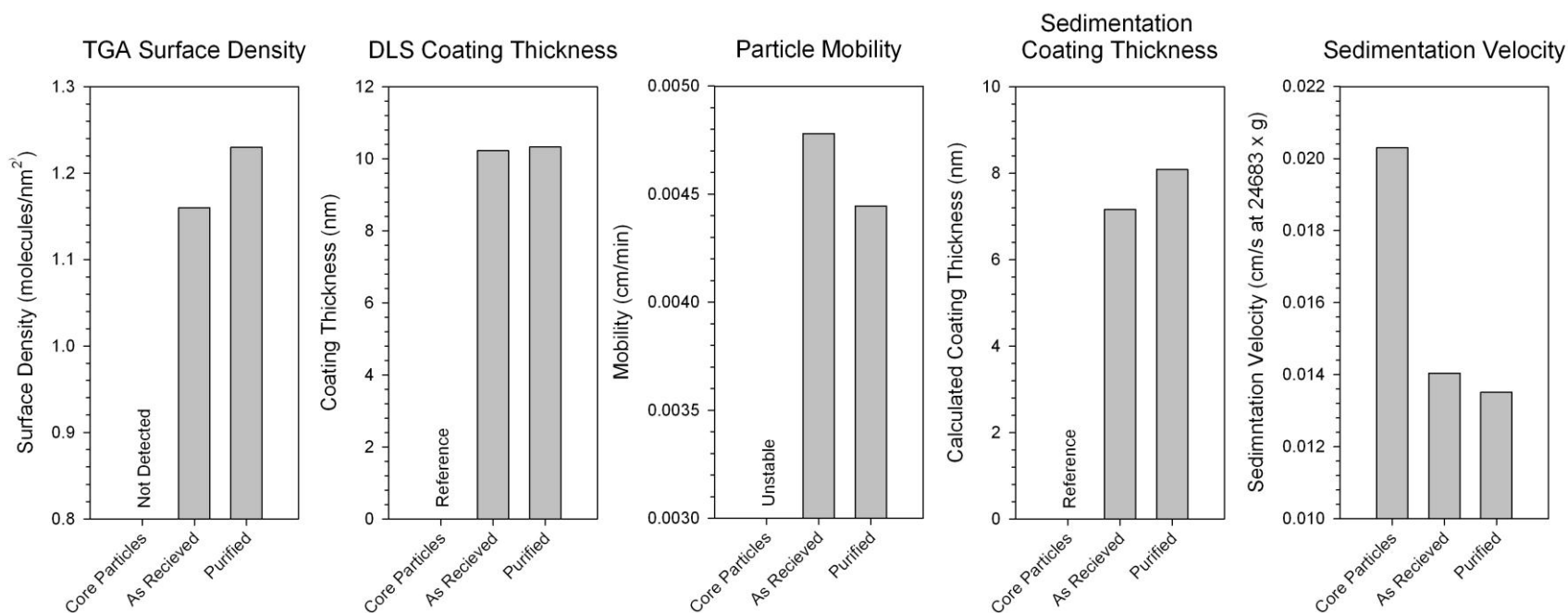


Figure 3-45. Comparative measurements of purified and as received PEG reagent (Reagent 2) using several coating characterization techniques. Significant increases in TGA surface density and sedimentation coating thickness were observed while significant decreases in particle mobility by electrophoresis and sedimentation velocity were observed after purification. No significant difference in coating thickness was observed by DLS. These differences are all consistent with a higher surface density of PEG caused by removal of a competing adsorbate.

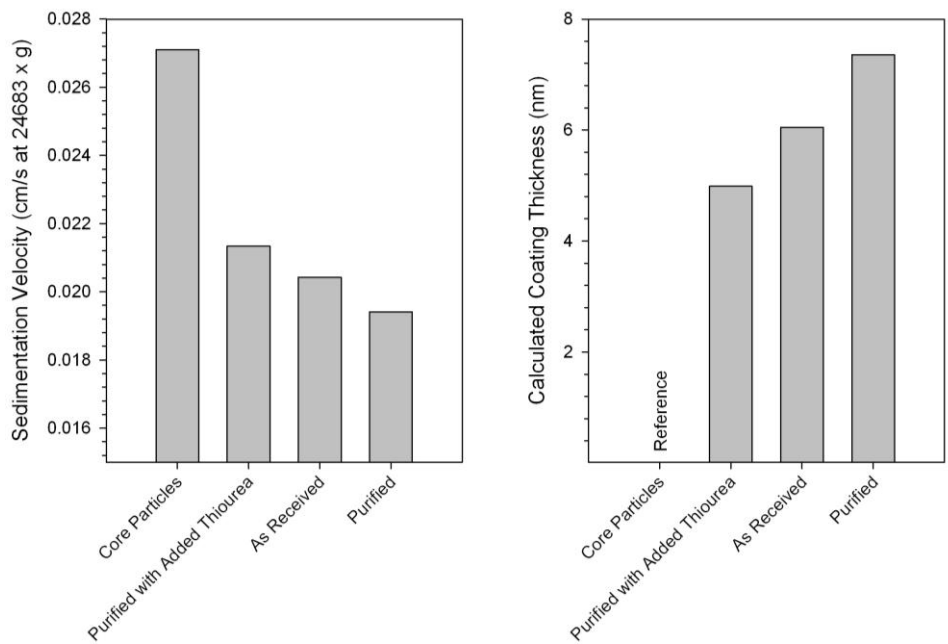


Figure 3-46. Sedimentation analysis demonstrating the effects of thiourea impurities on the PEG coating. As the concentration of thiourea in the PEG reagent increases, the coating thickness decreases as evidenced by the increase in sedimentation velocity and decrease in calculated thickness. The sample with thiourea added to purified PEG contained a 2:1 molar ratio of thiourea:PEG, which is higher than the concentration present in the reagent initially.

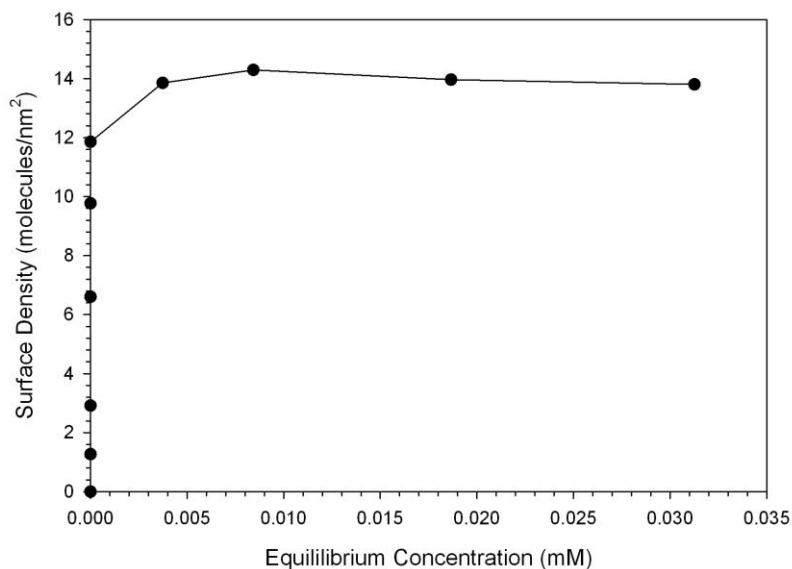


Figure 3-47. Adsorption isotherm of thiourea on nom. 20nm gold particles. Surface density at saturation was approximately 14 molecules/nm².

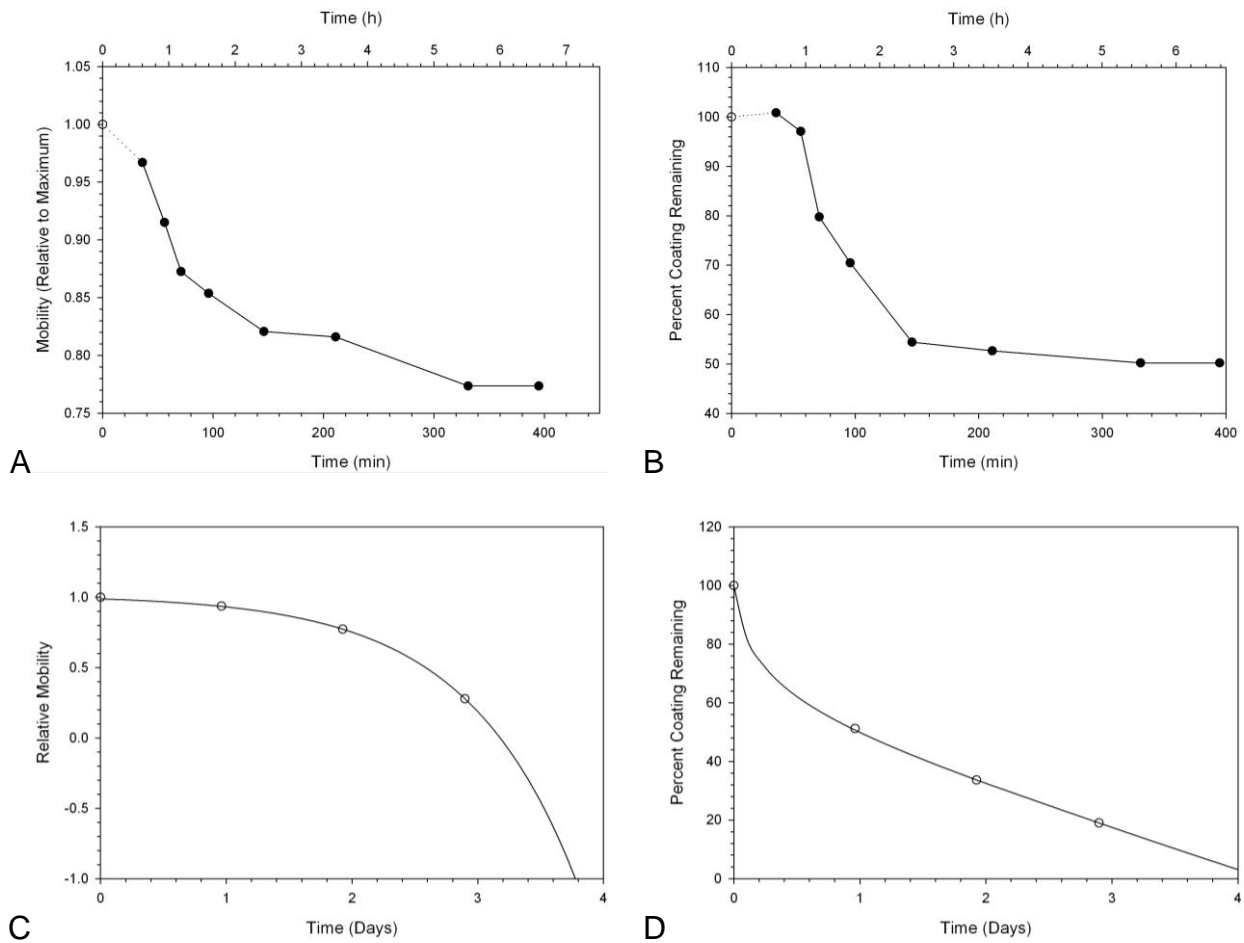


Figure 3-48. Time dependent mobility and coating density of PEG coated gold particles incubated at 37C in deionized water. Time dependent A) mobility and B) approximate coating density for PEG coated gold particles using Reagent 1. Time dependent C) mobility and D) approximate coating density for PEG coated gold particles using Reagent 2. Measurement at t=0 are fully coated particles with excess PEG. The source of the curve fitting the data in (D) is described previously in text.

Table 3-11. Summary of selected compounds possessing properties which are likely to influence the rate and mechanism of PEG coating degradation.

Sample Name	Preparation Details
Ascorbic Acid	Mild antioxidant
Uric Acid	Mild antioxidant
Glutathione	Mild antioxidant
Mercaptoethanol	Competing adsorbate, moderate thiol reductant
Thiourea	Competing adsorbate and lixivalent for gold, impurity in PEG reagents, mild antioxidant
TCEP (tris(2-carboxyethyl) phosphine HCl)	Strong thiol reductant
Sodium Borohydride	Strong reductant
Ferrous Chloride	Mild Oxidant
Hydrogen Peroxide	Strong Oxidant
Phosphate Buffered Saline	pH (7.2) and elevated (isotonic) salinity
Saturated Saline	High salinity (saturated NaCl)
Human Plasma	Whole human plasma
Human Plasma (Small molecules only)	Human plasma without large proteins and macromolecules (passed by 3kDa dialysis membrane)

Table 3-12. Degradation times for the least stable samples listed in Table 3-11 under buffered conditions.

Sample or Condition	Time to near complete removal of PEG coating.
Hydrogen Peroxide	Immediate
Mercaptoethanol	<1 day
Thiourea	<1 day
Deionized water (no buffer)	3 days
Sodium Borohydride	6 days

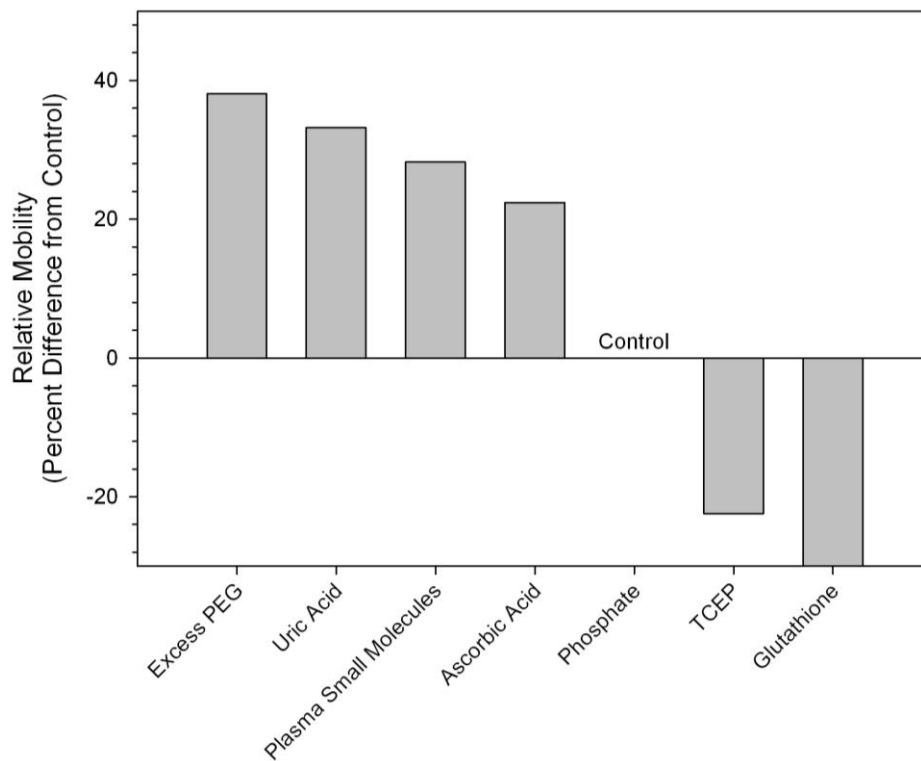


Figure 3-49. Change in mobility of buffered particles exposed to various compounds at 37C for 23 days. A relative mobility greater than the control (phosphate buffer only) indicates that the added compound decreases the rate of coating degradation.

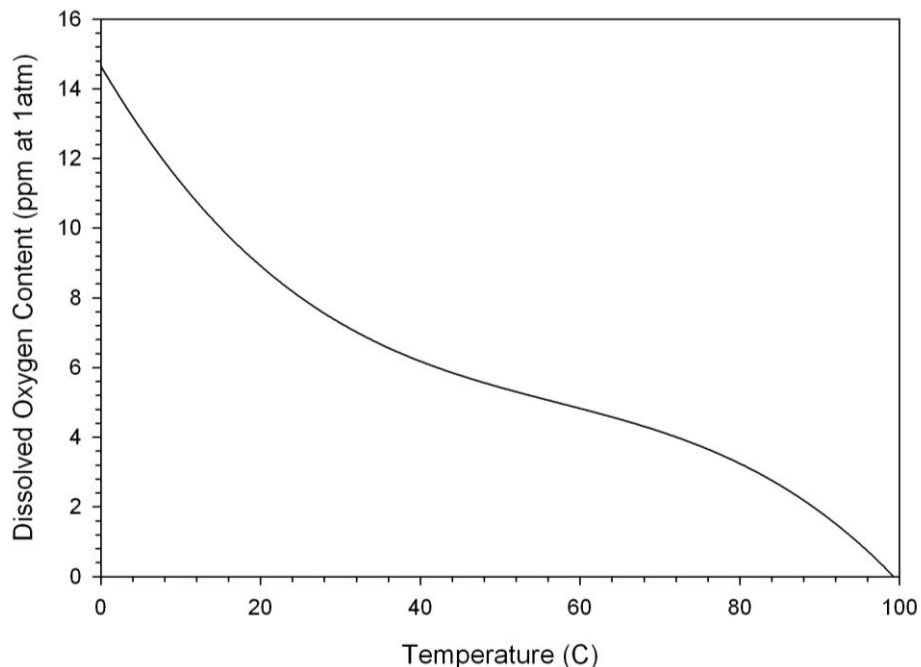


Figure 3-50. Dissolved oxygen content in deionized water equilibrated with air at STP.²¹¹

Table 3-13. Summary of samples prepared to screen for relationships between rate of coating degradation and common storage conditions.

Sample Name	Preparation Details
<i>Excess PEG</i> (Control)	At the time of analysis, a large excess of PEG-SH was added to a sample of the particle suspension used in this study.
<i>Ambient</i> (Equilibrated and Degassed)	Samples were left uncovered under ambient lighting conditions at ambient temperature (22C).
<i>Inert Ambient</i> (Equilibrated and Degassed)	Samples were left in the dark at ambient temperature (22C) and under an inert (Ar) atmosphere.
<i>37C</i> (Equilibrated and Degassed)	Samples were left in a dark and temperature controlled oven at 37C.

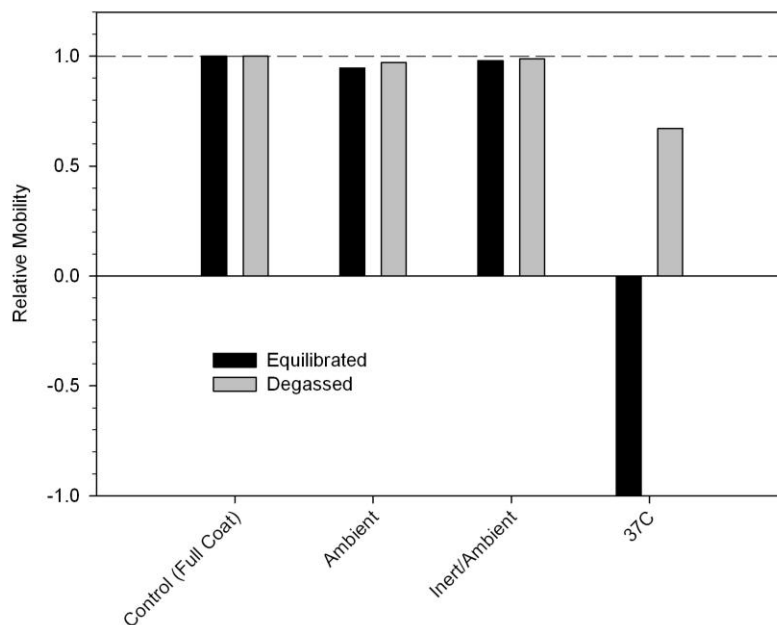


Figure 3-51. Comparison of particle mobilities in equilibrated and degassed media after 5 days under various conditions. Note that the equilibrated media sample at 37C showed high cathodal mobility, indicating that little coating remained.

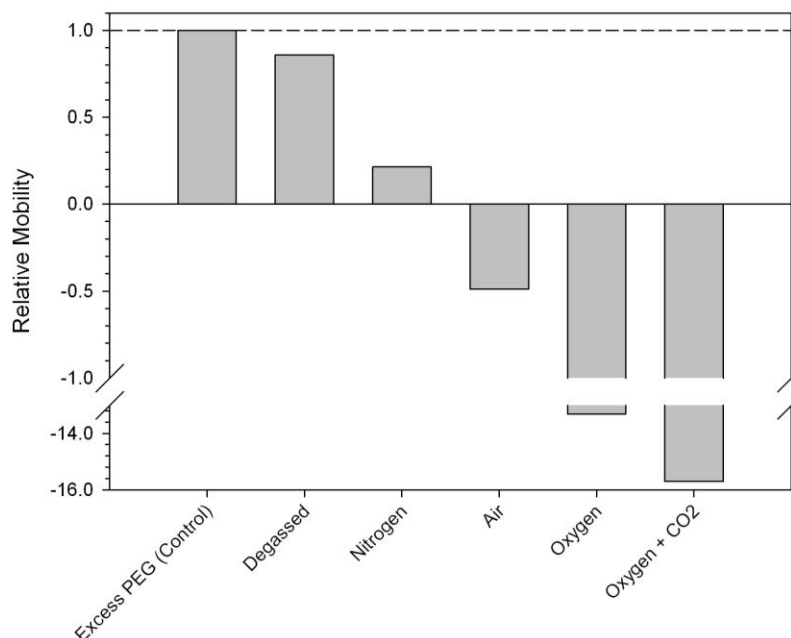


Figure 3-52. Relative mobilities of PEG coated gold particles incubated for 5 days at 37C in deionized water which was degassed and subsequently saturated with various gases and gas mixtures. Coating stability follows the trend: Degassed >> N₂ > Air > O₂ > O₂+CO₂.

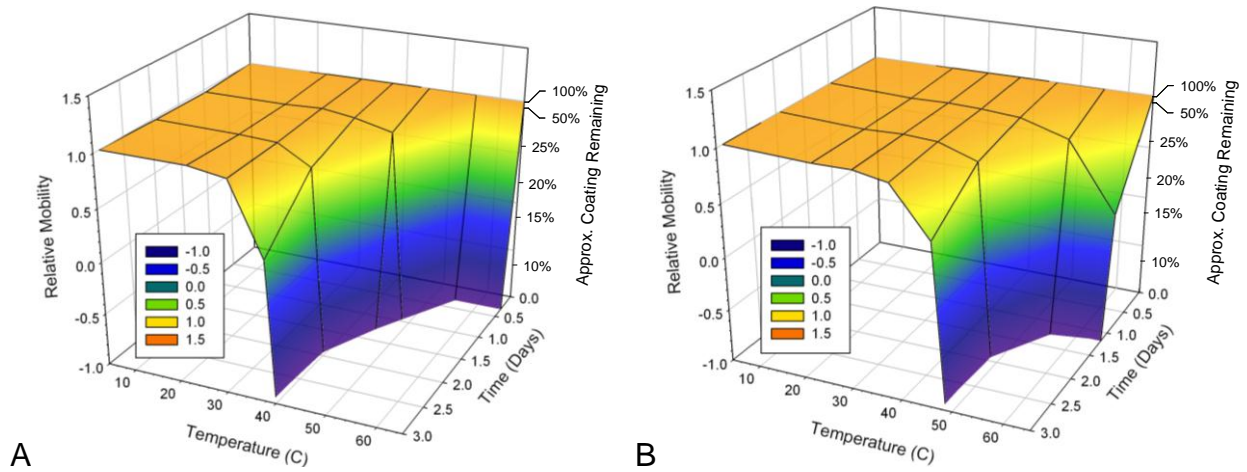


Figure 3-53. Relative particle mobility as a function of temperature and time over the first three days of incubation for A) Equilibrated water and B) Degassed water. Note the wider region of stability in the degassed water sample.

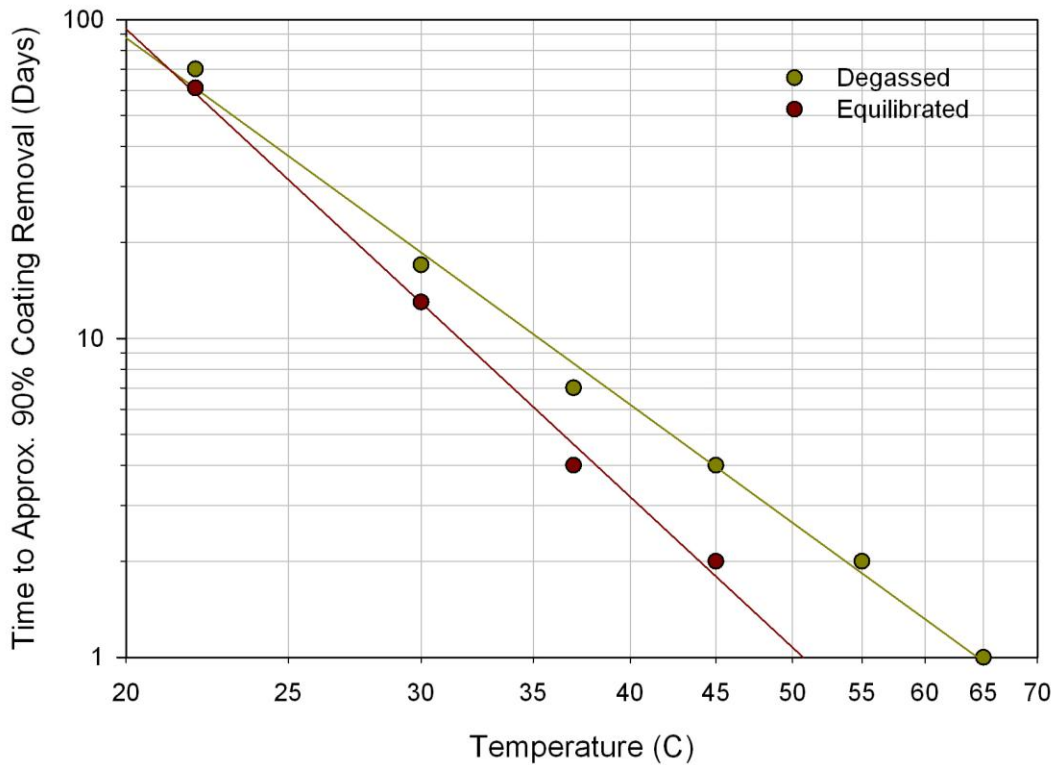


Figure 3-54. Time required to degrade approximately 90% of the PEG coating on nom. 20nm gold particles as a function of temperature in equilibrated and degassed water. At temperatures above body temperature, the time required to reach 90% coating removal in degassed water was at least twice that of air equilibrated water.

Table 3-14. Summary of samples prepared for analysis of the relationship between thiourea impurities in PEG reagents and particle degradation.

Sample Name	Preparation Details
As Received Excess	Particles were coated with excess thiolated PEG (Reagent 2 as received)
Cleaned Excess	Particles were coated with excess thiolated PEG (Reagent 2, purified by dialysis)
As Received	Particles were coated with excess thiolated PEG (Reagent 2 as received) then purified by diafiltration to remove an estimated 99.9999% of soluble residues.
Cleaned	Particles were coated with excess thiolated PEG (Reagent 2, purified by dialysis) then purified by diafiltration to remove an estimated 99.9999% of soluble residues.
Cleaned + Thiourea	Thiourea was added to particles coated with excess purified PEG.

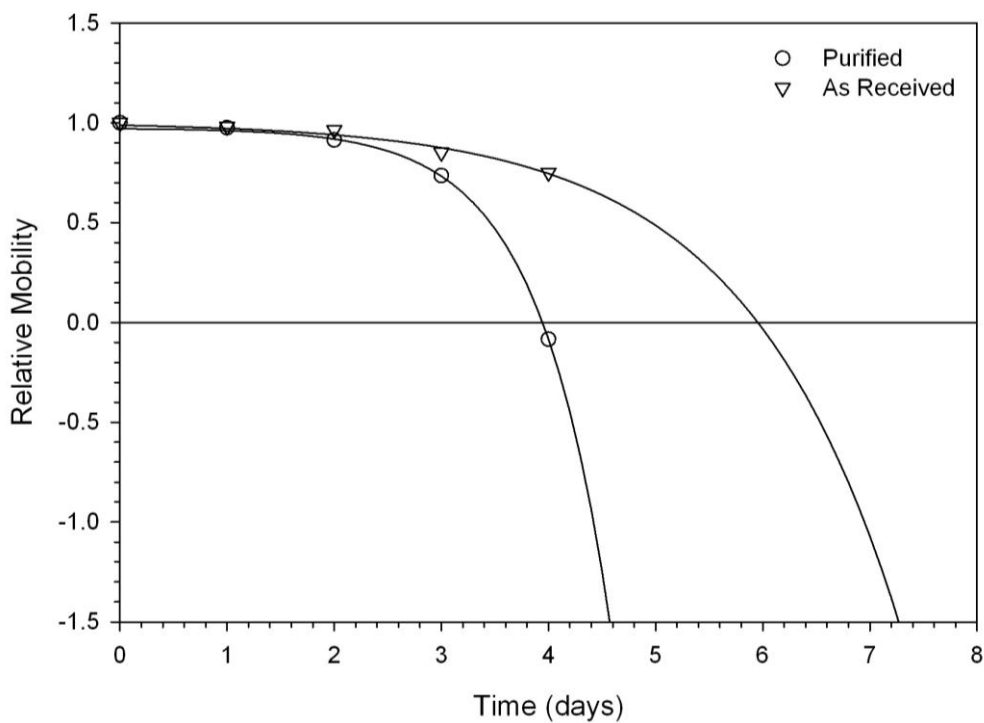


Figure 3-55. Time dependent relative mobilities of particles coated with purified and as-received thiolated PEG (Reagent 2). Purification of the PEG reagent caused a significant decrease in the particle stability.

Table 3-15. Literature reported salt effect parameters for selected salts²¹².

Salt	Salt Effect Parameter (L mol ⁻¹)
LiCl	0 – 0.112
NaCl	0.138 – 0.145
KCl	0.094 - 0.129
KBr	0.117
NaF	0.284
CaCl ₂	0.226
Na ₃ PO ₄	0.652
Na ₂ SO ₄	0.325 – 0.398
NaNO ₃	0.124
Na ₂ CO ₃	0.338 - 0.464
NH ₄ OH	0.006

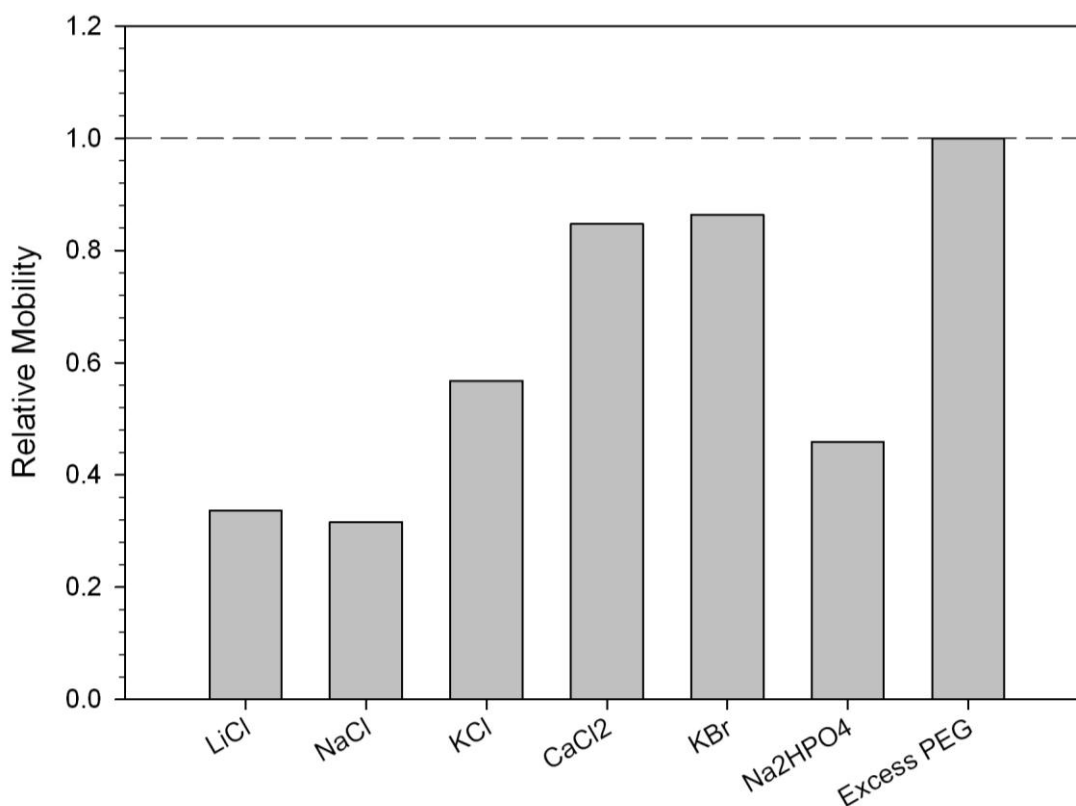


Figure 3-56. Relative mobilities of PEG coated (Reagent 2) particles in various 100mM salt solutions after approximately one month of incubation at 37C.

Table 3-16. Degradation times for the least stable samples listed in Table 3-15.

Solute	Time to near complete removal of PEG coating (≥80-90% of coating removed).
Deionized Water	3
PEG	3
NH4F	16
NaSO4	16
Sodium Citrate	22

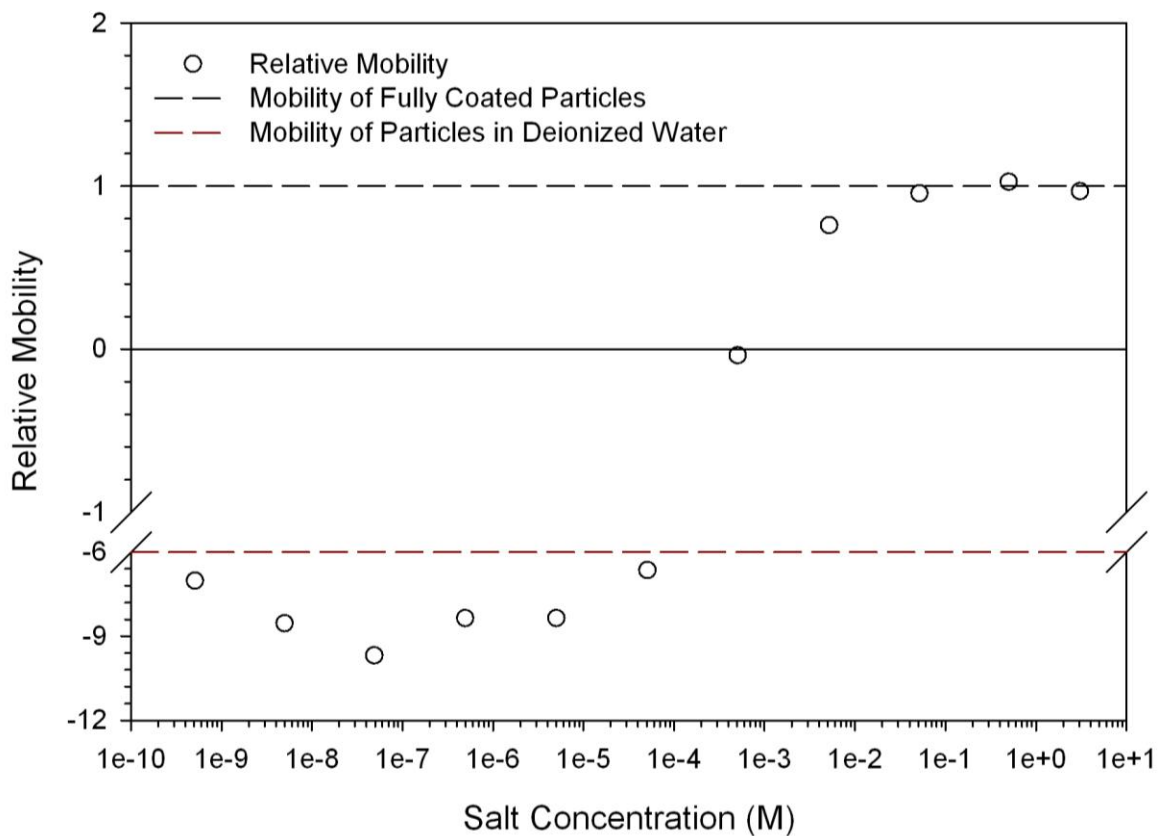


Figure 3-57. Concentration dependent mobility of coated gold particles (Reagent 2) as a function of salt (NaCl) concentration after incubation for 4 days at 37C. Particles with a salt concentration in the mM range showed significantly higher stability than those in deionized water. The suspension concentration was 500ppm (as gold).

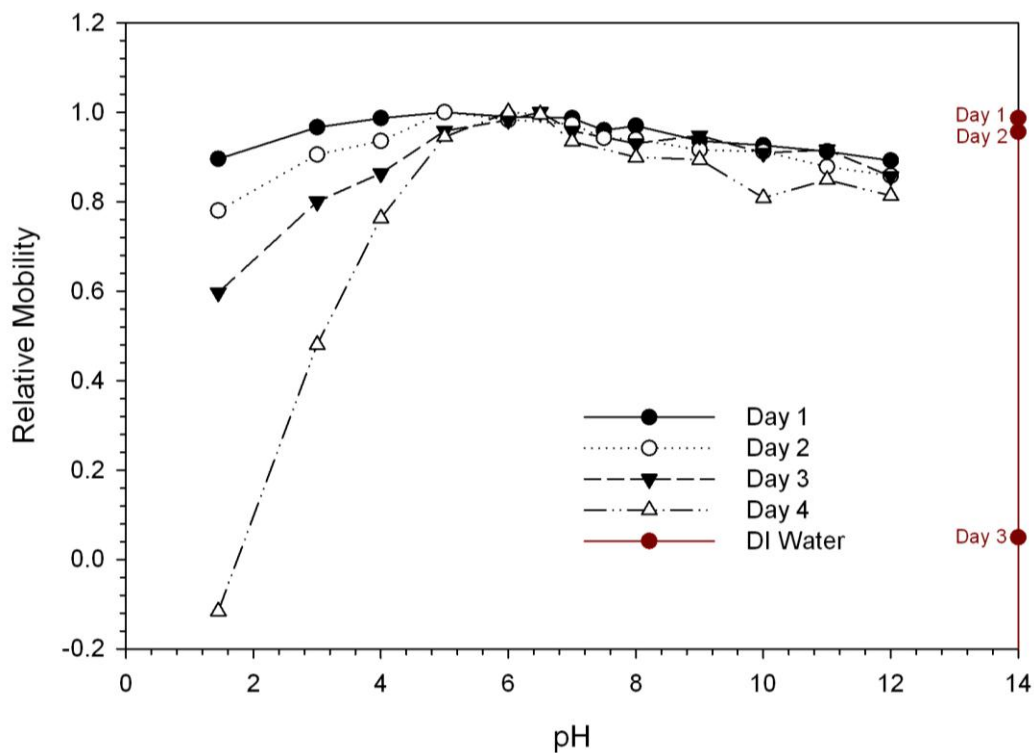


Figure 3-58. Time dependent degradation of PEG coated gold particles (Reagent 2) at various pHs. Samples were stored in 100mM phosphoric acid solutions adjusted to each desired pH with sodium hydroxide. Note that the degradation of particles occurred slower in the buffer solutions than in deionized water, which is consistent with previous observations (Figure 3-57).

CHAPTER 4 IN VITRO PARTICLE - PROTEIN INTERACTIONS

Chapter Introduction

The interactions of nanomaterials with the biological environment represent an area of increasing interest to toxicologists. Initially, many toxicological studies focused on relating *in vivo* and toxicological behavior of various nanomaterials to a particular core particle composition. As the complexity of many of these systems have been realized and sophistication in the field has increased, focus on assigning toxicological and biological properties has gradually shifted from an intrinsic material property of the core particle towards the particle surface chemistry instead. The stability and behavior of a particle *in vivo* to a large degree are mediated by the surface chemical interactions in the bloodstream.

In this chapter, the interactions of model proteins with coated and uncoated gold particles will be examined. Though intensely studied, the adsorption of proteins to solid surfaces is a highly complex subject and is not well understood^{184, 224}. One of the two major purposes for the coating of particles with PEG is the elimination or minimization of nonspecific protein adsorption, as this can lead to recognition. The PEG coating moderates interactions between the proteins in the fluid surrounding the particles and the core particle surface. The previous chapter established the stability of the coating and many of the factors which can enhance or retard its degradation. The behavior of the coating and protein binding properties of coated and uncoated particles in the presence of select proteins and plasma will be examined in this chapter to better understand the moderating effects of the PEG coating.

Selection of Model Proteins

Several factors were considered in the selection of individual model proteins used for this study. The primary reasons included relevancy to the system of interest, price, and commercial availability in significant quantities. Albumin (as BSA) was selected as the primary protein for this study due to its high concentration in the bloodstream, high affinity for gold particles relative to its concentration in serum (discussed in detail later), and availability in significant quantities. With an isoelectric point of approximately 5²²⁵, BSA is also within the IEP range observed for a large proportion of serum proteins. Lysozyme was selected primarily due to its relatively high isoelectric point of 10.3-11²²⁶, after initial protein binding experiments indicated that net protein charge played a major role in the adsorption of proteins to the gold surface (detailed in subsequent sections). Lysozyme is commercially isolated from chicken egg whites²²⁶⁻²²⁸, and is therefore readily available in significant quantities. Lysozyme is also considered a 'hard' protein in that its structure has a high degree of conformational stability, whereas serum albumin is considered 'soft'²²⁹. The protein pepsin was selected for the opposite reason – its isoelectric point is relatively low at 2.2²³⁰. Pepsin is also available in significant quantities and is typically isolated from the porcine stomach²³⁰.

Interactions of Proteins with Gold Particles

Before coatings and protein resistance can be considered, the protein adsorption behavior of the core particles will be addressed, as these interactions represent the core binding interactions between the particles and proteins. There are three potential mechanisms anticipated to promote association of proteins with the gold nanomaterials:

- Coulombic interactions between the charged particles and proteins
- Hydrophobic interactions involving the hydrophobic regions of proteins
- Chemisorption of proteins, particularly via sulfur groups.

These mechanisms and some of their impacts on protein adsorption with the core particles will be addressed in this section..

Measurements of Protein Adsorption

A wide variety of protein quantification methods are available, ranging from the optical absorbance of proteins at 280nm, to various colorimetric and fluorimetric methods, to more sensitive mass spectrometry methods. Routine total protein analysis is typically performed by colorimetry and fluorimetry, which provide adequate detection limits using readily available and flexible instrumentation. As with measurements of PEG adsorption, both qualitative and quantitative analysis techniques were employed, and many of the same methods used and parameters measured for PEG adsorption were repeated here.

Colorimetric assay methods

Due to simplicity, widespread use, and availability of instrumentation, colorimetric assay methods were selected for routine total protein analysis. Some of the most common colorimetric protein quantification methods are the Biuret assay, the Lowry and BCA (bicinchoninic acid) assays, the Bradford assay, and optical absorbance at 280nm. Though optical absorbance at 280nm would likely provide adequate quantification with no sample preparation, it was not selected as the primary quantification technique due to the potential for interference. Proteins exhibit optical absorbance maxima at wavelengths of 280 and 190-200nm due to aromatic amino acid groups (primarily tyrosine and tryptophan) and peptide bonds respectively, the latter being the more sensitive absorbance wavelength²²⁵. The optical absorbance (extinction coefficient) at 280nm can vary due to a number of common factors, such as the solution conditions

(pH, buffer, etc.) and interfering background species²²⁵. The Bradford dye-binding assay was ultimately selected due to its adequate limit of detection for the proteins of interest, simplicity, and the fact that it does not require incubation prior to analysis (unlike the BCA assay).

The Bradford assay was first described in 1976²³⁸ and involves the use of the acid dye Coomassie Brilliant Blue G-250. The dye, originally developed for wool textile dyeing applications, binds nonspecifically to a wide array of proteins, producing a bright blue color. Initially, the dye has a tan color under acidic conditions with observed optical absorbance maxima at approximately 467nm and 647nm (Figure 4-1). Binding to proteins occurs at basic and aromatic amino acid residues and hydrophobic sites^{238, 239}. Upon binding, the dye color shifts to a vibrant blue color with an observed optical absorbance maximum of 590nm with BSA (Figure 4-1). Quantification is performed using an assay wavelength of 595nm. Typical observed sensitivities are in the range of 100s of ppb for proteins such as albumin and lysozyme.

Electrophoretic techniques

Electrophoresis can be used to qualify or estimate the degree of protein adsorption on gold particles in a manner similar to the analysis of PEG coating density (provided that the protein adsorbate of interest is sufficiently charged). Like similar measurements with PEG, adsorption of a protein to a particle causes a change in the net charge of the particle which results in changes to the particle mobility. Measurements involving protein adsorption differ from those involving only PEG adsorbates in that the change in electrophoretic mobility arises from addition of charged protein molecules rather than exposure of a latent surface charge due to changes in coating thickness (Figure 4-3). This degree of charging is dependent on the number of charged species adsorbed, and

will increase the electrophoretic component of the observed mobility. In most cases involving a mildly alkaline electrolyte (pH ~8 typically used), the adsorbed protein will be negatively charged and will cause migration to occur opposite to the electroosmotic flow. The net effect is a transition of the particles toward cathodal migration with a velocity related to the protein adsorbate density. Using a set of standard particles with known protein and PEG adsorbate densities, the relationship between protein density and electrophoretic mobility can allow for (at a minimum) an estimation of the density of adsorbed proteins.

Other measurements

Similar to the analysis of PEG coatings, other measurements of the coating properties were performed. Protein coated particles were imaged by transmission electron microscopy, and coating thickness was analyzed by dynamic light scattering and sedimentation.

The thickness of the adsorbed serum protein layer coating the gold particles was measured using both dynamic light scattering and differential sedimentation as previously described. Since a certain level of reversibility exists in protein adsorption (detailed later) which can influence colloidal stability (Figure 4-7), excess quantities of proteins were used for differential sedimentation measurements to minimize the possibility of desorption during analysis. Regardless, sedimentation analysis should be considered with caution due to the possibility of desorption and shearing effects. The density of the protein layer was assumed to be 1.1g/cm^3 for the purpose of thickness calculations based on sedimentation. The calculated human plasma protein coating thickness by sedimentation on nom. 40nm gold particles was determined to be $16 \pm 0.8\text{nm}$. Analysis was also performed under buffered (pH 7.2 phosphate buffer) and

non-buffered (deionized water) conditions, neither of which showed a significant influence on the protein thickness. Dynamic light scattering measurements avoid some of the pitfalls associated with differential sedimentation when equilibration of an adsorbate with the bulk is an issue. However, interferences can result when protein concentrations are high since dynamic light scattering is also capable of measuring the size of macromolecules (such as proteins) in solution, and changes in solution properties such as viscosity and density due to dissolved protein must be accounted for. Analysis of larger particles is preferable for this purpose as the scattered light intensity is significantly higher. Analysis of protein coated nom. 40nm particles showed a size increase of approximately 40nm, corresponding to a 20nm coating thickness. As anticipated, this number was higher than the 16nm value obtained by sedimentation.

Protein coated nom. 40nm gold particles were supplied to Kerry Siebein for staining and TEM imaging. The particles were negatively stained to highlight the relatively difficult to image protein coating. Transmission electron micrographs (Figure 4-4) show a thin and inhomogeneous coating of protein around the particles while the uncoated particles did not show any coating. Since the samples had to be prepared and dried prior to imaging by TEM, this coating was not expected to represent the actual conditions in solution.

Protein Adsorption and Binding Behavior

Protein adsorption measurements were performed using the Bradford Assay for select model proteins by the depletion method. The adsorption isotherm for BSA on as prepared nom. 20nm particles (pH approximately 5) is shown in Figure 4-6. At saturation, the surface density was 0.034 ± 0.001 molecules/nm², which corresponds to an adsorbate footprint of approximately 30nm² (equivalent to a circular area with a

diameter of 6.1 nm). Initially, the adsorption isotherm demonstrated a high adsorbate affinity, as evidenced by the nearly undetectable equilibrium quantities of protein remaining in the medium. Unlike the adsorption of thiolated PEG, the adsorption isotherm of BSA demonstrated an extended region where equilibration with unbound protein occurred prior to surface saturation.

Depending on the protein surface density, stability also varied significantly. At low adsorbate concentrations, the particle suspension was stable, however as the concentration increased, a region of instability was observed prior to saturation. The first region of stability is likely due to the low concentration of adsorbate molecules, which are not present in sufficient quantities to interfere with the electrostatic repulsion of the parent particles. As the concentration increases, the levels of adsorbate are capable of destabilizing the suspension. Once the surface density approaches saturation, the steric or coulombic repulsion (or a combination thereof) imparted by the protein coating is sufficient to maintain colloidal stability. Some degree of adsorption reversibility was observed at or near saturation. When a small quantity of deionized water was added to a suspension of particles coated with BSA such that the surface density was just above saturation, the particles immediately aggregated. This demonstrates that the adsorption of protein around the saturation point does not occur via a strong chemical binding mechanism such as adsorption via a thiol (Figure 4-7). Subsequent experiments with higher concentrations of BSA at the same dilution did not aggregate, indicating that a certain minimum concentration of protein in equilibrium with the bound protein is necessary to prevent aggregation. Although the particles are initially indefinitely stable, it is possible that the region of aggregation may vary based on salt content. In the as-

prepared suspension used for this study, salt concentration is in the 10s of millimolar range. The influence of salt content on stability was not specifically studied in this work.

Proteins contain many pH sensitive functionalities, principally the carboxylic acid and amine groups of amino acids, which control the net charge on the macromolecule. At a certain pH, it is possible for the positive and negatively charged functionalities to balance, producing no net charge on the molecule. This is known as the isoelectric point (also known as the *pI* or IEP). The majority of protein isoelectric points exists at pH values between 5 and 7, but may vary considerably based on function. A brief list of some common proteins and their isoelectric points is shown in Table 4-1. All three of the aforementioned mechanisms of binding are impacted by solution pH and the isoelectric point of the adsorbed proteins. For adsorption based solely on coulombic attraction, the pH dependent protein charge is the primary controlling factor. Protein hydrophobicity and potential chemical binding sites can be exposed in a pH dependent manner²⁴⁰. Compared to synthetic polymers, proteins have an additional level of complexity in their conformation. Several studies have identified changes in protein conformation upon adsorption to particles and solid surfaces²⁴⁴. Protein conformations in albumin (BSA) can also vary based on solution pH²⁴⁵.

To better understand some of these pH dependent interactions, adsorption density measurements of select model proteins were performed using nom, 20nm gold particles. All suspension samples were pre-adjusted to the desired pH value and were then added to a small volume of BSA at a fixed concentration. The pH of the final suspension mixture after analysis was also measured to ensure that all values remained stable. The concentration used for this purpose was selected based on the adsorption

isotherm (Figure 4-6) to yield a well stabilized particle with a sufficient equilibrium concentration of BSA. After a brief incubation period, the particles were removed by centrifugation, and the supernatant analyzed for protein content. Five replicate measurements were performed at each pH value along with controls. Separate controls containing only pH adjusted protein solutions at a fixed concentration were performed at each pH value to identify any potential interference with the assay. The Bradford assay reagent contains a significant amount of acid (usually phosphoric acid) to ensure that the pH of the assay remains strongly acidic. Since pH values up to 10 were considered (particles were unstable beyond this point), controls were necessary to ensure that the high pH would not interfere with the assay. Any significant adhesion of the adsorbate to the sample containers would be also detected by these controls. The results for the positive controls showed that all assayed values were within 1-2% of the expected concentration with one exception (which was within 7% and not at a pH extreme or isoelectric point). Negative control values also returned background levels under all conditions.

The mean and standard deviations of the protein surface density relative to pH are shown in Figure 4-8. The adsorption density increased with pH until a maximum value was observed at the isoelectric point of the protein. The concentration then steadily declined until no statistically significant levels of adsorbed protein were detected at a pH of approximately 10. This behavior yields a key piece of information about the binding behavior of the protein on gold particles. At low pH, the net charge on BSA is positive, allowing for attraction to the particle via electrostatic interactions with the negatively charged gold surface (Figure 2-26). As the pH approaches the isoelectric point, the

adsorption density increases to a maximum value of approximately 0.04 molecules/nm² due to a combination of electrostatic and hydrophobic interactions. The hydrophobic interactions can easily be seen in Figure 4-9, where the protein coated particles adhere to the hydrophobic polypropylene container around the isoelectric point. As the pH increases beyond this point, the adsorption density rapidly declines to negligible levels due to coulombic repulsion between the negatively charged gold particles and negatively charged BSA molecules. In addition to particle - protein coulombic interactions, coulombic interactions between adsorbate molecules may also play a role in compaction of the adsorbed layer around the isoelectric point. In the vicinity of the isoelectric point, the net charge on the adsorbate molecules is low, allowing for the adsorbate molecules to more efficiently pack on the surface due to decreased inter-adsorbate coulombic repulsion. Though it was not directly investigated in this work, the presence of salts during adsorption may also alter the adsorption density through a similar mechanism of reducing inter-adsorbate coulombic repulsion. This phenomenon occurs in a species dependent fashion and has been described for adsorption at the oil-water interface for BSA^{241, 242}.

A similar procedure was performed on the protein lysozyme as a contrast to BSA. The isoelectric point of lysozyme is relatively high at pH 10.3-10.9²³⁵, and is therefore positively charged over a wide pH range (unlike BSA). The mean and standard deviation of the protein surface density relative to pH are shown in Figure 4-10. A trend similar to BSA was observed in the results where the adsorption density peaked around the isoelectric point. At lower pH values, lysozyme is positively charged and is attracted electrostatically to the negatively charged gold particles. There is a sharp increase in

surface density around the isoelectric point followed by a sharp decline in adsorption density due to electrostatic repulsion between the like-charged particles and adsorbate. Like BSA, this indicates that electrostatic and possibly hydrophobic interactions are the major contributing factors in the adsorption of proteins to gold particles. Lysozyme did not appear to be as effective as BSA in promoting colloidal stability, and stability was only achieved at pH values above 10.

Desorption of protein from particles may occur through several means, principally pH change, change in salt content, competitive adsorption, and reduction of the equilibrium adsorbate concentration²⁴³. The driving forces for these desorption effects are electrostatic repulsion, solvent effects/entropic considerations, preferential adsorption, and equilibrium shift respectively. Like many other polyelectrolyte adsorbates, complete desorption from a surface is possible but less likely due the higher number of binding sites, hydrophobic interactions (if present), conformational/entropy change on desorption, and solvent accessibility. Proteins also do not have a uniform charge distribution over their entire surface²²⁶, allowing certain locations on the protein to bind with greater affinity. Although studies of the desorption of proteins from surfaces can provide useful information on binding interactions, the primary concern in this work was adsorption of proteins. Desorption was therefore not pursued in this work.

Properties of Coated Particles

The protein coating on a gold particle can easily mask the particle surface and will be a strong mediator of the particle's behavior *in vivo*. The charge on nanomaterials is one major factor that can control biodistribution²²⁴. As discussed in the previous section, the adsorption affinity of proteins onto gold particles is strongly dependent on the

protein's net charge. The adsorption of these proteins can in turn alter the net particle charge as a function of pH. To illustrate this behavior, the zeta potential of nom. 20nm gold particles coated with BSA, lysozyme, and human serum proteins were analyzed by dynamic light scattering. The results for BSA are shown in Figure 4-11. The isoelectric point of the BSA coated particles was approximately 4.92, which is within the range of literature reported values (4.7-5.3). Similar behavior was observed with lysozyme (Figure 4-12), where an isoelectric point of 9.13 was observed. When gold particles and lysozyme were mixed directly, lysozyme coated particles were only stable at pH values above 9-10. To ensure that the particles were initially stable, the suspension was titrated down from an initial pH of 11. The coated particles were unstable during titration below a pH of 9-10, and appeared to be more dispersed at a pH <3, though they did not fully regain stability at these low pH values. The serum protein coated particles showed a zeta potential titration curve identical to BSA in isoelectric point (4.92) and shape (Figure 4-13). The magnitude of the values was significantly lower than BSA in deionized water, which is expected when charge screening due to the higher ionic strength in plasma is considered. The curves for BSA coated particles in deionized water and serum protein coated particles were practically superimposable when normalized. In all cases, the negative charge of the gold particles (Figure 2-26) can be easily reversed by the adsorbed protein coating at pH values below the isoelectric point.

Differential Binding of Serum Proteins

The ability of nanomaterials to differentially bind serum proteins has been noted for some materials in literature such as aluminum^{246, 247}, nickel^{248, 249}, gold²⁵⁰, diamond²⁵⁰, zinc oxide²⁵¹, iron oxide²⁵⁰, titania^{252,254}, silica^{253,254,252}, polystyrene (various surface functionalities)²⁵², and carbon black²⁵⁴. Since the composition of this protein

coating is ultimately what interacts with its surroundings, the layer of adsorbed protein is as important if not more important than the core particle composition. The protein coating consists not only of proteins which are bound directly to the core particle, but also proteins which weakly associate with the proteins bound to the particle surface. The composition of this layer may change based on the location in the body among other factors, This entire coating (sometimes called the protein 'corona') is highly complex, dynamic, and poorly understood²⁵⁴. Though a complete study of the protein binding characteristics of these particles is beyond the scope of this work, a study on the serum protein binding of several particles was performed. Gold particles of nom. 3, 20, and 40nm were provided to David Barber of the Center for Environmental and Human Toxicology for analysis of bound proteins. For contrast, commercial nom. 25nm titania particles were also analyzed. The results in Figure 4-14 showed striking differences in the quantity and type of protein adsorbed between gold and titania particles. Albumin was found to bind to gold in a far higher abundance relative to its concentration in serum, a fact which has been recently confirmed in literature²⁵⁵. This was particularly useful in validating the choice of BSA as the primary test protein used throughout this study. Since thiol chemistry can play a key role in adsorption to metal surfaces, an additional analysis was performed where the protein thiols were inactivated by acetylation prior to incubation with the particles. This would presumably reduce or eliminate binding based on thiol-metal bonds. When the results of this sample were compared to the particles coated with untreated protein, no significant differences were noted in the adsorbed protein abundance. Size dependent effects on adsorption of certain proteins were also noted, as shown in Figure 4-15. Some of the listed proteins

were bound in successively higher proportions as the size increased while others decreased or remained roughly the same.

Interactions of Proteins with PEG Coated Gold Particles

The protein resistance of PEG coated particles is predicated on the stability of the PEG coating. As the coating density decreases, the ability of the coating to resist protein adsorption by steric repulsion decreases, ultimately allowing opsonization to trigger clearance mechanisms. This behavior was investigated using BSA and human serum. The point at which the coating density is sufficient to resist detectable levels of protein adsorption was determined by depletion of a constant starting concentration of protein using particles with varying PEG coating densities. The results for BSA are shown in Figure 4-16. The point at which protein adsorption could no longer be detected coincided with the point at which the coating density of the particles was maximized, indicating that protein adsorption occurs almost immediately upon degradation of the PEG coating. Once the coating begins to degrade, protein adsorption increases exponentially as the PEG coating density decreases. This same analysis was performed using a degraded PEG reagent for comparison and showed a similar trend (Figure 4-17).

Time Dependent Interactions of Proteins with PEG Coated Gold Particles

In chapter three, the stability of the PEG coating under different conditions was investigated, and the previous sections in this chapter discussed the equilibrium adsorption behavior of proteins on coated and uncoated particles. In this section, these two concepts will be combined to understand the time dependent behavior of protein binding and suspension stability of PEG coated particles.

Protein Binding

In chapter three, the time dependent stability of PEG coated particles was established and related to the reagent source/quality (Figure 3-48). It was noted that the presence of other solutes and compounds can significantly alter the rate of coating degradation (Figure 3-56, Figure 3-49, Table 3-12, Table 3-16). Proteins and components of blood plasma may interact with the particles in similar ways to alter this stability. In this section, the time dependent adsorption of protein on PEG coated particles was examined. For these analyses, the model proteins were restricted to BSA, as it was previously found that albumin adsorbed to the gold particles with the highest observed affinity, and that many of the properties of the serum protein coated particles are similar (or identical) to particles coated with albumin.

The time dependent protein binding characteristics were measured using nom. 20nm gold particles which were initially coated using an excess of PEG (Reagent 1) before being cleaned by diafiltration. These particles were then exposed to BSA (at a concentration equivalent to serum reference levels) as well as pooled human plasma. Particles were coated with a freshly prepared solution of thiolated PEG and cleaned at each time point to eliminate the possibility of changes in the reagent or suspension during storage. The suspensions were analyzed by electrophoresis at time points selected based on the stability of the PEG coated particles in water. As detailed in a previous section, adsorption of proteins to gold particles results in cathodal migration due to the negative charge on the protein. Migration at a velocity less than the velocity of the reference PEG coated particles indicates adsorption of protein. Since the mobility distribution of protein coated particles does not remain constant and is fairly broad, it can not be easily deconvoluted from the particles with little to no adsorbed protein. For

this reason, the relative integrated intensity of particles with mobilities less than the control particles (fully PEG coated) was used to indicate the extent of protein adsorption rather than the peak mobility. Though the mean mobility and certain other metrics would also suffice, their poor sensitivity to low levels of protein binding decreased their utility. The mobility data for particles incubated in BSA and human plasma are shown in Figure 4-18. At the earliest time points, the particles did not exhibit any significant difference from the control particle samples (fully PEG coated). However, the particle mobilities began to decrease at the 1-2h time points, indicating the onset of protein adsorption. Extrapolation of the baseline and particles exhibiting significant protein adsorption allowed for a more precise estimation of the time to onset of protein adsorption, which was 85 and 90min for BSA and human plasma respectively. This coincided with the onset of coating degradation observed for Reagent 1 (Figure 3-48). The change in particle mobility did not occur as a continuous shift in mobility, as indicated by the mobility spectra (Figure 4-21). Over time, a second peak developed as protein adsorption occurred, and within two hours, two peaks are evident. The peak corresponding to the PEG coated particles can be seen decreasing over time relative to the peak corresponding to the protein coated particles. This indicates that at most early time points, both coated and uncoated particles are present in the suspension, but by approximately 2 days, virtually all PEG coated particles have at least some level of protein adsorbed. Using a set of calibration samples with known levels of bound BSA, the quantity of adsorbed BSA was estimated from the mobility data (Figure 4-19). To verify that this technique is an accurate means of estimating mean protein adsorption, a separate experiment was performed with larger sample quantities and lower protein

concentrations to facilitate adsorption measurements based on a total protein assay. Control samples containing only BSA in water were run concurrently to verify that incubation did not affect the assayed protein values. All control samples assayed to within 3% of the initial BSA concentration, indicating that no interferences were encountered. The results of this experiment, shown in Figure 4-20, closely matched the data gained by electrophoresis when calibrated with samples of known protein density. This indicated that calibrated electrophoresis was an effective means of estimating protein adsorption. A similar procedure was performed on Reagent 2, which previously demonstrated markedly higher stability under all circumstances than Reagent 1. It was generally observed that the rates of protein binding were significantly lower with this reagent than with particles prepared using Reagent 1. Electrophoresis analysis of the particles in human plasma showed that the onset of bulk protein adsorption occurred at approximately 1 day (Figure 4-22); however detailed analysis of earlier time points showed that small quantities of protein can adsorb after approximately 4h of incubation. Due to the higher activity of this reagent compared to reagent 1, these particles were particularly susceptible to interferences from unbound PEG concentrations.

Several other conditions were tested as single-point comparative measurements, such as whether or not the presence of unbound PEG would delay protein binding and whether or not elevated salt levels or timing of protein addition would influence binding. In all cases, BSA was used as a model protein and the final protein concentration was determined using the Bradford assay after incubation for three days at 37C. For particles coated with Reagent 1, the only factor which had a statistically significant difference in protein binding from the control sample was the presence of excess PEG

in the suspension medium. All samples which were cleaned of excess PEG, regardless of other factors, adsorbed nearly the same quantity of protein, while the samples containing unbound PEG showed no significant levels of protein binding.

The aforementioned observations on the presence of excess PEG in the suspension brought up the possibility of competitive adsorption between the PEG reagent and proteins. To identify whether or not the PEG reagent was capable of out-competing adsorbed protein for surface area, BSA coated particles were prepared and dosed with increasing concentrations of PEG-thiol (Reagent 2). All suspensions were buffered at physiological pH to ensure that the proteins were sufficiently negatively charged to provide repulsion from the surface. The equilibrium protein concentrations were then analyzed using the Bradford Assay, and qualitative electrophoresis measurements were also performed. The results(Figure 4-24) show that even in the presence of high levels of PEG thiol, little to no protein is desorbed from the particle surface. A slight trend in the data indicating possible desorption at high concentration of PEG was observed; however this could not be separated from a slightly elevated assay response due to the presence of high concentrations of PEG. Similar results were observed with Reagent 1. Electrophoresis measurements of these samples indicated that the protein coating was largely intact, as the particles had significant cathodal mobility.

The opposite case involving protein desorbing PEG from a coated particle was already considered in Figure 4-16 and Figure 4-17. Unlike proteins which may bind due to a variety of mechanisms (most notably coulombic attraction), PEG chemisorbs to the surface and is therefore less likely to desorb. This behavior was observed in previous

experiments, where no detectable levels of protein adsorption occurred at concentrations near saturation. If significant levels of PEG desorption did occur, protein binding should be detected above the point at which the particle surface is saturated with PEG.

The third and least likely case would involve competitive binding with both PEG and BSA initially mixed (competitive coadsorption). This has certain applications in preparing conjugated particles where a mixed coating is desired, and is used to prepare some conjugated therapeutic particles commercially¹⁸⁴. The relative quantities of adsorbed protein are dependent on the initial ratio of PEG and protein prior to adsorption as well as the affinity of the protein for the surface due to solution conditions.

Reagent Purity

In the previous chapter, the impact of impurities on the formation and stability of PEG coatings was extensively discussed. In addition to impacting coating formation and stability, these compounds may affect the adsorption of proteins. The typical impacts of impurities on the PEG coating involve competitive adsorption and effects on oxidation processes. These impacts may aid in exposing the surface of the particles to protein adsorbates; however, if the impurity is capable of strongly binding to the particle surface, the composition of the impurity itself also alters the local surface chemistry. This in turn can alter a protein's affinity for the surface. One of the primary ways for this to occur is via alteration of the surface charge. Under most conditions, a strong negative surface charge exists on the tested gold particles (Figure 2-26). Addition of adsorbates such as thiourea can decrease the net surface charge of the particles, allowing proteins to more readily adsorb. As demonstrated previously (Figure 4-8), the protein charge (due to pH) can greatly influence the quantity of bound protein on gold surfaces. In addition to the

change in surface charge, the presence of impurities in the PEG coating solution initially caused a small decrease in coating density (Figure 3-45) which was likely caused by competitive coadsorption during coating. The proposed effects of the thiourea impurity found in the PEG reagents are illustrated in Figure 4-25. Previous measurements of the rate of degradation with and without impurities indicated that the presence of small quantities of thiourea can increase the coating stability (in deionized water). Since effects due to thiourea which can both improve and reduce protein resistance exist, the time dependent protein resistance was characterized by electrophoresis in samples with and without purification as described in previous sections.

Surprisingly, the apparent increase in stability observed in deionized water when adsorbed thiourea is present does not translate to better protein resistance. Qualitative measurements of time dependent protein adsorption using BSA and human plasma showed lower protein binding in suspensions prepared with a purified PEG reagent (Figure 4-26). Additional measurements with coated gold particles using a purified reagent that was subsequently treated with thiourea lead to increased protein binding, indicating that the change is related to the presence of thiourea. These measurements were repeated several times with the same outcome each time: increased protein binding in the presence of thiourea.

To confirm the measurements made by electrophoresis, single point measurements were performed at 3 and 5 day intervals post-coating using the Bradford assay and BSA. These results (Figure 4-27) showed that protein adsorption by the particles coated with the PEG reagent as received was approximately 25% and 45% higher at the 3 and 5 day points respectively than the particles coated with purified

PEG. Additionally, when thiourea was added to the cleaned reagent in concentrations similar to the as received reagent, the quantity of protein bound by this particle was approximately the same as the quantity bound by the impure reagent.

Suspension Stability

Given that PEG coated particles continuously exchange the protective PEG coating for serum proteins under physiological conditions, it is possible that the suspension stability is compromised during this process. Aggregation is less likely to occur in the bloodstream (or any other compartment) where the high concentration of albumin and other stabilizing proteins can immediately stabilize the suspension upon loss of the PEG coating. Previous experiments also indicated that at physiological pH, albumin (the most prevalent serum protein) can readily bind to and stabilize uncoated gold particles. The conditions of these experiments, though, only involved a static system and single proteins or plasma rather than whole blood. To address any possibility of aggregation in whole blood, PEG coated gold particles (using Reagent 1) were incubated with whole mouse blood and analyzed at various time points by differential sedimentation (analysis details provided in Chapter 2). The concentration of gold particles was selected to mimic a dose of 1 mg/mouse as gold using an approximate blood volume of 2.4mL/mouse. Blood was heparinized when collected and supplemental oxygen added to the airspace in each sample container to preserve the blood. The blood was gently stirred to simulate circulation conditions throughout the 24h incubation period. Sedimentation velocity data for each time point is shown in Figure 4-28. During the course of the 9h incubation, no significant decrease in the peak corresponding to the primary coated gold particles was observed. The remaining sample was analyzed again after 3.5 days in whole blood, again showing no significant

change in the primary particle peak intensity. If appreciable levels of aggregation occurred in these samples, aggregate particles could be either detected directly (if the concentration of aggregates was sufficient and particle size was within the analysis range) or detected by a loss of primary particle concentration. Neither of these conditions was detected at any time during this experiment; however this does not exclude the possibility that small concentrations of aggregate particles were generated. Blood samples were examined by optical microscopy to verify that formation of larger aggregates in low concentration did not occur. Aggregate particles can be identified optically from other organic particles (Figure 4-29) in blood by their high optical density/opacity (brightfield) and yellow scattered light (darkfield). No aggregate particles were observed at any time point during this experiment optically.

To contrast the behavior of the PEG coated particles and better understand the indicators of aggregation in blood, uncoated particles were dosed into blood and were analyzed concurrently with the PEG coated particles. Unlike the PEG coated particles, the electrostatically stabilized gold particles aggregated immediately when introduced into blood. This behavior was observed optically at all time points (Figure 4-30) and by sedimentation at the earliest time points (Figure 4-31). The aggregate size observed optically ranged in excess of 30 μ m, which placed the bulk of the particles outside of the analysis range of the centrifuge and was a major cause of the weak and transient response observed at higher sedimentation velocities (Figure 4-31).

Mixing kinetics is a key factor in the formation and final size of aggregate particles in fluids such as blood or plasma (Figure 4-32). The components of plasma can be divided into three major classes in this case: salts, small organic molecules, and

macromolecules (proteins primarily). Neither the salts nor small organic molecules are capable of stabilizing the gold particles, while proteins (in sufficient concentration) can. The salt content alone in blood is capable of destabilizing the gold suspension through charge screening, and many of the small organic molecules are capable of decreasing the net particle charge. Of the three aforementioned classes, only certain small organic molecules and proteins found in plasma are typically capable of chemically adsorbing to the surface of the particles. When mixing occurs without high shear or slow addition, a high concentration gradient between the plasma and particles is maintained for an extended period of time, leading to aggregation. The higher viscosity and density of blood and plasma contribute to this decrease in mixing efficiency. Extended mixing times allow for the more mobile salts and small organics to destabilize the suspension before the stabilizing proteins can fully adsorb. The concentration gradient of plasma proteins caused by slow mixing can also contribute to aggregation when the local protein concentration is below a certain point (Figure 4-6). Under conditions mimicking circulation, the amount of shear used could not provide sufficient mixing to prevent aggregation. However if the same particles and plasma were combined under high shear mixing, particularly with gradual addition of particles, dispersed protein stabilized particles could easily be prepared.

Chapter Summary

Colloidal stability of BSA coated particles is highly dependent on the coating density. Three distinct regions of stability are observed: stable at low adsorbate concentrations, unstable at higher concentrations leading up to saturation, and stable at or above saturation (Figure 4-6). Adsorption of BSA is reversible to an extent, and can result in aggregation if the equilibrium concentration is decreased beyond a certain point

(Figure 4-7). The adsorption of protein to gold particles is strongly dependent on electrostatic and hydrophobic interactions. Adsorption follows a predictable trend with regards to electrostatic interactions. Around the isoelectric point of the protein, hydrophobic interactions and more favorable inter-adsorbate coulombic interactions are likely contributors to the observed sharp increase in adsorption (Figure 4-8, Figure 4-9, Figure 4-10). Hydrophobization of proteins near the isoelectric point promotes adhesion to hydrophobic surfaces, such as the surface of a container (Figure 4-9) or syringe, and should be avoided if possible when working with protein coated particles. When exposed to human serum, proteins adsorb differentially to the uncoated particle surfaces. Albumin was found to bind to gold particles with a high affinity relative to its concentration in the serum (Figure 4-14). Size dependent differential adsorption of proteins was also observed, with certain proteins adsorbing in higher or lower quantities as the particle size increased (Figure 4-15). Particle sizes of 3.5, 20, and 40nm were tested. Inactivation of thiols in human serum by alkylation does not significantly alter the on-particle protein abundance, indicating that chemisorption via thiols is less likely to be the primary driving factor of protein adsorption on gold particles. The zeta potential of protein coated gold particles is dependent on the pH of the system and type of protein adsorbed. Typically, the isoelectric point of the particles is close or identical to the isoelectric point of the adsorbed protein (Figure 4-11, Figure 4-12). Ex. 4.92 for BSA coated particles, and 9.13 for lysozyme coated particles were observed. The isoelectric point of serum protein coated gold particles is approximately 4.92 (Figure 4-13). Both the shape of the zeta potential titration curve and the isoelectric point of serum protein coated particles (Figure 4-13) are identical to those of albumin (Figure 4-11). The

thickness of the serum protein coating is measured at $16 \pm 0.8\text{nm}$ by differential sedimentation and 20nm by dynamic light scattering on 40nm gold particles.

Adsorption of protein (BSA) begins to occur shortly before the particle surface is saturated with thiolated PEG adsorbates. This indicates that only a small amount of coating degradation is required before the onset of protein (BSA) adsorption. The time dependent adsorption of protein on PEG coated gold particles does not occur uniformly to all particles, as evidenced by the electrophoresis data gathered over the course of several days (Figure 4-21). The peak corresponding to fully coated particles continuously decreased while shoulders and peaks for particles at lower mobilities began to appear. These peaks continuously exhibited higher cathodal migration as additional protein adsorbed. Analysis of time dependent electrophoresis and total protein assay data indicated that the onset of protein binding for particles coated with Reagent 1 was 85-90min for particles incubated with BSA and human serum (Figure 4-18), whereas Reagent 2 showed far smaller amounts of protein adsorption at similar time points. The onset of protein binding in Reagent 1 coincides with the onset of coating degradation observed previously. Analysis of the effects of various factors such as the addition timing of BSA to coated particles before and after incubation, elevated salt content, and the presence of excess PEG reagent indicated that the primary factor which inhibited protein adsorption was the presence of excess PEG reagent (Figure 4-23). This also confirmed that PEG can successfully outcompete protein (BSA) when the particles are initially coated in PEG. Competitive desorption of BSA and human serum proteins by PEG is not feasible under standard conditions. Although large excesses of PEG were added to protein coated gold particles, only a small quantity of BSA was

desorbed from the particle surface under standard conditions, a factor which did not change significantly over the course of several days (Figure 4-24).

Reagent purity played a major role in the adsorption of BSA and human serum proteins. Electrophoresis measurements of over a weeklong period showed that samples coated with PEG (Reagent 2 as received) had significantly higher cathodal mobility than those coated with the purified reagent (Figure 4-26). This was confirmed and quantified with single point protein adsorption measurements using a total protein assay at 3 and 5 days, which showed 25% and 45% higher levels of adsorbed protein respectively in the as-received reagent (Figure 4-27). Samples using purified PEG with thiourea added at approximately the same concentration as the as-received reagent adsorbed similar concentrations of BSA to the particles coated using the as-received reagent (Figure 4-27). The mechanism hypothesized for the increased level of protein binding involves a reduction of the core particle surface charge, which increases the affinity of the primarily negatively charged proteins for the surface as illustrated in Figure 4-25.

Analysis of the stability of uncoated particles dosed into whole blood under conditions designed to mimic normal circulation showed that the particles were highly unstable, forming large aggregates in the 10s of μm that could be observed optically (Figure 4-30). Aggregates of gold particles can be easily identified optically using transmitted illumination (where they appear as optically dense features), or as yellow features under reflected illumination (Figure 4-29). Sedimentation analysis of the blood samples at various time points showed only a weak signal for aggregate particles at the lowest time points (Figure 4-31). This lack of response was caused by the rapid

increase in size upon aggregation, which caused most aggregate particles to exceed the analysis window. No primary particles were detected at any time. Aggregation of the uncoated particles in blood can be controlled by mixing kinetics. Rapid, high shear mixing of particles of an appropriate concentration into plasma allows for stabilization of the uncoated particles with the plasma proteins. Slow mixing results in collapse of the suspension by charge screening and adsorption of various blood components at sub-optimal levels (Figure 4-32). Sedimentation analysis of PEG coated particles incubated in blood at times ranging from 5min to over 3.5 days indicated no loss in the intensity of the peak corresponding to the primary particles. No evidence of larger aggregate particles was observed in significant quantities (Figure 4-28) by both sedimentation and optical microscopy. Though the PEG coating can degrade, the presence of high concentrations of plasma proteins in blood allows for immediate stabilization of the particles upon loss of the protective PEG coating.

Table 4-1. Literature reported isoelectric points for some common proteins.

Protein	Isoelectric Point (pI)	Notes
HSA	4.6-5.3 ²³⁰	
BSA	4.7-5.3 ^{225, 231, 232}	Values for fatty acid free BSA are typically higher (4.95-5.3) ²³³
Lysozyme	9.2, 10.3-11.3	Calculated pI is ~9.3 ^{231, 233} , most reported values 10.3-10.9 ²²⁷ , some references show 11.2-11.35 ^{226, 234, 235} .
IgG	6.1-8.5 ²²⁸	Ranges vary based on source, but are typically between 6±0.5 to 9±0.5.
Pepsin	2.2 ²³⁶	Values of 2.8 reported ²³⁷
Hemoglobin	6.9-7.4 ^{225, 230}	

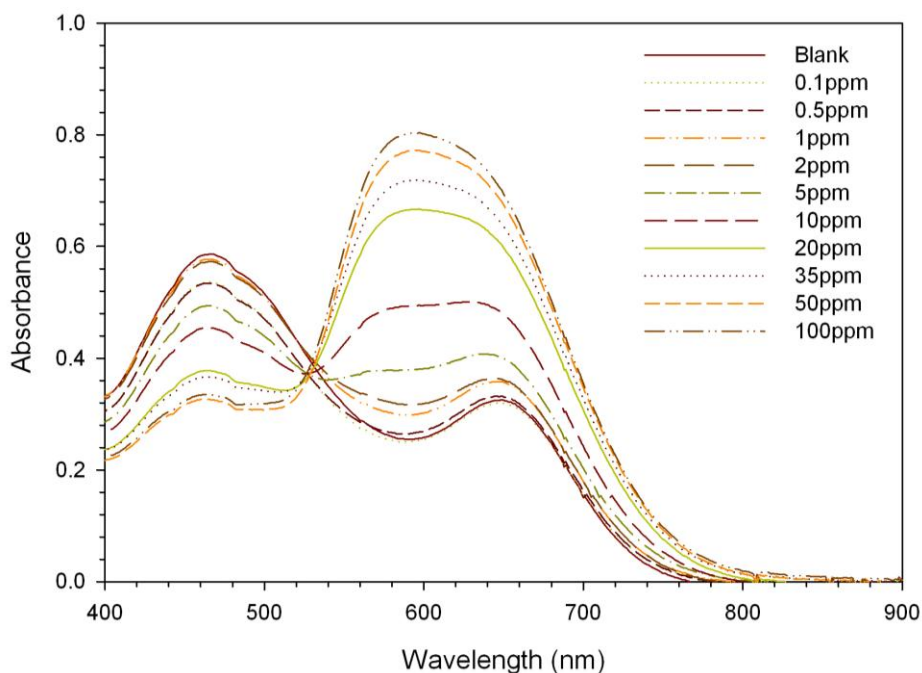


Figure 4-1. UV/Visible absorption spectrum of the Bradford Assay with various concentrations of BSA. The unbound reagent exhibits visible absorption bands at approximately 467nm and 647nm, and the bound dye exhibits a visible absorbance at approximately 590nm.

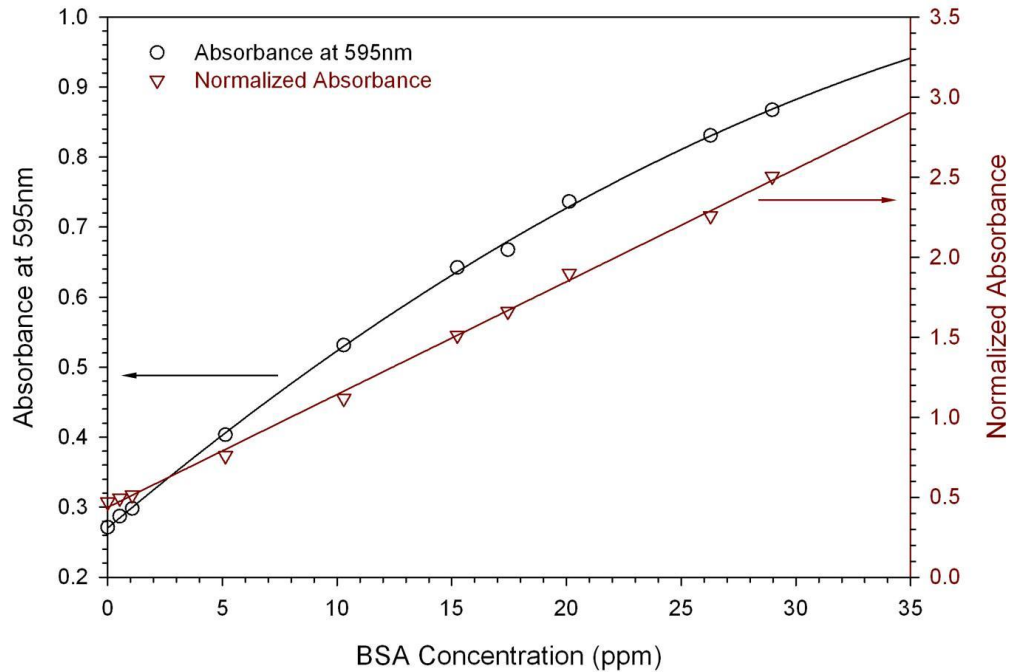


Figure 4-2. Typical response curves for the Bradford Assay using BSA. The assay response can be linearized by normalizing the absorbance at 595nm to the peak at approximately 467nm.

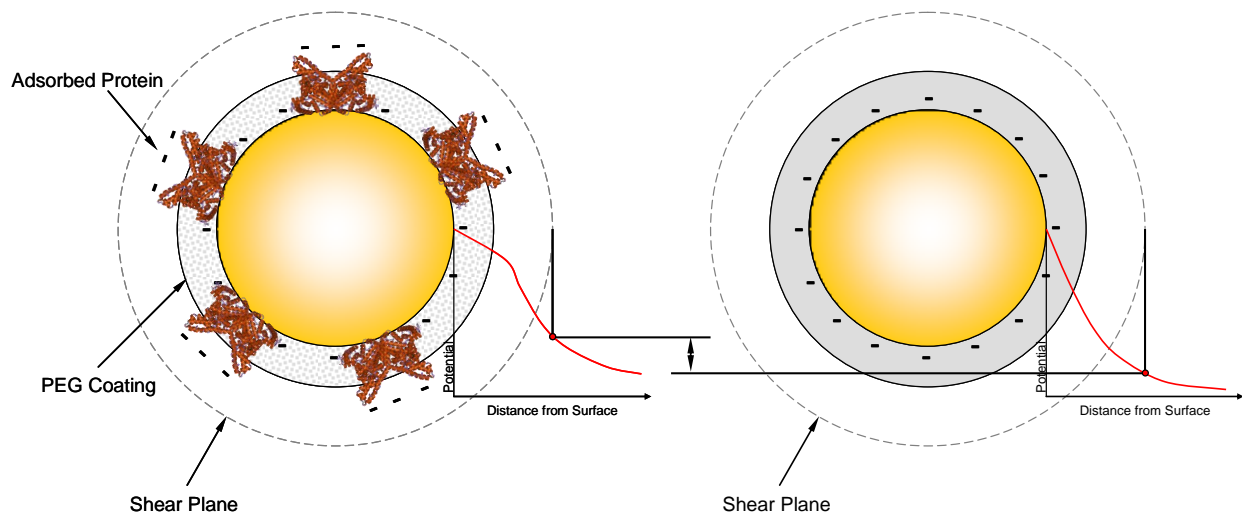


Figure 4-3. Schematic showing the effect of protein adsorption on the electrophoretic mobility. The potential difference between a PEG coated particle with adsorbed protein (left) and a fully PEG coated particle (right) is indicated by the double arrow in the center.

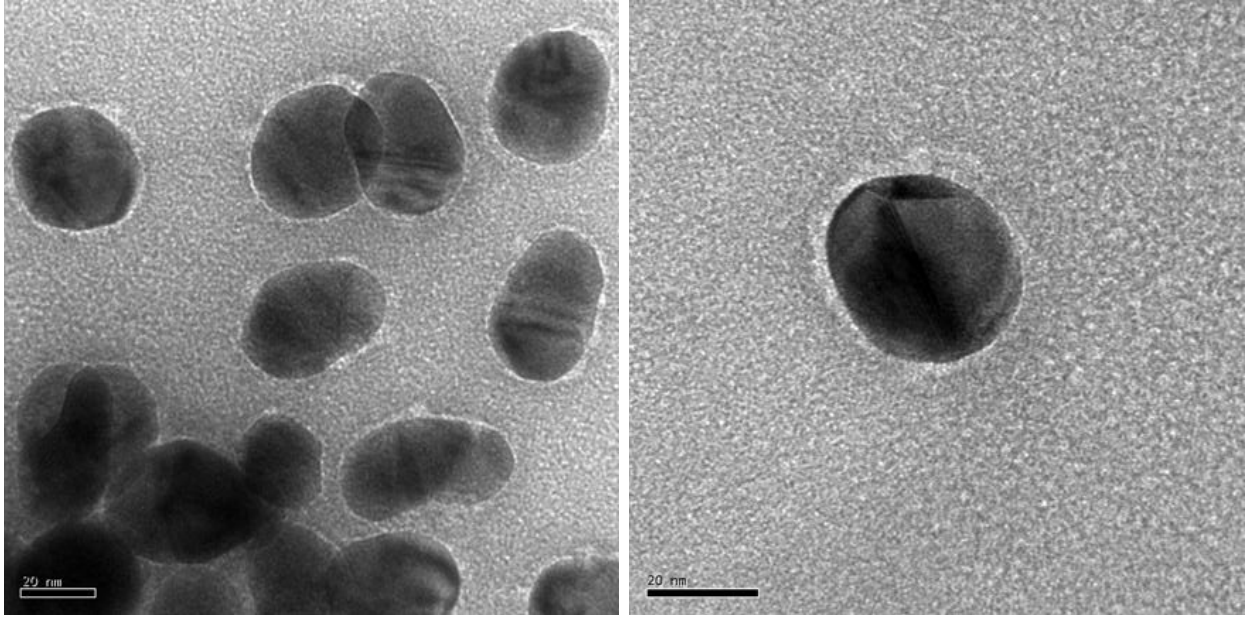


Figure 4-4. Transmission electron micrographs of negatively stained serum protein coated nominal 40nm gold particles. The protein coating can be seen as a light colored 'halo' around the particles. Particles were imaged by Kerry Siebein.

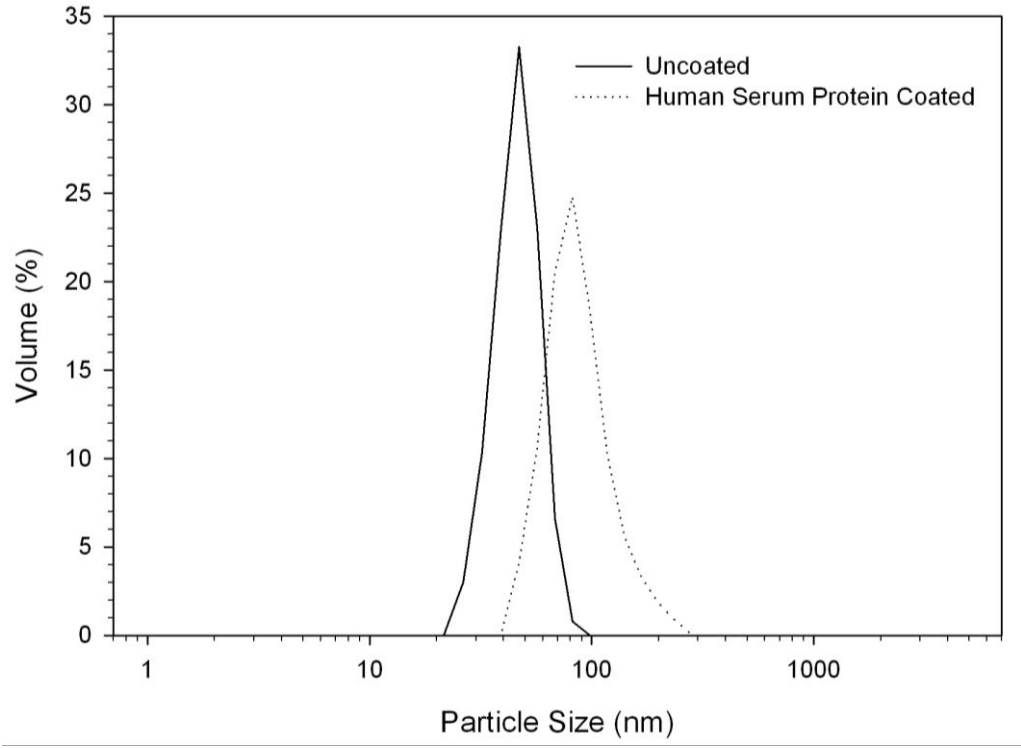


Figure 4-5. Dynamic light scattering particle size distributions of nominal 40nm gold particles showing an increase in size of approximately 40nm on coating with human plasma proteins.

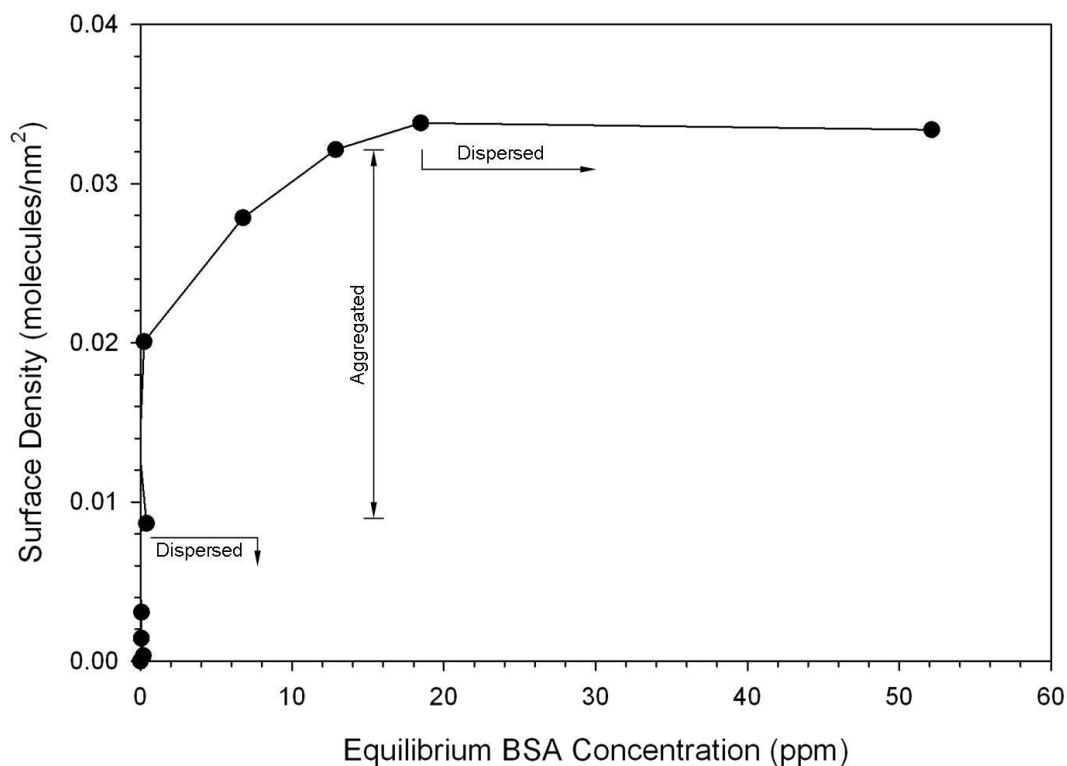


Figure 4-6. Adsorption isotherm of BSA onto as-prepared nom. 20nm gold particles with regions of colloidal stability and instability indicated. The pH of the suspension prior to adsorption was approximately 4.5-5, and the surface density at saturation was 0.034 ± 0.001 molecules/nm².

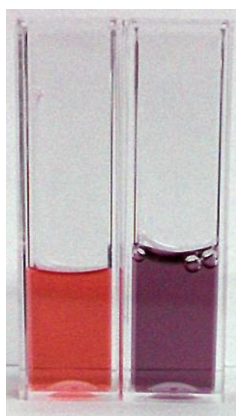


Figure 4-7. Aggregation of protein coated particles upon dilution with deionized water. The particles on the left were prepared with the minimum quantity of protein required to maintain stability (these regions are described in Figure 4-6). Aggregation of the suspension (right) occurred after addition of deionized water. This behavior illustrates the adsorbate equilibration occurring at or near surface saturation and its impact on suspension stability.

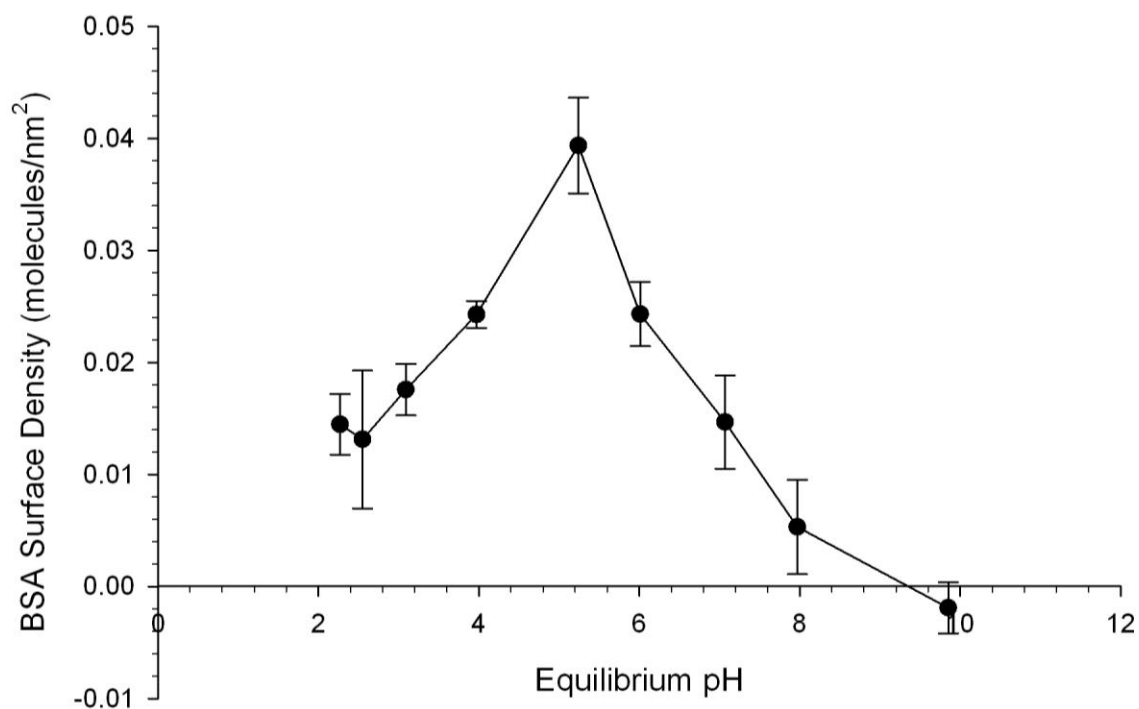


Figure 4-8. Adsorption density of BSA as a function of suspension pH on as prepared nom. 20nm gold particles. Five replicates were performed at each data point. The highest level of protein adsorption was observed at the isoelectric point of the protein.

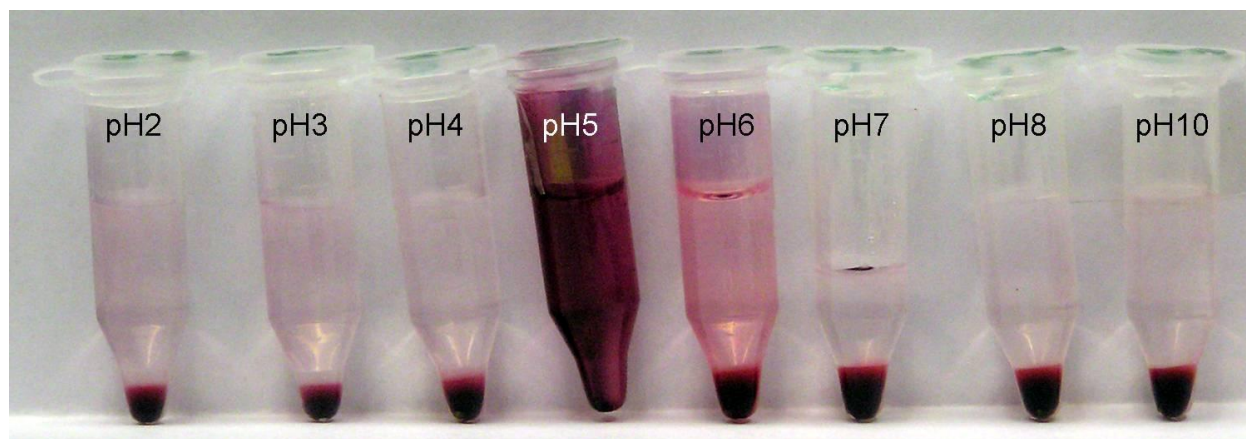


Figure 4-9. Adhesion of BSA coated gold particles to hydrophobic polypropylene containers. The highest level of adhesion occurred at the isoelectric point of the protein. Outside of this range, significant adhesion to the container did not occur.

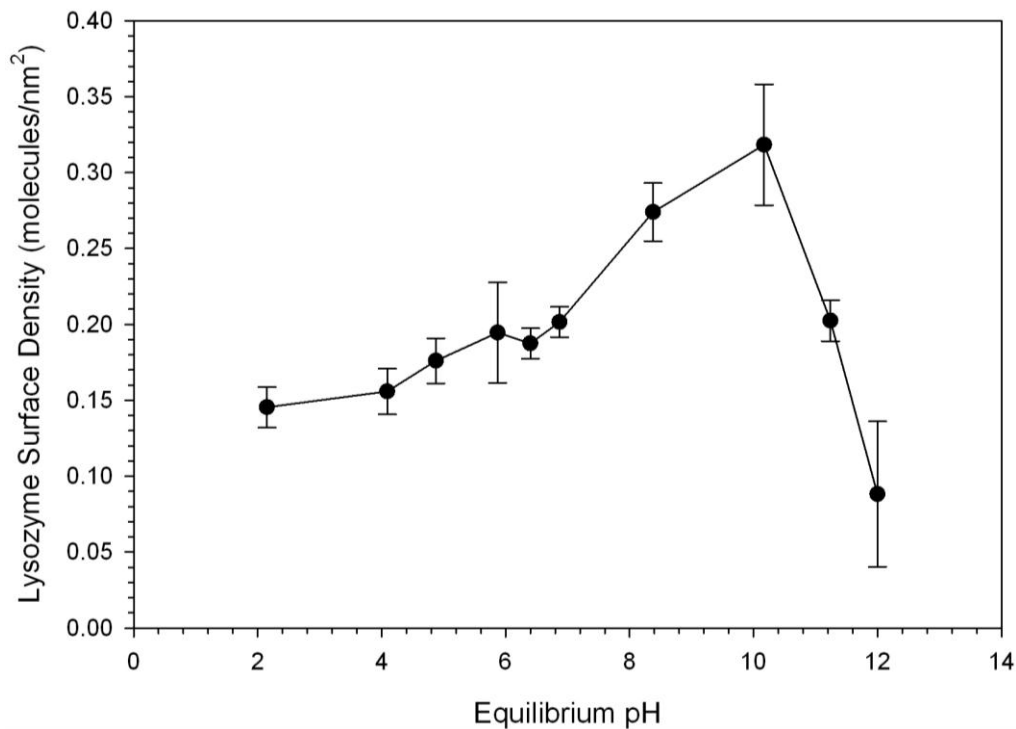


Figure 4-10. Adsorption density of Lysozyme as a function of suspension pH on as prepared nom. 20nm gold particles. Five replicates were performed at each data point. The highest level of protein adsorption was observed at the isoelectric point of the protein.

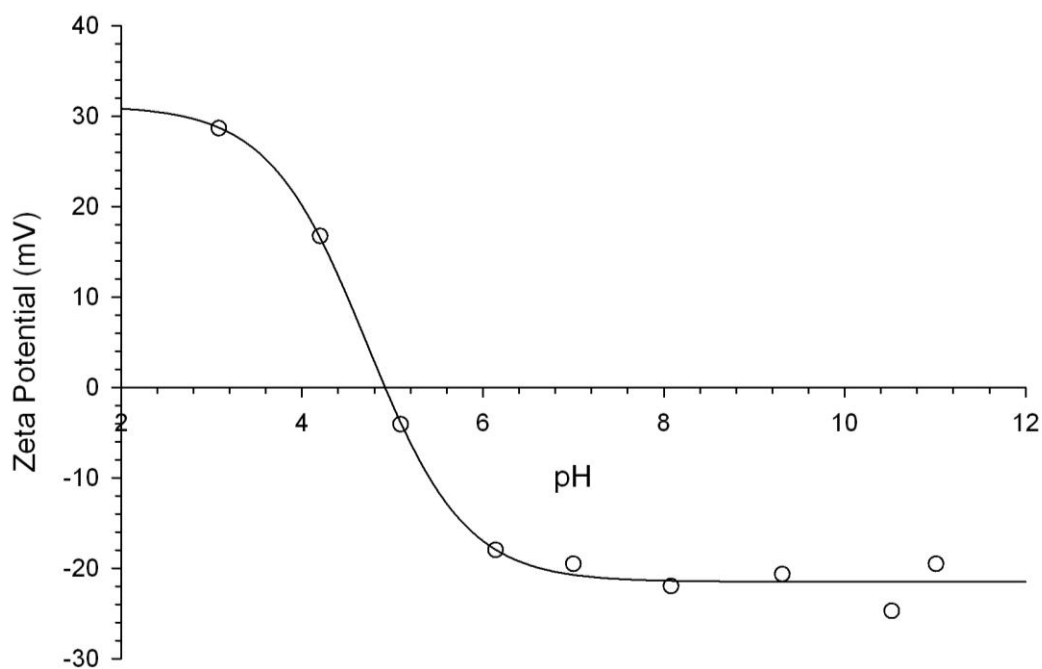


Figure 4-11. Zeta potential titration of BSA coated nom. 20nm gold particles. The isoelectric point is approximately 4.92.

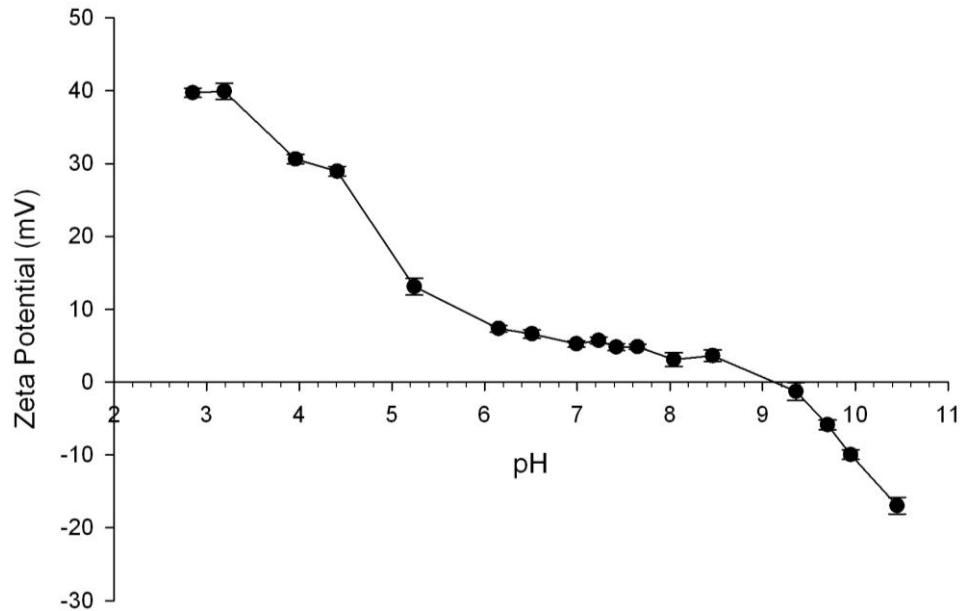


Figure 4-12. Zeta potential titration of lysozyme coated nom. 20nm gold particles. The isoelectric point is approximately 9.13. The suspension was titrated down from pH 11 since lysozyme coated particles are unstable at pH values below 9-10.

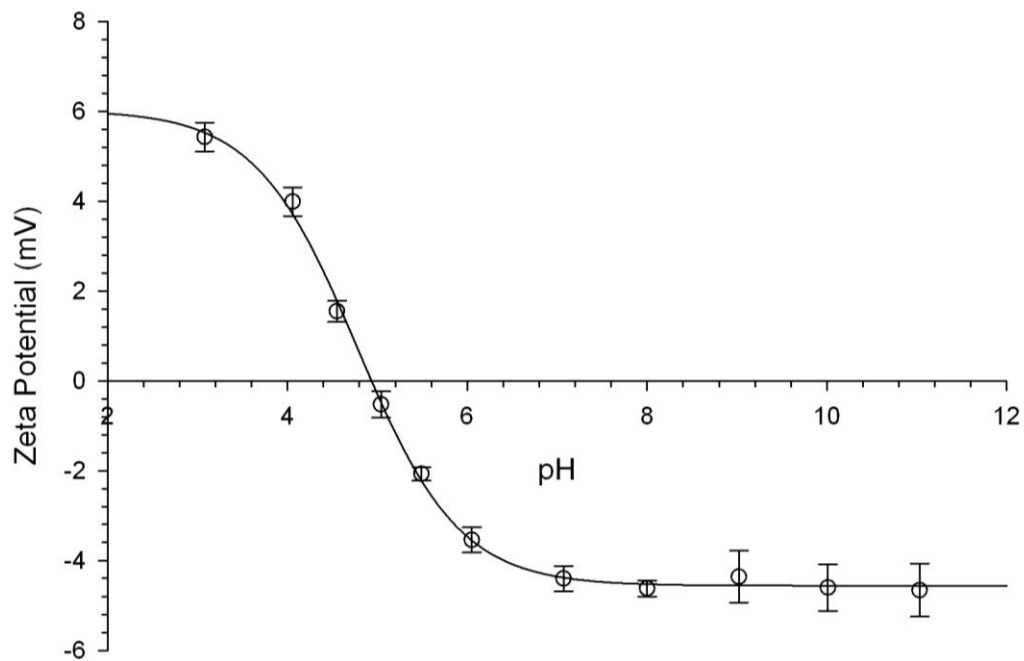


Figure 4-13. Zeta potential titration of serum protein coated 40nm gold particles. The isoelectric point is approximately 4.92. Both the curve shape and isoelectric point are virtually identical to the curve for similar albumin coated gold particles (Figure 4-11). The magnitude of the zeta potential is likely decreased due to the salt content in plasma.

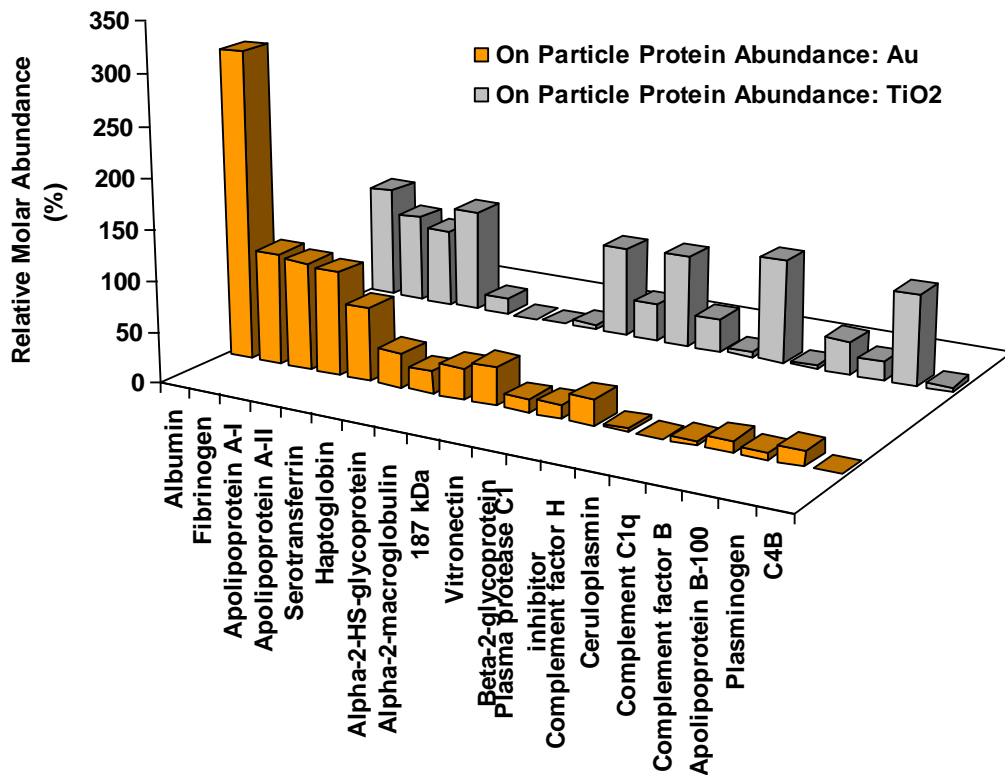


Figure 4-14. Comparison of serum protein binding characteristics of gold and titania particles. The molar abundance relative to the concentration in serum is presented. Graph was produced by David Barber.

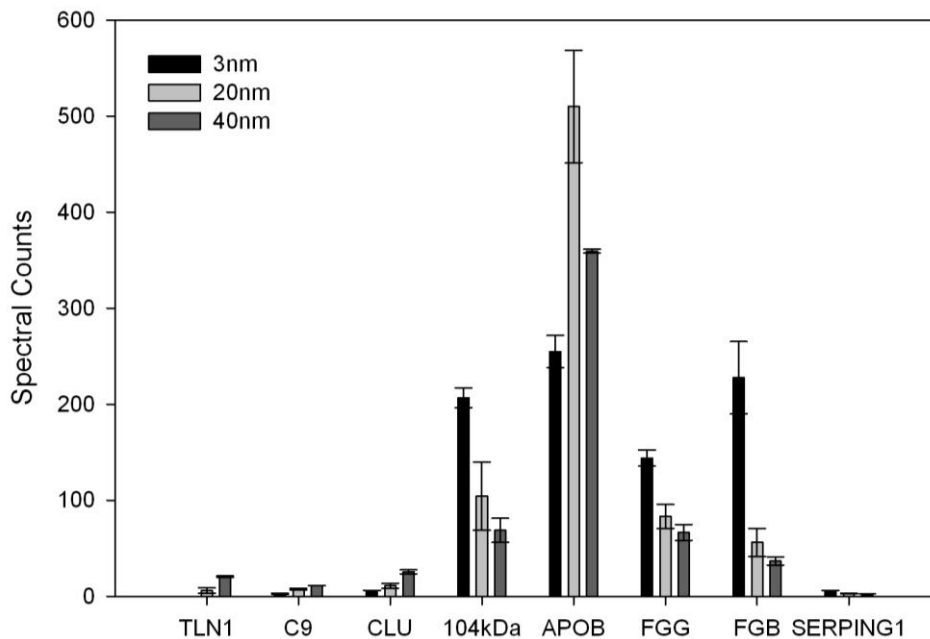


Figure 4-15. Size dependent binding of serum proteins to uncoated gold particles.

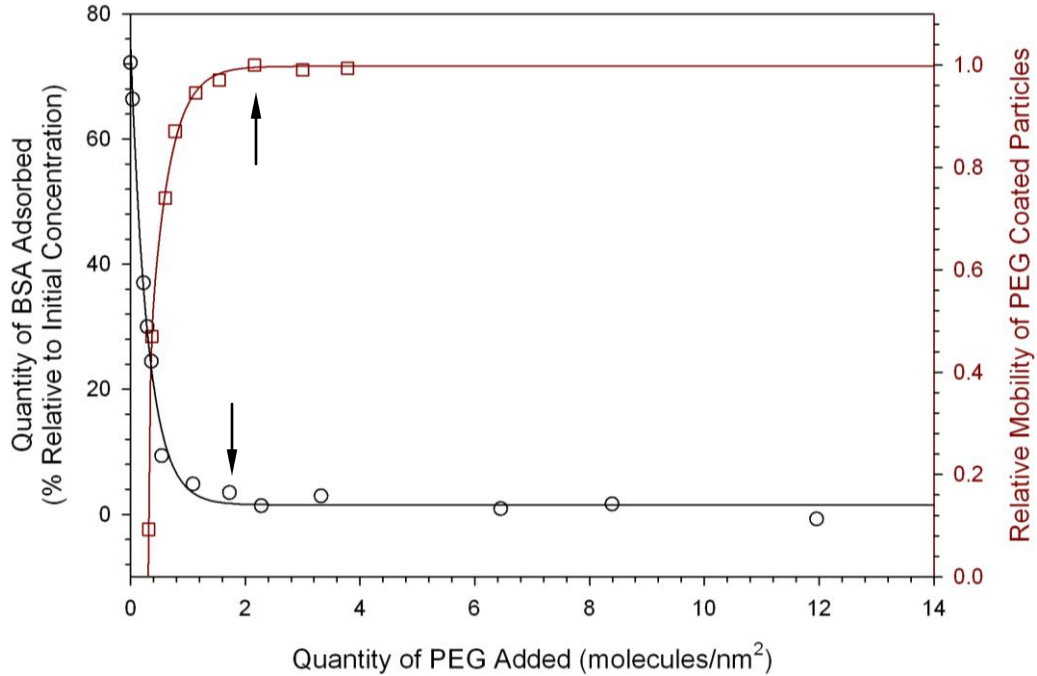


Figure 4-16. Adsorption of BSA relative to PEG coating density on nom. 20nm gold particles. Note that the point at which adsorption of BSA reaches a minimum occurs near the same point at which the surface is saturated with PEG.

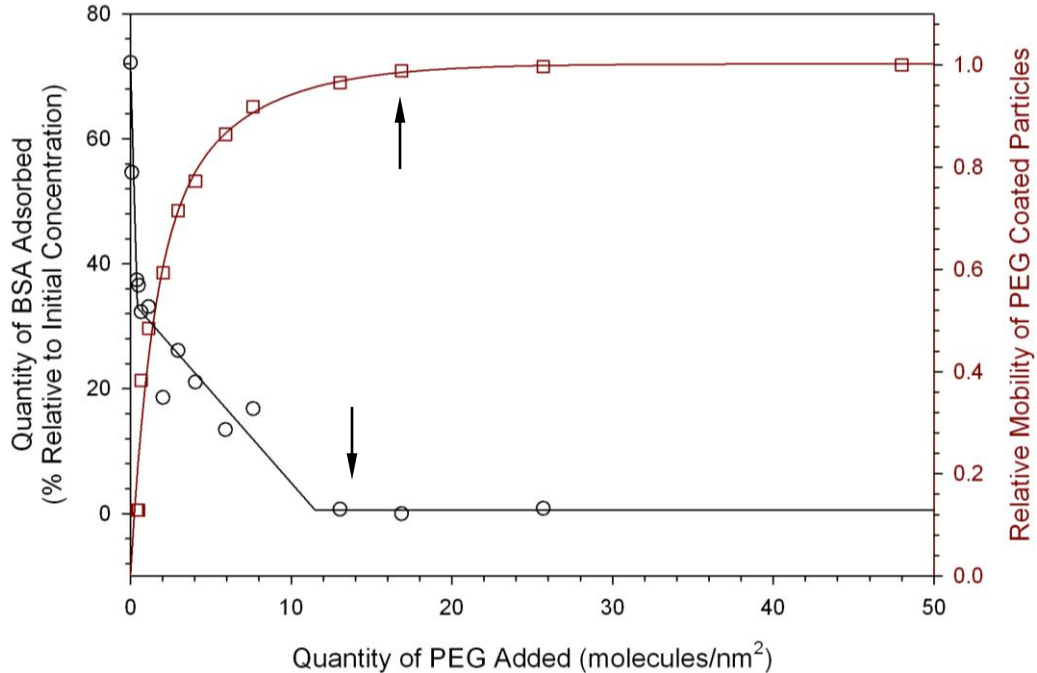
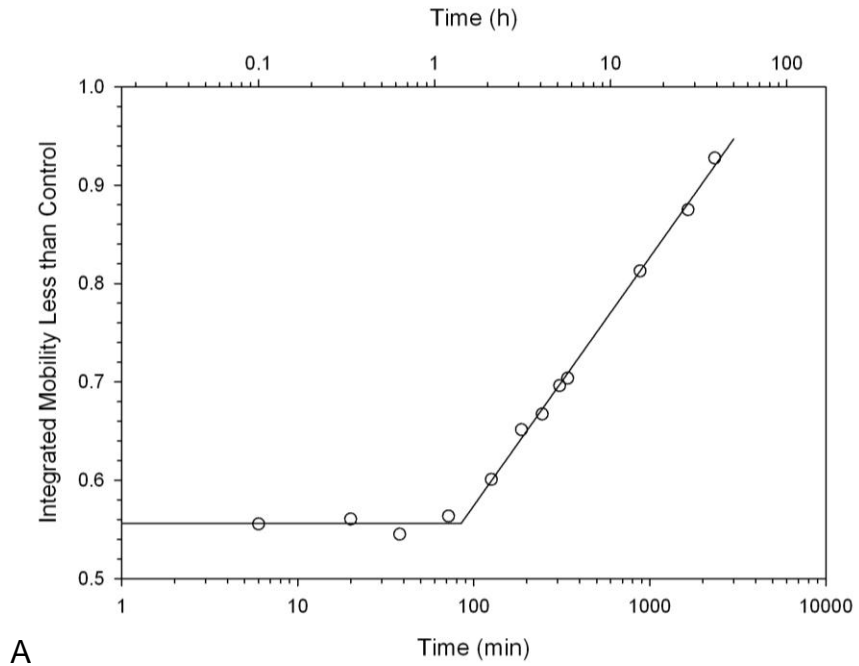
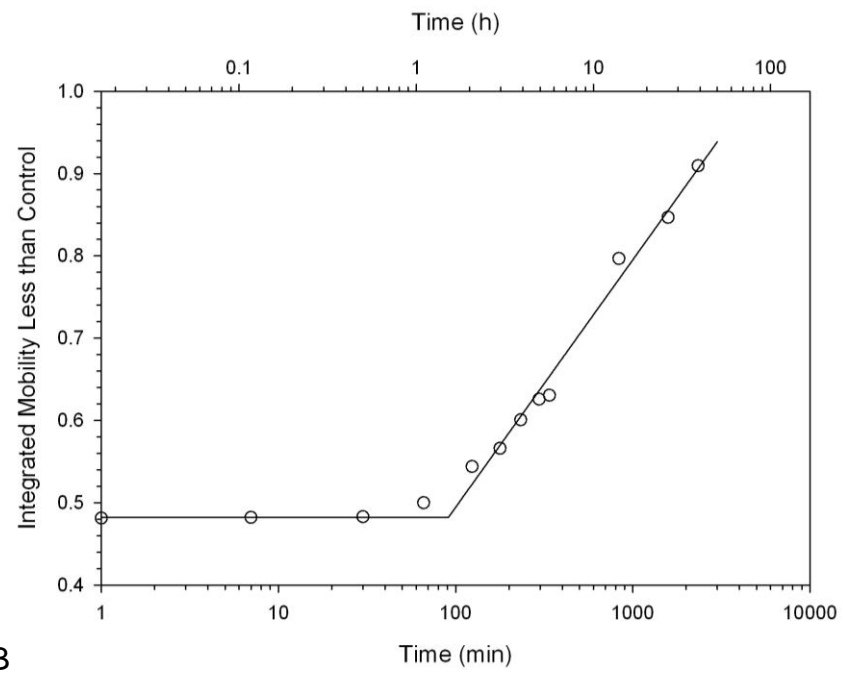


Figure 4-17. Adsorption of BSA relative to PEG coating density on nom. 20nm gold particles using a lower quality reagent. Note that the point at which adsorption of BSA reaches a minimum occurs near where the surface is saturated with PEG.

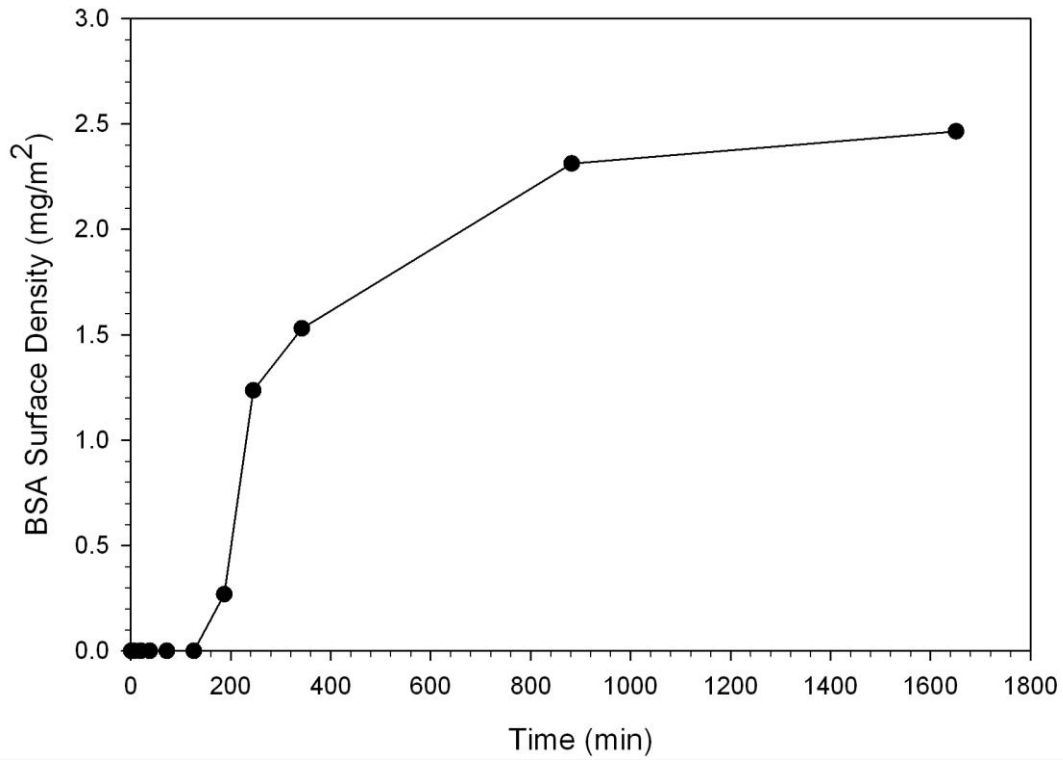


A

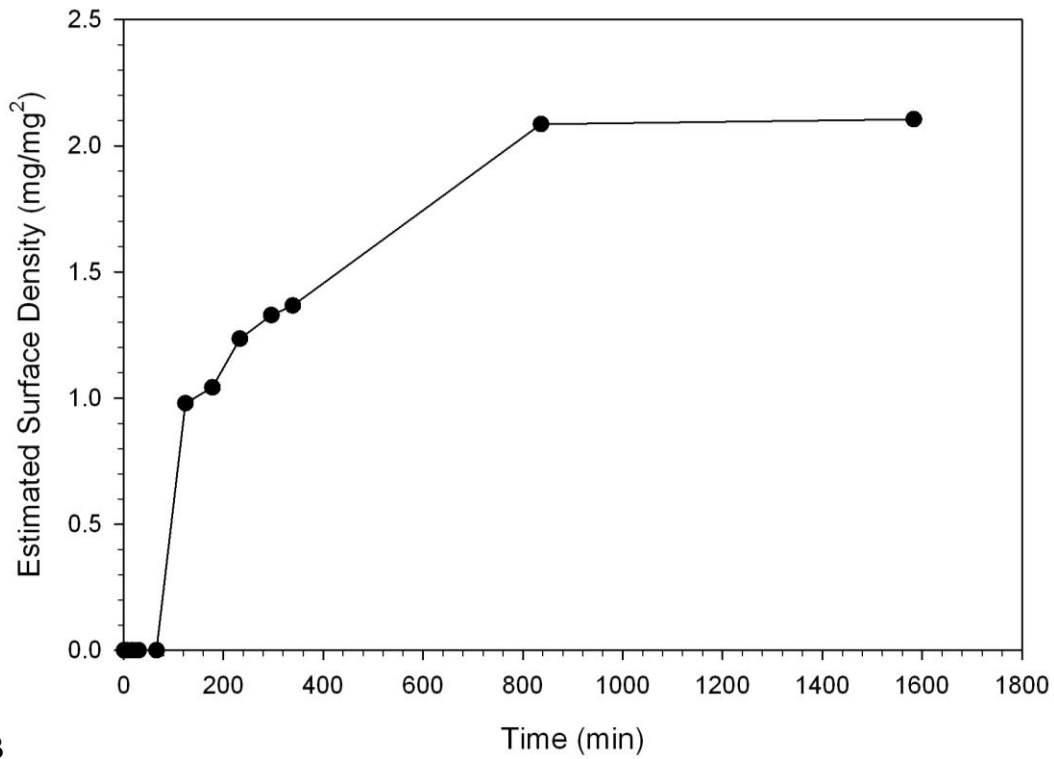


B

Figure 4-18. Time dependent integrated mobility of PEG coated gold particles (Reagent 1) in BSA and Human Serum. Particles incubated in: A) BSA (concentration approximately equal to reference serum albumin levels) B) Human plasma. The integrated mobility is the relative integrated signal strength of particles with a mobility less than that of the control (fully PEG coated) particles. Extrapolation of the baseline and data from the longest time points shows that the onset of protein binding occurs at approximately 85 and 90min for BSA and human plasma respectively.



A



B

Figure 4-19. Estimated quantities of protein adsorbed (as BSA) to PEG gold particles based on data shown in Figure 4-18. A) BSA and B) Human plasma (as albumin).

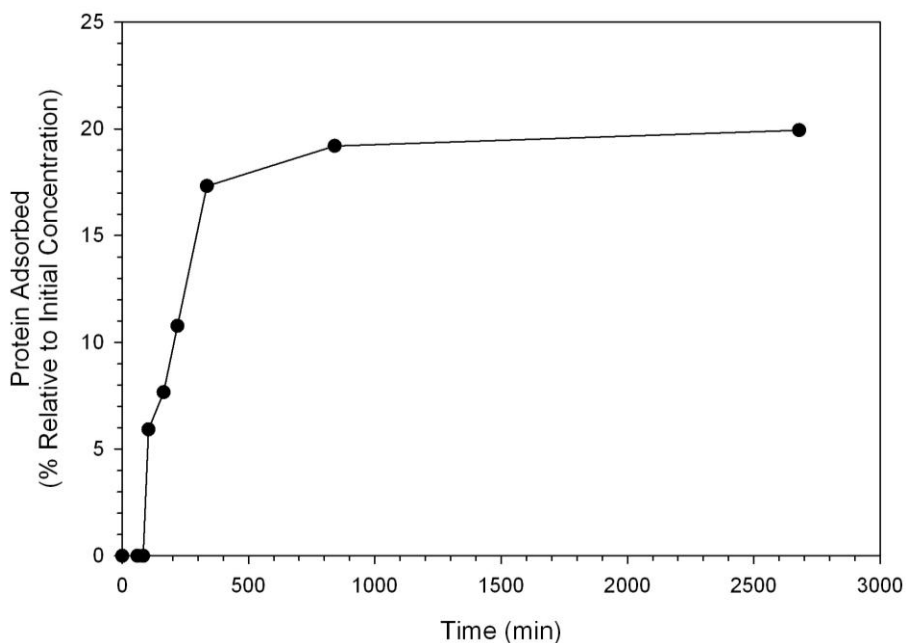


Figure 4-20. Time dependent BSA adsorption on PEG coated (Reagent 1) gold particles quantified by the Bradford total protein assay. The curve closely resembles the data shown in Figure 4-19.

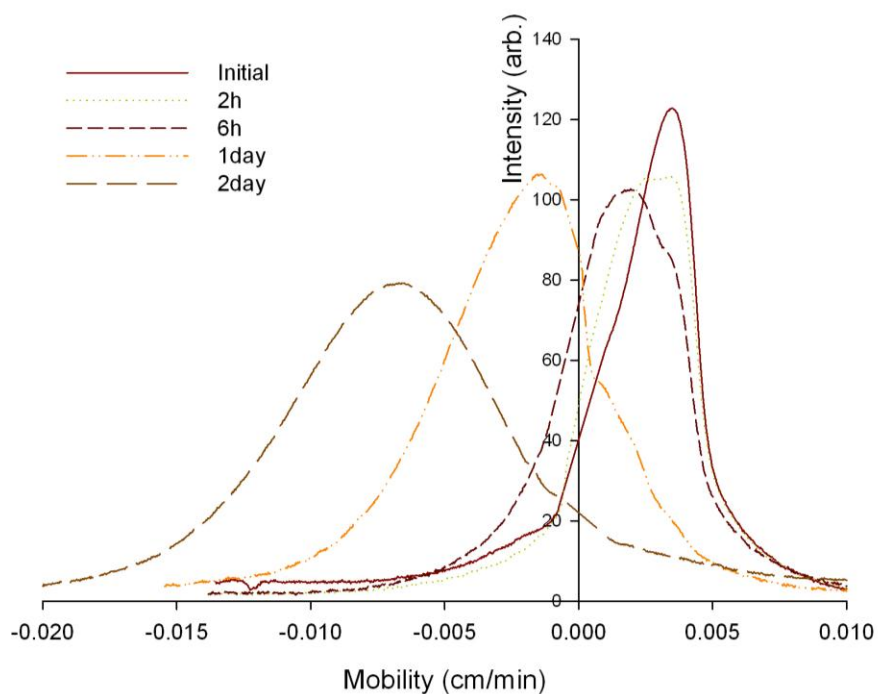


Figure 4-21. Mobility spectra of PEG coated gold particles (Reagent 1) incubated with BSA for various periods of time. Adsorption of the negatively charged protein BSA causes a decrease in mobility relative to the PEG coated particles.

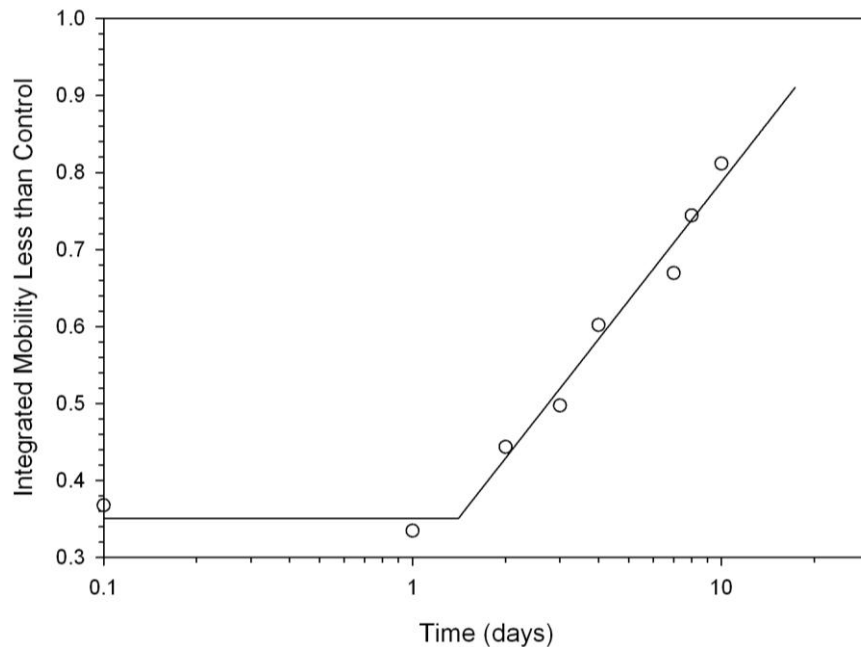


Figure 4-22. Time dependent integrated mobility of PEG coated gold particles (Reagent 2) in human plasma.

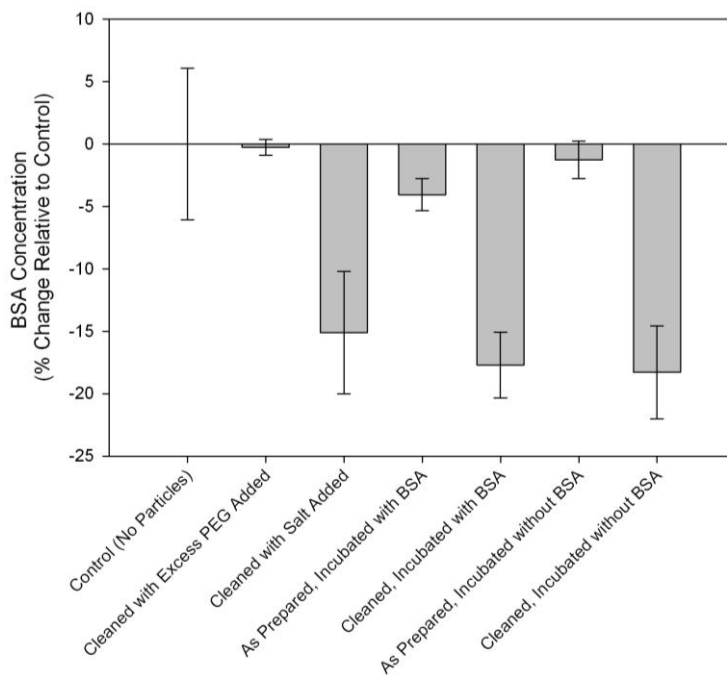


Figure 4-23. Protein adsorption in cleaned and as prepared PEG coated (Reagent 1) gold particles after incubation at 37C for three days under different conditions. Note that the primary factor which determined whether or not protein adsorption would occur was the presence of small quantities of excess (unbound) PEG-thiol.

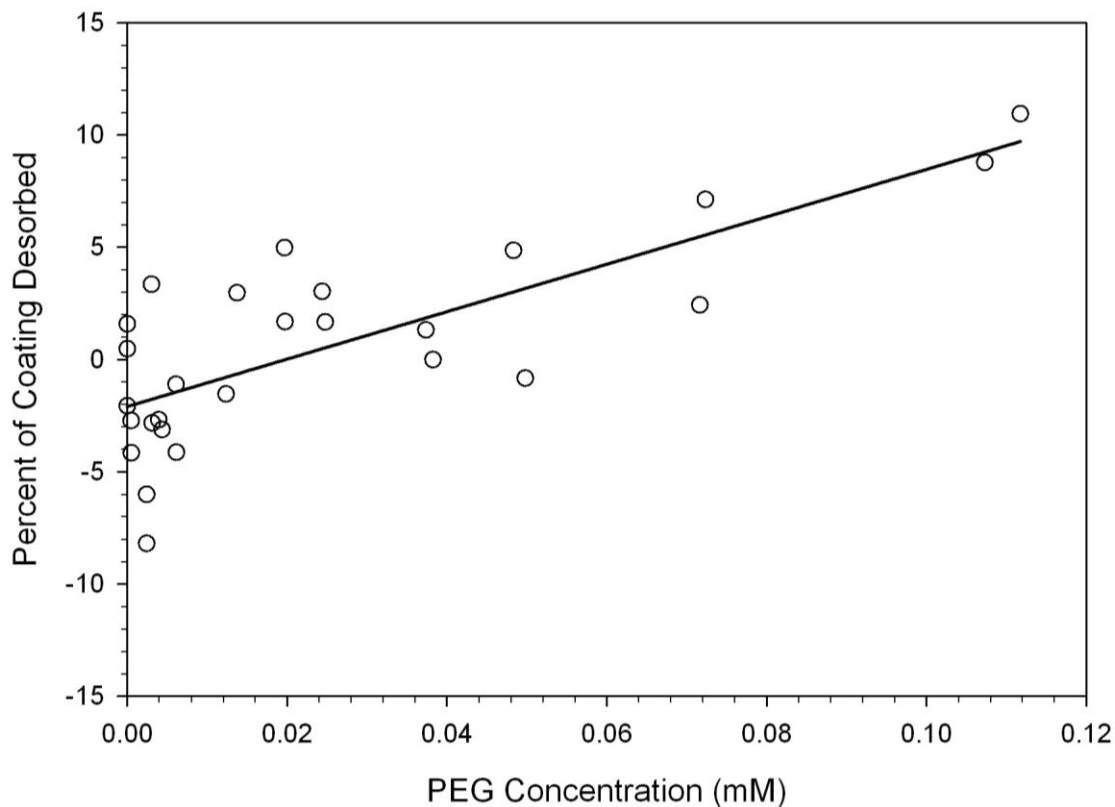


Figure 4-24. Competitive desorption of BSA from fully protein coated particles at physiological pH by thiolated PEG (Reagent 2). Only a small increase in supernatant protein concentration was observed, and most values were statistically indistinguishable from the parent suspension except at the highest level. PEG was added far in excess of the quantity required to fully coat the particles used. In certain cases, higher concentrations of PEG were found to produce a slight positive response from the tested assay when combined with protein.

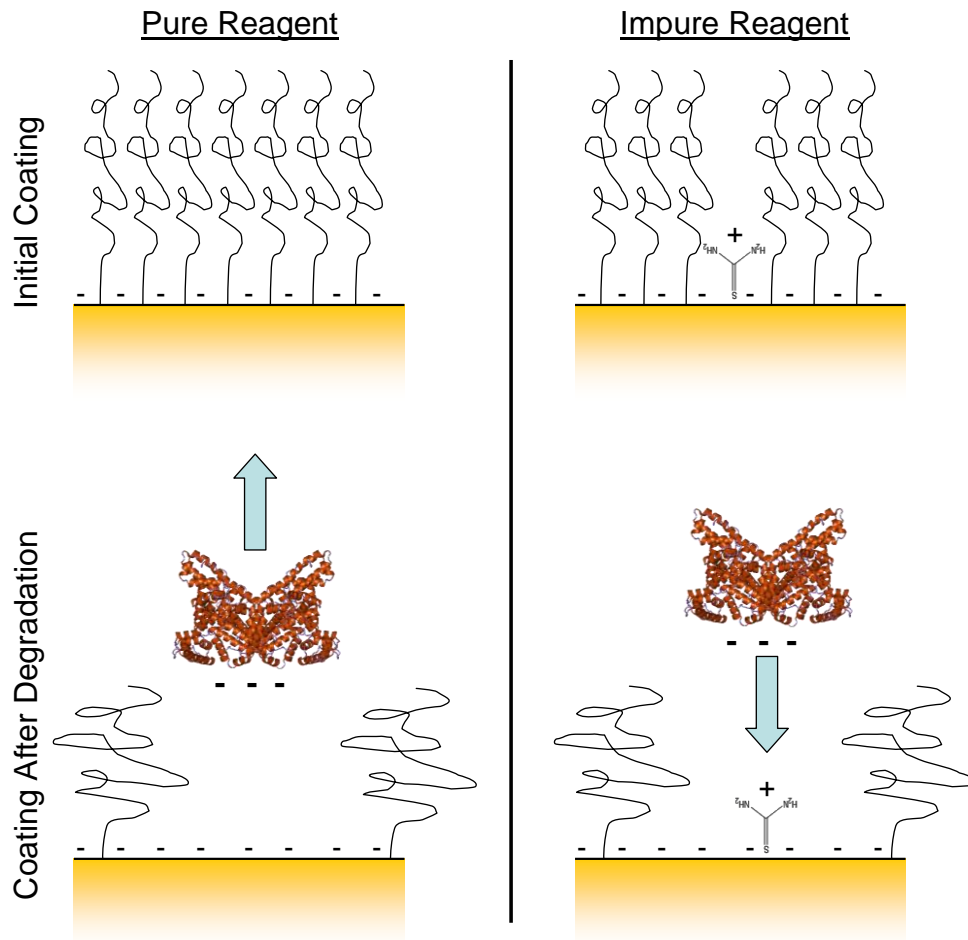


Figure 4-25. Illustration of the proposed relationship between impurity adsorption and protein binding on gold particles. In the impure reagent, the coating is initially less dense than the pure reagent due to competitive coadsorption of the impurity (thiourea). After degradation, the reduced surface charge caused by the presence of thiourea enhances adsorption of proteins due to decreased surface charge.

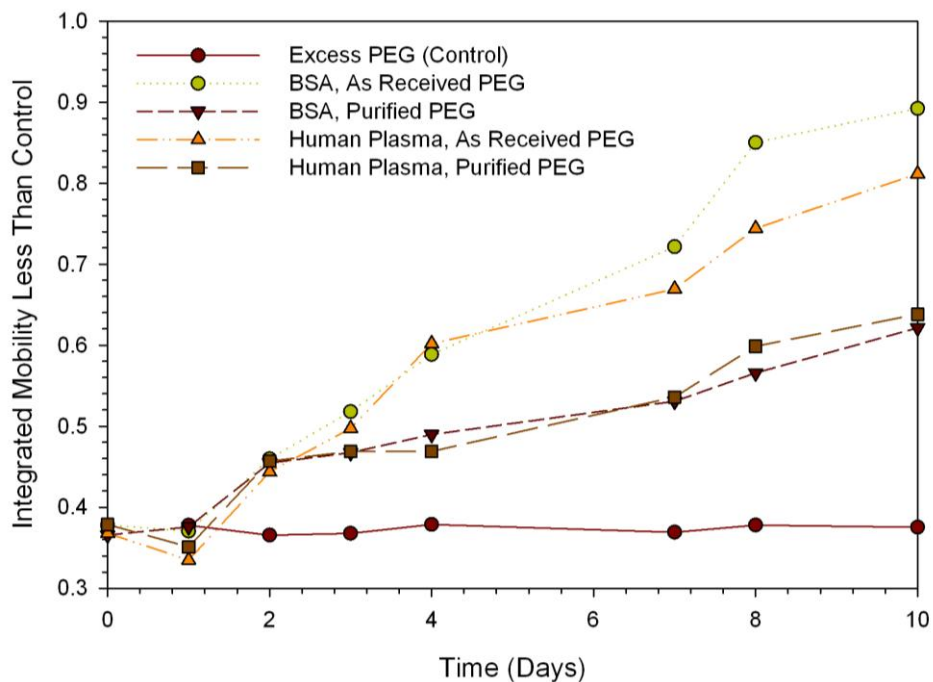


Figure 4-26. Time dependent integrated mobility of particles coated with purified and as-received PEG-thiol (Reagent 2) exposed to BSA and Human Serum at 37C. Note that the pairs of samples prepared with purified PEG bound less protein than the samples prepared with as-received PEG reagent, as indicated by the lower integrated mobility.

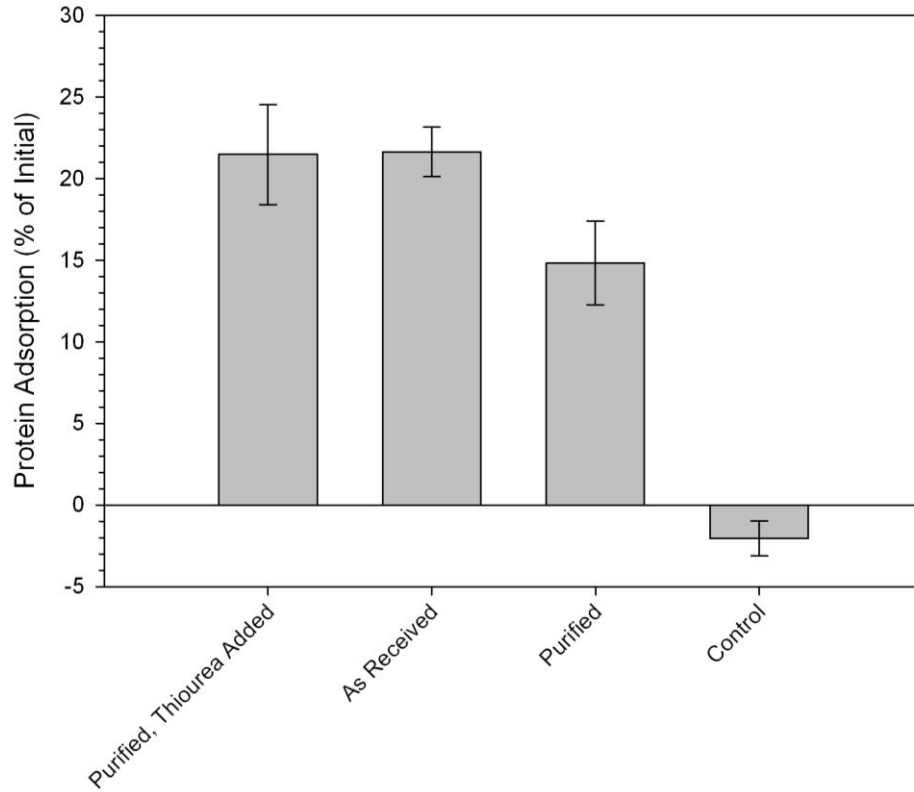


Figure 4-27. Single point adsorption measurement of BSA onto PEG coated (Reagent 2) nom. 20nm gold particles using the Bradford Assay after a 5 day incubation at 37C. The particles coated with PEG as received bound approximately 45% more protein than the particles coated with purified PEG.

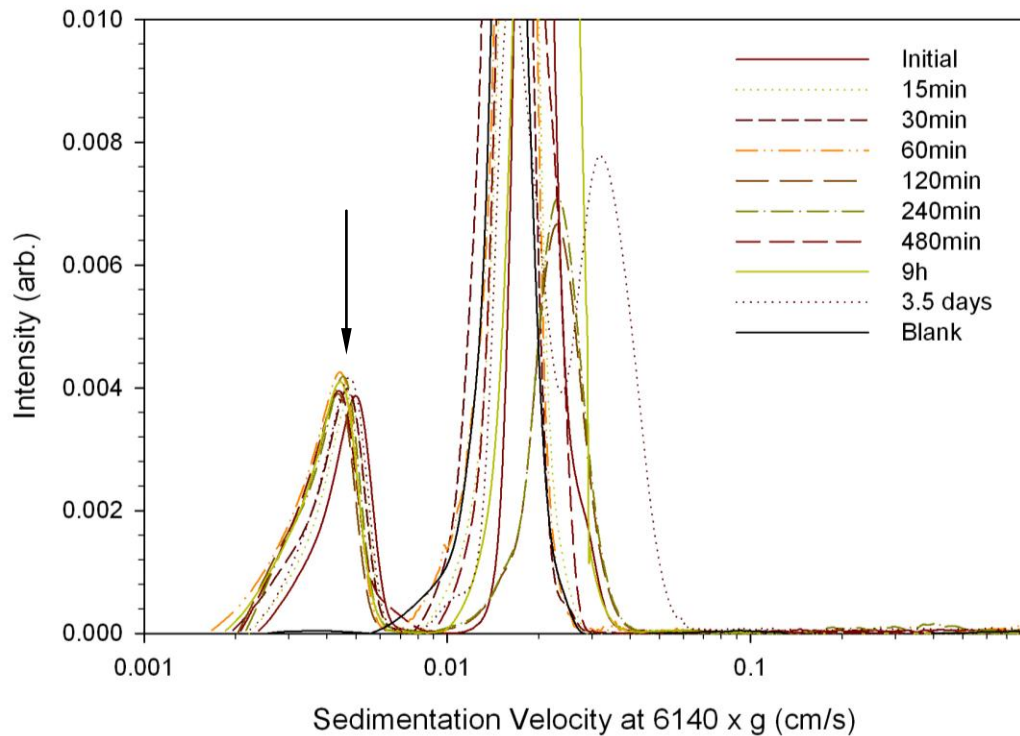


Figure 4-28. Sedimentation velocity distributions of PEG coated gold particles (Reagent 1) incubated at 37C in whole mouse blood for various times. The peak corresponding to the primary particles is indicated with an arrow. Note that the peak intensity does not change significantly over time, indicating that there is no loss of primary particle concentration due to aggregation.

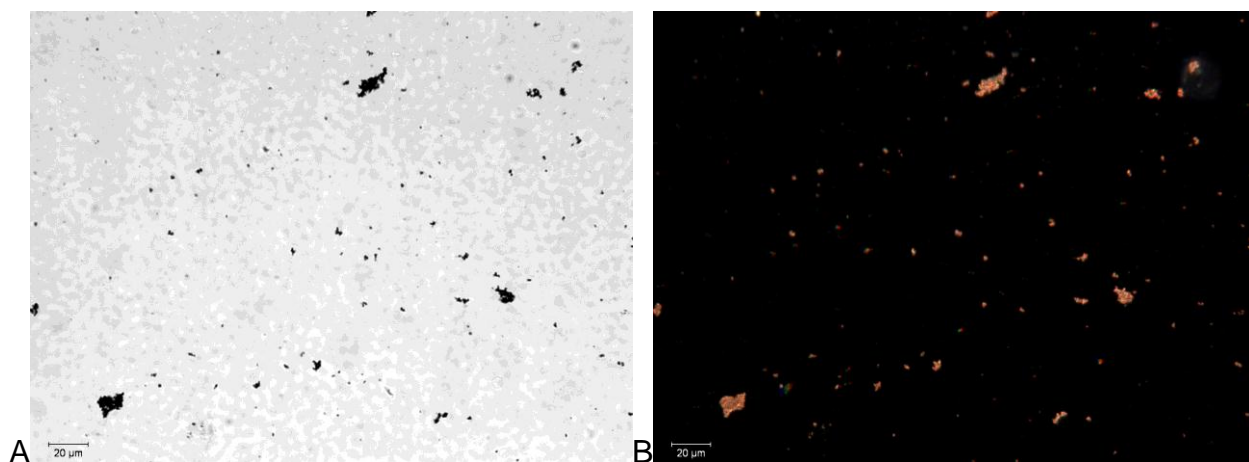


Figure 4-29. Optical micrographs of aggregated gold particles (uncoated) in whole blood after lysing cells in deionized water. A) Brightfield transmitted micrograph. B) Darkfield reflected micrograph. Gold particles of sufficient size appear as optically dense features under transmitted illumination and yellow features under reflected illumination.

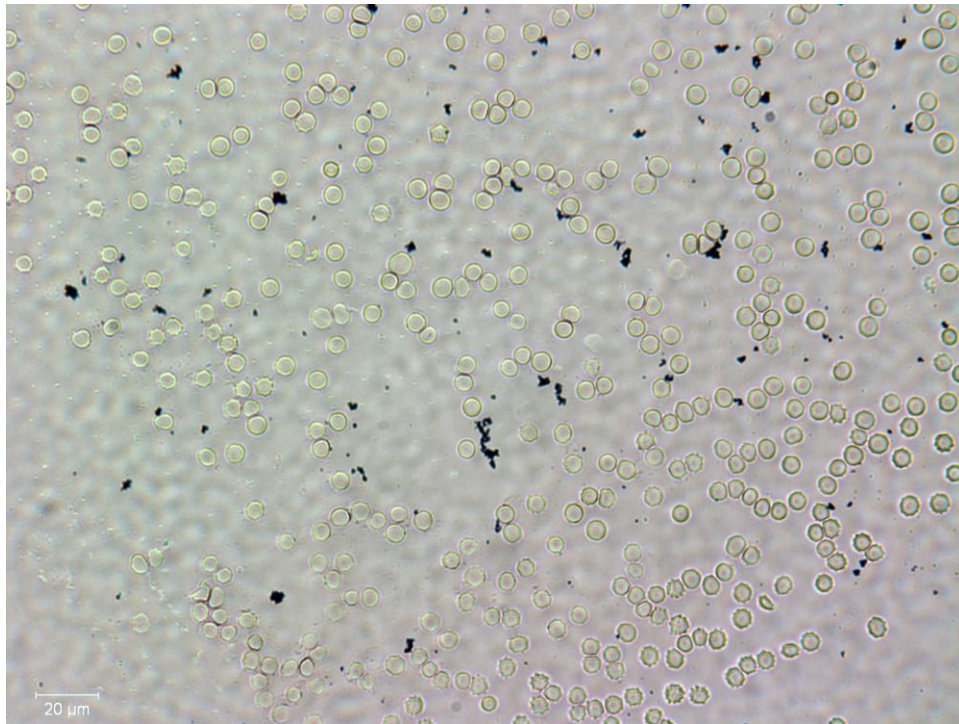


Figure 4-30. Optical micrograph of aggregated gold particles (uncoated) in whole blood. The gold aggregates are the dense features dispersed around blood cells.

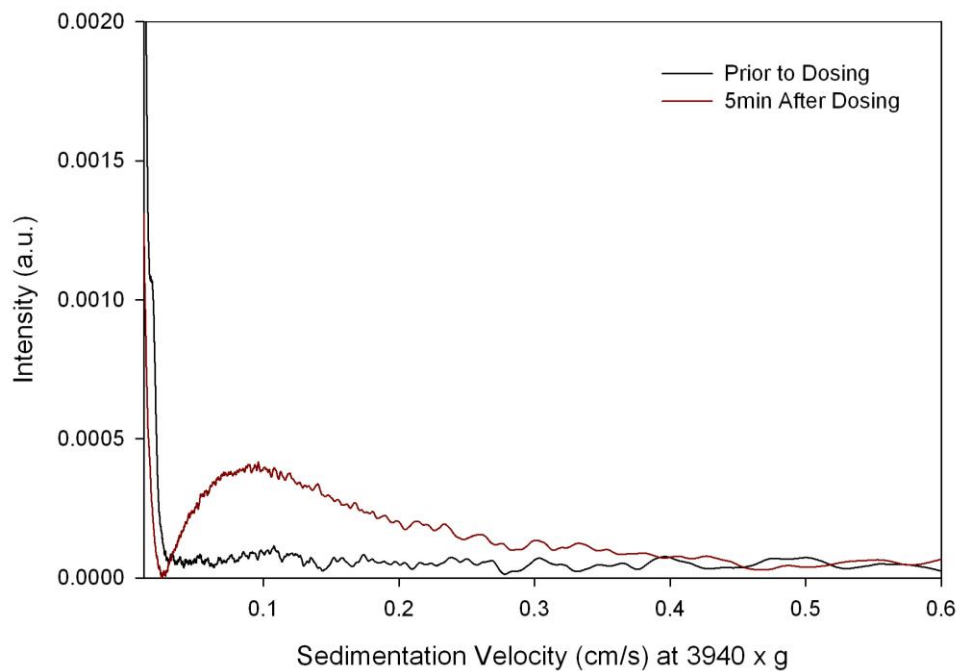


Figure 4-31. Sedimentation velocity distributions of blood before and after addition of uncoated gold particles. Weak and transient peaks corresponding to aggregate particles were observed at early time points while no peaks corresponding to the primary particles were observed at any time.

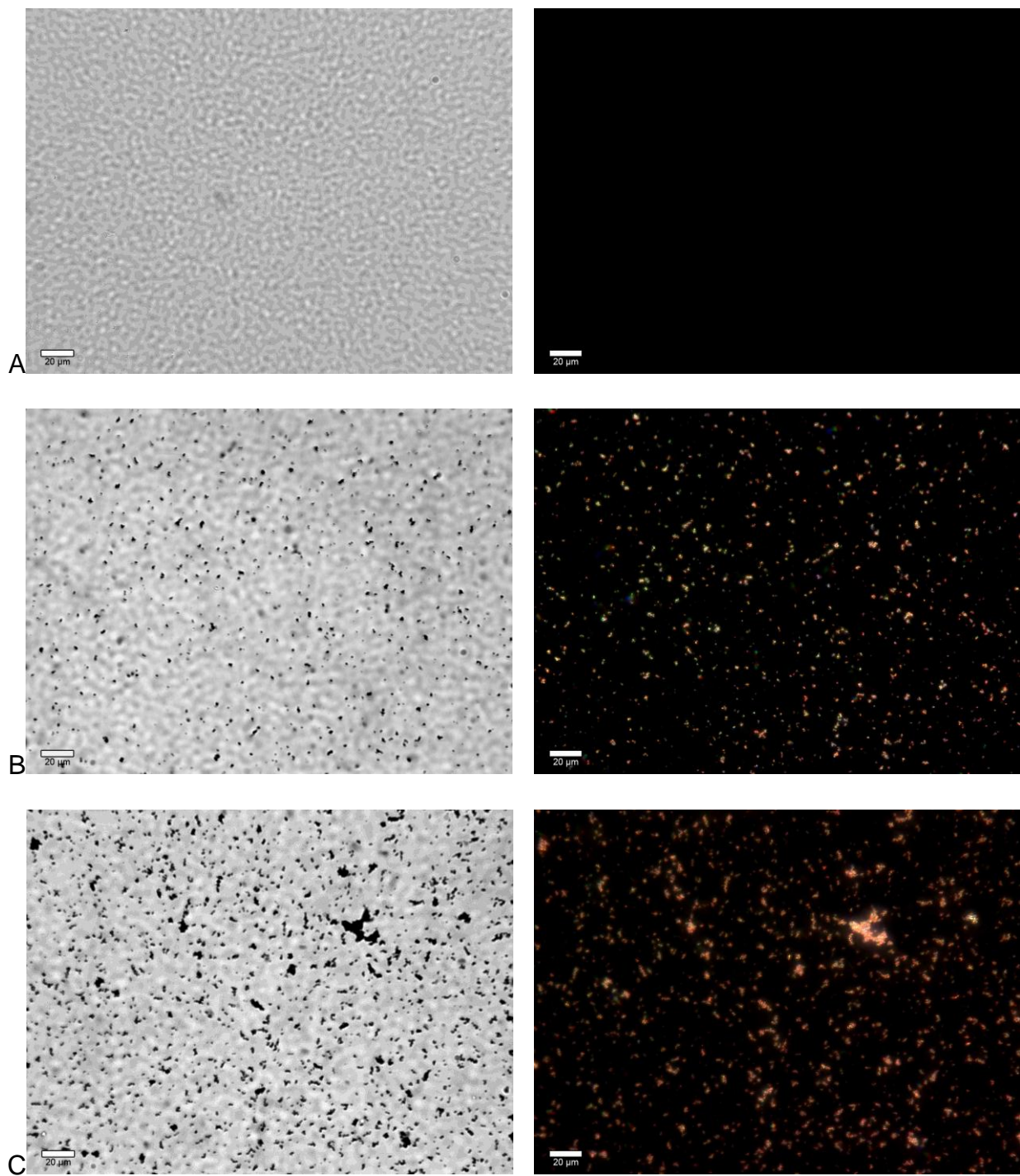


Figure 4-32. Optical micrographs of uncoated gold particles added to human plasma under different mixing conditions. Brightfield transmitted images are on the left, darkfield reflected images are on the right. A) Uncoated particles mixed gradually under high shear. B) Particles mixed under rapid stirring. C) Particles mixed under gentle stirring. An increase in aggregate size is evident with decreasing shear during mixing. Without higher illumination power, the well dispersed particles are not visible optically.

CHAPTER 5 IN VIVO BEHAVIOR OF NANOMATERIALS

Chapter Introduction

The previous chapters focused on the characterization and *in vitro* behavior of PEG coated particles. The stability of the PEG coated gold particles was characterized under a variety of conditions, and coatings were shown to degrade rapidly in deionized water. The presence of impurities in the reagent and exposure to various compounds were found to moderate the rate of degradation. Once sufficient degradation of the coating occurred, plasma proteins began to adsorb, signaling the point at which the coating failed. Although this is indicative of the point at which opsonization is likely to occur, the point at which recognition of the particles by the body could not be tested *in vitro*. Little evidence exists today to generally correlate properties of the particles such as size, charge, total quantity of protein adsorbed, stabilizing coating type, etc. to clearance and biodistribution²⁵¹. Despite the fact that most interactions which govern efficacy of nanomaterial based therapeutics occur *in vivo*, little data is available on the surface properties and colloidal stability of nanomaterials in the bloodstream⁶¹. The final stage in this work is to assess the colloidal stability and clearance rates of the aforementioned particles *in vivo*.

Polyethylene Glycol Surface Coatings for Improved Circulation Time

Polyethylene glycol was first used to improve blood circulation times of proteins in 1977¹⁸⁴. In the decade that followed, relatively limited widespread use or commercialization of products occurred²⁵⁶. The last two decades, on the other hand, have seen a considerable expansion of the use of PEG for both research and commercial medical applications. PEG and its derivatives have been widely employed

for solubilization, enhancing circulation times, increasing pharmaceutical molecular weight, and surface modification of various materials. The first reported use of PEGylation to increase circulation times of particles *in vivo* was in the early 1990s with liposomes³¹ and PLGA particles²⁵⁷. In one study²⁵⁸, the circulation times of PLGA particles were extended from minutes to hours upon PEGylation. These developments ultimately lead to the first FDA approved nanomaterial based commercial pharmaceutical: Doxil (PEGylated liposomal Doxorubicin) in 1995²⁵⁹. In this capacity, PEG continues to be the most effective and widely used polymer for improving nanomaterial stability in the bloodstream²⁵⁹.

Though the advantages to the use of PEG for enhancing circulation time are numerous, there are several important factors that can compromise its effectiveness. One major factor involves thermal and chemical degradation of the PEG chain. Previous discussion indicated that PEG may be degraded at temperatures as low as 30C⁵². Work performed on solid PEG at temperatures of 60C and less showed damage to and oxidation of the polymer under ambient conditions including addition of various oxygen containing functional groups and a decrease in the polymer molecular weight to 10% of its original value^{32, 33, 257}. Chain scission was also observed even without the presence of oxygen. UV damage at longer wavelengths and thermal oxidative damage have been identified in these polymers and occurs via the formation of peroxide and peroxy radicals¹⁸⁸. Degradation of the PEG polymer itself by oxidation under ambient conditions has been shown to cause complement activation²⁶⁰, and the presence of exposed terminal hydroxyls on PEG have been proposed as a site where complement activation can occur²⁶¹. Even if the PEG chain is undamaged, the presence of a naturally

occurring anti-PEG antibody has been identified and correlated with rapid clearance in coated liposomes²⁶², and hypersensitivity reactions have been identified for certain PEG-drug-nanoparticle preparations²⁶³. Although certain limited drawbacks to the use of PEG for improvement of biocompatibility exist, they are generally considered to be far outweighed by the beneficial properties of PEG²⁶⁴.

Clearance of particles from the bloodstream

Parenterally administered nanomaterials are typically cleared from circulation by three major mechanisms: extravasation, uptake by the RES system, and renal clearance. Of these three mechanisms, most nanomaterials are cleared by the RES system, and to a lesser extent, extravasation. Renal clearance does not play a role unless the particles are small (less than approximately 5-10nm^{265, 266}), in which case clearance occurs rapidly through excretion. Some evidence also suggests that excretion efficiency occurs in a charge dependent manner²⁵⁷. The major clearance pathways and their interactions with each other are detailed in Figure 5-1. Although polymer coated particles are engineered to resist opsonization and clearance, all engineered nanomaterials are eventually cleared from the blood by the RES, with a small size dependent number of particles removed through extravasation (smaller particles are more likely to pass through vessel walls)^{249, 267, 249}. Larger particles (~200nm and larger) are removed from the bloodstream and sequestered via filtration by the spleen and liver^{29, 264, 268, 269}. For most stable nanomaterials with intermediate sizes (between ~10 and 100nm), RES uptake processes generally result in a final biodistribution where the majority of particles are sequestered in the liver and spleen³⁷. The amount of time required for well stabilized materials to clear the bloodstream by this mechanism can range widely, with literature reported values in excess of 24h for iron oxides and over

15h for gold³⁷, whereas unstabilized materials immediately accumulate opsonins and are cleared in seconds to minutes²⁷⁰. Breakdown of the coating and accumulation of opsonins are hypothesized to be the two major causative events for the clearance of well stabilized materials; however the dynamics of the coating and the accumulation of opsonins on stabilized particles in the bloodstream are not well known. Once taken up, most inorganic materials are sequestered by the body due to their inert composition. Some materials, such as iron oxide, have the ability to dissolve and become bioavailable. Iron oxide administered in this form can be completely removed from the RES within 1-2 weeks after administration for some commercial MRI contrast agents¹⁵. Nanoscale silica particles are also known to dissolve slowly in aqueous environments at a size related rate²⁵⁹.

Though PEG coated particles are thought to be largely inert, significant evidence in literature indicates that the body is capable of recognizing repeated doses of PEG coated particles. Accelerated blood clearance is observed (primarily in liposomes but also in polymer and lipid particles) when repeated doses of PEG coated particles are administered to animals⁵³. Additional analysis of blood from animals dosed repeatedly with PEG coated liposomes revealed the presence of an anti-PEG IgM, which takes part in rapidly clearing the PEG coated particles^{271, 272}. The existence of a naturally occurring anti-PEG antibody has been known for decades^{264, 273-276}. Studies to determine the occurrence of this antibody among healthy blood donors found that the antibody is present in up to 25% of the tested population²⁷⁷.

Literature values of blood half-lives for PEGylated gold particles vary widely, with reported half-lives ranging from minutes to days (Table 5-1). A high degree of variability

in these values occurs within similar particle types and sizes. Some variability in these numbers is expected; however several references report extremes in clearance half lives for seemingly identical particles. Previously, evidence provided in this work showed large differences in the rates of protein adsorption based on reagent source and the presence of impurities in the reagent. It is possible that these factors could be at play in addition to variances based on the type of animal, dose concentration, and other similar factors.

***In vivo* Clearance and Biodistribution of PEG Coated Gold Particles**

Experimental work performed in chapters three and four established the stability of the PEG coating on gold particles as a function of the suspension environment and the protein adsorption characteristics of those particles. The previous work focused only on the *in vitro* properties of these particles, which were not complicated by the various interacting systems in the body. In this section, those interactions will be explored to identify any relationships between the *in vitro* particle properties and *in vivo* clearance of the gold nanomaterials. Two major factors affecting clearance were singled out for analysis: aggregation of the particles *in vivo* and protein binding.

Larger particles such as aggregates of the primary gold particles can be removed from clearance in a size dependent manner²⁹⁵. Aggregation may also imply a loss of or change in the coating chemistry, since steric repulsion is capable of maintaining dispersion over a vast range of conditions. Previous *in vitro* experiments and theory indicate that this type of aggregation is less likely to occur, even on coating loss. The presence of high concentrations of protein, namely albumin, offers a ready supply of stabilizing adsorbates in the event of coating loss. Reference serum albumin levels and total protein levels are 3.4-5.4 g/dL²⁸⁶ and 6.0-8.3 g/dL¹⁸⁴ respectively in healthy

individuals. Experiments performed previously (Figure 4-6 and Figure 4-8) show that uncoated gold particles at the typical solids loading used can be effectively stabilized at concentrations of protein that are thousands of times lower than these serum protein levels. It is therefore unlikely that aggregation of the coated particles in the bloodstream would occur, provided that strong protein mediated adhesive interactions do not occur between particles (Examples of this adhesion is shown previously in Figure 4-9, Figure 3-28). This lack of aggregation was observed under simulated *in vivo* conditions previously (Figure 4-28) over a period of time well beyond where the particles begin to adsorb serum proteins.

The second major factor, protein binding, was also addressed *in vitro*. The time dependent change in protein binding was characterized and found to be dependent on a variety of factors. The protein binding clearly followed the rapid loss of PEG coating density after 1-2h of incubation (Reagent 1). It is important to note that binding of serum proteins to particles does not necessarily guarantee that a particle will be cleared via the RES; however it does indicate that a higher probability of opsonization exists.

The behavior of these particles *in vivo* was examined using a mouse model at time points up to 48h. Aggregation during circulation, accumulation of the particles in the liver and spleen, and the quantity of particles circulating in the bloodstream were examined in this experiment. PEG coated (Reagent 1) gold particles and uncoated gold particles with a nominal size of 40nm were administered to ICR outbred mice in a 100uL dose via tail vein injection at a concentration of 10mg/mL (as gold). To enable IV injection, the animals were restrained by enclosing them in a ventilated polycarbonate frame allowing only the tail to be exposed. The tail was immersed in warm water (<40°C) until the tail

veins appeared dilated. Using a 1ml syringe with a 26 gauge, 5/8" needle attached, the gold suspension was injected into the tail vein as a single bolus. Pressure was applied to the wound for 60 seconds to occlude any bleeding before the mouse was returned to its cage. Mice were allowed normal food and water during the period from dose to tissue harvest. Mice were euthanized by CO₂ inhalation and samples collected at the following time points: 5, 15, 60, 240, 480min, 24h, 48h. Analyses were performed in triplicate for each time point. Blood samples were collected immediately by cardiac puncture with a heparin rinsed syringe for analysis by differential sedimentation as described previously. Aliquots of the blood were retained for analysis of gold content by ICP-MS at a later time. Samples of the liver and spleen were taken for histology and analysis of gold content by ICP-MS at a later time. Tissue samples for histology were immediately placed in a fixative solution upon collection (4% Paraformaldehyde with 2% Glutaraldehyde in Sodium Cacodylate buffer at pH 7.24). The tissue and blood samples were digested with aqua regia for 24h and subsequently filtered and diluted for analysis. Tissue samples were provided to Kerry Siebein for sectioning and imaging by TEM and optical microscopy according to the following procedure: The samples were dissected into cubes of approximately 1.5mm, and washed in sodium cacodylate buffer. Samples for optical imaging were dehydrated in graded water/ethanol solutions (70%/30%, 50%/50%, 30%/70%, 10%/90%, and two times 100% ethanol) and cleared by soaking in xylene. The samples were then vacuum infiltrated with paraffin four times, sectioned, stained with Haematoxylin and Eosin (H&E), and mounted on glass slides. Tissue samples for TEM imaging were fixed a second time in Trumps Solution followed by two washing stages in sodium cacodylate buffer for 45 seconds in the microwave at 180

watts. The cells were post fixed in 2% Osmic Acid in 0.1 M Phosphate Buffer for one minute at room temperature, 45 seconds in the microwave under vacuum, and 3 minutes at room temperature. The osmic acid was drained and the samples were rinsed two times with Phosphate Buffer for 45 seconds in the microwave at 180 watts. The tissues were dehydrated in graded water/ethanol solutions (70%/30%, 50%/50%, 30%/70%, 10%/90%, and two times 100% ethanol). Each step was 45 seconds in the microwave at 180 watts followed by 1 min at room temperature. The tissue was vacuum infiltrated in graded Ethanol/Spurrs Resin mixtures (70%/30%, 50%/50%, 70%/30%, and 100%) in the microwave at 250 watts for 3 minutes. The samples remained at room temperature for 24 hours followed by a second infiltration with 100% Spurr's Resin for 48 hours at room temperature. The samples were placed in silicone molds, filled with Spurr's Resin, and cured at 68 F for 48 hours. The tissue blocks were trimmed then sectioned using an ultramicrotome. Thick 500nm sections were cut for optical microscopy and thin 70-100 nm sections were cut for TEM.

The time dependent concentration of gold particles in the bloodstream and body tissues is shown in Figure 5-3 for both coated and uncoated particles. After the PEG coated particles were administered, the concentration of gold in the bloodstream remained relatively constant until after the 2h time point, when the concentration began to decrease. As the concentration in the blood decreased, the tissue concentrations began to increase, indicating that the particles were being cleared by the RES system after 2h. In contrast to the behavior observed with the PEG coated particles, the uncoated particles were immediately cleared, with the majority of the particles recovered in the liver within 5min of dosing. The tissue and blood concentrations

remained constant throughout the remainder of the 48h exposure. Analysis of blood samples obtained at each time point by differential sedimentation showed no direct evidence of aggregation during the exposure (peaks corresponding to larger aggregate particles were not detected at any point). Comparison of the primary particle peak intensity (from differential sedimentation) to the total gold concentration in the blood (Figure 5-3) for mice dosed with PEG coated gold showed good agreement at early time points. At times greater than or equal to 2h, a difference was observed in the sedimentation data and ICP data. The sedimentation data began to decline at a higher rate than the ICP data (illustrated in Figure 5-4). There are several possibilities for this difference, neglecting sampling and instrument related issues:

- Aggregation (with aggregates remaining in circulation). Aggregation would cause a decrease in the primary particle peak intensity in sedimentation without changing the concentration of gold in the blood (as determined by ICP-MS).
- Adhesion to or internalization of particles in cellular components in the blood. Adhesion would cause the particles to sediment with the attached cellular components at a different rate from the primary particles. This is less likely to occur since the blood was lysed prior to analysis.
- Protein binding. Protein binding alters the sedimentation velocity of the particles (Figure 2-10) in a manner dependent on the quantity and type of protein adsorbed. Though this would not cause a dramatic difference in the sedimentation velocity as in the previous cases, it would cause some of the particles to sediment at varying rates lower than the fully PEG coated particles. This in turn would cause the peak to broaden and decrease in height with part of the signal lost to background.

Sedimentation data from mice dosed with uncoated particles did not yield any detectable primary particles or aggregate particles at the earliest time points. To provide the best possibility of detection, an additional time point (not shown) at approximately 1min was added. This time point would allow the blood volume in the mouse to be circulated approximately one time before a blood sample was obtained. Even at this

time point, no primary particles or aggregate particles were detected. Combined with the ICP data, which showed that the vast majority of the recovered dose was in the liver, this indicated that uncoated gold particles are cleared almost immediately after dosing.

Images of the liver tissue sections at various time points followed the trends observed by ICP and differential sedimentation. Optical images of tissues from animals dosed with uncoated gold particles at short time points showed large numbers of optically dense features located throughout the tissues (Figure 5-5). This remained constant throughout the exposure. Transmission electron micrographs of liver tissue sections showed that the dark features were large clusters of the parent gold particles located throughout the Kupffer cells (Figure 5-6). In contrast to this behavior, the optical micrographs of liver sections from animals exposed to PEG coated gold particles did not contain any of the aforementioned dark features (Figure 5-7A) at the early time points. Transmission electron micrographs of these sections at early time points revealed small numbers of individual particles or occasionally small clusters of a few particles (Figure 5-8A). Optical micrographs of the liver tissues at later time points showed the presence of dark clusters of particles dispersed throughout the tissue as observed in the uncoated particles at early time points (Figure 5-7B). Transmission electron micrographs showed large concentrations of the parent gold particles within the Kupffer cells (Figure 5-8B).

The clearance behavior of these particles is consistent with the onset of protein adsorption observed *in vitro*. Measurement of the concentration of gold in the blood and the primary particle peak intensity indicated that the onset of clearance occurred after approximately 2h of exposure (Figure 5-3), and the onset of protein adsorption was found to occur at a similar time point (Figure 4-18, Figure 4-19, Figure 4-20).

Microscopic investigation confirmed these results, with little accumulation of particles in the liver tissue samples at early time points while later time points contained large numbers of particles accumulated in the Kupffer cells.

Chapter Summary

Administration of native (uncoated) nom. 40nm gold particles to mice showed that clearance occurred extremely rapidly (Figure 5-1). No significant quantities of gold were detected in the bloodstream within 5min by ICP-MS, and no primary particles were detected within 1min by sedimentation. Sedimentation data from mice dosed with uncoated particles showed neither the presence of primary particles nor the presence of aggregate particles at any time during the exposure, suggesting that the particles either aggregated beyond the analysis range of the instrument or were cleared from the blood stream. ICP-MS data confirmed that the latter outcome was the case. Optical micrographs of liver histology sections from mice exposed to uncoated particles showed large numbers particles accumulated in the Kupffer cells within 5min (Figure 5-7A), a fact which did not change over the 48h exposure (Figure 5-7B). Transmission electron microscopy was used to identify the particles (Figure 5-9) and showed that they existed in the Kupffer cells as large clusters of primary gold particles (Figure 5-6). The behavior of PEG coated (Reagent 1) nom. 40nm particles was significantly different, demonstrating enhanced stability *in vivo*. The concentration of particles in the bloodstream remained relatively constant for approximately the first 2h of exposure before beginning to decline (Figure 5-3, Figure 5-2). The PEG coated (Reagent 1) primary particles were identified by sedimentation *in vivo*; however no aggregates were observed at any time during the exposure. ICP-MS analysis of liver and spleen tissue concentrations showed that gold levels in the liver remained relatively constant until the

coated (Reagent 1) particles began to clear, at which time the concentration of gold in the liver tissue began to increase (Figure 5-2). Unlike the uncoated particles, optical micrographs of the liver tissue samples from mice dosed with PEG coated (Reagent 1) particles did not exhibit any concentrations of gold particles at early time points (Figure 5-5A). Concentrations were observed in the Kupffer cells at longer time points (Figure 5-5B), consistent with the ICP-MS data. Transmission electron micrographs of liver sections from mice dosed with PEG coated gold particles (Reagent 1) at early time points showed only small numbers of isolated particles, in contrast to the large number of large clusters observed in the uncoated particles (Figure 5-8A). Later time points showed concentrations of gold particles accumulated in the Kupffer cells (Figure 5-8B).

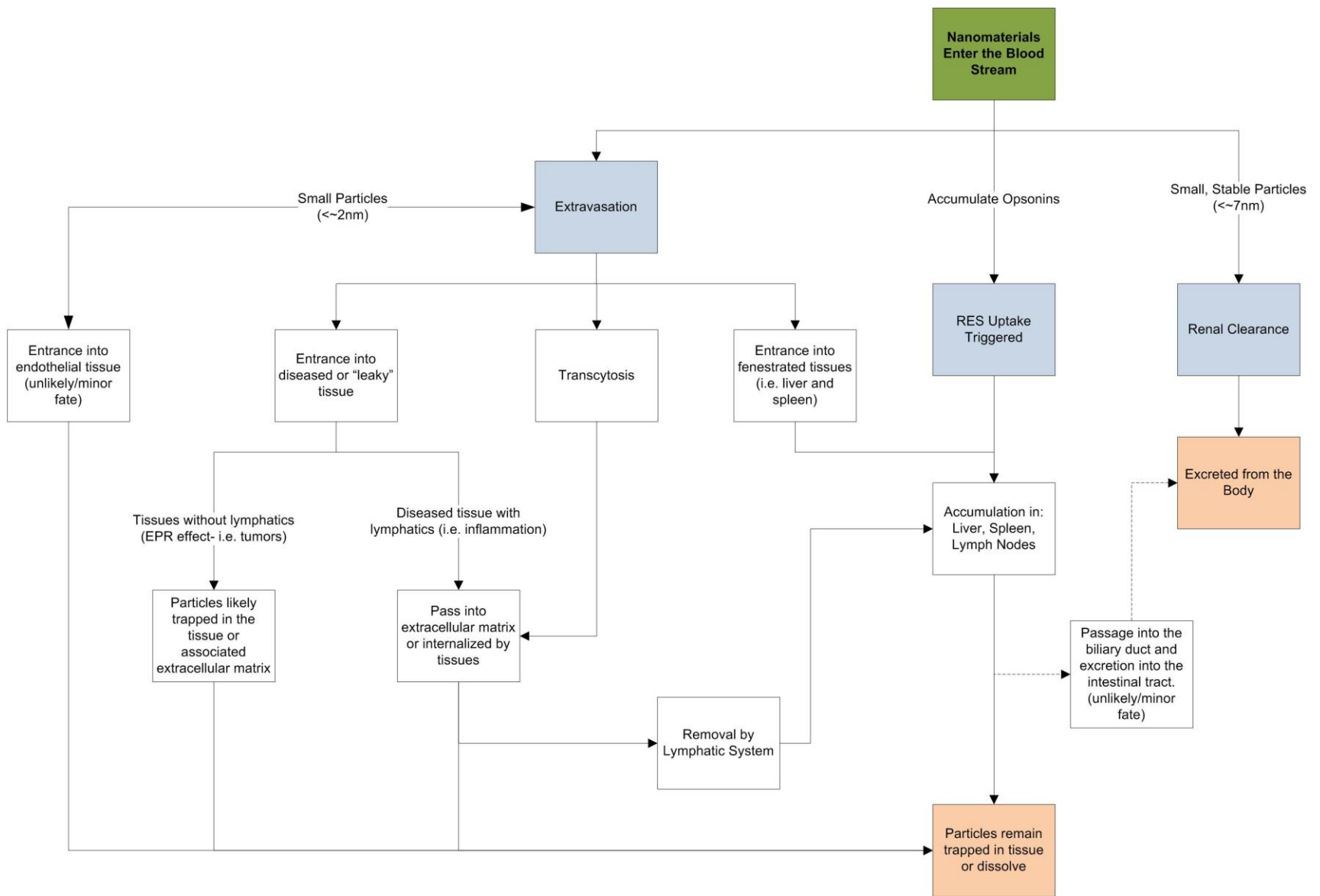


Figure 5-1. Clearance pathways for particles in the bloodstream.

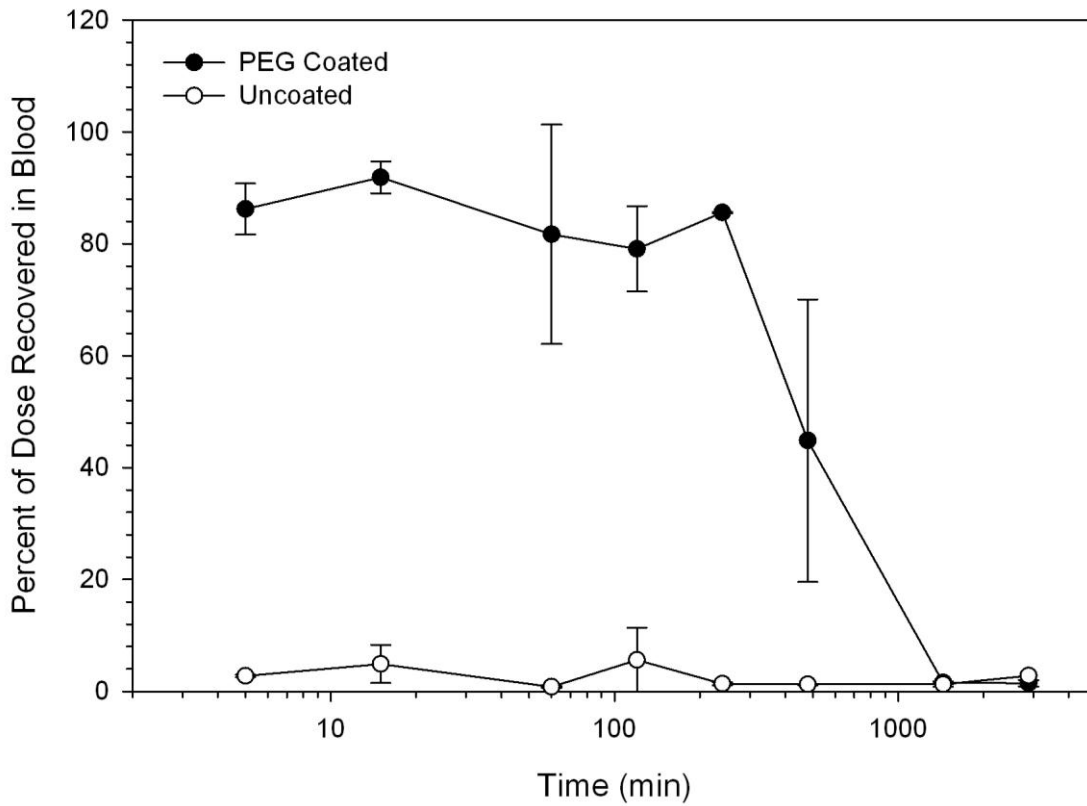
Table 5-1. Literature reported clearance characteristics of gold particles *in vivo*.

Reference	Particle Size and Type	Approximate Half Life	Comments
Goel et al. (2009) ²⁷⁸	33nm spherical, 5kDa PEG coated	2.2h	Mice
Kawano et al. (2006) ²⁷⁹⁻²⁸¹	47nm spherical, 5kDa PEG coated.	2h	Mice
Cho et al. (2009) ²⁸²	13nm spherical, 5kDa PEG coated.	30-33h	Mice
Cho et al. (2010) ²⁸³	4nm 13nm 100nm Spherical with PEG coating	12h 74h 49h	Mice
Dutta (2009) ²⁸⁴	15nm spherical, 5kDa PEG coated	9h	Rats
Zhang et al. (2009) ²⁸⁵	80nm 40nm 20nm Spherical with 5kDa PEG coating	16h 10h 23h	Mice. Thiocctic acid terminal group on PEG.
Wang et al. (2004) ²⁸⁶	125nm gold nanoshell, 5kDa PEG coated	3.7h	Mice
Xie et al. (2007) ¹⁰⁷	125nm gold nanoshell, 5kDa PEG coated	4.2h	Mice
James et al. (2007) ²⁸⁷	120nm gold nanoshell, PEG coated	3.7h	Mice
Michalak et al. (2009) ²⁸⁸	Gold nanoshell (coating unspecified)	7-8min and 43-77min	Mice
Michalak et al. (2010) ²⁸⁹	160-170nm Gold nanoshell, PEG coated	5.3h	Mice
Michalak et al. (2010) ²⁹⁰	Gold nanoshell (coating unspecified)	3-43min	Mice
Niidome et al. (2006, 2008) ²⁹¹	65x11nm gold nanorod, 5kDa PEG coated.	<1h	Mice
Lankveld, et al. (2011) ²⁹²	55.3x18.5nm gold nanorod, 5kDa PEG coated.	19h	Rats
Von Maltzahn et al. (2009) ^{293, 294}	47x13nm gold nanorod, 5kDa PEG coated.	17h	Mice
Lankveld, et al. (2011) ²⁹⁵	55.3x18.5nm gold nanorod, uncoated (CTAB surface).	<15min	Rats
Dutta (2009) ¹⁵	15nm uncoated gold particles	<5min	Rats

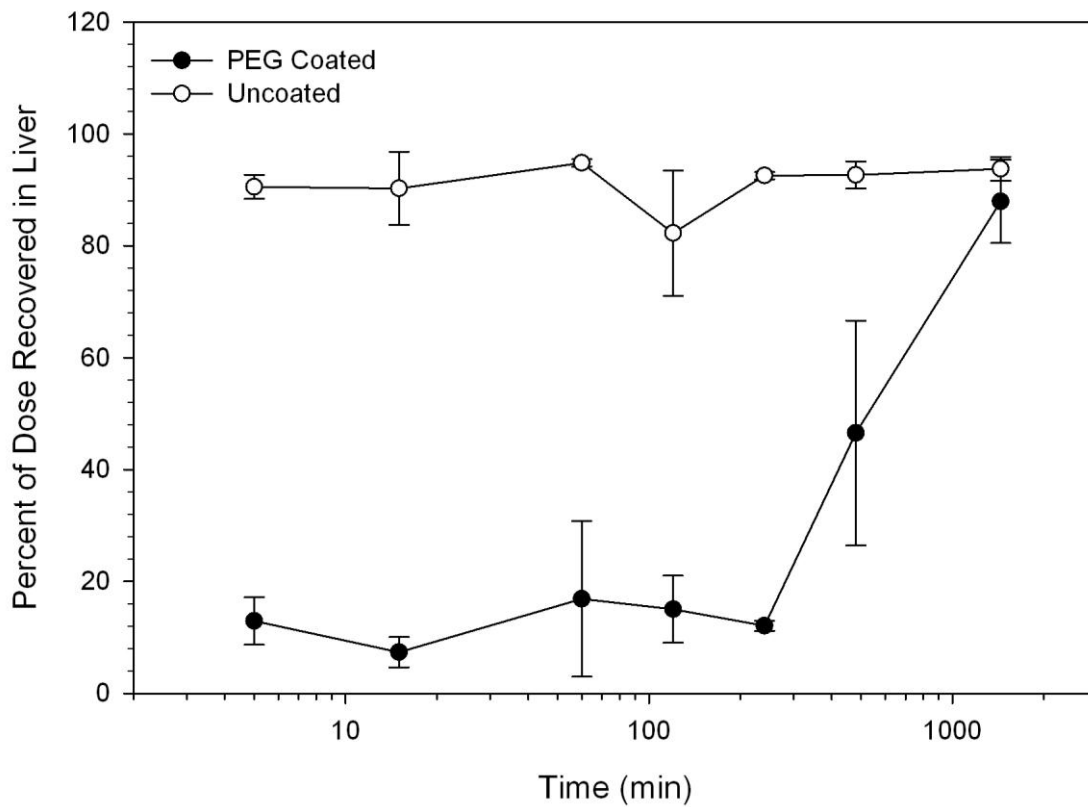
Table 5-2. Summary of particles tested *in vivo*.

Particle stability under physiological conditions	Protein binding particles	Protein resistant particles
Stable	Serum Protein Coated	Polyethylene Glycol Coated
Unstable	Uncoated/Native Particles	N/A

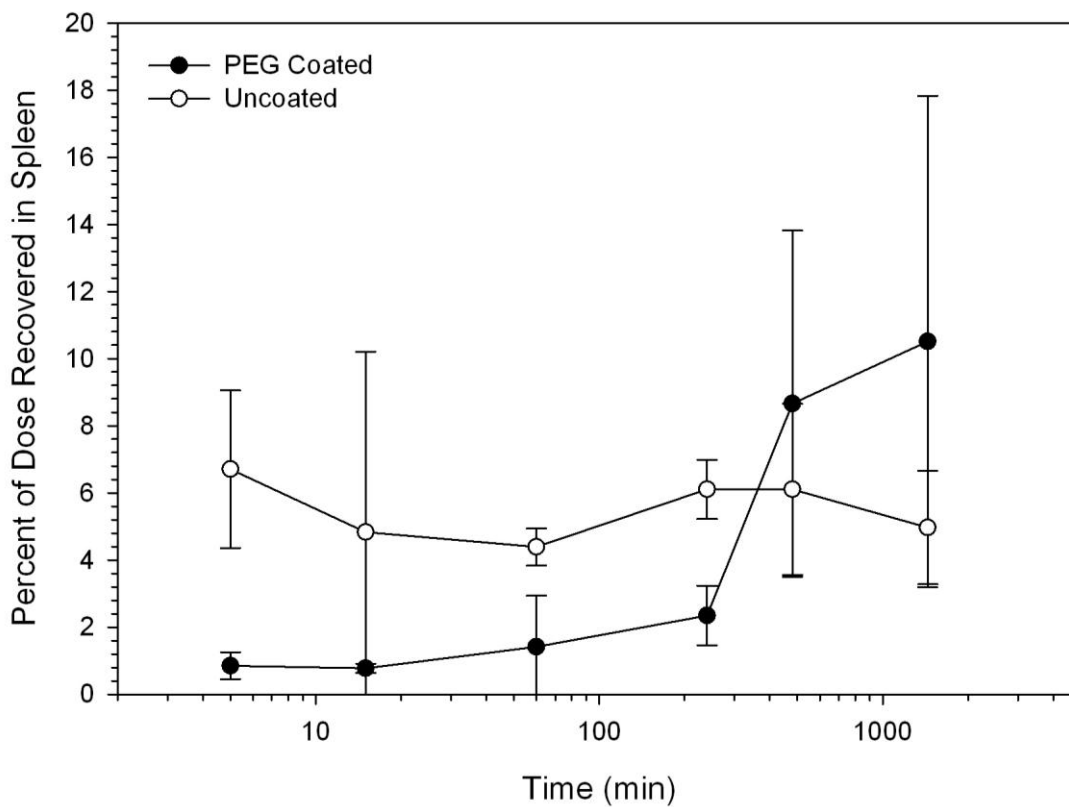
Figure 5-2. Percent of dose recovered in the blood and body tissues. A) Blood. B) Liver. C) Spleen. Gold content was determined by ICP-MS. Note that the concentration of PEG coated particles in the blood began to decrease as the concentrations in the liver and spleen began to increase after the 2h time point. The uncoated particles showed nearly constant levels of gold in all tissue and blood samples.



A



B



C

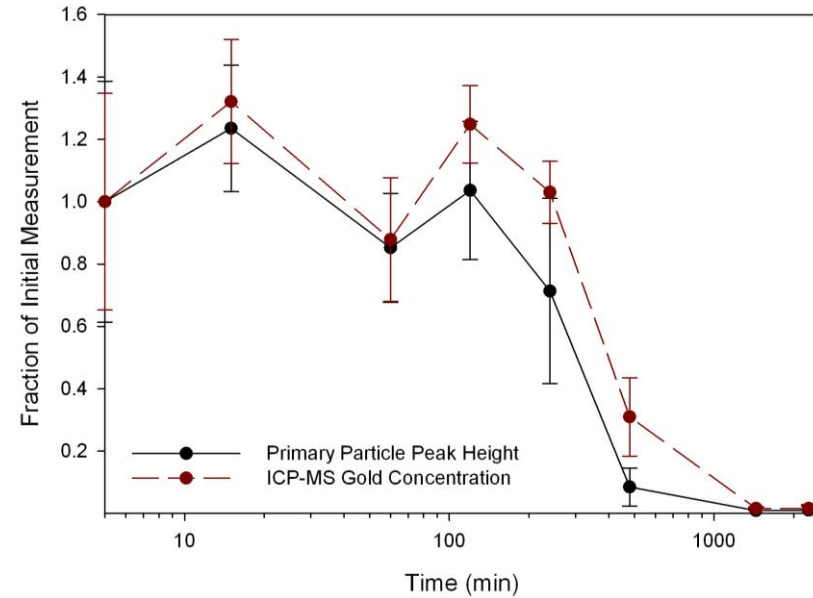


Figure 5-3. Gold concentration and primary particle peak intensity in blood as a function of time. Note that at the earliest time points, the values closely match; however at time points of 2h and greater, the primary particle peak intensity decreases at a faster rate than the total gold content by ICP. Due to a higher than anticipated demand for particles, a second batch of particles was used for the 5min and 1h time points, resulting in a lower concentration of gold at those points.

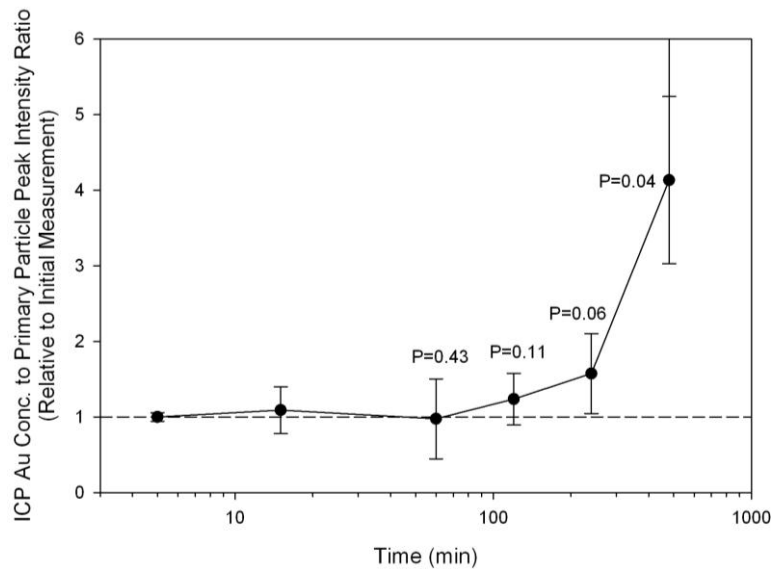


Figure 5-4. Ratio of gold concentration in blood by ICP-MS to primary particle peak intensity. P values shown are the probability that the relative gold concentration in the blood and primary particle peak intensity do not statistically differ. Note that the values begin to differ from 1 at the 2h time point.

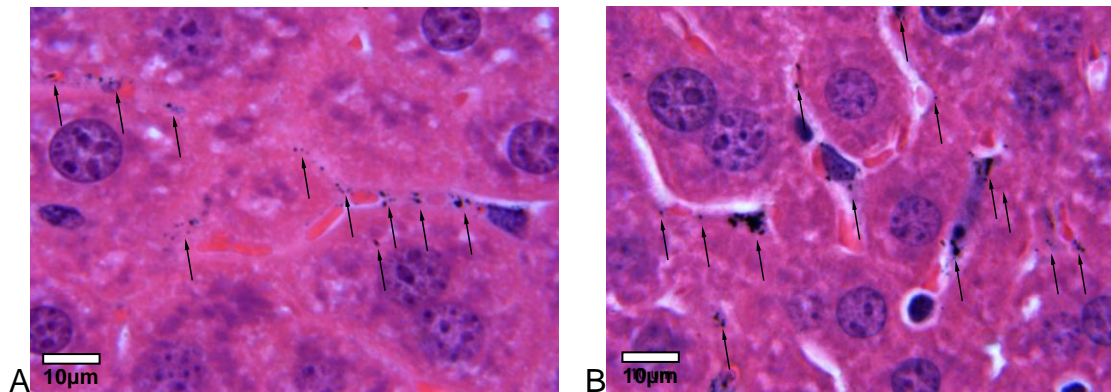


Figure 5-5. Histology sections of liver tissue from mice after dosing with uncoated gold particles. A) 5min and B) 24h after dosing. Gold particles (appearing as optically dense features) are marked with arrows. Samples imaged by Kerry Siebein.

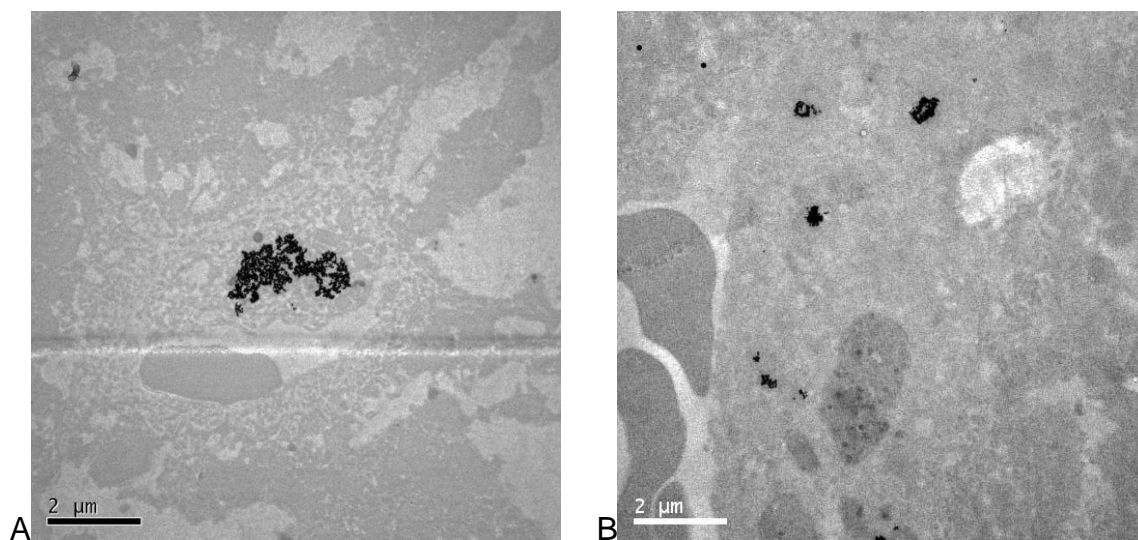


Figure 5-6. Transmission electron micrographs of clusters of gold particles in liver tissue after administration of uncoated particles. A) After 15min and B) after 24h. Samples imaged by Kerry Siebein.

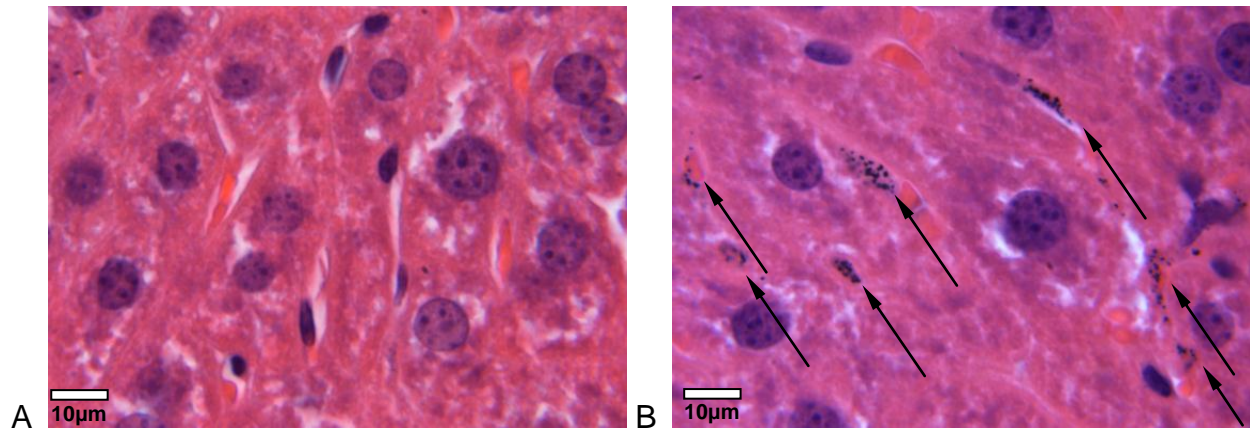


Figure 5-7. Histology sections of liver tissues from mice dosed with PEG coated (Reagent 1) gold particles. A) 2h after dosing. B) 24h after dosing. Gold particles (appearing as optically dense features) are marked with arrows. Note that these collections of gold particles are not observed at the 2h time point, but are present at later time points. Samples imaged by Kerry Siebein.

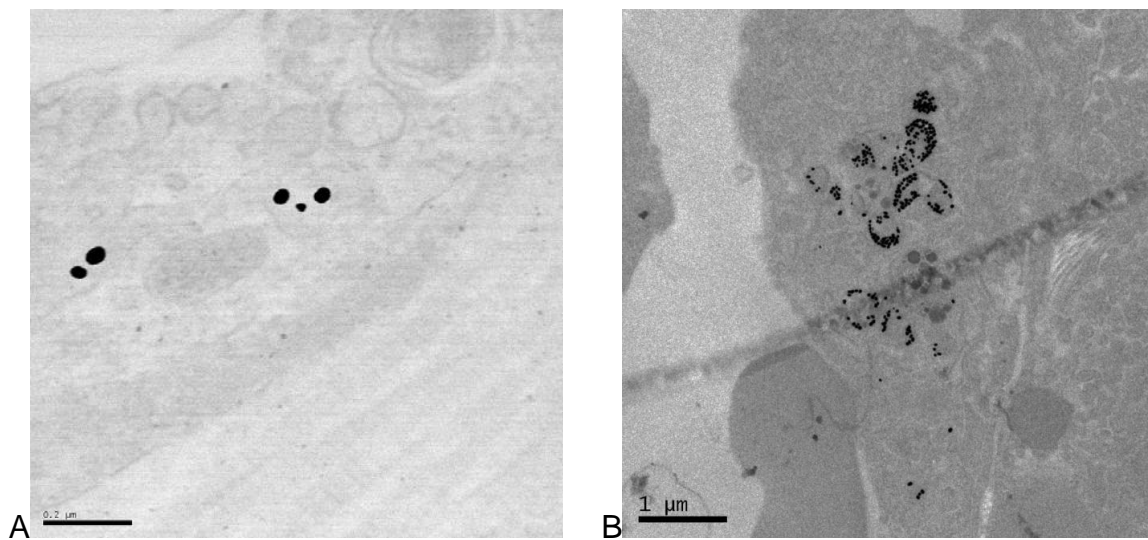


Figure 5-8. Transmission electron micrographs of liver tissues after administration of uncoated particles. A) After 15min and B) after 24h. Individual particles can be seen at early time points, while large clusters and concentrations can be seen at later time points. Samples imaged by Kerry Siebein.

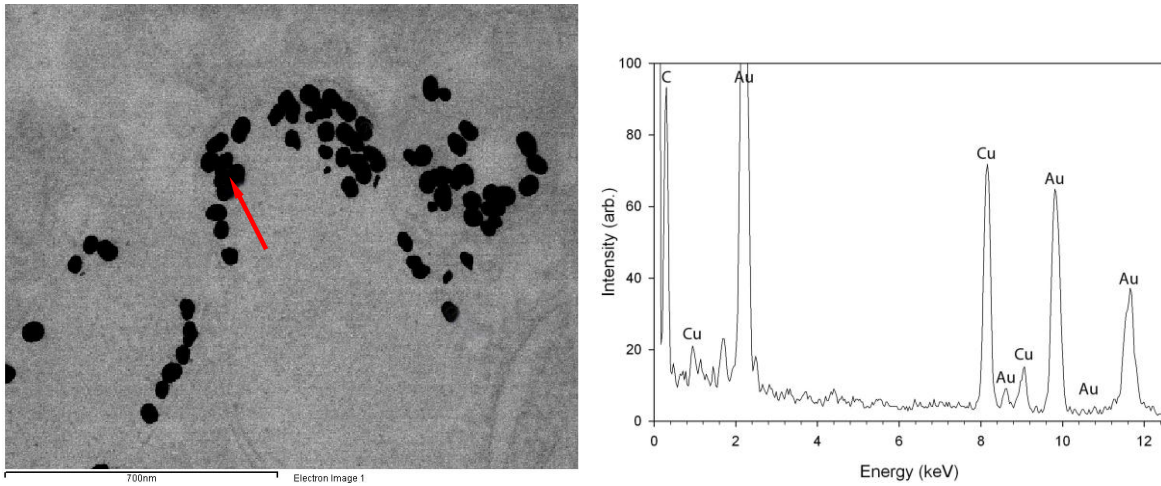


Figure 5-9. EDS analysis of dark features observed in tissue sections to confirm composition. The EDS spectrum of the location indicated by the red arrow is shown on the right. The particles were both morphologically and compositionally consistent with the dosed particles. The presence of copper in the sample was from the grid. Analysis performed by Kerry Siebein.

CHAPTER 6 SUMMARY AND CONCLUSIONS

In this work, the formation, properties, and stability of PEG coated gold particles were traced from the formation of the coating, through *in vitro* stability experiments, and finally *in vivo*. The properties, mechanisms and timing of degradation, and *in vivo* stability of PEG coated particles are largely unknown. In many cases, this lack of information is related to the complexity of measurements associated with each of these topics. Measurement techniques were first developed or adapted for efficient characterization of the selected particles and their coatings. Some of the major interactions governing stability and degradation of the PEG coating and accumulation of proteins were then studied *in vitro*. In the final stage of this work, the behavior of the selected particles was investigated *in vivo*.

The first issue addressed was characterization of the particles and coating. Determination of the coating condition at a given time is typically difficult and/or requires excessive quantities of suspension to perform accurate measurements. Interferences from a variety of sources and inadequate measurement techniques can result in measurement errors, some of which were illustrated previously. This has contributed to the widely varying values given for coating density shown previously. Examples of interferences with colorimetric assays and gravimetric methods were demonstrated. Gravimetric analysis of the coating thickness is a popular method of measuring the coating density; however analysis of particles produced using methods which involve strongly adsorbing species (e.g. quaternary ammonium phase transfer catalysts) to the gold surface during synthesis are a potential source of error. Coincidentally, all referenced measurements which involved particles produced using phase transfer

catalysts showed relatively high adsorbate densities. Accurate measurements of the initial coating density are a strong indicator of the quality of the reagent and coating. A comparison between two theoretically identical commercial PEG reagents on the same core particles showed that one reagent (which was later identified to be less active) produced a coating with significantly lower adsorbate density even when an excess of reagent was supplied initially. A variety of indirect techniques are employed to estimate the density of the PEG coating, such as prevention of salt induced aggregation and the minimization of zeta potential. Analysis of these methods indicated that neither is an effective means of quantifying or estimating the PEG coating density since salt induced aggregation and zeta potential (as measured by DLS) are all neutralized well before the point of surface saturation. Measurements in this work were performed with several direct and indirect methods. The direct measurements of the coating density by gravimetric analysis and colorimetry produced coating thicknesses of $1 \text{ molecule/nm}^2 \pm 0.2$ with most measurements observed between 1 and $1.2 \text{ molecules/nm}^2$. With proper preparation and attention paid to potential sources of interference, the two techniques used produced nearly identical surface densities. Error in the estimated specific surface area was found to be a contributor to some of the variance observed in the measured surface densities in this work and likely also in literature. Unfortunately, due limits of expense and practicality, measurements of specific surface area by traditional means such as gas sorption are not feasible. Particularly for smaller particles, differences in shape and size can be magnified significantly when the specific surface area is calculated. The particles synthesized by the citrate method (including those used in this work) are often anisotropic or faceted. Factors such as anisotropy, faceting and other

surface features, and variation in particle size can cause the surface area estimated by ensemble particle size analysis (assuming uniform spheres) to vary. More accurate finite element based image analysis measurements were performed utilizing truncated conical sections, though these measurements still can not fully account for the 3-dimensionality of the particles. Three dimensional data is not gathered by direct TEM imaging, necessitating the assumption of a symmetric (circular) cross sectional area. Image analysis using methods to account for some of the particle anisotropy showed that errors of up to 20% (compared to assumed spherical geometry) were possible due to particle shape and size distribution. The techniques for estimating specific surface area demonstrated in this work were able to account for the major component of the particles anisotropy.

Several qualitative methods of evaluating coating condition were utilized throughout this work where comparative results were required or experimental conditions prohibited direct measurements. The two techniques used for this purpose were differential sedimentation and electrophoresis. Differential sedimentation analyzed the differences in sedimentation velocity of a coated particle relative to the core particle. Coating causes both a decrease in the net particle density as well as an increase in the particle diameter. These factors cause the particle sedimentation velocity to decrease and increase respectively, the balance of which determine the final sedimentation velocity. Measurements of the relative sedimentation velocity can be used to calculate the coating thickness if the coating density is known or assumed. The calculated coating thickness increases exponentially with the quantity of PEG-thiol added until a maximum value is obtained. Qualitatively, the sedimentation velocity can be used to evaluate the

coating condition by comparison to this curve. Coating thicknesses calculated based on this technique ranged from 6nm to 10nm with most values between 6-8nm. These values were dependent on (among other factors) reagent source. Coating thickness measured with this technique was slightly lower than those measured by dynamic light at approximately 10nm. Electrophoresis provides information similar to sedimentation, though through a different mechanism. In electrophoresis, as the coating density increases, the particle surface charge is masked by extending the shear plane farther from the particle surface. This causes an exponential decrease in the cathodal mobility of the particles until a minimum value is reached. Electrophoresis provides complementary information to sedimentation on the adsorption of charged molecules to the particle surface, a fact which is useful for analysis of protein binding. An additional benefit to electrophoresis is that the quantity of sample required is extremely small.

The aforementioned techniques were used to analyze the time and condition dependent particle and PEG coating stability. Initial experiments identified two major sources of coating degradation: oxidation and competing adsorbates. Treatment of coated particles with oxidizers such as peroxide and Fe (III) resulted in rapid coating degradation and particle aggregation. Reaction with peroxide resulted in virtually instantaneous oxidation and desorption of the coating. Treatment of the particles with competing adsorbates, such as small molecular weight thiols, also resulted in destabilization of the suspension over the course of several hours (depending on concentration). Reducing agents either enhanced stability or promoted coating degradation depending on strength. Strong reducing agents, such as borohydride,

increased the rate of coating degradation significantly while weaker reducing agents such as ascorbic acid had the opposite result.

The presence of dissolved oxygen in particular was found to be a major contributor to the rate of coating degradation. Since oxygen is an omnipresent source of oxidation, it is often overlooked as a potential problem. Various reports lauding the stability of thiol based monolayer coatings under ambient conditions or indicating that oxygen alone is incapable of desorbing the coatings add to the confusion. Under standard preparation procedures, the time required to remove the vast majority of the PEG coating was three to four days at 37C. Analysis of the coating at shorter time scales showed that coating degradation does not occur at a constant rate. Several hours after the start of the incubation at 37C, a rapid initial loss of coating is sometimes observed. When the medium containing the particles was degassed, degradation occurred at approximately half of the rate of the particles in water containing dissolved oxygen. This rate of degradation was highly dependent on temperature and the availability of oxygen (including the effectiveness of the container at sealing out oxygen). Analyses of coating degradation with and without dissolved oxygen at temperatures ranging from 4C to 65C were performed. Degradation of the coating occurred extremely rapidly at elevated temperatures, with the majority of the coating removed in less than 24h at 65C when dissolved oxygen is present. Samples at room temperature degraded at a far slower rate than body temperature, requiring almost 60 days to remove the majority of the coating. Samples kept under refrigeration for over 8 months showed no significant signs of coating degradation even in the presence of dissolved oxygen. This temperature dependence is an important factor to consider, especially if the particles are intended for

use *in vivo*, as the seemingly small change in temperature from room temperature to body temperature can significantly elevate the rate of degradation.

One major and often overlooked confounding factor in the analysis of these particles is the removal of unbound adsorbate left over after coating. Trace quantities of the unbound adsorbate were found to significantly increase the amount of time required for a coated particle to degrade. The loss of thiol activity was quantified in the tested reagents, and was dependent on storage temperature. Rates of thiol activity loss were constant over the temperature range tested. Reagents stored at 65C, 37C, and 4C lost approximately 4.6%, 0.86%, and $\leq 0.38\%$ per day respectively of their thiol activity at a 0.1mM starting concentration. In this work, removal of unbound adsorbate was performed using multiple centrifugal diafiltration stages. This process allowed for very efficient purification without large losses of particles.

The quality and purity of the commercially produced PEG reagents were critical factors in the formation and stability of the coating. Two different commercial reagents were tested in the course of this work, and each exhibited significantly different properties. Analysis of the quantity and type of sulfur in the reagents indicated that the thiol content of one reagent (referred to as Reagent 1) was significantly lower than the second (referred to as Reagent 2). A higher than stoichiometric ratio of sulfur was found when the total sulfur content of each reagent was analyzed, particularly in Reagent 2 which contained 6-9% higher levels of sulfur than anticipated. When this data was compared to the concentration of reduced thiols in the reagent, a large mismatch was observed, indicating that not all sulfur was present as an active thiol. The concentration of sulfur (as thiol) in all reagents was significantly lower than the theoretical quantity. As

predicted by the aforementioned results, Reagent 2 saturated the surface of gold particles at a significantly lower initial concentration than Reagent 1. Reagent 2 also produced a less dense coating (as determined by TGA), though it is unknown whether or not degradation occurred during the sample preparation period. Analysis of the near ultraviolet absorption spectra of the PEG compounds yielded an unexpected peak at 235nm. This peak did not correspond with any structural element of the specified compound. When the ultraviolet absorption spectra of the reagent before and after adsorption onto gold surfaces were obtained, the peak at 235nm was no longer present. Combined with previous data on the sulfur content and other observations, the possibility existed that these phenomena could be caused by the presence of an impurity in the reagents. Dialysis and chromatographic separations were able to isolate the impurity from the reagent, and the UV absorption spectrum was compared with compounds which would likely be used to thiolate the PEG during synthesis. The unknown impurity precisely matched the spectrum for thiourea. The identity of this impurity was subsequently confirmed by HPLC. Deconvolution of the absorption spectra and comparison to a standard curve yielded an approximate concentration of 2100ppm thiourea in the tested reagent (Reagent 2). The presence of this impurity was not an isolated instance, and was found in different lots from of both Reagent 1 and Reagent 2. The presence and behavior of this compound has several far reaching effects on the behavior and stability of the particles. Thiourea has the ability to adsorb to gold particles and compete with the thiolated PEG for surface area, can dissolve gold via the formation of a gold (I)-thiourea complex, and has the ability to take part in oxidation processes. Analysis of particles coated with purified PEG and as received PEG showed

that the purified reagent was able to form a denser coating, as measured by several techniques. The likely cause of this behavior is the initial competition between the thiolated PEG and thiourea. This was verified as the cause by reintroducing thiourea to the cleaned reagent and analyzing the resultant coating. This reintroduction of thiourea in the initial coating solution caused the coating density to decrease once again.

Analysis of the rates of degradation upon purification yielded unexpected results. The particles coated using the purified reagent degraded at a much faster rate than the as-received reagent. Addition of small quantities of thiourea to particles coated with purified PEG caused a decrease in the rate of degradation, confirming that thiourea was the cause of this behavior. The particles coated with purified and unpurified PEG were also exposed to oxidizers (peroxide and Iron (III)) and competitive adsorbates (mercaptoethanol and thiourea), which showed qualitatively that the particles coated with the purified reagent were more susceptible to these sources of degradation.

Two other factors which influenced particle stability were examined in addition to those previously described: pH of the particle medium and salt content. Initial experiments showed that the presence of salts or other solutes in the coated particles considerably decreased the rate of degradation. Partitioning of coated particles at the gas-liquid and liquid-container interface was also observed at higher salt concentrations. The potential interactions driving these behaviors involve salting-out of the polymer coating and possibly a small percentage of the dissolved oxygen. Salting out of the polymer could create a more cohesive interfacial layer while the decrease in oxygen solubility would decrease the availability of oxygen to the particles. Various solutes were tested for their impact on the suspensions. Though no direct correlations

between literature reported cloud point measurements for PEG and particle stability could be drawn, certain extreme cases involving uncharged molecules and salts that are less effective at salting out PEG were consistent with this possibility. Although the primary application of these gold particles involves parenteral administration, the pH in other compartments of the body can vary. For this reason, the coating stability as a function of pH was also investigated. The results showed that the highest level of degradation occurred in acidic environments with peak stability occurring at a pH of 6. This pH appeared to be somewhat of a 'pivot point' where degradation below a pH of 6 occurred at a rapid rate while degradation at higher pH values occurred slowly. Control of the pH was maintained using non complexing buffer systems since systems containing complexing species (such as chloride) may interact with the particle surface. This experiment was repeated for particles coated with purified PEG to determine whether or not the presence of thiourea was a contributing factor; however the results for this experiment were similar to the results with the reagent as received, indicating no correlation.

Up to this point, stability and preparation of the coating in deionized water and simple salt and buffer systems were the sole concern. The elimination of protein binding is the second major concern which was addressed, as elimination of opsonization leads to a more effective particle for *in vivo* applications. The interactions of proteins with the core particles were the first concepts explored since these interactions represent the core attraction between serum proteins and the particle surface. BSA was selected as the primary model protein since differential binding experiments identified it as the

protein which bound with highest affinity to the gold particles used in this study relative to its concentration in serum.

The adsorption of protein on uncoated particles was first addressed. Proteins can effectively stabilize gold particles provided that they are mixed with high enough shear and in a high enough concentration. The major mechanisms by which proteins bind to particles include electrostatic interactions, hydrophobic interactions, and chemisorption (ex. via exposed thiols). The adsorption isotherm of BSA onto gold particles showed a relatively high affinity for gold. A region of suspension instability was observed immediately preceding surface saturation. Once the surface was saturated with BSA, the particles remained indefinitely stable. Some reversibility of adsorption was observed at or near the point of surface saturation. If the equilibrium concentration of BSA was diluted below the point of saturation, the suspension immediately aggregated. With a complete coating of protein, the particles exhibited many of the characteristics of the adsorbed protein. A zeta potential titration of the coated particles demonstrated an isoelectric point of 4.9, which is consistent with literature reported values for BSA. The same measurement was performed on particles coated with human plasma proteins, and showed a similar isoelectric point, though the magnitude of the particle charge was considerably less due to salt content. Analysis of particles coated with lysozyme was consistent with its isoelectric point, though the particles were unstable over the majority of the pH range. To aid in elucidating the mechanism by which albumin bound to gold particles, adsorption measurements were performed at pH values spanning pH 2 to pH 10. The sign and magnitude of the charge on a protein is dependent on solution pH, while the charge on the gold particles is negative across the entire region of stability.

The electrostatic attraction of the particles and proteins would therefore be mediated primarily by the charge on the protein. The results of this experiment reflected this, as the binding of BSA remained at a steady value at low pH before increasing to peak at the isoelectric point and subsequently dropping to undetectable levels at higher pH values. A similar behavior was observed with lysozyme coated particles. The increase in binding near the isoelectric point is not predicted exclusively by electrostatic interactions between the particle surface and protein, and likely involves both hydrophobic interactions and decreased inter-adsorbate electrostatic repulsion. Hydrophobic interactions were observed around the isoelectric point, where coated particles would completely partition out of the aqueous phase and adhere to hydrophobic container walls. This is an important pH region to avoid if protein coated particles are to be used.

The preceding work provided the foundation for the adsorption interactions between the core particles and selected proteins. Once the PEG coating is introduced, these interactions are now mediated by the applied coating and its stability. The ability of BSA to adsorb to PEG coated particles with varying coating densities was examined and showed that protein adsorption begins just before the completion of PEG adsorption, indicating that only a small amount of PEG desorption is required before the onset of protein adsorption. Previous work showed that the PEG coating is sensitive to a variety of factors, such as pH and the presence of salts and other competing adsorbates. Blood plasma contains many of these components which can interact with the PEG coating to either increase or decrease stability. The time dependent protein adsorption was measured using several techniques for both PEG reagents tested. The

results of the time dependent protein binding analysis on particles coated using Reagent 1 paralleled the measured coating degradation. The onset of protein binding was measured at approximately 90min in both BSA and human plasma. Reagent 2 showed a higher degree of protein resistance, with the onset of trace protein adsorption calculated to be approximately 4h and bulk adsorption at much longer times (approximately 1 day). Agreement was achieved between the measurement methods used for these experiments.

Reagent purity was found to interact with the protein binding of the particles. Although measurements of the PEG coating stability showed that the presence of the impurity thiourea slowed the rate of coating degradation, the protein binding was higher in the particles with the impurity present. It was hypothesized that the difference is related to the surface charge of the core particles. Adsorption of the cationic thiourea onto the surface of the gold particles decreases the net surface charge which in turn increases protein affinity for the particle surface. Under physiological conditions, the particles and albumin molecules (as well as most other proteins and biomolecules) are negatively charged. This introduces a repulsive interaction between the surface and proteins (observed in the pH dependent adsorption measurements). Decreasing this repulsion leads to a more favorable surface for protein adsorption. Incubation of particles coated with PEG as received showed a 25% to 45% higher level of protein adsorption than the sample particles coated with purified PEG at three and five days respectively.

The final topic examined *in vitro* was the colloidal stability of the particles under simulated *in vivo* conditions. Coated particles were exposed to whole mouse blood for a

period of up to 3 days at 37C under agitation designed to mimic circulation. Analysis of the particles in blood by differential sedimentation indicated no loss of the peak corresponding to the primary particles as well as no detected aggregate particles. Optical micrographs confirmed that there were no large aggregates present in the blood samples. The high concentration of protein in blood provided a ready supply of stabilizing adsorbates as the PEG coating degraded and desorbed. For contrast, uncoated gold particles were also analyzed. These particles aggregated rapidly, with aggregates exceeding 30um present within minutes of dosing. Differential sedimentation analysis showed no primary particles present even at the earliest time points.

The final stage in relating the behavior of the PEG coating stability and protein adsorption properties to clearance is *in vivo* exposures. Both PEG coated (Reagent 1) and uncoated particles were administered to mice via tail vein injection. Blood, liver, and spleen samples were collected at various time points over the course of a 48h exposure and analyzed by ICP-MS for gold content, sedimentation (in blood) for particle size, and microscopy to identify the particles in tissues. Analysis of samples from mice dosed with uncoated particles showed that the particles were cleared almost immediately from circulation and sequestered in the liver and spleen. The coated particles were far more stable *in vivo*. The concentration of particles remained stable in the bloodstream until approximately 2h, after which the particles began to clear from the bloodstream and appear in the liver and spleen. Analysis of liver tissue sections by microscopy paralleled the behavior observed by ICP and sedimentation. Large clusters of particles were observed in liver tissue sections immediately after uncoated particles were administered

to mice. Few coated particles were observed in the liver at early time points, while large concentrations of particles were observed at later time points. The clearance of the particles paralleled the protein binding and degradation behavior observed in the *in vitro* experiments. This data suggests that for the PEG coated particles tested, clearance is mediated by the breakdown of the coating after approximately 2h, which allows for opsonization of particles and subsequent clearance by the RES.

APPENDIX A ESTIMATION OF PARTICLE SPECIFIC SURFACE AREA BY IMAGE ANALYSIS

As discussed previously, the sphericity and monodispersity of gold particles can cause significant deviation in the specific surface area from actual values when particles are assumed to be spherical and/or monodisperse. The prohibitive expense of direct specific surface area analysis by traditional means (such as gas-sorption methods) is often the driving force to estimate surface area based on ensemble particle size analysis. In order to provide a better estimation of the specific surface area, several different schemes based on image analysis were considered for the analysis of particle specific surface area. The particles produced by the citrate method are anisotropic over a wide size range, decreasing the effectiveness of most ensemble sizing methods and calculations based on the assumption of perfectly spherical particles. Most particles generally exhibit radial symmetry along a major axis; however the surface may exhibit gentle curves which decrease that level of symmetry. SEM imaging of the particles showed that the particle surfaces were relatively smooth and the particle shape ranged from spherical to roughly prolate spheroidal. To account for this anisotropy, several different image analysis models were explored, as outlined in Figure A-1. The capsule and prolate spheroid models use the measured major and minor axes to compute the volume and specific surface area of the particles. These models collapse to spherical when the aspect ratio of the particles approaches 1. The finite element model is the most capable model, as it can handle arbitrary shapes (provided that the particles exhibit radial symmetry about one axis). An algorithm was written to compute the precise axis of highest symmetry about the major axis of the particle from image analysis data. This precise axis of symmetry and 2D image analysis data were then

passed into the finite element algorithm, which is described in Figure A-2, for computation of the specific surface area. The resulting specific surface area values are shown in Table A-1 for all models. It is important to note that although these image analysis methods provide a far more accurate estimation of particle specific surface area, they do not account for all possible complexity of the particle shape. All methods assume symmetry along at least one axis, which may or may not adequately account for the entire complexity of the particle. The specific surface areas computed by the anisotropic models were between 15 and 20% higher than those calculated assuming that the particles were spherical for standard citrate particles. Similarly sized higher sphericity particles were analyzed for comparison, and all specific surface area values produced by both the anisotropic and spherical models were similar.

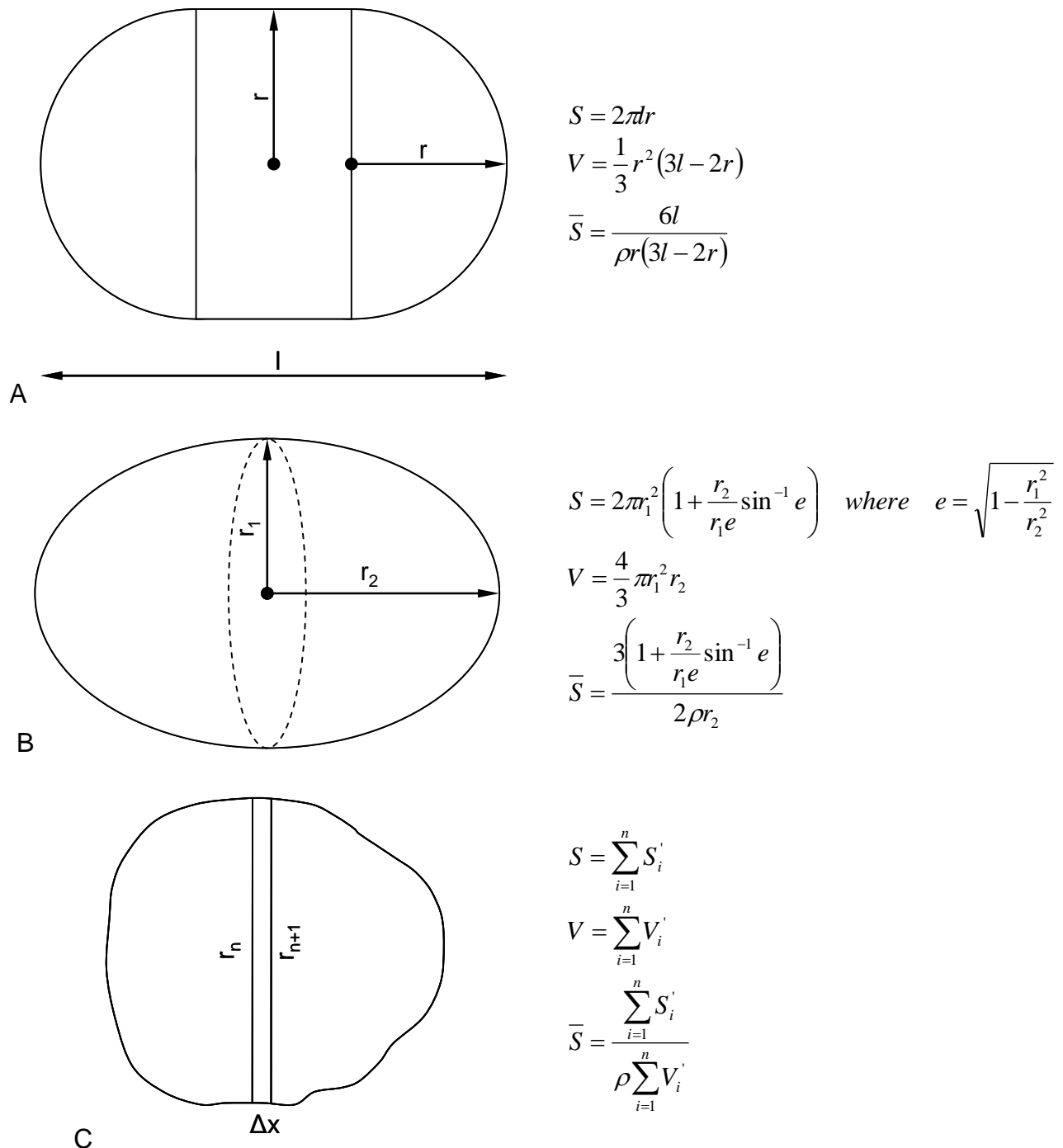
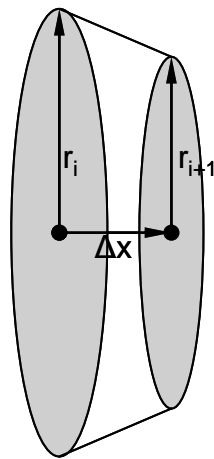
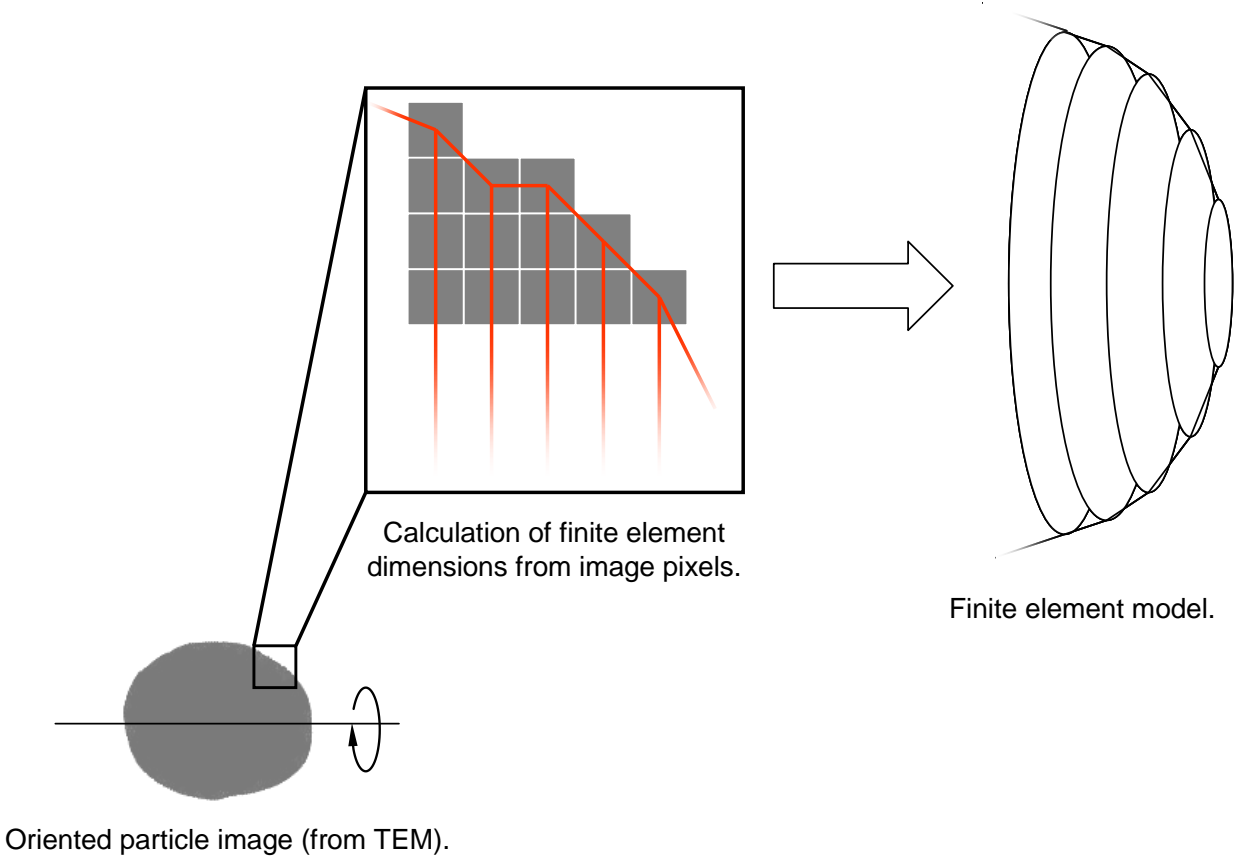


Figure A-1. Image analysis schemes for approximating the specific surface area of certain anisotropic particles. A) Capsule model, B) Prolate spheroid model, C) Finite element model. All models assume radial symmetry about the major axis. S is defined to be the surface area, V is the volume, \bar{S} is the specific surface area, ρ is the particle density, S' and V' are the finite element exterior surface area and volume respectively.



$$S_{ext} = \sum_{i=0}^n \pi(r_i + r_{i+1}) \sqrt{\Delta x^2 + (r_i - r_{i+1})^2}$$

$$V = \sum_{i=0}^n \frac{1}{3} \pi \Delta x (r_i^2 + r_{i+1}^2 + r_i r_{i+1})$$

$$\bar{S} = \sum_{i=0}^n \frac{3(r_i + r_{i+1}) \sqrt{\Delta x^2 + (r_i - r_{i+1})^2}}{\rho \Delta x (r_i^2 + r_{i+1}^2 + r_i r_{i+1})}$$

Figure A-2. Image analysis scheme based on finite element analysis using truncated conical elements.

Table A-1. Comparison of mean specific surface area values produced by various models of particle shape (by TEM image analysis). All values are given in m^2/g .

	Spherical	Capsule model	Prolate spheroid model	Finite element model
High Sphericity nom. 40nm Au	7.30	7.61	7.72	7.73
Standard Citrate nom. 40nm Au	6.95	8.12	8.37	8.39

APPENDIX B
ADDITIONAL PHYSICOCHEMICAL CHARACTERIZATION DATA

This appendix contains miscellaneous physicochemical characterization data on some of the materials used in this work. These items include:

- Concentration dependent near UV absorption spectra of thiourea in water.
- Changes in relative intensities of thiourea peak absorbances vs. concentration.
- TGA curves of C₁₆TAB and thiourea
- Raman spectra of hydroxyl terminated and functionalized PEG compounds.
- Raman spectrum of thiourea.
- Titration curve of thiourea

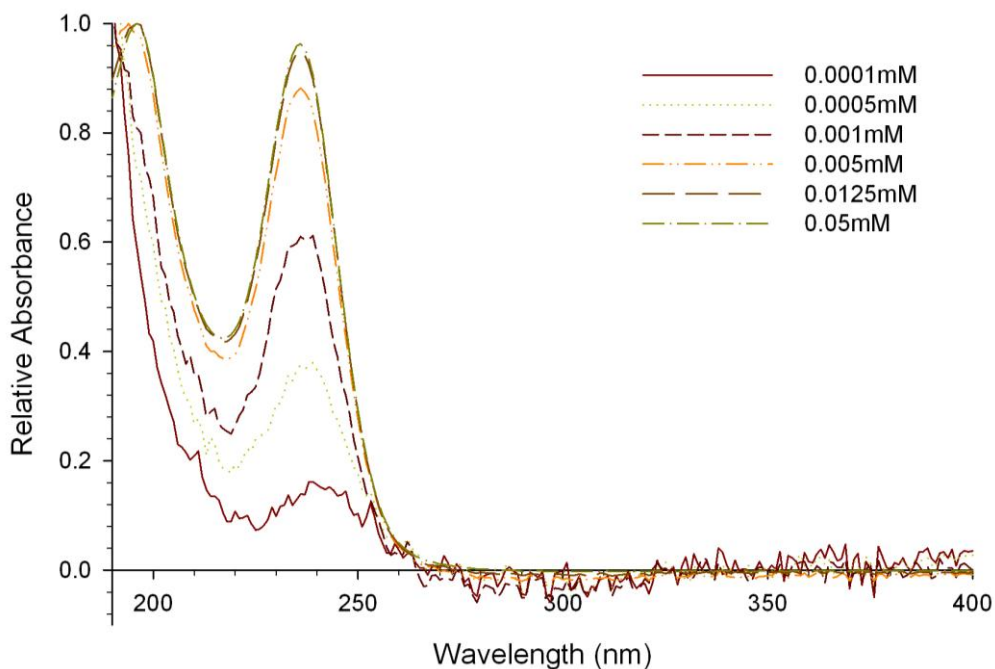


Figure B-1. Relative near ultraviolet absorption spectra of thiourea at various concentrations. Note that the relative intensities of the peaks at 196 and 236 are not constant until higher concentrations (greater than $\sim 0.05\text{mM}$).

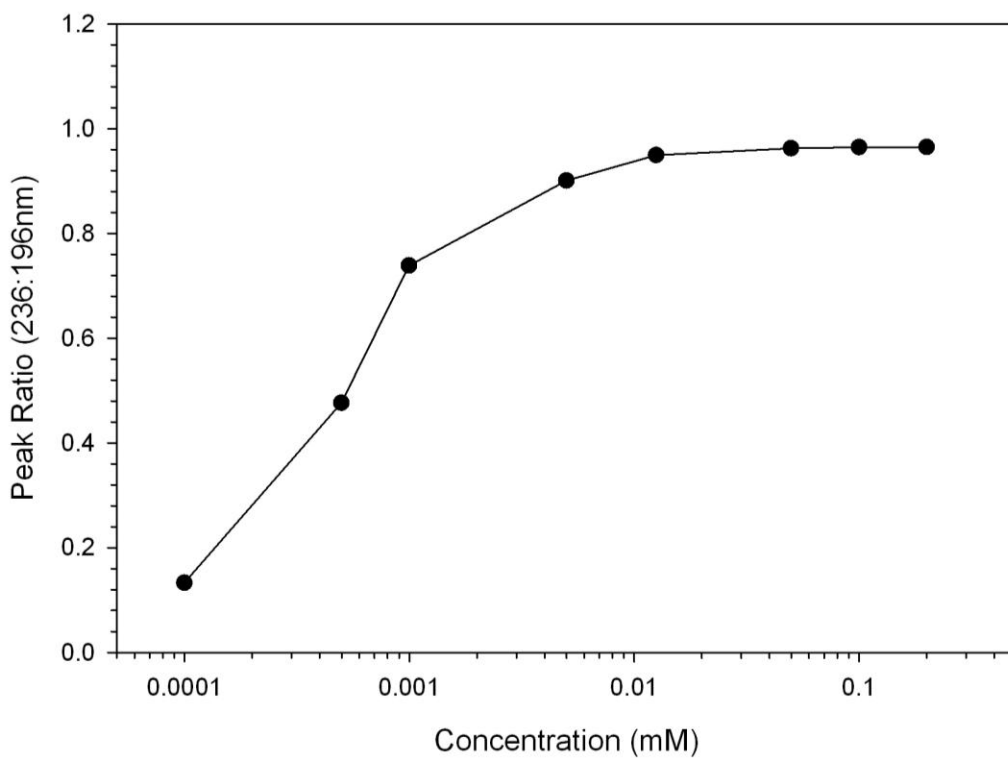


Figure B-2. Ratio of absorbance peak intensities at 236nm and 196nm as a function of thiourea concentration.

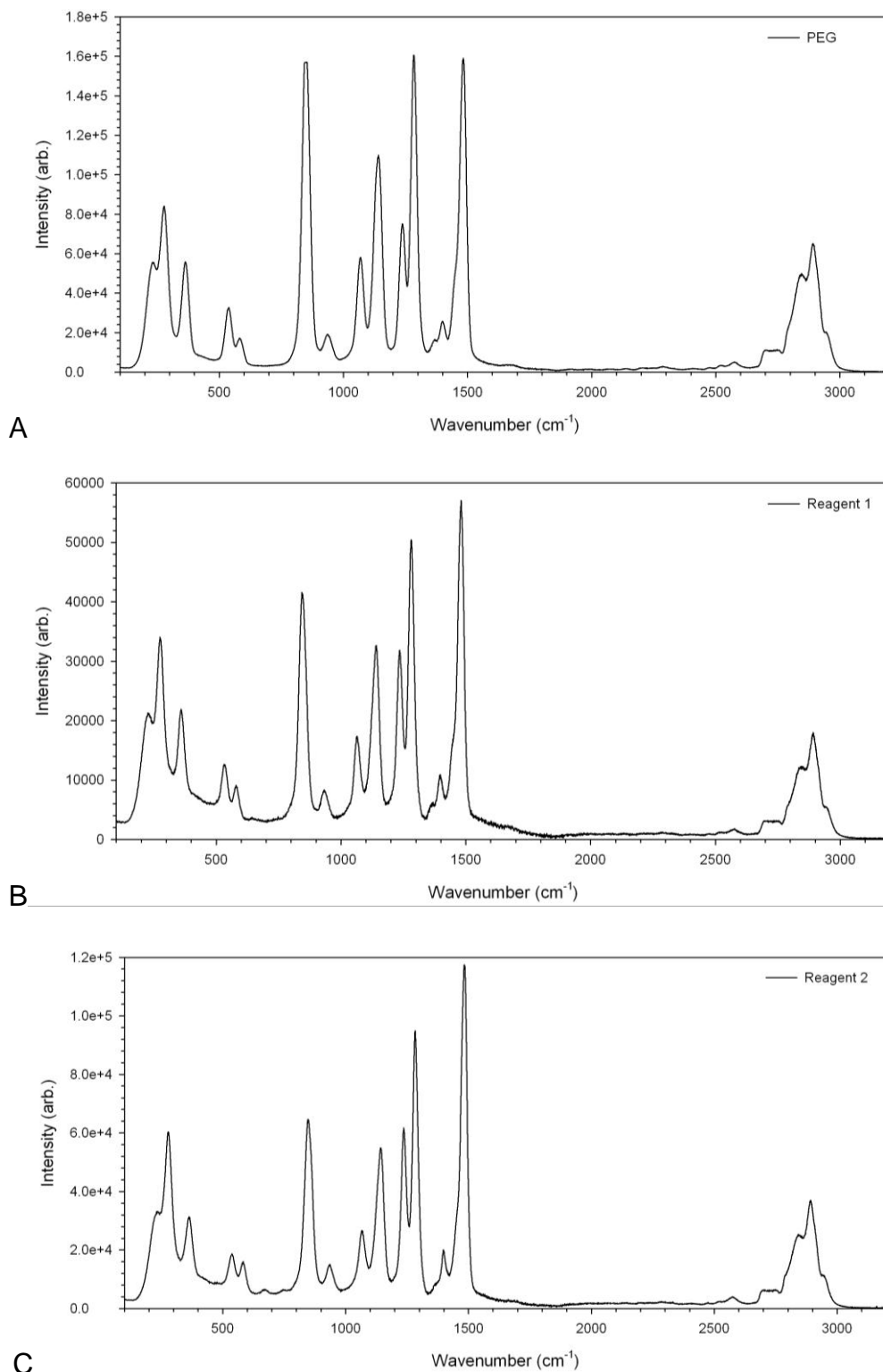


Figure B-3. Raman spectra of various PEG and functionalized PEG reagents. A) Hydroxyl terminated PEG. B) Thiolated methoxy-PEG (Reagent 1). C) Thiolated methoxy-PEG (Reagent 2).

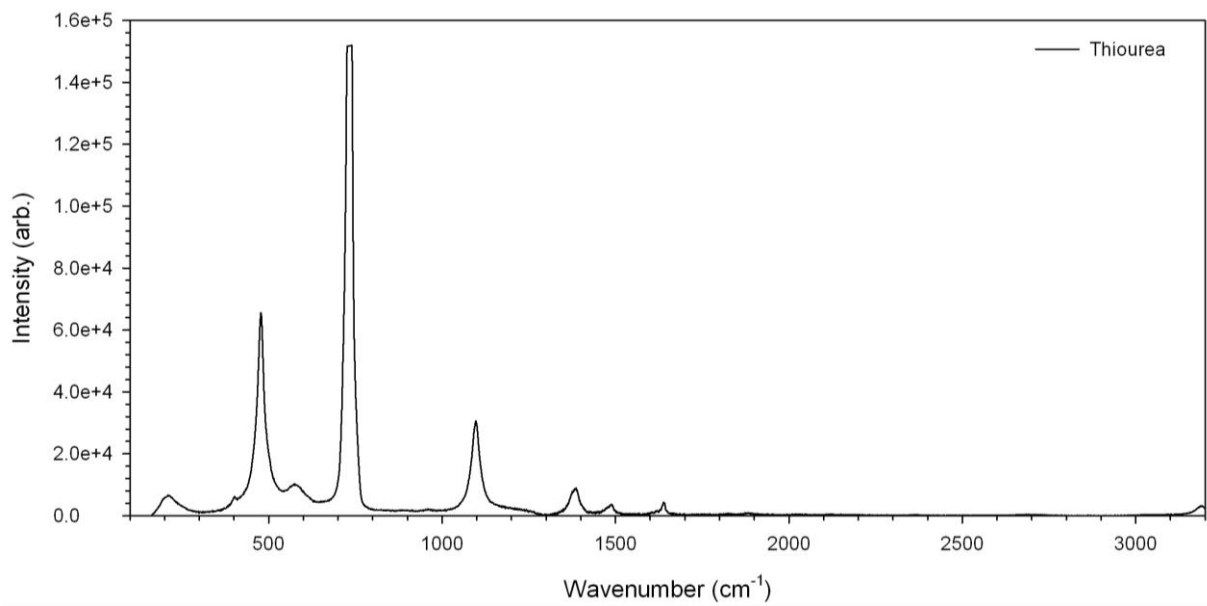


Figure B-4. Raman spectrum of thiourea.

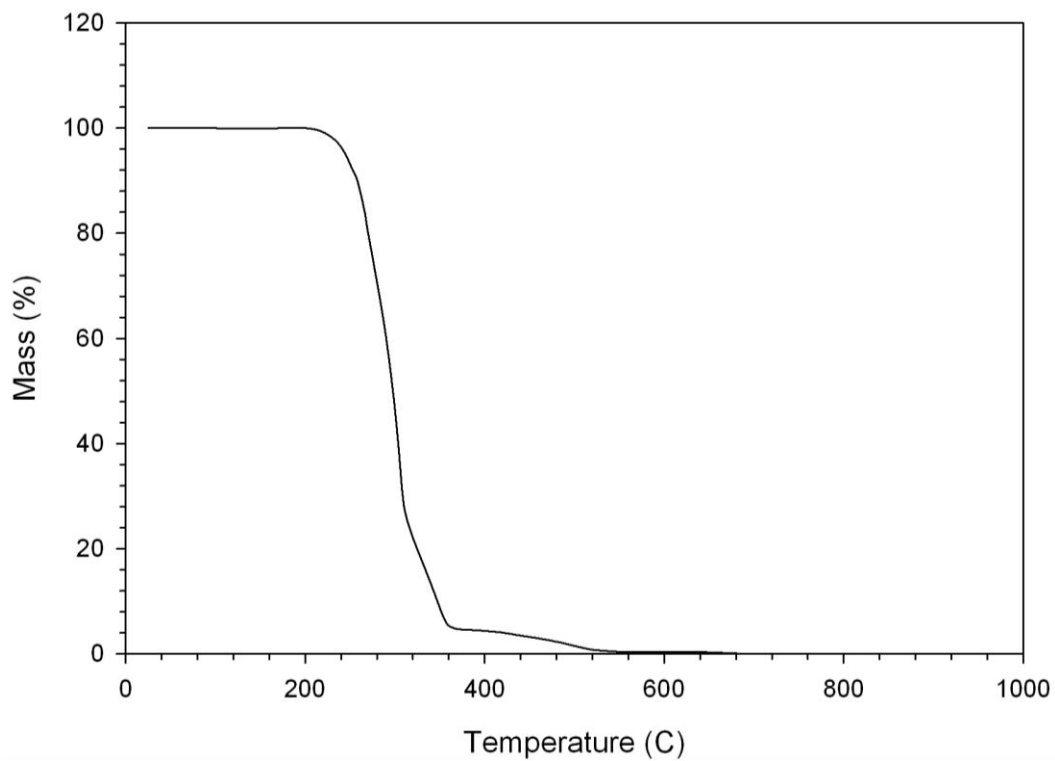


Figure B-5. TGA curve of C₁₆TAB in air up to 1000C.

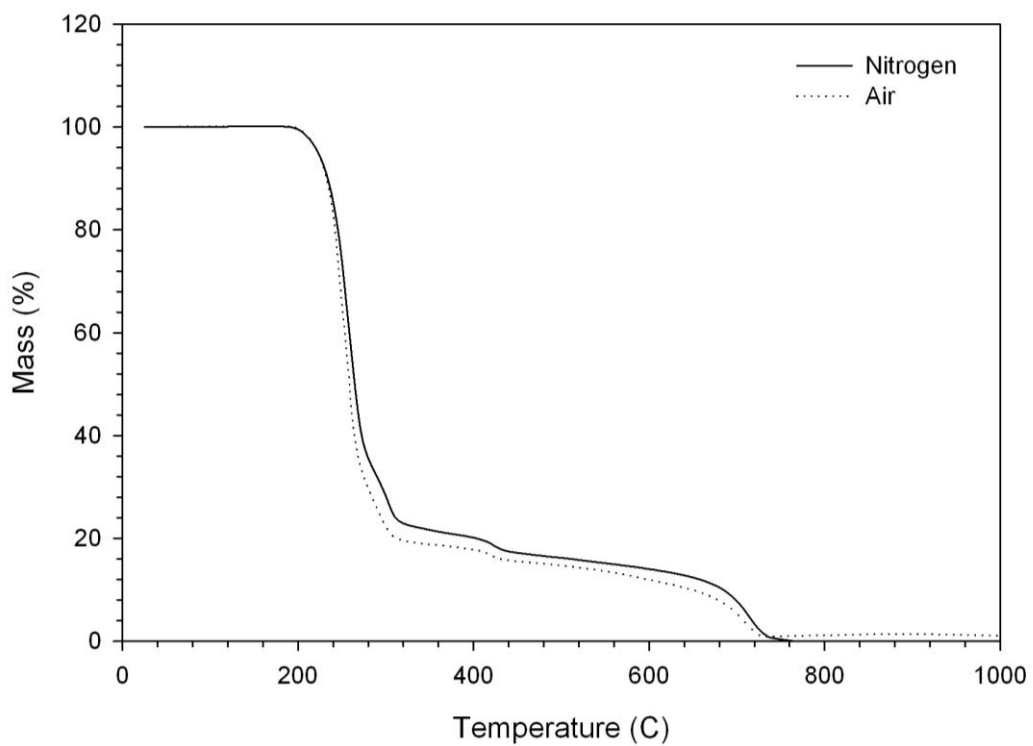


Figure B-6. TGA curves of thiourea under nitrogen and air up to 1000C.

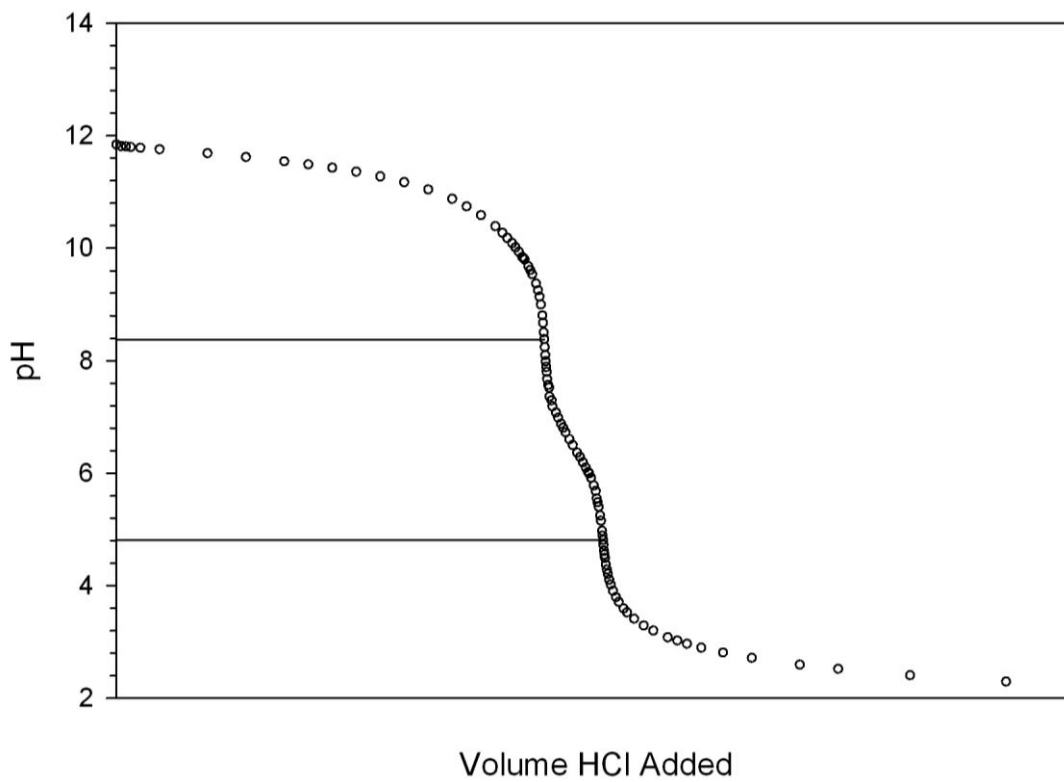


Figure B-7. Titration curve of thiourea. pH was initially adjusted to approximately 12, and then back-titrated to pH 2 with HCl.

APPENDIX C

EFFECTS OF CONTAINER TYPE ON DEGRADATION RATE MEASUREMENTS

The type of container used during the analysis of coating degradation rate is an important and often overlooked consideration. Plastic containers were initially selected in this work to minimize extractibles from glass, as certain experiments were to involve pH modification. Since salts were initially found to impact the rate of coating degradation, leaching of salts from glass was an additional motivation to select plasticware. The ubiquitous and convenient disposable polypropylene plasticware such as conical centrifuge tubes are often used without a thought about potential purity issues. Previous reports of compounds (most notably the plasticizer bisphenol-A) leached from polycarbonate containers led to considerable toxicological concerns due to widespread use both in and out of the laboratory³⁰⁰. Though plasticizers are typically not required with polypropylene, manufacturers employ a variety of additives²⁹⁸ to improve performance, aesthetics, and manufacturability of the containers. Common additives include light stabilizers, antioxidants, and chemicals to improve flowability and molding processes^{299,300}. These compounds can leach from plasticware and contaminate the solutions held in the containers, leading to measurement interferences. Particularly for sensitive biological experiments, leaching from polypropylene containers have been identified as a significant interference in various techniques^{300, 301}. The effects of container selection were investigated as a potential source of variance in the measurements made. The following items were specifically investigated:

- Leaching of additives from plastic containers
- Leaching of salts from glass containers
- Effectiveness of seals and oxygen availability.

The presence of leaching additives was identified by near ultraviolet absorption spectroscopy. Analysis of deionized water placed into various common plastic containers for 24h at 37C showed that small amounts of leaching did occur and was dependent on the manufacturer and type of container (Figure C-1). As expected, the amount of leaching was also found to be time and temperature dependent. Research into the types of additives included in polypropylene plasticware showed that sulfur based antioxidant additives are used in some plastics and can leach³⁰³. This is particularly concerning for the system of interest in this work as the sulfur based additives can adsorb to gold surfaces competitively (demonstrated previously). Analysis of the leachate from all containers used in this study with ICP did not show any detectable level of sulfur even at extremes in temperature and leaching times.

Analysis of the rates of degradation in glass and plastic containers under different conditions was performed. Surprisingly, the rates of degradation in the glass containers were significantly lower than those in plastic at the tested temperatures of 37C and 65C (Figure C-2). To verify that the presence of the leachates from the plastic containers were not the source of this difference, concentrated particles were added to both fresh deionized water and deionized water which was stored in plastic containers at 65C for several days (the presence of leached compounds was confirmed by UV absorption spectroscopy). These samples were placed into glass vials and incubated at 65C for three days. The resulting mobilities for both samples incubated in deionized water and leachate were indistinguishable from one another and showed far greater stability than the same particles in plastic containers. In order to rapidly screen potential influences on coating stability, most experiments performed after this point were run at 65C as an

accelerated life test. Due to both the significant increase in coating lifetime and the fact that the coating lifetime was enhanced nonspecifically over a wide range of conditions (data not shown), it was hypothesized that the presence of salts leached from the glass containers was the major contributing factor to the observed increase in stability. The effects of salts on the coating lifespan were noted previously (Figure 3-57) at relatively low concentrations. To test this hypothesis, deionized water was placed into a glass container and held at 65C for one day. A sample of this leachate was then added to PEG coated particles and placed into a plastic container. This sample was compared to the same particles in fresh deionized water in plastic and glass containers. Additionally, the conductivities of fresh deionized water, deionized water equilibrated with the ambient atmosphere, and water after incubation in glass for 24h were measured. The results of this experiment confirmed that species leached from the glass container were the cause of the increase in stability (Table C-1). Water pre-incubated at 65C in glass before mixing with particles in plastic containers showed minimal degradation after one day, while particles in fresh deionized water degraded rapidly in the same plastic container. Conductivity measurements provided additional support for this hypothesis, as the conductivity of water stored in glass at 65C was significantly elevated while not elevated when stored in plastic at the same temperature. The solubility of silicates and other glass components is dependent on the type of glass, leaching temperature, and available surface area³⁰².

The influence of oxygen availability due to permeability and sealing efficiency were examined both to verify the previous hypothesis as well as investigate the effects of oxygen availability as mediated by the container used. All experiments were performed

with deionized water in polypropylene containers. A summary selected samples analyzed are shown in Table C-2. It is clear from these results that the availability of dissolved oxygen, storage conditions, and the ability of oxygen to permeate the containers all have a significant effect on the rate of degradation.

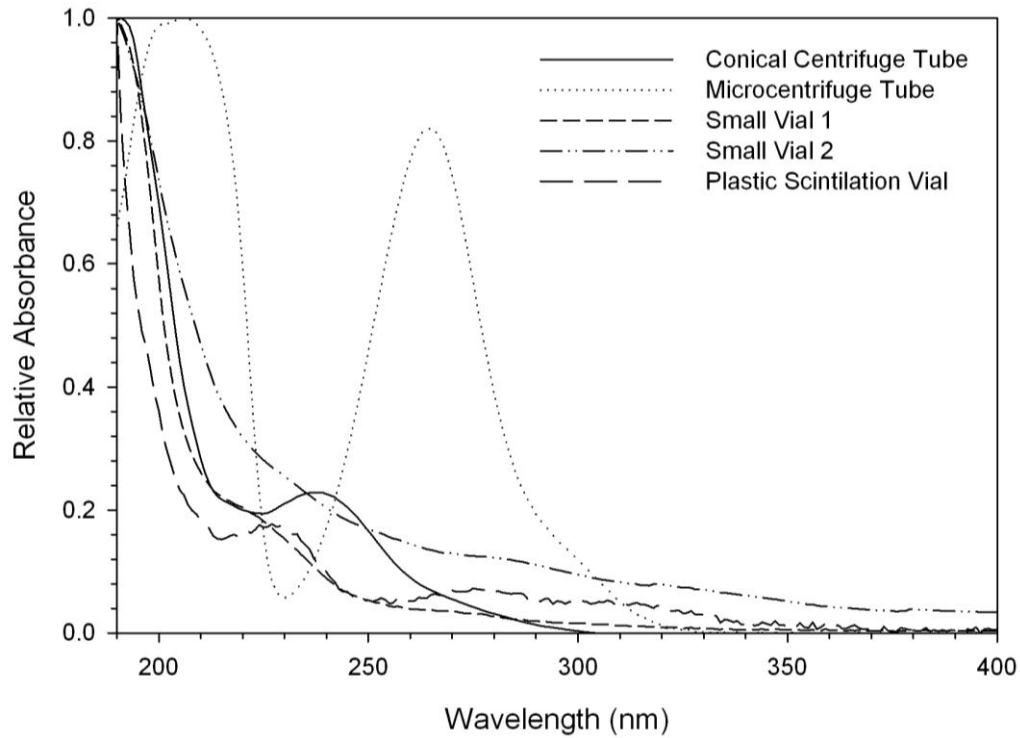


Figure C-1. Near ultraviolet absorption curves of water after leaching in various plastic containers for approximately 24h at 65C.

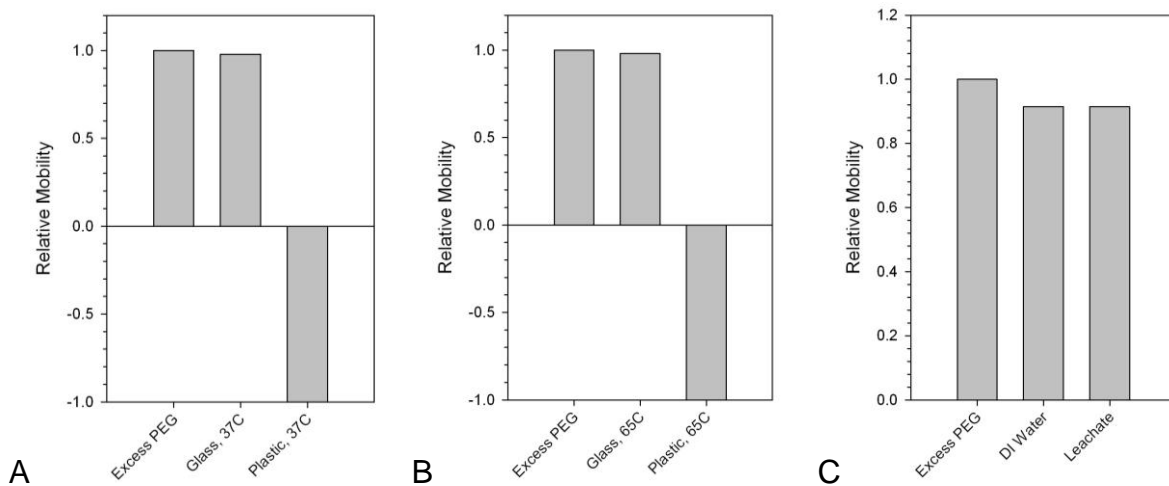


Figure C-2. Relative mobilities of PEG coated (Reagent 2) gold particles under various conditions. A) Particles incubated at 37C for 5 days. Note that degradation occurred more rapidly in the plastic container. B) Particles incubated at 65C for 1 day. C) Particles incubated at 65C for three days in glass containers. Concentrated particles were added to either deionized water or leachate (water) from plastic containers after several days at 65C. Note that the presence of the leachate does not have a significant effect on the degradation of the particles.

Table C-1. Summary of leaching experiment results at 65C. A concentrate of PEG coated (Reagent 2) gold particles was added to a selected medium and incubated at 65C for 24h before analysis by electrophoresis.

Medium used	Container used during incubation	Results after 24h of incubation at 65C
DI Water	Glass	Little degradation observed
DI Water	Plastic	Majority of coating removed
DI water leached in glass for 24h	Glass	Little degradation observed
DI water leached in glass for 24h	Plastic	Little degradation observed
DI water leached in plastic for 3 days	Glass	Little degradation observed

Table C-2. Summary of samples prepared for analysis of container sealing and oxygen availability in plastic containers.

Sample Preparation	Comments
Plastic/Ambient	Sample stored in a plastic container
Oil Layer	Sample stored in a plastic container with hexadecane layer above to minimize contact with air
Inert storage	Sample in an unpurged plastic container placed in an inert (argon) environment.
Full Purge	Sample in a purged (argon) plastic container in an inert (argon) environment.
Argon purged in an oxygen atmosphere	Sample argon purged in a plastic container and placed in a pure oxygen environment.
Argon purged in an air atmosphere	Sample argon purged in a plastic container and left in the ambient environment.
Oxygen Full Purge	Sample in a purged (pure oxygen) environment placed in an oxygen purged environment.

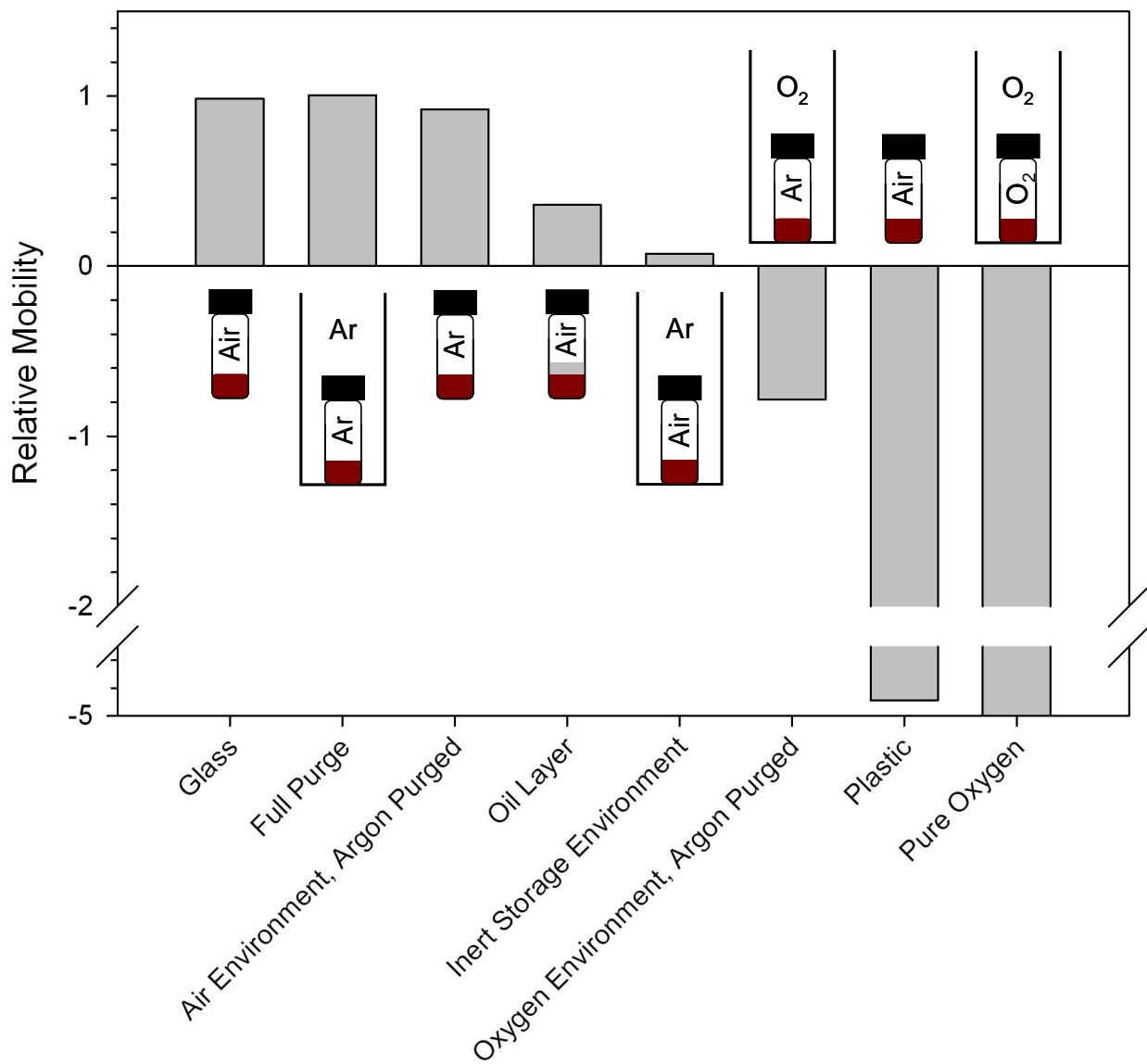


Figure C-3. Relative mobilities of PEG coated (Reagent 2) gold particles under various conditions to illustrate the influence of dissolved oxygen availability on coating degradation. Details of sample preparation are provided in Table C-2, and particles were incubated at 65C for 24h.

LIST OF REFERENCES

- (1) Lövestam, G.; Rauscher, H.; Roebben, G.; Sokull Klüttgen, B.; Gibson, N.; Putaud, J.; Stamm, H. Considerations on a Definition of Nanomaterial for Regulatory Purposes. **2010**.
- (2) National Nanotechnology Initiative (NNI) Glossary | Nano
<http://www.nano.gov/about-nni/glossary> (accessed 9/20/2012, 2012).
- (3) Meyer, M.; Persson, O.; Power, Y. Mapping excellence in nanotechnologies: preparatory study. **2001**.
- (4) American Chemical Council Definition for Engineered Nanomaterials. **2007**.
- (5) The European Commission Commission Recommendation of 18 October 2011 on the definition of nanomaterial. **2011**.
- (6) He, X. M.; Carter, D. C. Atomic structure and chemistry of human serum albumin *Nature* **1992**, *358*, 209-215.
- (7) Kiselev, M. A.; Gryzunov, I.; Dobretsov, G. E.; Komarova, M. N. Size of a human serum albumin molecule in solution. *Biofizika* **2001**, *46*, 423-427.
- (8) Horbett, T. A.; Brash, J. L. Proteins at Interfaces II **1995**, 602.
- (9) Furgeson, D. Y. Nanotools for Toxicity Assessment of Nanomedicines. **2008**.
- (10) Moghimi, S. M.; Hunter, A. C.; Murray, J. C. Nanomedicine: current status and future prospects *FASEB J.* **2005**, *19*, 311-330.
- (11) Freedomia Group Inc. Nanotechnology in Health Care. **2010**.
- (12) Department for Environment, Food and Rural Affairs, HM Government
Characterising the potential risks posed by engineered nanoparticles: A first UK Government Research Report. **2005**.
- (13) Szebeni, J.; Baranyi, L.; Savay, S.; Lutz, H. U.; Jelezarova, E.; Bunger, R.; Alving, C. R. The Role of Complement Activation in Hypersensitivity to Pegylated Liposomal Doxorubicin (Doxil®) *J. Liposome Res.* **2000**, *10*, 467-481.
- (14) Bawa, R. Nanoparticle-Based Therapeutics in Humans: A Survey. *Nanotech. L. & Bus.* **2008**, *5*, 9.
- (15) von Maltzahn, G.; Park, J. H.; Agrawal, A.; Bandaru, N. K.; Das, S. K.; Sailor, M. J.; Bhatia, S. N. Computationally guided photothermal tumor therapy using long-circulating gold nanorod antennas *Cancer Res.* **2009**, *69*, 3892-3900.

- (16) Libutti, S. K.; Paciotti, G. F.; Byrnes, A. A.; Alexander, H. R.; Gannon, W. E., Jr; Walker, M.; Seidel, G. D.; Yuldasheva, N.; Tamarkin, L. Phase I and Pharmacokinetic Studies of CYT-6091, a Novel PEGylated Colloidal Gold-rhTNF Nanomedicine *Clin. Cancer Res.* **2010**.
- (17) CytImmune Sciences, I. Drug Pipeline :: CytImmune Sciences, Inc. <http://www.cytimmune.com/go.cfm?do=Page.View&pid=19> (accessed 9/17/2012, 2012).
- (18) Huang, X.; El-Sayed, I. H.; Qian, W.; El-Sayed, M. A. Cancer Cell Imaging and Photothermal Therapy in the Near-Infrared Region by Using Gold Nanorods *J. Am. Chem. Soc.* **2006**, *128*, 2115-2120.
- (19) Huff, T. B.; Tong, L.; Zhao, Y.; Hansen, M. N.; Cheng, J. X.; Wei, A. Hyperthermic effects of gold nanorods on tumor cells *Nanomedicine (Lond)* **2007**, *2*, 125-132.
- (20) Oldenburg, S. J.; Averitt, R. D.; Westcott, S. L.; Halas, N. J. Nanoengineering of optical resonances *Chemical Physics Letters* **1998**, *288*, 243-247.
- (21) Bulte, J. W. M.; Kraitchman, D. L. Iron oxide MR contrast agents for molecular and cellular imaging *NMR Biomed.* **2004**; **2004**, *17*, 484-499.
- (22) Sonvico, F.; Mornet, S.; Vasseur, S.; Dubernet, C.; Jaillard, D.; Degrouard, J.; Hoebeke, J.; Duguet, E.; Colombo, P.; Couvreur, P. Folate-Conjugated Iron Oxide Nanoparticles for Solid Tumor Targeting as Potential Specific Magnetic Hyperthermia Mediators: Synthesis, Physicochemical Characterization, and in Vitro Experiments *Bioconjug. Chem.* **2005**, *16*, 1181-1188.
- (23) Velikov, K. P.; van Blaaderen, A. Synthesis and Characterization of Monodisperse Core-Shell Colloidal Spheres of Zinc Sulfide and Silica *Langmuir* **2001**, *17*, 4779-4786.
- (24) Slowing, I. I.; Vivero-Escoto, J. L.; Wu, C. W.; Lin, V. S. Mesoporous silica nanoparticles as controlled release drug delivery and gene transfection carriers *Adv. Drug Deliv. Rev.* **2008**, *60*, 1278-1288.
- (25) Slowing, I. .; Trewyn, B. .; Giri, S.; Lin, V. . -. Mesoporous Silica Nanoparticles for Drug Delivery and Biosensing Applications *Advanced Functional Materials* **2007**, *17*, 1225-1236.
- (26) Vivero-Escoto, J.; Slowing, I. I.; Wu, C.; Lin, V. S. -. Photoinduced Intracellular Controlled Release Drug Delivery in Human Cells by Gold-Capped Mesoporous Silica Nanosphere. *J. Am. Chem. Soc.* **2009**, *131*, 3462-3463.

- (27) Love, J. C.; Estroff, L. A.; Kriebel, J. K.; Nuzzo, R. G.; Whitesides, G. M. Self-assembled monolayers of thiolates on metals as a form of nanotechnology *Chem. Rev.* **2005**, *105*, 1103-1169.
- (28) Moghimi, S. M.; Hunter, A. C.; Murray, J. C. Long-circulating and target-specific nanoparticles: theory to practice *Pharmacol. Rev.* **2001**, *53*, 283-318.
- (29) Gabizon, A.; Papahadjopoulos, D. The role of surface charge and hydrophilic groups on liposome clearance in vivo *Biochimica et Biophysica Acta (BBA) - Biomembranes* **1992**, *1103*, 94-100.
- (30) Szebeni, J.; Savay, S.; Alving, C.; Hunter, A.; Moghimi, S. In *In Proc Int Symp Control Rel Bioact Mater.* 2001; .
- (31) Abuchowski, A.; McCoy, J. R.; Palczuk, N. C.; van Es, T.; Davis, F. F. Effect of covalent attachment of polyethylene glycol on immunogenicity and circulating life of bovine liver catalase *J. Biol. Chem.* **1977**, *252*, 3582-3586.
- (32) Mrksich, M. Using self-assembled monolayers to understand the biomaterials interface *Current Opinion in Colloid & Interface Science* **1997**, *2*, 83-88.
- (33) Kingshott, P.; Griesser, H. J. Surfaces that resist bioadhesion *Current Opinion in Solid State and Materials Science* **1999**, *4*, 403-412.
- (34) Yang, M.; Chung, F. L.; Thompson, M. Acoustic network analysis as a novel technique for studying protein adsorption and denaturation at surfaces *Anal. Chem.* **1993**, *65*, 3713-3716.
- (35) Hlady, V.; Buijs, J. Protein adsorption on solid surfaces *Curr. Opin. Biotechnol.* **1996**, *7*, 72-77.
- (36) Wang, J.; Achilefu, S.; Nantz, M.; Kang, K. A. Gold nanoparticle-fluorophore complex for conditionally fluorescing signal mediator *Anal. Chim. Acta* **2011**, *695*, 96-104.
- (37) Gupta, A. K.; Gupta, M. Synthesis and surface engineering of iron oxide nanoparticles for biomedical applications *Biomaterials* **2005**, *26*, 3995-4021.
- (38) Faraday, M. The Bakerian Lecture: Experimental Relations of Gold (and Other Metals) to Light *Philosophical Transactions of the Royal Society of London* **1857**, *147*, 145-181.
- (39) Ferin, J.; Oberdörster, G.; Penney, D. P.; Soderholm, S. C.; Gelein, R.; Piper, H. C. Increased pulmonary toxicity of ultrafine particles? I. Particle clearance, translocation, morphology *J. Aerosol Sci.* **1990**, *21*, 381-384.

- (40) Oberdörster, G.; Ferin, J.; Finkelstein, G.; Wade, P.; Corson, N. Increased pulmonary toxicity of ultrafine particles? II. Lung lavage studies *J. Aerosol Sci.* **1990**, *21*, 384-387.
- (41) Service, R. F. American Chemical Society meeting. Nanomaterials show signs of toxicity *Science* **2003**, *300*, 243.
- (42) The Royal Society and The Royal Academy of Engineering Nanoscience and nanotechnologies: opportunities and uncertainties . **2004**.
- (43) Fadeel, B.; Garcia-Bennett, A. E. Better safe than sorry: Understanding the toxicological properties of inorganic nanoparticles manufactured for biomedical applications *Adv. Drug Deliv. Rev.* **2010**, *62*, 362-374.
- (44) Landsiedel Staal, e. a. In *In Inhalational Toxicity Studies with Twelve Nanomaterials Using Different Dosimetries – None Fitted All*. Society of Toxicology Meeting 2010; 2010; .
- (45) Crist, R. M.; Grossman, J. H.; Patri, A. K.; Stern, S. T.; Dobrovolskaia, M. A.; Adisheshaiah, P. P.; Clogston, J. D.; McNeil, S. E. Common pitfalls in nanotechnology: lessons learned from NCI's Nanotechnology Characterization Laboratory *Integr. Biol. (Camb)* **2012**.
- (46) Adisheshaiah, P. P.; Hall, J. B.; McNeil, S. E. Nanomaterial standards for efficacy and toxicity assessment *Wiley Interdisciplinary Reviews: Nanomedicine and Nanobiotechnology* **2010**; **2009**, *2*, 99-112.
- (47) Powers, K. W.; Palazuelos, M.; Moudgil, B. M.; Roberts, S. M. Characterization of the size, shape, and state of dispersion of nanoparticles for toxicological studies *Nanotoxicology* **2007**, *1*, 42-51.
- (48) California Department of Toxic Substances Control Chemical Information Call-In - Nano Metals, Nano Metal Oxides, and Quantum Dots
<http://www.dtsc.ca.gov/TechnologyDevelopment/Nanotechnology/nanometalcallin.cfm> (accessed 9/19/2012, 2012).
- (49) Community Environmental Advisory Commission Berkeley Municipal Code. **2006**, *15.12.040*.
- (50) Organisation for Economic Co-operation and Development (OECD) CURRENT DEVELOPMENTS/ACTIVITIES ON THE SAFETY OF MANUFACTURED NANOMATERIALS. **2011**, *29*.

- (51) Organisation for Economic Co-operation and Development (OECD) Report of the OECD Workshop on the Safety of Manufactured Nanomaterials: Building Co-operation, Co-ordination and Communication. **2005**, 1.
- (52) Barenholz, Y. C. Doxil®—The first FDA-approved nano-drug: Lessons learned. *J. Controlled Release* **2012**.
- (53) National Institutes of Health FERIDEX (FERUMOXIDES) SOLUTION [BAYER HEALTHCARE PHARMACEUTICALS INC.]
<http://dailymed.nlm.nih.gov/dailymed/drugInfo.cfm?id=6934> (accessed 9/19/2012, 2012).
- (54) Organisation for Economic Co-operation and Development (OECD) LIST OF MANUFACTURED NANOMATERIALS AND LIST OF ENDPOINTS FOR PHASE ONE OF THE SPONSORSHIP PROGRAMME FOR THE TESTING OF MANUFACTURED NANOMATERIALS: REVISION. **2010**, 27.
- (55) Nelson, B. C.; Petersen, E. J.; Marquis, B. J.; Atha, D. H.; Elliott, J. T.; Cleveland, D.; Watson, S. S.; Tseng, I. H.; Dillon, A.; Theodore, M.; Jackman, J. NIST gold nanoparticle reference materials do not induce oxidative DNA damage *Nanotoxicology* **2011**.
- (56) National Cancer Institute NCL supports the first biocompatible NIST nanoparticulate reference material - Nanotechnology Characterization Laboratory
http://ncl.cancer.gov/resources_news_06292007.asp (accessed 10/28/2012, 2012).
- (57) Barcikowski, S.; Rehbock, C.; Merk, V.; Gamrad, L.; Taylor, U.; Kues, W.; Rath, D. In *In Additive-free gold nanoparticles as toxicity reference materials in reproduction biology*; Proceedings of SPIE; SPIE: 2013; Vol. 8595.
- (58) Chen, Y. S.; Hung, Y. C.; Liao, I.; Huang, G. S. Assessment of the In Vivo Toxicity of Gold Nanoparticles *Nanoscale Res. Lett.* **2009**, 4, 858-864.
- (59) Stone, V.; Nowack, B.; Baun, A.; van den Brink, N.; von der Kammer, F.; Dusinska, M.; Handy, R.; Hankin, S.; Hassellöv, M.; Joner, E. Nanomaterials for environmental studies: classification, reference material issues, and strategies for physico-chemical characterisation. *Sci. Total Environ.* **2010**, 408, 1745-1754.
- (60) Handley, D. A. In *History of Colloidal Gold as a Microscopic Probe*. Hayat, M. A., Ed.; Colloidal gold: principles, methods, and applications; San Diego : Academic Press: 1989; .
- (61) Paciotti, G. F.; Myer, L.; Weinreich, D.; Goia, D.; Pavel, N.; McLaughlin, R. E.; Tamarkin, L. Colloidal gold: a novel nanoparticle vector for tumor directed drug delivery *Drug Deliv.* **2004**, 11, 169-183.

- (62) Nanospectra Biosciences, I. Nanospectra Biosciences, Inc.
<http://www.nanospectra.com/> (accessed 9/17/2012, 2012).
- (63) Chamberland, D. L.; Agarwal, A.; Kotov, N.; Brian Fowlkes, J.; Carson, P. L.; Wang, X. Photoacoustic tomography of joints aided by an Etanercept-conjugated gold nanoparticle contrast agent-an ex vivo preliminary rat study *Nanotechnology* **2008**, *19*, 095101.
- (64) Kim, D.; Park, S.; Lee, J. H.; Jeong, Y. Y.; Jon, S. Antibiofouling Polymer-Coated Gold Nanoparticles as a Contrast Agent for in Vivo X-ray Computed Tomography Imaging *J. Am. Chem. Soc.* **2007**, *129*, 7661-7665.
- (65) Baes Jr, C.; Mesmer, R. In *The Hydrolysis of Cations*; Wiley: New York, 1976; Vol. 1, pp 489.
- (66) Turkevich, J.; Stevenson, P. C.; Hillier, J. A study of the nucleation and growth processes in the synthesis of colloidal gold *Discuss. Faraday Soc.* **1951**, *11*, 55.
- (67) Frens, G. Controlled nucleation for the regulation of the particle size in monodisperse gold suspensions. *Nature (London)* **1973**, *241*, 20.
- (68) Powers, K. W.; Brown, S. C.; Krishna, V. B.; Wasdo, S. C.; Moudgil, B. M.; Roberts, S. M. Research strategies for safety evaluation of nanomaterials. Part VI. Characterization of nanoscale particles for toxicological evaluation *Toxicol. Sci.* **2006**, *90*, 296-303.
- (69) Andreasen, A. *Kolloid Beith* **1928**, *27*, 405.
- (70) Andreasen, A. L., JJV. *Ber. Dt. Keram. Ges.* **1930**, *11*, 312.
- (71) Yusah, N. SediGraph™ III 5120. **2003**.
- (72) Bettersize Instruments Ltd. BT-1500 Centrifugal Sedimentation Particle Size Analyzer <http://www.bettersize.com/en/products/psa/bt-1500.htm> (accessed April 1, 2012).
- (73) Brookhaven Instrument Corporation Brookhaven Instruments BI-DCP High Resolution Particle Size Analyzer
<http://www.brookhaveninstruments.com/products/particle-sizing/particle-size-BI-DCP.html> (accessed 3/31/2012, 2012).
- (74) CPS Instruments Particle Size Analysis: Welcom to CPS Instruments.
<http://www.cpsinstruments.com/> (accessed March 31, 2012).
- (75) LUM GmbH LUMiSizer® - The All-in-One Dispersion Analyser. <http://www.lum-gmbh.com/product-information.html> (accessed April 1, 2012).

- (76) Marshall, C. E. A New Method of Determining the Distribution Curve of Polydisperse Colloidal Systems *Proceedings of the Royal Society A: Mathematical, Physical and Engineering Sciences* **1930**, 126, 427-439.
- (77) Slater, C.; Cohen, L. A centrifugal particle size analyser *J. Sci. Instrum.* **1962**; **2002**, 39, 614-617.
- (78) Allen and Svarowsky *Dechema Monogram.* **1975**, 1589-1625, 279-292.
- (79) Beckman Coulter ProteomeLab™ XL-A/XL-I - Beckman Coulter, Inc.
<https://www.beckmancoulter.com/wsrportal/wsr/research-and-discovery/products-and-services/centrifugation-analytical/index.htm> (accessed 4/2/2012, 2012).
- (80) Stokes, G. G. In *Mathematical and Physical Papers*; Cambridge University Press: London, 1880; .
- (81) Voros, J. The density and refractive index of adsorbing protein layers *Biophys. J.* **2004**, 87, 553-561.
- (82) Nakeff, A.; Floeh, D. P. Separation of megakaryocytes from mouse bone marrow by density gradient centrifugation. *Blood* **1976**, 48, 133-138.
- (83) Xu, J.; Plaxco, K. W.; Allen, S. J. Probing the collective vibrational dynamics of a protein in liquid water by terahertz absorption spectroscopy. *Protein Sci.* **2006**, 15, 1175-1181.
- (84) Welle, A.; Chiumiento, A.; Barbucci, R. Competitive protein adsorption on micro patterned polymeric biomaterials, and viscoelastic properties of tailor made extracellular matrices *Biomol. Eng.* **2007**, 24, 87-91.
- (85) Dow Chemical Company CARBOWAX PEGs Densities vs Temperature.
https://dow-answer.custhelp.com/app/answers/detail/a_id/3591/kw/carbowax%208000 (accessed March 31, 2012).
- (86) Gonzalez-Tello, P.; Camacho, F.; Blazquez, G. Density and Viscosity of Concentrated Aqueous Solutions of Polyethylene Glycol *Journal of Chemical & Engineering Data* **1994**, 39, 611-614.
- (87) Dow Chemical Company CARBOWAX™ Polyethylene Glycols. **2011**.
- (88) MetLab Corporation Materials Safety Data Sheet: Polyethylene Glycol. **2011**.
- (89) Fisher Scientific Materials Safety Data Sheet:Carbowax PEG 7000-8000. **2007**, 9.

- (90) Fischer, H.; Polikarpov, I.; Craievich, A. F. Average protein density is a molecular-weight-dependent function *Protein Science* **2009**, *13*, 2825-2828.
- (91) Rappaz, B.; Barbul, A.; Emery, Y.; Korenstein, R.; Depeursinge, C.; Magistretti, P. J.; Marquet, P. Comparative study of human erythrocytes by digital holographic microscopy, confocal microscopy, and impedance volume analyzer *Cytometry Part A* **2008**, *73A*, 895-903.
- (92) McLaren, C. E.; Brittenham, G. M.; Hasselblad, V. Statistical and graphical evaluation of erythrocyte volume distributions *Am. J. Physiol.* **1987**, *252*, H857-66.
- (93) Young, B.; Wheeler, P. R.; Lowe, J. N.; Stevens, A.; Heath, J. E. In *Wheeler's Functional histology: a text and colour atlas* Churchill Livingstone Elsevier: Philadelphia, PA, 2006; , pp 437.
- (94) National Cancer Institute Electron Microscopy Lab EML Image Gallery | Advanced Technology Program (ATP) <http://atp.ncifcrf.gov/imaging-and-nanotechnology/electron-microscopy-laboratory/eml-protocols-and-resources/eml-image-gallery/> (accessed 4/14/2012, 2012).
- (95) Meyers, R. A. In *Encyclopedia of analytical chemistry: applications, theory, and instrumentation*; Wiley: New York, 2000; .
- (96) Malvern Instruments Ltd. Zetasizer Nano ZS particle size, zeta potential and molecular weight http://www.malvern.com/labeng/products/zetasizer/zetasizer_nano/zetasizer_nano_zs.htm (accessed 4/22/2012, 2012).
- (97) QuantomiX :: QuantomiX WETSEM® Technology :: <http://www.wetsem.com/> (accessed 11/4/2012, 2012).
- (98) Takae, S.; Akiyama, Y.; Otsuka, H.; Nakamura, T.; Nagasaki, Y.; Kataoka, K. Ligand Density Effect on Biorecognition by PEGylated Gold Nanoparticles: Regulated Interaction of RCA120Lectin with Lactose Installed to the Distal End of Tethered PEG Strands on Gold Surface *Biomacromolecules* **2005**, *6*, 818-824.
- (99) MATSUMURA, H.; ATSUTA, M.; TANOUE, N. Evaluation of two thione primers and composite luting agents used for bonding a silver-palladium-copper-gold alloy *J. Oral Rehabil.* **2002**, *29*, 842-846.
- (100) Troughton, E. B.; Bain, C. D.; Whitesides, G. M.; Nuzzo, R. G.; Allara, D. L.; Porter, M. D. Monolayer films prepared by the spontaneous self-assembly of symmetrical and unsymmetrical dialkyl sulfides from solution onto gold substrates: structure, properties, and reactivity of constituent functional groups *Langmuir* **1988**, *4*, 365-385.

- (101) Zhu, H.; Coleman, D. M.; Dehen, C. J.; Geisler, I. M.; Zemlyanov, D.; Chmielewski, J.; Simpson, G. J.; Wei, A. Assembly of Dithiocarbamate-Anchored Monolayers on Gold Surfaces in Aqueous Solutions *Langmuir* **2008**, *24*, 8660-8666.
- (102) Zhao, Y.; Perez-Segarra, W.; Shi, Q.; Wei, A. Dithiocarbamate assembly on gold *J. Am. Chem. Soc.* **2005**, *127*, 7328-7329.
- (103) Arduengo, A. J.; Moran, J. R.; Rodriguez-Parada, J.; Ward, M. D. Molecular control of self-assembled monolayer films of imidazole-2-thiones: adsorption and reactivity *J. Am. Chem. Soc.* **1990**, *112*, 6153-6154.
- (104) Ion, A.; Partali, V.; Sliwka, H.; Gabriel Banica, F. Electrochemistry of a carotenoid self-assembled monolayer *Electrochemistry Communications* **2002**, *4*, 674-678.
- (105) Ihs, A.; Uvdal, K.; Liedberg, B. Infrared and photoelectron spectroscopic studies of ethyl and octyl xanthate ions adsorbed on metallic and sulfidized gold surfaces. *Langmuir* **1993**, *9*, 733-739.
- (106) von Wrochem, F.; Gao, D.; Scholz, F.; Nothofer, H. G.; Nelles, G.; Wessels, J. M. Efficient electronic coupling and improved stability with dithiocarbamate-based molecular junctions *Nat. Nanotechnol* **2010**.
- (107) Zhang, G.; Yang, Z.; Lu, W.; Zhang, R.; Huang, Q.; Tian, M.; Li, L.; Liang, D.; Li, C. Influence of anchoring ligands and particle size on the colloidal stability and in vivo biodistribution of polyethylene glycol-coated gold nanoparticles in tumor-xenografted mice *Biomaterials* **2009**, *30*, 1928-1936.
- (108) Langry, K. C.; Ratto, T. V.; Rudd, R. E.; McElfresh, M. W. The AFM Measured Force Required to Rupture the Dithiolate Linkage of Thiocetic Acid to Gold Is Less than the Rupture Force of a Simple Gold-Alkyl Thiolate Bond *Langmuir* **2005**, *21*, 12064-12067.
- (109) Willey, T. M.; Vance, A. L.; van Buuren, T.; Bostedt, C.; Terminello, L. J.; Fadley, C. S. Rapid degradation of alkanethiol-based self-assembled monolayers on gold in ambient laboratory conditions *Surf. Sci.* **2005**, *576*, 188-196.
- (110) Laibinis, P. E.; Whitesides, G. M. Self-assembled monolayers of n-alkanethiolates on copper are barrier films that protect the metal against oxidation by air *J. Am. Chem. Soc.* **1992**, *114*, 9022-9028.
- (111) Brewer, N. J.; Rawsterne, R. E.; Kothari, S.; Leggett, G. J. Oxidation of Self-Assembled Monolayers by UV Light with a Wavelength of 254 nm *J. Am. Chem. Soc.* **2001**, *123*, 4089-4090.

- (112) Lee, M.; Hsueh, C.; Freund, M. S.; Ferguson, G. S. Air Oxidation of Self-Assembled Monolayers on Polycrystalline Gold: The Role of the Gold Substrate *Langmuir* **1998**, *14*, 6419-6423.
- (113) Hasan, M.; Bethell, D.; Brust, M. The Fate of Sulfur-Bound Hydrogen on Formation of Self-Assembled Thiol Monolayers on Gold: ¹H NMR Spectroscopic Evidence from Solutions of Gold Clusters *J. Am. Chem. Soc.* **2002**, *124*, 1132-1133.
- (114) Vericat, C.; Vela, M. E.; Benitez, G.; Carro, P.; Salvarezza, R. C. Self-assembled monolayers of thiols and dithiols on gold: new challenges for a well-known system *Chem. Soc. Rev.* **2010**.
- (115) Woodruff, D. P. The interface structure of n-alkylthiolate self-assembled monolayers on coinage metal surfaces *Physical Chemistry Chemical Physics* **2008**, *10*, 7211.
- (116) Weisbecker, C. S.; Merritt, M. V.; Whitesides, G. M. Molecular Self-Assembly of Aliphatic Thiols on Gold Colloids *Langmuir* **1996**, *12*, 3763-3772.
- (117) Kankate, L.; Turchanin, A.; Götzhäuser, A. On the Release of Hydrogen from the S-H groups in the Formation of Self-Assembled Monolayers of Thiols *Langmuir* **2009**, *25*, 10435-10438.
- (118) Kodama, C.; Hayashi, T.; Nozoye, H. Decomposition of alkanethiols adsorbed on Au (1 1 1) at low temperature. *Appl. Surf. Sci.* **2001**, *169-170*, 264-267.
- (119) Vericat, C.; Vela, M. E.; Andreasen, G.; Salvarezza, R. C.; Vázquez, L.; Martín-Gago, J. A. Sulfur-Substrate Interactions in Spontaneously Formed Sulfur Adlayers on Au(111) *Langmuir* **2001**, *17*, 4919-4924.
- (120) Schlenoff, J. B.; Li, M.; Ly, H. Stability and Self-Exchange in Alkanethiol Monolayers. *J. Am. Chem. Soc.* **1995**, *117*, 12528-12536.
- (121) Ulman, A. Formation and Structure of Self-Assembled Monolayers *Chem. Rev.* **1996**, *96*, 1533-1554.
- (122) Nuzzo, R. G.; Zegarski, B. R.; Dubois, L. H. Fundamental studies of the chemisorption of organosulfur compounds on gold(111). Implications for molecular self-assembly on gold surfaces. *J. Am. Chem. Soc.* **1987**, *109*, 733-740.
- (123) Lustemberg, P. G.; Vericat, C.; Benitez, G. A.; Vela, M. E.; Tognalli, N.; Fainstein, A.; Martiarena, M. L.; Salvarezza, R. C. Spontaneously Formed Sulfur Adlayers on Gold in Electrolyte Solutions: Adsorbed Sulfur or Gold Sulfide? *Journal of Physical Chemistry C* **2008**, *112*, 11394-11402.

- (124) Bourg, M.; Badia, A.; Lennox, R. B. Gold-Sulfur Bonding in 2D and 3D Self-Assembled Monolayers: XPS Characterization. *J Phys Chem B* **2000**, *104*, 6562-6567.
- (125) Joseph, Y.; Besnard, I.; Rosenberger, M.; Guse, B.; Nothofer, H.; Wessels, J. M.; Wild, U.; Knop-Gericke, A.; Su, D.; Schlögl, R.; Yasuda, A.; Vossmeier, T. Self-Assembled Gold Nanoparticle/Alkanedithiol Films: Preparation, Electron Microscopy, XPS-Analysis, Charge Transport, and Vapor-Sensing Properties† *The Journal of Physical Chemistry B* **2003**, *107*, 7406-7413.
- (126) Tanaka, A.; Takeda, Y.; Imamura, M.; Sato, S. Dynamic final-state effect on the Au 4f core-level photoemission of dodecanethiolate-passivated Au nanoparticles on graphite substrates *Physical Review B* **2003**, *68*.
- (127) Zhang, P.; Sham, T. X-Ray Studies of the Structure and Electronic Behavior of Alkanethiolate-Capped Gold Nanoparticles: The Interplay of Size and Surface Effects *Phys. Rev. Lett.* **2003**, *90*.
- (128) Tanaka, A.; Takeda, Y.; Nagasawa, T.; Takahashi, K. Chemical states of dodecanethiolate-passivated Au nanoparticles: synchrotron-radiation photoelectron spectroscopy *Solid State Commun.* **2003**, *126*, 191-196.
- (129) Kitsudo, Y.; Iwamoto, A.; Matsumoto, H.; Mitsuhara, K.; Nishimura, T.; Takizawa, M.; Akita, T.; Maeda, Y.; Kido, Y. Final state effect for Au 4f line from gold-nanoparticles grown on oxides and HOPG supports *Surf. Sci.* **2009**, *603*, 2108-2114.
- (130) Jokerst, J. V.; Lobovkina, T.; Zare, R. N.; Gambhir, S. S. Nanoparticle PEGylation for imaging and therapy. *Nanomedicine* **2011**, *6*, 715-728.
- (131) Oxford Journals Oxford Journals | Life Sciences & Medicine | Toxicological Sciences | Manuscript Preparation Guidelines.
http://www.oxfordjournals.org/our_journals/toxsci/for_authors/msprep_submission.html (accessed 6/9/2012, 2012).
- (132) MINChar Initiative Characterization Matters — <http://characterizationmatters.org/> (accessed 7/8/2012, 2012).
- (133) Corbierre, M. K.; Cameron, N. S.; Sutton, M.; Mochrie, S. G. J.; Lurio, L. B.; Rühm, A.; Lennox, R. B. Polymer-Stabilized Gold Nanoparticles and Their Incorporation into Polymer Matrices *J. Am. Chem. Soc.* **2001**, *123*, 10411-10412.
- (134) Corbierre, M. K.; Cameron, N. S.; Lennox, R. B. Polymer-Stabilized Gold Nanoparticles with High Grafting Densities *Langmuir* **2004**, *20*, 2867-2873.

- (135) Corbierre, M. K.; Cameron, N. S.; Sutton, M.; Laaziri, K.; Lennox, R. B. Gold nanoparticle/polymer nanocomposites: dispersion of nanoparticles as a function of capping agent molecular weight and grafting density *Langmuir* **2005**, *21*, 6063-6072.
- (136) Manson, J.; Kumar, D.; Meenan, B. J.; Dixon, D. Polyethylene glycol functionalized gold nanoparticles: the influence of capping density on stability in various media *Gold Bulletin* **2011**; **2011**, *44*, 99-105.
- (137) Karunamuni, R. Targeted Gold Nanoparticle Contrast Agent for Digital Breast Tomosynthesis and Computed Tomography **2011**.
- (138) Wuelfing, W. P.; Gross, S. M.; Miles, D. T.; Murray, R. W. Nanometer Gold Clusters Protected by Surface-Bound Monolayers of Thiolated Poly(ethylene glycol) Polymer Electrolyte *J. Am. Chem. Soc.* **1998**, *120*, 12696-12697.
- (139) Walkey, C. D.; Olsen, J. B.; Guo, H.; Emili, A.; Chan, W. C. W. Nanoparticle Size and Surface Chemistry Determine Serum Protein Adsorption and Macrophage Uptake. *J. Am. Chem. Soc.* **2012**, *134*, 2139-2147.
- (140) Zhang, Q.; Iwakuma, N.; Sharma, P.; Moudgil, B. M.; Wu, C.; McNeill, J.; Jiang, H.; Grobmyer, S. R. Gold nanoparticles as a contrast agent for in vivo tumor imaging with photoacoustic tomography *Nanotechnology* **2009**, *20*, 395102.
- (141) Xia, X.; Yang, M.; Wang, Y.; Zheng, Y.; Li, Q.; Chen, J.; Xia, Y. Quantifying the Coverage Density of Poly(ethylene glycol) Chains on the Surface of Gold Nanostructures *ACS Nano* **2012**, *6*, 512-522.
- (142) Bell, C. S. A "label-free" method for the determination of polyethylene-glycol functionalization efficiency on gold monolayer protected clusters. **2009**, 123.
- (143) Tsai, D. H.; DelRio, F. W.; MacCuspie, R. I.; Cho, T. J.; Zachariah, M. R.; Hackley, V. A. Competitive adsorption of thiolated polyethylene glycol and mercaptopropionic acid on gold nanoparticles measured by physical characterization methods. *Langmuir* **2010**, *26*, 10325-10333.
- (144) Qian, X.; Peng, X. H.; Ansari, D. O.; Yin-Goen, Q.; Chen, G. Z.; Shin, D. M.; Yang, L.; Young, A. N.; Wang, M. D.; Nie, S. In vivo tumor targeting and spectroscopic detection with surface-enhanced Raman nanoparticle tags *Nat. Biotechnol.* **2008**, *26*, 83-90.
- (145) Levin, C. S.; Bishnoi, S. W.; Grady, N. K.; Halas, N. J. Determining the Conformation of Thiolated Poly(ethylene glycol) on Au Nanoshells by Surface-Enhanced Raman Scattering Spectroscopic Assay *Anal. Chem.* **2006**, *78*, 3277-3281.

- (146) Akiyama, Y.; Mori, T.; Katayama, Y.; Niidome, T. The effects of PEG grafting level and injection dose on gold nanorod biodistribution in the tumor-bearing mice. *J. Controlled Release* **2009**, *139*, 81-84.
- (147) Yamashita, S.; Niidome, Y.; Katayama, Y.; Niidome, T. Photochemical Reaction of Poly(ethylene glycol) on Gold Nanorods Induced by Near Infrared Pulsed-laser Irradiation. *Chem. Lett.* **2009**, *38*, 226-227.
- (148) Oh, E.; Susumu, K.; Blanco-Canosa, J. B.; Medintz, I. L.; Dawson, P. E.; Mattoussi, H. Preparation of Stable Maleimide-Functionalized Au Nanoparticles and Their Use in Counting Surface Ligands *Small* **2010**.
- (149) Unsworth, L. D.; Tun, Z.; Sheardown, H.; Brash, J. L. Chemisorption of thiolated poly(ethylene oxide) to gold: surface chain densities measured by ellipsometry and neutron reflectometry *J. Colloid Interface Sci.* **2005**, *281*, 112-121.
- (150) Maccarini, M.; Briganti, G.; Rucareanu, S.; Lui, X.; Sinibaldi, R.; Sztucki, M.; Lennox, R. B. Characterization of Poly(ethylene oxide)-Capped Gold Nanoparticles in Water by Means of Transmission Electron Microscopy, Thermogravimetric Analysis, Mass Density, and Small Angle Scattering. *J. Phys. Chem. C* **2010**, *114*, 6937-6943.
- (151) Sebyy, K.; Mansfield, E. The stability and surface coverage of polymer stabilized gold nanoparticles. *European Cells and Materials* **2010**, *20*, 234.
- (152) Ansari, D. O. Raman-encoded nanoparticles for biomolecular detection and cancer diagnostics. **2008**.
- (153) Choi, C. H.; Zuckerman, J. E.; Webster, P.; Davis, M. E. Targeting kidney mesangium by nanoparticles of defined size *Proc. Natl. Acad. Sci. U. S. A.* **2011**, *108*, 6656-6661.
- (154) Larson-Smith, K.; Pozzo, D. C. Scalable synthesis of self-assembling nanoparticle clusters based on controlled steric interactions *Soft Matter* **2011**, *7*, 5339.
- (155) Larson-Smith, K.; Pozzo, D. C. Competitive adsorption of thiolated polyethylene glycol and alkane-thiols on gold nanoparticles and its effect on cluster formation *Langmuir* **2012**.
- (156) Doane, T. L.; Cheng, Y.; Babar, A.; Hill, R. J.; Burda, C. Electrophoretic Mobilities of PEGylated Gold NPs *J. Am. Chem. Soc.* **2010**.
- (157) ELLMAN, G. L. Tissue sulfhydryl groups. *Arch. Biochem. Biophys.* **1959**, *82*, 70-77.

- (158) Riddles, P. W.; Blakeley, R. L.; Zerner, B. Ellman's reagent: 5,5'-dithiobis(2-nitrobenzoic acid)—a reexamination *Anal. Biochem.* **1979**, *94*, 75-81.
- (159) Riddles, P. W.; Blakeley, R. L.; Zerner, B. Enzyme Structure Part I; [8] Reassessment of Ellman's reagent **1983**, *91*, 49-60.
- (160) Benedict, R. C.; Stedman, R. L. Ellman's reagent: interference in mercapto group determination, with special reference to cigarette smoke *Analyst* **1970**, *95*, 296.
- (161) Humphrey, R. E.; Ward, M. H.; Hinze, W. Spectrophotometric determination of sulfite with 4,4'-dithio-dipyridine and 5,5'-dithiobis(2-nitrobenzoic acid) *Anal. Chem.* **1970**, *42*, 698-702.
- (162) Gao, X.; Zhang, Y.; Weaver, M. J. Observing surface chemical transformations by atomic-resolution scanning tunneling microscopy: sulfide electrooxidation on gold(111) *J. Phys. Chem.* **1992**, *96*, 4156-4159.
- (163) Hill, H. D.; Millstone, J. E.; Banholzer, M. J.; Mirkin, C. A. The Role Radius of Curvature Plays in Thiolated Oligonucleotide Loading on Gold Nanoparticles. *ACS Nano* **2009**, *3*, 418-424.
- (164) Reuss, F. *Mém. Soc. Impériale Naturalistes de Moscow* **1809**, *2*, 327.
- (165) von Helmholtz, H. *Wied. Ann.* **1879**, *7*, 337.
- (166) von Smoluchowski, M. *Bull. Int. Acad. Sci. Cracovie* **1903**, 184.
- (167) Gouy, G. *J. Phys.* **1910**, *9*, 457.
- (168) Gouy, G. *Compt. Rend.* **1909**, *149*, 654.
- (169) Hückel, E. *Physik. Z.* **1924**, *25*, 204.
- (170) Wiersema, P. H.; Loeb, A. L.; Overbeek, J. T. Calculation of the electrophoretic mobility of a spherical colloid particle. **1966**.
- (171) Faraday, M. *Exp. Res. Nr.* **1838**, 1562.
- (172) Bier, M., In *Electrophoresis: theory, methods, and applications*. Academic Press: [New York, 1959; .
- (173) Tiselius, A. A new apparatus for electrophoretic analysis of colloidal mixtures *Transactions of the Faraday Society* **1937**, *33*, 524.
- (174) SMITHIES, O. Zone electrophoresis in starch gels: group variations in the serum proteins of normal human adults *Biochem. J.* **1955**, *61*, 629-641.

- (175) ORNSTEIN, L. Disc Electrophoresis. I. Background and Theory *Ann. N. Y. Acad. Sci.* **1964**, *121*, 321-349.
- (176) DAVIS, B. J. Disc Electrophoresis. II. Method and Application to Human Serum Proteins *Ann. N. Y. Acad. Sci.* **1964**, *121*, 404-427.
- (177) Sharp, P. A.; Sugden, B.; Sambrook, J. Detection of two restriction endonuclease activities in *Haemophilus parainfluenzae* using analytical agarose-ethidium bromide electrophoresis *Biochemistry (N. Y.)* **1973**, *12*, 3055-3063.
- (178) Schirmer, R. H. In *Modern methods of pharmaceutical analysis* Boca Raton, Fla. : CRC Press, c1982-: .
- (179) Brust, M.; Walker, M.; Bethell, D.; Schiffrin, D. J.; Whyman, R. Synthesis of thiol-derivatised gold nanoparticles in a two-phase Liquid-Liquid system. *J. Chem. Soc., Chem. Commun.* **1994**, 801-802.
- (180) Connor, E.; Mwamuka, J.; Gole, A.; Murphy, C.; Wyatt, M. Gold Nanoparticles Are Taken Up by Human Cells but Do Not Cause Acute Cytotoxicity *Small* **2005**, *1*, 325-327.
- (181) Bain, C. D.; Troughton, E. B.; Tao, Y. T.; Evall, J.; Whitesides, G. M.; Nuzzo, R. G. Formation of monolayer films by the spontaneous assembly of organic thiols from solution onto gold *J. Am. Chem. Soc.* **1989**, *111*, 321-335.
- (182) Luedtke, W. D.; Landman, U. Structure and Thermodynamics of Self-Assembled Monolayers on Gold Nanocrystallites *The Journal of Physical Chemistry B* **1998**, *102*, 6566-6572.
- (183) Terrill, R. H.; Postlethwaite, T. A.; Chen, C.; Poon, C.; Terzis, A.; Chen, A.; Hutchison, J. E.; Clark, M. R.; Wignall, G. Monolayers in Three Dimensions: NMR, SAXS, Thermal, and Electron Hopping Studies of Alkanethiol Stabilized Gold Clusters *J. Am. Chem. Soc.* **1995**, *117*, 12537-12548.
- (184) Aggarwal, P.; Hall, J. B.; McLeland, C. B.; Dobrovolskaia, M. A.; McNeil, S. E. Nanoparticle interaction with plasma proteins as it relates to particle biodistribution, biocompatibility and therapeutic efficacy *Adv. Drug Deliv. Rev.* **2009**, *61*, 428-437.
- (185) Hostetler, M. J.; Green, S. J.; Stokes, J. J.; Murray, R. W. Monolayers in Three Dimensions: Synthesis and Electrochemistry of ω -Functionalized Alkanethiolate-Stabilized Gold Cluster Compounds *J. Am. Chem. Soc.* **1996**, *118*, 4212-4213.
- (186) Hostetler, M. J.; Templeton, A. C.; Murray, R. W. Dynamics of Place-Exchange Reactions on Monolayer-Protected Gold Cluster Molecules *Langmuir* **1999**, *15*, 3782-3789.

- (187) Dubois, L. H.; Nuzzo, R. G. Synthesis, Structure, and Properties of Model Organic Surfaces. *Annu. Rev. Phys. Chem.* **1992**, *43*, 437-463.
- (188) Dow Chemical Company CARBOWAX PEGs - Thermal Degradation. Dow Perf Materials & Basic Chem Answer Center. [https://dow-answer.custhelp.com/app/answers/detail/a_id/3821/~carbowax-pegs---thermal-degradation](https://dow-answer.custhelp.com/app/answers/detail/a_id/3821/~/carbowax-pegs---thermal-degradation) (accessed 6/17/2012, 2012).
- (189) Mitchell, S. C.; Steventon, G. B. THIOUREA AND ITS BIOLOGICAL INTERACTIONS *Sulfur reports* **1994**, *16*, 117-137.
- (190) Rostkowska, H.; Lapinski, L.; Khvorostov, A.; Nowak, M. J. Proton-Transfer Processes in Thiourea: UV Induced Thione → Thiol Reaction and Ground State Thiol → Thione Tunneling *The Journal of Physical Chemistry A* **2003**, *107*, 6373.
- (191) Jayaram, P. N.; Roy, G.; Mugesh, G. Effect of thione—thiol tautomerism on the inhibition of lactoperoxidase by anti-thyroid drugs and their analogues *Journal of Chemical Sciences* **2008**, *120*, 143.
- (192) Marsden, J.; House, I. In *The chemistry of gold extraction* Society for Mining, Metallurgy, and Exploration: Littleton, Colo., 2006; , pp 651.
- (193) Groenewald, T. The dissolution of gold in acidic solutions of thiourea *Hydrometallurgy* **1976**, *1*, 277-290.
- (194) Deng, T.; Liao, M. Gold recovery enhancement from a refractory flotation concentrate by sequential bioleaching and thiourea leach. *Hydrometallurgy* **2002**, *63*, 249-255.
- (195) Van Driessche, E.; Beeckmans, S.; Dejaegere, R.; Kanarek, L. Thiourea: The antioxidant of choice for the purification of proteins from phenol-rich plant tissues *Anal. Biochem.* **1984**, *141*, 184-188.
- (196) Mendoza, G.; Alvarez, A. I.; Pulido, M. M.; Molina, A. J.; Merino, G.; Real, R.; Fernandes, P.; Prieto, J. G. Inhibitory effects of different antioxidants on hyaluronan depolymerization *Carbohydr. Res.* **2007**, *342*, 96-102.
- (197) Araujo, M. C. P.; Antunes, L. M. G.; Takahashi, C. S. Protective effect of thiourea, a hydroxyl - radical scavenger, on curcumin - induced chromosomal aberrations in an in vitro mammalian cell system. *Teratog. , Carcinog. Mutagen.* **2001**, *21*, 175-180.
- (198) Ziegler-Skylakakis, K. Thiourea. *Concise International Chemical Assessment Document* **2003**, 49.
- (199) Hoffmann, M.; Edwards, J. O. Kinetics and mechanism of the oxidation of thiourea and N,N'-dialkylthioureas by hydrogen peroxide *Inorg. Chem.* **1977**, *16*, 3333-3338.

- (200) Shashoua, V. E. Formamidine Sulfinic Acid as a Biochemical Reducing Agent *Biochemistry (N. Y.)* **1964**, 3, 1719-1720.
- (201) ARIFOGLU, M.; MARMER, N. Reaction of thiourea with hydrogen peroxide: ¹³C NMR studies of an oxidative/reductive bleaching process. *gen* **1992**, 95.
- (202) Shaw, W. H. R.; Walker, D. G. The decomposition of thiourea in water solutions. *J. Am. Chem. Soc.* **1956**, 78, 5769-5772.
- (203) Love, J. C.; Wolfe, D. B.; Haasch, R.; Chabynec, M. L.; Paul, K. E.; Whitesides, G. M.; Nuzzo, R. G. Formation and Structure of Self-Assembled Monolayers of Alkanethiolates on Palladium. *J. Am. Chem. Soc.* **2003**, 125, 2597-2609.
- (204) Schoenfish, M. H.; Pemberton, J. E. Air Stability of Alkanethiol Self-Assembled Monolayers on Silver and Gold Surfaces *J. Am. Chem. Soc.* **1998**, 120, 4502-4513.
- (205) Flynn, N. T.; Tran, T. N. T.; Cima, M. J.; Langer, R. Long-Term Stability of Self-Assembled Monolayers in Biological Media. *Langmuir* **2003**, 19, 10909-10915.
- (206) Deschaines, T. O.; Carron, K. T. Stability and Surface Uniformity of Selected Thiol-Coated SERS Surfaces. *Appl. Spectrosc.* **1997**, 51, 1355-1359.
- (207) Mrksich, M.; Dike, L. E.; Tien, J.; Ingber, D. E.; Whitesides, G. M. Using microcontact printing to pattern the attachment of mammalian cells to self-assembled monolayers of alkanethiolates on transparent films of gold and silver *Exp. Cell Res.* **1997**, 235, 305-313.
- (208) Dasog, M.; Scott, R. W. Understanding the oxidative stability of gold monolayer-protected clusters in the presence of halide ions under ambient conditions *Langmuir* **2007**, 23, 3381-3387.
- (209) Yuan, M.; Zhan, S.; Zhou, X.; Liu, Y.; Feng, L.; Lin, Y.; Zhang, Z.; Hu, J. A Method for Removing Self-Assembled Monolayers on Gold *Langmuir* **2008**, 24, 8707-8710.
- (210) Lewis, M. E. In *Dissolved Oxygen*; U.S. Geological Survey, Ed.; U.S. Geological Survey Techniques of Water-Resources Investigations; U.S. Geological Survey: 2006; Vol. 9, .
- (211) Weiss, R. F. The solubility of nitrogen, oxygen and argon in water and seawater. *Deep Sea Research and Oceanographic Abstracts* **1970**, 17, 721-735.
- (212) Battino, R.; Rettich, T. R.; Tominaga, T. The Solubility of Oxygen and Ozone in Liquids *Journal of Physical and Chemical Reference Data* **1983**, 12, 163.
- (213) The BOC Group Reference Manuals: Pure Gases. **2006**.

- (214) Jaffey, D. M.; Madix, R. J. Reactivity of Sulfur-Containing Molecules on Noble Metal Surfaces. 2. tert-Butyl Thioalcohol on Au(110). *J. Am. Chem. Soc.* **1994**, *116*, 3012-3019.
- (215) Delamarche, E.; Michel, B.; Kang, H.; Gerber, C. Thermal Stability of Self-Assembled Monolayers. *Langmuir* **1994**, *10*, 4103-4108.
- (216) Maltesh, C.; Somasundaran, P. Effect of binding of cations to polyethylene glycol on its interactions with sodium dodecyl sulfate *Langmuir* **1992**, *8*, 1926-1930.
- (217) Ananthapadmanabhan, K. P.; Goddard, E. D. Aqueous biphasic formation in polyethylene oxide-inorganic salt systems *Langmuir* **1987**, *3*, 25-31.
- (218) Nozary, S.; Modarress, H.; Eliassi, A. Cloud-point measurements for salt + poly(ethylene glycol) + water systems by viscometry and laser beam scattering methods *J Appl Polym Sci* **2003**; **2003**, *89*, 1983-1990.
- (219) Harris, D. C. In *Quantitative Chemical Analysis* W.H. Freeman & Company: New York, 2007; .
- (220) Bettelheim, F. A.; Brown, W. A.; Campbell, M. K.; Farrell, S. O. In *Introduction to Organic and Biochemistry* Brooks Cole: 2008; .
- (221) Banker, G. S.; Rhodes, C. T. In *Modern pharmaceuticals* New York Marcel Dekker: 2002; , pp 838.
- (222) Alberts, B. In *Essential cell biology: an introduction to the molecular biology of the cell* Garland Pub.: New York, 1998; .
- (223) Ho, P. In *Biological and Physiological Features of the Gastrointestinal Tract Relevant to Oral Drug Absorption* ; Hu, M., Li, X., Eds.; **Oral Bioavailability: Basic Principles, Advanced Concepts, and Applications**; Wiley: New Jersey, USA, 2011; pp 51.
- (224) Roach, P.; Farrar, D.; Perry, C. C. Interpretation of Protein Adsorption: Surface-Induced Conformational Changes. *J. Am. Chem. Soc.* **2005**, *127*, 8168-8173.
- (225) Malamud, D.; Drysdale, J. W. Isoelectric points of proteins: A table. *Anal. Biochem.* **1978**, *86*, 620-647.
- (226) Roche Diagnostics GmbH Lysozyme. **2006**.
- (227) Worthington Biochemical Corporation Lysozyme - Worthington Enzyme Manual. <http://www.worthington-biochem.com/ly/default.html> (accessed 8/11/2012, 2012).

- (228) WETTER, L. R.; DEUTSCH, H. F. Immunological studies on egg white proteins. IV. Immunochemical and physical studies of lysozyme *J. Biol. Chem.* **1951**, *192*, 237-242.
- (229) Efimova, Y. M.; Haemers, S.; Wierczinski, B.; Norde, W.; van Well, A. A. Stability of globular proteins in H₂O and D₂O *Biopolymers* **2007**, *85*, 264-273.
- (230) Mohan, C. Buffers: A guide for the preparation and use of buffers in biological systems. **2003**.
- (231) Foster, J. F.; Kaplan, L. J. Isoelectric focussing behavior of bovine plasma albumin, mercaptalbumin, and β -lactoglobulins A and B *Biochemistry (N. Y.)* **1971**, *10*, 630-636.
- (232) Rex M. C. Dawson; Elliott, D. C.; Elliott, W. R. In *Data for biochemical research* Clarendon Press: Oxford, 1989; , pp 580.
- (233) Yadav, S.; Shire, S. J.; Kalonia, D. S. Viscosity Analysis of High Concentration Bovine Serum Albumin Aqueous Solutions *Pharm. Res.* **2011**.
- (234) Tanford, C.; Roxby, R. Interpretation of protein titration curves. Application to lysozyme *Biochemistry (N. Y.)* **1972**, *11*, 2192-2198.
- (235) Zayas, J. F. In *Functionality of proteins in foods* Springer: New York, 1997; , pp 373.
- (236) Chiodi, F.; Sidén, Å.; Ösby, E. Isoelectric focusing of monoclonal immunoglobulin G, A and M followed by detection with the avidin-biotin system *Electrophoresis* **1985**, *6*, 124-128.
- (237) Agrisera Antibodies Information about IgG antibodies
<http://www.agrisera.com/en/info/igg.html> (accessed 10/20/2012, 2012).
- (238) Aitken, A.; Learmonth <component_number> Chapter 1, M. The Protein Protocols Handbook; Protein Determination by UV Absorption **1996**, 3-6.
- (239) Pace, C. N.; Vajdos, F.; Fee, L.; Grimsley, G.; Gray, T. How to measure and predict the molar absorption coefficient of a protein *Protein Sci.* **1995**, *4*, 2411-2423.
- (240) Bradford, M. M. A rapid and sensitive method for the quantitation of microgram quantities of protein utilizing the principle of protein-dye binding *Anal. Biochem.* **1976**, *72*, 248-254.
- (241) Compton, S. J.; Jones, C. G. Mechanism of dye response and interference in the Bradford protein assay *Anal. Biochem.* **1985**, *151*, 369-374.

- (242) Georgiou, C. D.; Grintzalis, K.; Zervoudakis, G.; Papapostolou, I. Mechanism of Coomassie brilliant blue G-250 binding to proteins: a hydrophobic assay for nanogram quantities of proteins *Anal. Bioanal Chem.* **2008**, *391*, 391-403.
- (243) Das, K. P.; Chatteraj, D. K. Adsorption of proteins at the polar oil—water interface *J. Colloid Interface Sci.* **1980**, *78*, 422-429.
- (244) Norde, W.; MacRitchie, F.; Nowicka, G.; Lyklema, J. Protein adsorption at solid-liquid interfaces: Reversibility and conformation aspects *J. Colloid Interface Sci.* **1986**, *112*, 447-456.
- (245) Carter, D. C.; Ho, J. X. Structure of serum albumin *Adv. Protein Chem.* **1994**, *45*, 153-203.
- (246) Bhattacharya, M.; Jain, N.; Bhasne, K.; Kumari, V.; Mukhopadhyay, S. pH-induced Conformational Isomerization of Bovine Serum Albumin Studied by Extrinsic and Intrinsic Protein Fluorescence *J. Fluoresc.* **2012**, *21*, 1083-1090.
- (247) Ahmad, B.; Parveen, S.; Khan, R. H. Effect of Albumin Conformation on the Binding of Ciprofloxacin to Human Serum Albumin: A Novel Approach Directly Assigning Binding Site. *Biomacromolecules* **2006**, *7*, 1350-1356.
- (248) McNeil, S. E. Nanoparticle therapeutics: a personal perspective *Wiley Interdisciplinary Reviews: Nanomedicine and Nanobiotechnology* **2009**, *1*, 264.
- (249) Soo Choi, H.; Liu, W.; Misra, P.; Tanaka, E.; Zimmer, J. P.; Itope, B.; Bawendi, M. G.; Frangioni, J. V. Renal clearance of quantum dots *Nat. Biotechnol.* **2007**, *25*, 1165-1170.
- (250) Wasdo, S. C.; Barber, D. S.; Denslow, N. D.; Powers, K. W.; Palazuelos, M.; Jr., S. M. S.; Moudgil, B. M.; Roberts, S. M. Differential binding of serum proteins to nanoparticles *International Journal of Nanotechnology* **2008**, *5*, 92.
- (251) Casals, E.; Pfaller, T.; Duschl, A.; Oostingh, G. J.; Puentes, V. Time Evolution of the Nanoparticle Protein Corona *ACS Nano* **2010**.
- (252) Deng, Z. J.; Mortimer, G.; Schiller, T.; Musumeci, A.; Martin, D.; Minchin, R. F. Differential plasma protein binding to metal oxide nanoparticles *Nanotechnology* **2009**, *20*, 455101.
- (253) Ruh, H.; Kuhl, B.; Brenner-Weiss, G.; Hopf, C.; Diabate, S.; Weiss, C. Identification of serum proteins bound to industrial nanomaterials *Toxicol. Lett.* **2011**.

- (254) Tenzer, S.; Docter, D.; Rosfa, S.; Wlodarski, A.; Kuharev, J.; Rekik, A.; Knauer, S. K.; Bantz, C.; Nawroth, T.; Bier, C.; Sirirattanapan, J.; Mann, W.; Treuel, L.; Zellner, R.; Maskos, M.; Schild, H.; Stauber, R. H. Nanoparticle Size Is a Critical Physicochemical Determinant of the Human Blood Plasma Corona: A Comprehensive Quantitative Proteomic Analysis *ACS Nano* **2011**.
- (255) Zhang, H.; Burnum, K. E.; Luna, M. L.; Petritis, B. O.; Kim, J.; Qian, W.; Moore, R. J.; Heredia-Langner, A.; Webb-Robertson, B. M.; Thrall, B. D.; Camp, D. G.; Smith, R. D.; Pounds, J. G.; Liu, T. Quantitative proteomics analysis of adsorbed plasma proteins classifies nanoparticles with different surface properties and size *Proteomics* **2011**, *11*, n/a-n/a.
- (256) Fischer, H. C.; Chan, W. C. Nanotoxicity: the growing need for in vivo study *Curr. Opin. Biotechnol.* **2007**, *18*, 565-571.
- (257) Knop, K.; Hoogenboom, R.; Fischer, D.; Schubert, U. S. Poly(ethylene glycol) in Drug Delivery: Pros and Cons As Well as Potential Alternatives *Angewandte Chemie International Edition* **2010**.
- (258) Klibanov, A. L.; Maruyama, K.; Torchilin, V. P.; Huang, L. Amphipathic polyethyleneglycols effectively prolong the circulation time of liposomes *FEBS Lett.* **1990**, *268*, 235-237.
- (259) Gref, R.; Minamitake, Y.; Peracchia, M. T.; Trubetsky, V.; Torchilin, V.; Langer, R. Biodegradable long-circulating polymeric nanospheres *Science* **1994**, *263*, 1600-1603.
- (260) Scheirs, J.; Bigger, S. W.; Delatycki, O. Characterizing the solid-state thermal oxidation of poly(ethylene oxide) powder *Polymer* **1991**, *32*, 2014-2019.
- (261) Morlat, S.; Gardette, J. Phototransformation of water-soluble polymers. I: photo- and thermooxidation of poly(ethylene oxide) in solid state *Polymer* **2001**, *42*, 6071-6079.
- (262) Toda, M.; Arima, Y.; Iwata, H. Complement activation on degraded polyethylene glycol-covered surface *Acta Biomater.* **2010**.
- (263) Szebeni, J.; Alving, C. R.; Muggia, F. M. Complement Activation by Cremophor EL as a Possible Contributor to Hypersensitivity to Paclitaxel: an In Vitro Study *JNCI Journal of the National Cancer Institute* **1998**, *90*, 300-306.
- (264) Dams, E. T.; Laverman, P.; Oyen, W. J.; Storm, G.; Scherphof, G. L.; van Der Meer, J. W.; Corstens, F. H.; Boerman, O. C. Accelerated blood clearance and altered biodistribution of repeated injections of sterically stabilized liposomes *J. Pharmacol. Exp. Ther.* **2000**, *292*, 1071-1079.

- (265) Szebeni, J. Complement activation-related pseudoallergy: a new class of drug-induced acute immune toxicity *Toxicology* **2005**, *216*, 106-121.
- (266) Judge, A.; McClintock, K.; Phelps, J. R.; Maclachlan, I. Hypersensitivity and loss of disease site targeting caused by antibody responses to PEGylated liposomes *Mol. Ther.* **2006**, *13*, 328-337.
- (267) Shubayev, V. I.; Pisanic, T. R., 2nd; Jin, S. Magnetic nanoparticles for theragnostics *Adv. Drug Deliv. Rev.* **2009**, *61*, 467-477.
- (268) Moghimi, S. M.; Gray, T. A single dose of intravenously injected poloxamine-coated long-circulating particles triggers macrophage clearance of subsequent doses in rats *Clin. Sci. (Lond)* **1997**, *93*, 371-379.
- (269) Moghimi, S. M.; Murray, J. C. Poloxamer-188 revisited: a potentially valuable immune modulator *J. Natl. Cancer Inst.* **1996**, *88*, 766-768.
- (270) Duguet, E.; Vasseur, S.; Mornet, S.; Devoisselle, J. M. Magnetic nanoparticles and their applications in medicine *Nanomedicine (Lond)* **2006**, *1*, 157-168.
- (271) Misra, S. K.; Dybowska, A. D.; Berhanu, D.; Boccaccini, A. R.; Luoma, S. N.; Plant, J. A.; Valsami-Jones, E. In *In The solubility and reactivity of silica nanoparticles*. Goldschmidt Conference Abstracts; 2009; .
- (272) Iler, R. K. In *The chemistry of silica: solubility, polymerization, colloid and surface properties, and biochemistry* Wiley: New York, 1979; , pp 866.
- (273) Ishida, T.; Harada, M.; Wang, X. Y.; Ichihara, M.; Irimura, K.; Kiwada, H. Accelerated blood clearance of PEGylated liposomes following preceding liposome injection: Effects of lipid dose and PEG surface-density and chain length of the first-dose liposomes. *J. Controlled Release* **2005**, *105*, 305-317.
- (274) Laverman, P.; Carstens, M. G.; Boerman, O. C.; Dams, E. T. M.; Oyen, W. J. G.; van Rooijen, N.; Corstens, F. H. M.; Storm, G. Factors affecting the accelerated blood clearance of polyethylene glycol-liposomes upon repeated injection. *J. Pharmacol. Exp. Ther.* **2001**, *298*, 607-612.
- (275) Ishihara, T.; Takeda, M.; Sakamoto, H.; Kimoto, A.; Kobayashi, C.; Takasaki, N.; Yuki, K.; Tanaka, K.; Takenaga, M.; Igarashi, R.; Maeda, T.; Yamakawa, N.; Okamoto, Y.; Otsuka, M.; Ishida, T.; Kiwada, H.; Mizushima, Y.; Mizushima, T. Accelerated blood clearance phenomenon upon repeated injection of PEG-modified PLA-nanoparticles *Pharm. Res.* **2009**, *26*, 2270-2279.
- (276) Zhao, Y.; Wang, L.; Yan, M.; Ma, Y.; Zang, G.; She, Z.; Deng, Y. Repeated injection of PEGylated solid lipid nanoparticles induces accelerated blood clearance in mice and beagles *Int. J. Nanomedicine* **2012**, *7*, 2891-2900.

- (277) Wang, X.; Ishida, T.; Kiwada, H. Anti-PEG IgM elicited by injection of liposomes is involved in the enhanced blood clearance of a subsequent dose of PEGylated liposomes *J. Control. Release* **2007**, *119*, 236-244.
- (278) Richter, A. W.; & Aring; kerblom, E. Polyethylene Glycol Reactive Antibodies in Man: Titer Distribution in Allergic Patients Treated with Monomethoxy Polyethylene Glycol Modified Allergens or Placebo, and in Healthy Blood Donors *Int. Arch. Allergy Immunol.* **1984**, *74*, 36-39.
- (279) Leger, R.; Arndt, P.; Garratty, G.; Armstrong, J.; Meiselman, H.; Fisher, T. Normal donor sera can contain antibodies to polyethylene glycol (PEG). *Transfusion* **2001**, *41*, 29S.
- (280) Armstrong, J.; Leger, R.; Wenby, R.; Meiselman, H.; Garratty, G.; Fisher, T. Occurrence of an antibody to poly (ethylene glycol) in normal donors. *Blood* **2003**, *102*, 556A.
- (281) Armstrong, J. K.; Hempel, G.; Koling, S.; Chan, L. S.; Fisher, T.; Meiselman, H. J.; Garratty, G. Antibody against poly(ethylene glycol) adversely affects PEG-asparaginase therapy in acute lymphoblastic leukemia patients *Cancer* **2007**; **2007**, *110*, 103-111.
- (282) Goel, R.; Shah, N.; Visaria, R.; Paciotti, G. F.; Bischof, J. C. Biodistribution of TNF-alpha-coated gold nanoparticles in an in vivo model system. *Nanomedicine (Lond)* **2009**, *4*, 401-410.
- (283) Kawano, T.; Yamagata, M.; Takahashi, H.; Niidome, Y.; Yamada, S.; Katayama, Y.; Niidome, T. Stabilizing of plasmid DNA in vivo by PEG-modified cationic gold nanoparticles and the gene expression assisted with electrical pulses *J. Control. Release* **2006**, *111*, 382-389.
- (284) Cho, W. S.; Cho, M.; Jeong, J.; Choi, M.; Cho, H. Y.; Han, B. S.; Kim, S. H.; Kim, H. O.; Lim, Y. T.; Chung, B. H.; Jeong, J. Acute toxicity and pharmacokinetics of 13 nm-sized PEG-coated gold nanoparticles *Toxicol. Appl. Pharmacol.* **2009**, *236*, 16-24.
- (285) Cho, W. S.; Cho, M.; Jeong, J.; Choi, M.; Han, B. S.; Shin, H. S.; Hong, J.; Chung, B. H.; Jeong, J.; Cho, M. H. Size-dependent tissue kinetics of PEG-coated gold nanoparticles *Toxicol. Appl. Pharmacol.* **2010**.
- (286) Dutta, D. Engineered nanoparticles as contrast agents. **2009**.
- (287) Wang, Y.; Xie, X.; Wang, X.; Ku, G.; Gill, K. L.; O'Neal, D. P.; Stoica, G.; Wang, L. V. Photoacoustic Tomography of a Nanoshell Contrast Agent in the in Vivo Rat Brain *Nano Letters* **2004**, *4*, 1689-1692.

- (288) Xie, H.; Gill-Sharp, K. L.; O'Neal, D. P. Quantitative estimation of gold nanoshell concentrations in whole blood using dynamic light scattering *Nanomedicine* **2007**, *3*, 89-94.
- (289) James, W. D.; Hirsch, L. R.; West, J. L.; O'Neal, P. D.; Payne, J. D. Application of INAA to the build-up and clearance of gold nanoshells in clinical studies in mice *J. Radioanal. Nucl.* **2007**, *271*, 455-459.
- (290) Michalak, G. J.; Schwartz, J. A.; O'Neal, D. P. In *In Circulation time estimates of optically active nanoparticles using a pulse photometer*; Proceedings of SPIE. 2009; , pp 71880M.
- (291) Michalak, G. J.; Goodrich, G. P.; Schwartz, J. A.; James, W. D.; O'Neal, D. P. Murine photoplethysmography for in vivo estimation of vascular gold nanoshell concentration *J. Biomed. Opt.* **2010**, *15*, 047007.
- (292) Michalak, G. J.; Anderson, H. A.; O'Neal, D. P. Feasibility of Using a Two-Wavelength Photometer to Estimate the Concentration of Circulating Near-Infrared Extinguishing Nanoparticles *Journal of Biomedical Nanotechnology* **2010**, *6*, 73-81.
- (293) Niidome, T.; Yamagata, M.; Okamoto, Y.; Akiyama, Y.; Takahashi, H.; Kawano, T.; Katayama, Y.; Niidome, Y. PEG-modified gold nanorods with a stealth character for in vivo applications *J. Control. Release* **2006**, *114*, 343-347.
- (294) Niidome, T.; Akiyama, Y.; Shimoda, K.; Kawano, T.; Mori, T.; Katayama, Y.; Niidome, Y. In Vivo Monitoring of Intravenously Injected Gold Nanorods Using Near - Infrared Light *Small* **2008**, *4*, 1001-1007.
- (295) Lankveld, D. P. K.; Rayavarapu, R. G.; Krystek, P.; Oomen, A. G.; Verharen, H. W.; van Leeuwen, T. G.; De Jong, W. H.; Manohar, S. Blood clearance and tissue distribution of PEGylated and non-PEGylated gold nanorods after intravenous administration in rats. *Nanomedicine* **2011**, *6*, 339-349.
- (296) National Institutes of Health Albumin - serum: MedlinePlus Medical Encyclopedia <http://www.nlm.nih.gov/medlineplus/ency/article/003480.htm> (accessed 9/9/2012, 2012).
- (297) National Institutes of Health Total protein: MedlinePlus Medical Encyclopedia <http://www.nlm.nih.gov/medlineplus/ency/article/003483.htm> (accessed 9/9/2012, 2012).
- (298) FTIRsearch Commercial Materials Polypropylene Additives Library. [https://ftirsearch.com/features/libraries/PDFs/Commercial Materials Polypropylene Additives Library.pdf](https://ftirsearch.com/features/libraries/PDFs/Commercial%20Materials%20Polypropylene%20Additives%20Library.pdf) (accessed November 29, 2012).

- (299) Mansouri, H.; Yagoubi, N.; Ferrier, D. Extraction of polypropylene additives and their analysis by HPLC *Chromatographia* **1998**, *48*, 491-496.
- (300) McDonald, G. R.; Kozuska, J.; Holt, A. Bioactive leachates from lab plastics. Use of plastic disposables may compromise bioassay results. *G. I. T. Lab. J. Eur.* **2009**, *13*, 2-4.
- (301) Sachon, E.; Matheron, L.; Clodic, G.; Blasco, T.; Bolbach, G. MALDI TOF-TOF characterization of a light stabilizer polymer contaminant from polypropylene or polyethylene plastic test tubes *Journal of Mass Spectrometry* **2010**, *45*, 43-50.
- (302) SCHOTT Technical Glass Solutions GmbH SCHOTT Technical Glasses: Physical and technical properties. **2010**, 90491.
- (303) Xia, Y. Q.; Patel, S.; Bakhtiar, R.; Franklin, R. B.; Doss, G. A. Identification of a new source of interference leached from polypropylene tubes in mass-selective analysis. *J. Am. Soc. Mass Spectrom.* **2005**, *16*, 417-421.

BIOGRAPHICAL SKETCH

Paul Carpinone was born and raised in Tampa, Florida and began his undergraduate studies at the University of Florida in 2004. In 2008 he received his bachelor's degree in Chemical Engineering. The same year, he began his graduate studies at the Particle Engineering Research Center focusing on nanotoxicology and surface chemistry. He received his doctorate degree from the Department of Materials Science and Engineering in 2012.